Advancing risk assessment of climate change and the resiliency of cities

by

Hiva Viseh

M.Sc. Polytechnic University of Milan, 2020

A Dissertation Submitted in Partial Fulfillment of the

Requirements for the Degree of

DOCTOR OF PHILOSOPHY

in the Department of Civil Engineering

Advancing risk assessment of climate change and the resiliency of cities

By

Hiva Viseh

M.Sc. Polytechnic University of Milan, 2020

Supervisory Committee

Dr. David Bristow, Supervisor

(Department of Civil Engineering)

Dr. Tara Troy, Departmental Member

(Department of Civil Engineering)

Dr. David Atkinson, Outside Member

(Department of Geography)

Abstract

Climate change is widely acknowledged to have significant impacts on socio-ecological systems, affecting different regions to varying extents through shocks and stresses related to extreme weather events, sea level rise, and other climate-related changes. This highlights the critical role of adaptation measures in reducing the imposed cost of climate change by increasing urban resilience under a variety of likely climate change-induced scenarios while capitalising on the opportunities presented by a changing climate. The initial step in comprehending the importance of investing in adaptation measures, and subsequently implementing effective strategies in urban areas, is to disseminate information regarding the risks posed by climate change and cultivate awareness and understanding of these risks. While the magnitude of climate change impacts and their resulting socioeconomic consequences still remain uncertain, the increasing complexity and interconnection of diverse social and environmental systems has dramatically impacted our ability to foresee future-imposed threats from climate change.

This PhD thesis aims to foster advances in risk perceptions of climate change by progressing risk assessment of potential hazards and changes imposed by climate change on urban areas, as well as by proposing new methods to assess the vulnerability and reliability of complex systems and networks that cities rely on under stresses and shocks, while using all available data and sources, and communicating the complex and multifaceted aspects of climate change in such a way that the data can be used practically in resilience planning and resource allocation. The proposed new methods are: using Euclidean distance in conjunction with the modified Mann-Kendall test to capture both the direction and magnitude of changes in climate data derived from a large number of models; using the Epps-Singleton test to compare climate change in neighbouring cities to see the degree to which it may be possible for adaptation plans to be similar; combining damage functions and probability bound analysis to estimate potential flood damage caused by different climate change-driven flood scenarios at a regional scale by measuring a fraction of the buildings while addressing often-missing uncertainty quantification in damage estimates; and estimating time to failure and repair time of complex systems and networks when dealing with uncertainty in input parameters as well as indeterminant functional dependency using imprecise probability analysis in a probability box approach. In addition, the introduced methods were used to assess the potential variations in diverse climate variables across Canadian cities; to estimate the impact of climate change on flood damage to residential buildings in Metro Vancouver, Canada; to quantify time to failure and repair time of power, water, and wastewater networks, and to calculate the time to failure that an average utility customer of a two-story office building may experience for different types of internal and external functional dependencies.

Table of Content

Acknowledgements

I would like to express my sincere gratitude to my supervisor, Professor David Bristow, for giving me the incredible opportunity to join the Cities and Infrastructure Systems lab in the beautiful city of Victoria. His support, invaluable guidance, and expertise have been instrumental in bringing this work to completion.

I am also deeply grateful to my committee members, Professors Tara Troy and Professor David Atkinson, for their time and constructive feedback. I would also like to extend my thanks to the University of Victoria, especially the administrative team of the Department of Civil Engineering.

I cannot forget to mention my family - my loving mom, dad, and dear brother Sina whose unwavering love and support have been a source of strength and inspiration, motivating me to push beyond my limits and strive for excellence. Thank you for always being there for me, through this journey.

Lastly, I would like to express my appreciation to the funding programs that supported my research and enabled me to present it at various conferences.

Hiva Viseh

Dedication

I dedicate this thesis to my dearest mom, dad, and brother Sina with all my heart. I am forever grateful for your presence in my life and for being my best friends.

With all my love,
Hiva

Chapter 1: Introductory Remarks

1. Introduction

There is a growing scientific consensus on climate change and the new and unique risks that it poses to socio-ecological systems, especially in urban areas. Due to high population density, concentrated economic activities, large-scale infrastructures, and exacerbated impacts such as urban heat island, climate change-induced shocks and stresses could result in extensive socioeconomic loss in urban areas.

Mitigation and adaptation are two critical tools for reducing the impacts of stresses associated with climate change (Chen & Gong, 2021). In terms of mitigation, many international climate negotiations and agreements, such as the Paris Agreement, have been made to reduce global greenhouse gas (GHG) emissions and slow global warming. Anthropogenic climate change has been occurring despite efforts to reduce greenhouse gas emissions. This highlights the important role of adaptation measures in reducing the imposed cost of climate change by increasing urban resilience under a variety of likely climate change-induced scenarios (Brugmann, 2012). The first step in implementing effective adaptation measures in urban areas is to provide information and foster perceptions about the risks posed by climate change. According to Lehmann et al. (2015), whether decision-makers implement adaptation measures is influenced by three factors: 1) information, 2) available resources, and 3) incentives to act. Furthermore, the U.S. National Research Council (1997) argues that the perception of individuals towards global phenomena, e.g., climate change, is an important contributor to both environmental problems and potential solutions. According to Wachinger et al. (2013), the main factors that shape individual risk perception in complex arrangements with many intervening factors are their personal experience with the hazard and their level of trust in authorities and experts. However, since climate change is a slow and gradual modification of climate conditions and the majority of its effects will be felt in the future, detecting and tracking climate trends based on personal experience is difficult (Weber, 2010). As a result, information provided by scientists and experts will be the only remaining resource for improving risk perceptions of climate change.

Based on the Sixth Assessment Report of the Intergovernmental Panel on Climate Change (AR6), “risks arise from dynamic interactions between climate-related hazards and the exposure and vulnerability of the affected human or ecological system”, where AR6 defines hazard as “the potential occurrence of a natural or human-induced physical event or trend that could cause any kinds of loss or damage”, vulnerability as “the propensity or predisposition to be adversely affected”, and exposure as the presence of people, infrastructure, assets, etc. in places and settings that could be adversely affected”. While the role of uncertainty in the AR6 definition of risk is completely ignored, the increasing complexity of social and environmental systems, as well as climate change, have significantly impacted our ability to predict future risks imposed by climate change, implying the need for communicating the associated uncertainty in risk analysis, along with attempts to reduce the degree of uncertainty, in order to improve risk perception.

This thesis aims to foster and improve risk perceptions of climate change by advancing risk assessment of potential hazards and changes imposed by climate change on urban areas (Chapter 2) and by proposing new methods to assess the vulnerability and reliability of a region, complex system, or network under stresses and shocks (Chapters 3 and 4), while using all available data and sources

and transparently communicating the involved uncertainty with the analysis. This thesis is a compilation of three research efforts which are summarized in the following sections.

2. Chapter 2

To implement mitigation and adaptation plans that take advantage of the opportunities that a changing climate will bring while reducing the cost of the negative effects of climate change, it is critical to provide data at the scales at which organisations have responsibility. This chapter investigates the potential climate risks to Canadian cities using data derived from General Circulation Models (GCMs) of a future climate scenario to advance understanding for potential needs of municipality-scale climate adaptation.

GCMs are one of the most important tools in the study of climate change. However, there is uncertainty in GCMs projections due to the simplification of highly complex atmospheric physics in GCMs (Hughes et al., 2014), resulting in either overestimation or underestimation of values of the considered climate variable. At finer spatial resolutions, the associated uncertainty with the simulated climate is much higher, and therefore, for a specific region, not all GCMs can perform satisfactorily. However, the literature provides little guidance on how to select GCMs for a specific location. Other than the country in which the research was conducted, no additional justification was provided in those studies that used a specific GCM. Crosbie et al. (2011) investigates the uncertainty caused by the choice of GCMs, downscaling methods, and hydrological models in projecting the impact of future climate on groundwater recharge and claims that the choice of GCM is the most significant source of uncertainty. Bosshard et al. (2013) quantifies the uncertainties in climate impact projections on river streamflow and concludes that GCMs are the dominant source of uncertainty in summer and autumn projections. The literature suggests using multi-model ensembles rather than single GCMs to minimise and compensate for individual GCM biases and uncertainty (Hughes, Mantel and Mohobane (2014); Yan et al. (2016); He et al. (2019)). Therefore, we use statistically downscaled and bias corrected climate data (bias correction/constructed analogues with quantile delta mapping reordering (BCCAQv2) downscaling method) of twenty-six GCMs, from 2015 to 2100, based on the high-end emission scenario of the Shared Socioeconomic Pathway 5 (SSP5-8.5), from the Coupled Model Intercomparison Project Phase 6. However, since we use a large number of GCMs, the Sen's slope estimator which is a common approach for evaluating the magnitude and direction of changes across cities and variables is no longer valid. To address the issue, we employ both the modified Mann-Kendall test and the Euclidean distance to determine the magnitude and direction of changes in a wide variety of climate variables across the cities. We communicate the complex and multifaceted aspects of climate change in such a way that the data can be used practically in resilience planning and resource allocation.

3. Chapter 3

One of the most destructive natural disasters is flooding. According to the IPCC Sixth Assessment Report, floods cost the world economy 914 billion USD between 2000 and 2018, accounting for more than 21% of all economic damages brought on by natural disasters. Flood risks are expected to increase globally as a result of socio-economic development, climate change and its impact on the hydrological cycle (Kam et al., 2021), and the rate of sea level rise and subsidence.

In times of increasing flood risk, a thorough and comprehensive understanding of potential flood damage caused by future climate change-induced flood scenarios is crucial for developing adaptation plans and policies as well as enhancing the coping capacities of society. However, one of the biggest obstacles to estimating potential flood damage is a lack of data. Obtaining precise data is a very

demanding and challenging task, especially at a regional scale, and that is the reason flood damage analyses are typically limited to local scales. In chapter 3, we attempt to address this issue by proposing a new methodology that enables the analyst to estimate potential damage caused by different flood scenarios on a regional scale by measuring a fraction of the buildings and presenting the uncertainties associated with the estimates. The method distinguishes between aleatory and epistemic uncertainty allowing for identification of how additional data collection may or may not be helpful in reducing uncertainty. In addition to this benefit, the method is also shown to outperform more traditional methods from a computational perspective.

4. Chapter 4

As the reliance of cities on complex systems (e.g., power supply) and networks (e.g., electric transmission network) grows, the increasing frequency and length of heat waves caused by climate change can reduce the reliability of these systems. This reliability reduction can be attributed to, for example, the compounding effect of high energy demand for cooling and high temperatures on the capacity and efficiency of these systems. This implies the need for adaptation plans to improve the capacity and performance of complex systems and networks within cities to withstand shocks and stresses caused by climate change.

Given the growing complexity and interdependence of utility systems and infrastructure, adaptation projects must shift from a singular, special-purpose focus on specific systems and locations to a more integrated approach. The first step in accomplishing this is to consider functional and probabilistic dependencies both within and between complex systems. However, identifying dependencies between components and subsystems of modern systems and networks is extremely challenging, if not often impossible, given their increasing complexity. Using imprecise probability analysis in a probability box approach, we introduce a novel method to evaluate the reliability of complex systems and networks when dealing with indeterminant dependency between functions or components of the systems that are often either ignored or previously required a great deal of knowledge and effort to define as well as uncertainty in input parameters.

5. List of submitted papers

The following are the three research efforts presented in this thesis:

Chapter 2

Viseh, H., Bristow, D.N., 2023. How climate change could affect different cities in Canada and what that means for the risks to the built-environment functions. Under Review. Submitted to Urban Climate on February 15th, 2023.

Viseh, H. (first author): data curation, methodology, data analysis, experiment and cross-validation, data modelling, visualization, writing the manuscript.

Bristow, D.N. (co-author): supervision, data curation, manuscript proofreading and revising.

Chapter 3

Viseh, H., Bristow, D.N., 2023. Residential Flood Risk in Metro Vancouver Due to Climate Change Using Probability Boxes. Journal of River Basin Management. https://doi.org/10.1080/15715124.2023.2200006.

Viseh, H. (first author): data acquisition and curation, methodology, data analysis, experiment, data modelling, visualization, writing the manuscript.

Bristow, D.N. (co-author): supervision, data acquisition, manuscript proofreading and revising.

Chapter 4

Viseh, H., Bristow, D.N., 2022. Probability Box Method for Assessing Networked Reliability of Infrastructure and Buildings. Under Review. Submitted to Risk Analysis on September 26th, 2022.

Viseh, H. (first author): data curation, methodology, data analysis, experiment, data modelling, visualization, writing the manuscript.

Bristow, D.N. (co-author): supervision, data acquisition, methodology, manuscript proofreading and revising.

Chapter 2: How climate change could affect different cities in Canada and what that means for the risks to the built-environment functions

Abstract

This research aims to advance risk perceptions of climate change and understanding of the potential needs of municipal-scale climate adaptation across seventeen Canadian cities. To do so, the rate and direction of changes in a wide variety of climate variables are examined in all the capital cities and some other major cities like Montreal, Vancouver, and Calgary, by analyzing downscaled data from twenty-six General Circulation Models (GCMs) from Coupled Model Intercomparison Project Phase 6 (CMIP6) to the year 2100, using the modified Mann-Kendall test and Euclidean distance. The findings of this study suggest that under SSP5-8.5 scenario, Canadian cities will experience more extreme heat and heavy rainfall but less extreme cold in the future, especially when compared to SSP2-4.5, where for example, the number of models showing an increasing trend for annual precipitation is about 60% higher under SSP5-8.5 than under SSP2-4.5 over the 17 cities. In addition, using Epps-Singleton test, climate change in neighboring cities is compared to see how similar adaptation plans are possible. The results show that coastal cities, even those located relatively close to one another, such as Vancouver and Victoria, follow different trends for most of the variables (22 out of 28). Furthermore, a qualitative assessment of which built environment aspects of these cities may require more rapid modification than others is provided to assist decision-makers and planners in resilience planning and resource allocation.

1. Introduction

Global changes in the atmosphere, ocean, cryosphere, and biosphere have occurred rapidly and extensively. The influence of human-caused climate change is already evident in the increasing frequency and severity of weather and climate extremes such as heatwaves, altering the frequency and duration of drought events, increasing the pressure on agricultural production (Arora, 2019), and water resources, resulting in widespread adverse impacts on both ecosystems and human society (IPCC, 2023). The magnitude of these impacts varies across sectors, systems, regions, and timeframes, with some being substantial while others may seem less significant.

The impact of climate change in Canada is expected to be significant. NRTEE (2011) anticipates the cost of climate change in Canada to increase from an average of $5 billion per year in 2020 across all scenarios, to $21 billion and $43 billion per year in the low climate change–slow growth scenario and in the high climate change[1]–rapid growth scenario[2], respectively, by 2050. Kompas et al. (2018) estimates the annual GDP change in Canada will be -0.10% (Representative

[1] Definition of the high climate change scenario (IPCC "A2") and low climate change scenario (IPCC "B1") can be found in (Nakicenovic et al., 2000)

[2] NRTEE (2011) considers an annual growth of 1.3% and 3% in gross domestic product (GDP) as slow-growth scenario and rapid-growth scenario, respectively.

Concentration Pathway (RCP) 2.6) to -0.32% (RCP 8.5) in 2100, relative to projected GDP without the impacts of climate change. Also, Cleary and Willcot (2022) estimates that Canada will lose $2.773 trillion (+2 °C) to $5.520 trillion (+5 °C) in capital output between 2015 and 2100.

Climate change is projected to have a particularly pronounced impact on cities, where over 80 percent of Canadians reside. Urban areas are susceptible to the urban heat island effect, resulting in higher surface temperatures(Health Canada, 2009; Marcotullio and Schmeltz, 2021). Additionally, cities are highly vulnerable to climate change due to concentrated populations, social inequality, aging infrastructure, high-risk exposure of urban assets, and stressed ecosystems (Maxwell et al., 2018). These factors collectively increase the adverse impacts on human health, livelihoods, and critical infrastructure in urban areas.

Given the great size of Canada, the rate of climate change, as well as its impact and cost, will vary across regions and be unevenly distributed across the country. For instance, the greatest rate of temperature change is occurring in the northern parts of Canada (Warren and Lulham, 2021), by the 2050s estimated costs of dwellings damage induced by climate and non-climate related factors are anticipated to be higher than the national average in New Brunswick, and GDP reduction caused by impacts of climate change on the timber supply will be higher than average national GDP reductions in British Columbia (NRTEE, 2011).

To enhance climate resilience and leverage the opportunities arising from a changing climate, providing data at the scales for which organizations have responsibility is essential. Therefore, we intend to explore the potential impact of climate change on all the capital cities and some other major cities like Montreal, Vancouver, and Calgary across Canada.

Numerous studies have been conducted to investigate the impact of climate change in various cities around the world. Nematchoua et al. (2019) estimates the change in cooling energy demand of residential buildings for seven Central African countries and finds that, under scenarios RCP 4.5 and RCP 8.5, the average monthly cooling energy demand in residential buildings will rise to 81.6% and 167.3%, respectively, by 2100, compared to 2016. To project climate change, Nematchoua et al. (2019) uses downscaled results from five GCMs, including CGCM3, CNRM-CM3, GFDL CM2.0, HadCM3, and PCM from the CMIP5 climate projections. H. Wang and Chen (2014) uses one GCM (HadCM3) to project the change in energy use for fifteen cities in the United States, based on three CO2 emission scenarios. Based on their findings, under the high emission scenario (A1F1), ten of these fifteen cities will experience a net increase in source energy (natural gas for heating and electricity for cooling) intensity by the 2080s. L. Wang et al. (2017) examines the impacts of climate change on the energy consumption of an office building in five different cities in the United States, using two GCMs (HadCM3 and CESM) and three scenarios (RCP 2.6, RCP 4.5, and RCP 8.5), from the fifth assessment report of the Intergovernmental Panel on Climate Change (IPCC). Their findings show discrepancies in the annual average dry bulb temperature projections of the two models. Using the Delta downscaling approach, Luo et al. (2018) calculates changes in precipitation and temperature amounts in Xinjiang (northwestern China) based on the ensemble of 37 GCMs in 2021–2060. The Delta downscaling approach is based on the use of a change factor, which for precipitation is the ratio between the average monthly precipitation of the GCM scenarios and the historical run, and for temperature is obtained by subtracting the average monthly temperatures of the GCM scenarios from the historical period. Malik et al. (2020) investigates the change in precipitation in the Kolkata Metropolitan Area (KMA) based on 11 GCMs from the Fifth Assessment Report (AR5) of the IPCC. The authors used the Mann-Kendall test and Sen's slope estimator test to detect the trend and the magnitude of the trend in the datasets, respectively. Zhai et al. (2019) explores the trend of changes

in daily maximum, minimum, and mean temperatures in Ottawa based on downscaled data from three GCMs (CanESM2, GFDL-ESM2M, and IPSL-CM5A-LR) from CMIP5. Using Mann-Kendall and Sen's slope estimator test, the authors found a significant increase in temperature trends from 2007 to 2099 under RCP 8.5.

The literature review shows that previous studies either focused on investigating the impact of climate change in one city or, if they investigated the impact of climate change in more than one city, their analysis was based on one or a small number of GCMs. Although GCMs are one of the most important tools in the study of climate change, there is uncertainty in their projections due to the simplification of highly complex atmospheric physics in them (Hughes et al., 2014), resulting in either overestimation or underestimation of values of the considered climate variable. At finer spatial resolutions, the associated uncertainty with the simulated climate is much higher, and therefore, for a specific region, not all GCMs can perform satisfactorily. However, the literature provides little guidance on how to select GCMs for a specific location. Other than the country in which the research was conducted, no additional justification was provided in those studies that used a specific GCM. Crosbie et al. (2011) investigates the uncertainty caused by the choice of GCMs, downscaling methods, and hydrological models in projecting the impact of future climate on groundwater recharge and claims that the choice of GCM is the most significant source of uncertainty. Bosshard et al. (2013) quantifies the uncertainties in climate impact projections on river streamflow and concludes that GCMs are the dominant source of uncertainty in summer and autumn projections. Therefore, single model projections are likely to be biased and misleading, and they are also associated with a significant degree of uncertainty, particularly for precipitation, as reported in Luo et al. (2018), which compares the reliability of single run and ensemble downscaling results from 37 GCMs. The literature suggests using multi-model ensembles rather than single GCMs to minimize and compensate for individual GCM biases and uncertainty (Hughes et al., 2014; Yan et al., 2016; He et al., 2019). Therefore, in this study, climate data derived from multi-model ensembles of twenty-six GCMs that are presently available for Canada from 2015 to 2100, based on the emission scenario of the Shared Socioeconomic Pathways 5 (SSP5-8.5) and 2 (SSP2-4.5), from the CMIP6 are used. A concern when studying more than one or two cities using large ensembles of global circulation models is determining the magnitude of the changes for different variables across these cities. One common approach to show the magnitude of the trends is using Sen's slope estimator test. In such a case, we have two options: using the average value of GCMs per year, month, or day before applying Sen's slope estimator test, or apply the test to each GCM individually and then averaging the obtained slopes and intercepts. However, using the mean value can be problematic as it is sensitive to outliers, leading to potentially misleading results. Additionally, using the mean or median of the slopes and intercepts obtained from applying Sen's slope estimator test to each GCM individually may not always fit the data. The methodology section further elaborates on this issue.

This paper proposes a method for calculating the magnitude of changes when dealing with data from a large number of GCMs. Furthermore, unlike most previous studies that have almost exclusively focused on a small set of climate variables, such as total precipitation and maximum, minimum, and mean temperature, this study uses a wide variety of climate variables, considering a survey of infrastructure performance and emergency medical service in Canada with respect to past climate extremes.

2. Background on sensitivity to climate

2.1. Precipitation-related parameters

Under climate change, both dry events and wet events may be problematic. PIEVC (2014), a protocol for conducting vulnerability assessments on infrastructure, considers ten consecutive days with precipitation below 0.2 mm as an indicator of drought. Usually, precipitation of less than 0.2 mm in 24 hours is used to indicate a dry day. The reason for using 0.2 mm rather than 0 mm is to avoid confusing days with precipitation and days with frost, fog, or dew.

To gain insights into when and how wet events may cause an impact, it is instructive to review past events. For this purpose, an extensive search of relevant literature, news sources, and the Canadian Disaster Database was done to identify problematic wet events. On September 13, 2022, heavy rain in Montreal, caused roadway closures, sewer overflow, and underpasses being flushed with up to one meter of water (Laframboise and O'Malley, 2022; Roy, 2022). The measured precipitation at the Montreal International Airport weather station on that day was recorded as 24.8 mm (Government of Canada, n.d.). Another event occurred on July 19, 2022, in Regina, where heavy rain caused street closures and flooded underpasses (Stein, 2022; Whibbs and Postey, 2022). The total precipitation recorded at the Regina RCS weather station on that day was 47.4 mm (Government of Canada, n.d.).Furthermore, on November 14, 2021, floods in British Columbia severely disrupted all highways, rail links, and pipelines connecting Vancouver and southwestern British Columbia to the rest of Canada (Gillett et al., 2022). This event, as reported by Gillett et al. (2022), was the costliest natural disaster in the history of British Columbia and led to the loss of at least five lives. The total precipitation recorded at Vancouver International Airport on that day was 52.5 mm (Government of Canada, n.d.). These events show differing sensitivities in infrastructure disruptions to increases in rainfall.

In addition to disruption to infrastructure networks like roads, there can be other affects from large rainfall episodes. According to WSP Canada Inc. (2021), 40 mm of rain in 24 hours has the potential to increase contaminants by resuspension of bottom sediments in the water source and, as a result, increase disinfection by-products in water treatment plants. WSP Canada Inc. (2021)also stated that a 44 mm in 24 hours rainfall event will increase the potential of a wastewater treatment plant temporarily exceeding its design capacity. Moreover, PIEVC (2010) evaluated the anticipated changes to risks induced by climate change for Canadian public infrastructure, considers precipitation greater than 76 mm over 24 hours as an indicator of extreme rainfall.

2.2. Temperature-related parameters

Extremely hot temperatures have serious implications for both human health and infrastructure. McKeown (2015) has highlighted that temperatures above 26°C are associated with increased premature mortality and emergency medical service calls in Toronto. Also, Goldberg et al. (2011) found a strong non-linear association between daily maximum temperatures greater than 27°C and daily mortality in Montreal. Examining specific past events reveals the potential scale of losses of life due to high temperature. During the eight-day heatwave in 2009 (July 27 to August 3), Vancouver International Airport recorded temperatures as high as 34 and 34.4°C. As reported by the Fraser and Vancouver Health Authorities, during that period, 455 deaths were registered, significantly higher than the average of 321 death during the same eight-day period in previous years. Furthermore, during the 2021 Western North America heatwave, the maximum daily temperature at Vancouver International Airport exceeded 32°C twice between June 25 and July 1. The BC Coroners Service reported a loss of 808 lives due to that heatwave.

Heat warnings are issued in various regions of Canada based on specific temperature criteria, as outlined by Gachon et al. (2016). In British Columbia (Vancouver), a heat warning is issued when the average daily temperature at 14:00 local time and the forecast for the next day at Vancouver Airport are expected to be ≥ 29°C, or at Abbotsford Airport when expected to be ≥ 34 °C. In Alberta (Calgary, and Edmonton), a heat warning is issued when the maximum daily temperature (Tmax) exceeds 29°C and the minimum daily temperature (Tmin) exceeds 14°C. In Manitoba (Winnipeg) and Saskatchewan (Regina), a heat warning is issued when the temperature is expected to be ≥ 40°C, the humidex ≥ 40, and the dew point to be ≥15°C. In Southern Ontario (Toronto, and Ottawa), a heat warning is issued when Tmax ≥ 31°C and Tmin ≥ 20°C, or when the humidex ≥ 40. In Québec (Québec City and Montreal), a heat warning is issued when the humidex is ≥ 40 and the temperature is ≥ 30°C, and both conditions persist for at least one hour, or when the temperature is ≥ 40°C. In Nova Scotia (Halifax), New Brunswick (Fredericton), Prince Edward Island (Charlottetown), and Newfoundland and Labrador (St. Johns), a heat warning is issued when the temperature is expected to be ≥ 40°C, or the humidex ≥ 40, for at least one hour.

Extreme heat has adverse impacts on infrastructure as well. WSP Canada Inc. (2021), which conducted a climate change vulnerability assessment of infrastructure located within or associated with Canada's Northwest Territories, has identified 34°C as a threshold for extremely hot days based on historical and projected climate change data, as well as design codes and standards in effect.

AECOM Consultants Inc. (2015) studied the impacts of climate change on different parts of the electrical distribution infrastructure and supporting civil infrastructure in Toronto from 2015 to 2050. Based on their findings, high ambient air temperatures of 25°C and above (excluding humidity) degrade the lifespan of station batteries; heat waves, defined as three consecutive days with a daily maximum temperature exceeding 30°C, as well as maximum daily air temperatures higher than 35°C, negatively affect the station power transformers by increasing the electrical load on transformers and by reducing the effectiveness of natural or mechanical cooling; furthermore, heatwaves and high temperatures above 40°C pose a risk to underground and overhead feeder systems; additionally, transmission and municipal stations are at risk on days with peak temperatures above 40°C.

Transportation infrastructure is also susceptible to the negative impacts of extreme hot temperatures. Rail track warping and sun kinks, which are buckles in railroad tracks that can lead to derailments, can occur when temperatures rise above 32°C (Chiotti et al., 2017). Moreover, heatwaves, defined as periods with maximum temperatures of 32°C or higher for more than three consecutive days according to Environment Canada, further increase the risks to rail track integrity (Chiotti et al., 2017). Additionally, according to WSP Canada Inc. (2021), heat waves and temperatures above 34°C will increase the potential for maintenance, pavement softening, asphalt bleeding, cracking, and igniting, infrastructure failure due to thaw settlement of permafrost, and damage to steel and road components of bridges.

Transport Canada (2021) sets speed limit regulations for Class 1 railways, which are the largest railways in Canada. When the air temperature is between 30 and 32°C and the fire danger level is "extreme", the track speed limit is reduced to 25 and 26 mph for permitted track speeds of 26 and 35 mph, and 36 mph or greater, respectively. Similarly, when the air temperature is 33°C or higher and the fire danger level is "extreme", the track speed limit is reduced to 25 and 30 mph for permitted track speeds of 26-50 mph, and 51 mph or greater, respectively.

Extreme cold, like extreme heat, has negative impacts both human health and infrastructure. In the PIEVC (2014) and GENIVAR (2010) reports, a "cold wave" is defined as three or more consecutive days with a minimum temperature below -20°C and a maximum below -10°C. Also,

GENIVAR (2010) considers a threshold of -30°C to be representative of an extremely low temperature. Environment Canada has different threshold criteria for issuing extreme cold alerts depending on the region, ranging from -30°C for at least two hours in south-central and southwest Ontario to -55°C for at least two hours in the Northwest Territories, Baffin, and western and northern Nunavut.

As with high temperatures, low temperatures can affect transportation infrastructure. According to the Rail Association of Canada, when temperatures drop below -35 °C, the maximum safe length of an intermodal train with distributed power decreases by 39% (Palko and Lemmen, 2017). Moreover, temperatures below -23°C can cause rail tracks to break (Chiotti et al., 2017). In addition, reviewing past events such as the extreme cold weather (temperatures as low as -39°C with wind chill) experienced in Eastern Ontario and other parts of Canada from January 5 to 9, 2014, which severely disrupted passenger travel at many airports, including Toronto Pearson International, and caused some equipment to fail (Palko and Lemmen, 2017) and the winter of 2013-2014, in which some of the scheduled flights of the U.S. carriers to western Canada were cancelled because the aircraft were only certified to -30°C (Palko and Lemmen, 2017) highlight the adverse impact of extreme cold weather on aerial transportation.

Permafrost thaw, or an increase in the frequency of freeze-thaw cycles that, according to the Climate Data Portal of Canada (ClimateData.ca) occurs when the daily maximum temperature is greater than 0°C and the daily minimum temperature is less than or equal to -1°C, is also known as one of the most negative climate change-induced impacts in Canada. This phenomenon causes slope instability, soil instability and subsidence, ground movement, damage to building foundations, and a reduction or loss of functionality in infrastructure (WSP Canada Inc., 2021).

2.3. Cooling and heating degree days

The change in energy consumption brought on by the temperature change is one of the most significant effects of climate change. Cooling degree days (CDD) and heating degree days (HDD) are two common variables used to predict the impact of climate change on energy demand. Cooling degree days are calculated by subtracting the mean temperature from the base temperature when the daily average outdoor temperature is above the base temperature, and heating degree days are calculated by subtracting the base temperature from the mean temperature when the daily average outdoor temperature is below the base temperature. Therefore, the annual amount of energy required to heat or cool a building in a specific location is roughly proportional to the sum of heating and cooling degree days in that location over a year.

Different countries use different base temperatures for calculating cooling and heating degree days; for example, the used base temperature in the United States is 18.3°C, 15.0°C in Germany, and 15.5 °C in the United Kingdom (Bhatnagar et al., 2018). In Canada, the base temperature is 18 degrees Celsius.

Degree-day data can also be weighted according to different influential factors, such as the population of the region, to estimate climate-induced energy demand. Rivers and Shaffer (2020) propose temperature response functions for calculating the log (electricity demand) for ten Canadian provinces, taking into account the mean penetration of air conditioners and electric heating systems per household, as well as the total electricity demand attributed to the residential sector from 2001 to 2015. We use their proposed functions in this study and compare the trend of change in energy demand across the cities with and without considering influential factors such as the mean penetration

rate of air conditioners and electric heating systems per household. The results can be found in section 4.

3. Methodology

For this study, the statistically downscaled and bias-corrected daily climate data from the Pacific Climate Impacts Consortium (PCIC, 2021) with a gridded resolution of 300 arc-seconds are used. PCIC used bias correction/constructed analogues (BCCA) with quantile delta mapping reordering to statistically downscale and bias correct this climate data. The quantile mapping bias correction technique is often employed to correct systematic distributional biases in climate model precipitation outputs (Cannon et al., 2015). BCCA is one of the regression techniques used to extrapolate data to higher resolutions based on the identified relationship between large scale GCM output and local/regional climate variables, also known as predictors and predictands respectively (Keller et al., 2022). Bias correction and spatial disaggregation (BCSD) and constructed analog method (CA) are two other statistically downscale regression methods. BCSD was originally developed to downscaling monthly precipitation and temperature variables. Although this method can be used to directly downscaled daily GCM output, realistic spatial variability of daily precipitation events may not be reproduced (Hwang & Graham, 2013). According to Maurer and Hidalgo, (2008), the constructed analog method (CA) outperforms the BCSD method, particularly in reproducing extreme temperature events. Both methods, however, perform poorly in reproducing daily precipitation extremes. Despite the fact that BCCA may not precisely reproduce the mean and variance of precipitation at downscaled resolution, this method, which improves the CA method by removing GCMs biases, demonstrates better accuracy in simulating hydrologic extremes (Maurer et al., 2010), and also outperforms the other two methods in simulating streamflow (Maurer et al., 2010). Furthermore, BCCA can be used to directly downscale daily GCM output.

The analysis is performed for seventeen Canadian cities (Figure 1 shows major Canadian cities): Calgary, Charlottetown, Edmonton, Fredericton, Halifax, Iqaluit, Montreal, Ottawa, Quebec City, Regina, St Johns, Toronto, Vancouver, Victoria, Whitehorse, Winnipeg, and Yellowknife.

Under the RCP4.5 scenario, PCIC offers multimodal ensemble of twelve GCMs as part of the CMIP5 to effectively capture 90% of the variability in projected changes in temperature and precipitation, in across all seasons for different regions Canada, (Cannon, 2015). To maintain consistency, as well as to be conservative and capture more of the variation in the seventeen considered cities, data in this study is from all currently available GCMs from PCIC (Table 1). These twenty-six GCMs (Table 1) were developed by various countries and institutions and have distinct configurations, resulting in differences in performance and resolution. For instance, MPI-ESM1.2-HR, which has been developed by the Max Planck Institute for Meteorology Earth System Model (MPI-ESM1.2), is the higher-resolution version of the former MPI-ESM1.2-LR 11 (Gutjahr et al., 2019). As another example, ACCESS-CM2 and ACCESS-ESM1-5 have both been developed by the Australian Community Climate and Earth System Simulator (ACCESS). ACCESSCM2, as described in Bi et al. (2020), simulates the physical climate, while ACCESS-ESM1.5, as detailed in Ziehn et al. (2020), is designed to simulate a fully interactive carbon cycle.

Figure 1. Canada cities map.

Table 1. Twenty-six global climate models of CMIP6 considered in this study (institution and grid resolution of the models derived from Di Virgilio et al., (2022)).

Model	Institution	Atmosphere latitude and longitude grid
ACCESS-CM2	CSIRO	1.2 × 1.8
ACCESS-ESM1-5	CSIRO	1.2 × 1.8
BCC-CSM2-MR	Beijing Climate Center	1.1 × 1.1
CanESM5	Canadian Center for Climate Modeling and Analysis	2.8 × 2.8
CMCC-ESM2	Euro-Mediterranean Center	0.9 × 1.25
CNRM-CM6-1	National Center of Meteorological Research (NCMR), France	1.4 × 1.4

CNRM-ESM2-1	National Center of Meteorological Research (NCMR), France	1.4 × 1.4
EC-Earth3	EC-EARTH consortium, The Netherlands/Ireland	0.7 × 0.7
EC-Earth3-Veg	EC-EARTH consortium, The Netherlands/Ireland	0.7 × 0.7
FGOALS-g3	Chinese Academy of Sciences, China	2.3 × 2.0
GFDL-ESM4	NOAA Geophysical Fluid Dynamics Laboratory	1.0 × 1.3
HadGEM3-GC31-LL	UK Met Office Hadley Center	2.2 × 2.2
INM-CM4-8	Institute for Numerical Mathematics (INM), Russia	1.5 × 2.0
INM-CM5-0	Institute for Numerical Mathematics (INM), Russia	1.5 × 2.0
IPSL-CM6A-LR	Institute Pierre Simon Laplace, France	1.3 × 2.5
KACE-1-0-G	Nat. Inst. of Meteorological Sciences/Korea Meteorological Admin	2.2 × 2.2
KIOST-ESM	Korean Institute of Ocean Science and technology	2.2 × 2.2
MIROC-ES2L	National Institute for Environmental Studies, Japan	4.5 × 4.5
MIROC6	National Institute for Environmental Studies, Japan	1.4 × 1.4
MPI-ESM1-2-HR	Max Planck Institute for Meteorology (MPI), Germany	~0.9
MPI-ESM1-2-LR	Max Planck Institute for Meteorology (MPI), Germany	~2.0
MRI-ESM2-0	Meteorological Research Institute, Japan	1.1 × 1.1
NorESM2-LM	Norwegian Climate Center, Norway	1.9 × 2.5
NorESM2-MM	Norwegian Climate Center, Norway	0.9 × 0.9
TaiESM1	Taiwan Earth System Model	0.9 × 0.9
UKESM1-0-LL	UK Met Office and NERC research centers	1.3 × 1.9

3.1. Climate parameters

Twenty-eight climate parameters, including six precipitation-related parameters, and twenty-two temperature-related parameters are selected to be used in this research. These relevant climate parameters and threshold values at which human health and infrastructure performance would be affected were identified through an extensive literature review and analysis of past events that mentioned in the Section 2.

The precipitation-related variables used in this study can be found in Table 2. There are many factors that determine whether a certain amount of precipitation can be considered a risk for a city, such as intensity, duration, and type of precipitation, the nature and condition of the drainage system, and the climate, making it difficult to specify a threshold to derive heavy precipitation days for seventeen cities. However, based on historical weather events in the cities studied and literature review, thresholds of 20, 40, and 76 mm in 24 hours were selected. These are the threshold values at which the considered cities in this study have experienced different events in the past, including disrupted transport and communications, overflowing rivers and runoffs, and flooding, which led to road closures, infrastructure damage and debris. Higher thresholds such as 100 mm precipitation per day were not considered since GCMs are unable to simulate such extreme precipitation events.

The downscaled projected precipitation data that is available from the PCIC website, is a combination of both rainfall and snowfall. To derive the rainfall data, the xclim Python package (xclim.indices._conversion.rain_approximation) was used to approximate rainfall from total precipitation and temperature (see Appendix A). However, there are two caveats regarding using this function for our data: first, precipitation and temperature variables were downscaled individually, and

therefore the relationships between them are lost; second, the decision regarding which temperature parameter to use, whether it be the daily mean, maximum, or minimum temperature, must be made. Considering the mentioned caveats, the decision has been made to conduct the analysis using precipitation data rather than rainfall data. Given that snowfall contribution to runoff can influence water yield (Hunsaker et al., 2012) and also adds to the snowpack, which is a critical source of freshwater during the summer for many regions that rely on wintertime snowfall (Behrangi et al., 2018), the findings in this study cannot comment on water management adaptation measures.

The temperature-related variables used in this study can be found in Table 3. As an indicator of freeze-thaw days, we use the same thresholds as the Climate Data Portal of Canada (ClimateData.ca).

In addition, differences greater than 25°C were used as the threshold for extreme diurnal temperature variability based on the analysis in PIEVC (2014). Given that the IPCC global climate projections show a decrease in diurnal temperature variation in most regions and that the PEIVC (2014) analysis of daily temperature data for Toronto Pearson International Airport from 1971 to 2000 shows five occurrences of extreme diurnal temperature variability (difference greater than 25°C) during this 30-year period, PIEVC (2014) chose a difference greater than 25°C as an indicator of extreme diurnal temperature variability.

Moreover, the thresholds for the "comfort_zone_sum" variable, which indicates the total number of days when the temperature is between 18 and 24°C, are based on WHO guidance for appropriate air temperatures in the home for protecting health (Ormandy and Ezratty, 2011).

Furthermore, for the purpose of this study, the common set-point temperature of 18°C was used for the CDD and HDD variables.

Table2. List of the precipitation related variables considered in this study to evaluate climate change across the major cities in Canada.

Variable	Definition
pr_sum	Sum of daily precipitation per year (mm per year)
dry_day0p2_sum	Total number of days with precipitation =< 0.2 mm per year
dry_day0p2_max_streak	Maximum number of consecutive days with daily precipitation =< 0.2 mm per year
heavy_pr20_sum	Total number of days with precipitation > 20 mm per year
heavy_pr40_sum	Total number of days with precipitation > 40 mm per year
heavy_pr76_sum	Total number of days with precipitation > 76 mm per year

Table 3. List of temperature related variables considered in this study to evaluate climate change across the major cities in Canada.

Variable	Definition
tasmax_max	Maximum daily temperature per year (°C per year)
tasmin_min	Minimum daily temperature per year (°C per year)
above_tmax26_sum	Total number of days with maximum daily temperature > 26°C per year
above_tmax26_max_streak	Maximum number of consecutive days with maximum daily temperature > 26°C per year
above_tmax30_sum	Total number of days with maximum daily temperature > 30°C per year

above_tmax30_max_streak	Maximum number of consecutive days with maximum daily temperature > 30°C per year
above_tmax32_sum	Total number of days with maximum daily temperature > 32°C per year
above_tmax32_max_streak	Maximum number of consecutive days with maximum daily temperature > 32°C per year
above_tmax34_sum	Total number of days with maximum daily temperature > 34°C per year
above_tmax34_max_streak	Maximum number of consecutive days with maximum daily temperature > 34°C per year
above_tmax40_sum	Total number of days with maximum daily temperature > 40°C per year
above_tmax40_max_streak	Maximum number of consecutive days with maximum daily temperature > 40°C per year
above_tmax32_heat_wave_count	Total number of heat waves (three or more consecutive days with maximum temperature > 32 °C) per year
cdd_sum_18	Sum of the difference between average daily temperature and base temperature (18°C), where average daily temperature > base temperature, per year (°C per year)
hdd_sum_18	Sum of the difference between base temperature (18°C) and average daily temperature, where average daily temperature < base temperature, per year (°C per year)
below_tmin_30_sum	Total number of days with minimum daily temperature < -30°C per year
below_tmin_30_max_streak	Maximum number of consecutive days with minimum daily temperature < -30°C per year
cold_wave_count	Total number of cold waves (three or more consecutive days with minimum temperature < -20°C and maximum temperature < -10°C) per year
freeze_thaw_day_sum	Total number of days with minimum daily temperature =< -1°C and maximum daily temperature > 0°C per year
freeze_thaw_day_max_streak	Maximum number of consecutive days with minimum daily temperature =< -1°C and maximum daily temperature > 0°C per year
comfort_zone_sum	Total number of days with minimum temperature >= 18°C and maximum temperature <= 24°C per year
extreme_tvar_day_sum	Total number of days experiencing a diurnal temperature variability greater than 25°C per year

3.2. Direction and magnitude of climate parameters

To minimize future societal risks from climate change, we need to increase climate resilience. Climate resilience is multidimensional and scale-, time-, and location-specific, requiring comprehensive measurement and analysis. Evaluating the rate and direction of change in climate variables is an important first step.

3.2.1. Modified Mann-Kendall trend test (m-MK test)

Trend analysis is a widely used technique for detecting changes in climate data. Among the available Statistical tests for determining the significance of trends in climatic and hydrologic time series, one of the commonly used non-parametric ones is the Mann-Kendall trend test. The Mann-Kendall test statistic S (Mann, 1945; Kendall, 1975) is given by:

$$S = \sum_{i=1}^{n-1} \sum_{j=i+1}^{n} \operatorname{sgn}(x_j - x_i) \quad (1)$$

$$\operatorname{sgn}(x_j - x_i) = \begin{cases} 1, \text{if } x_j - x_i > 0 \\ 0, \text{if } x_j - x_i = 0 \\ -1, \text{if } x_j - x_i < 0 \end{cases} \quad (2)$$

where x_i and x_j are the values of sequence i, and j (j>i), n is the length of the time series, and sgn $(x_j - x_i)$ is the sign function. The variance of the statistics S is calculated as follows:

$$\text{Var}(S) = \frac{n(n-1)(2n+5) - \sum_{i=1}^{m} t_i(t_i-1)(2t_i+5)}{18} \quad (3)$$

where m is the number of tie groups in the data and t_i is the number of data in the i-th tie group. The MK test statistic (Z_{MK}) is calculate as follows:

$$Z_{MK} = \begin{cases} S - 1/\sqrt{\text{Var}(S)}, \text{if } S > 0 \\ 0, \text{if } S = 0 \\ S + 1/\sqrt{\text{Var}(S)}, \text{if } S < 0 \end{cases} \quad (4)$$

Positive values of Z_{MK} shows an increasing trend while negative value indicates a decreasing trend.

The null hypothesis of the Mann-Kendall test is that the data are independent and randomly ordered and that there is no serial correlation among them. However, climate data are often autocorrelated, which can result in misinterpretation of the trend test results (Hamed & Ramachandra Rao, 1998). Therefore, in this study, modified Mann-Kendall (m-MK) trend test, in which the variance is adjusted by a correction factor (C_f) to account for the autocorrelation of all lags $\rho_s(i)$ in the data, proposed by Hamed & Ramachandra Rao (1998), is used to determine whether there is a trend (monotonic) for each variable over time, and if so, whether it is statistically significant, while avoiding the misjudgment in trend detection caused by serial autocorrelation among the data.

The modified variance $V^*(s)$ is given by (Swain et al., 2022):

$$V^*(s) = \text{Var}(S).\ C_f \quad (5)$$

where:

$$C_f = 1 + \frac{2}{n(n-1)(n-2)} \sum_{i=1}^{n-1} (n-i)(n-i-1)(n-i-2)\,\rho_s(i) \quad (6)$$

3.2.2. Euclidean distance

The modified Mann-Kendall test does not evaluate the magnitude of the changes. A standard method for comparing the magnitude of change in a climate parameter across different locations is to use Sen's Slope estimator. However, Sen's slope estimator did not perform well for the data from the set of modeled data in this study in initial testing and so is not examined further. Also, using the polynomial fit to the data caused overfitting and consequently misinterpretation of the results (Figure 6 in Appendix B shows fitting two linear and one non-linear model to one of the variables). Thus, as an alternative way to consider the amount of change, we use the Euclidean distance of the value of each variable in each city between the 2020s and 2080s. This timescale (60 years) has been selected based on a literature review, which indicates that a 60-year time horizon is commonly used in life-cycle assessments of infrastructure and buildings (Lausselet et al., 2019; Capacci & Biondini, 2020; Lausselet et al., 2020;). To do so, each variable in each city is first assigned an index based on its year and GCM model. For example, for the variable "cdd_sum_18" in Toronto, index 1 is assigned to the variable value from ACCESS-CM2 in 2021, and index 2 is assigned to the variable value from ACCESS-ESM1-5 in 2021. This assignment of indices is carried out for the remaining variable values from other models and years in the 2020s. The same procedure is repeated for the 2080s, where index 1 is assigned to the variable value from ACCESS-CM2 in 2081, and index 2 is assigned to the variable

value from ACCESS-ESM1-5 in 2081, and so on. The variables are then sorted according to those indices. The Euclidean distance for each variable and city is calculated between the 2020s and 2080s through the following formula:

$$(\sum(u_i - v_i)^2)^{(\frac{1}{2})} \quad (7)$$

where i is the assigned index to the variable value, u is the array of variable values in 2020s, and v is the array of variable values in 2080s. Finally, to make the results comparable, we normalize them as follows:

$$(x - x_{min}) / (x_{max} - x_{min}) \quad (8)$$

where for each variable, x is the Euclidean distance between the 2020s and the 2080s for each city, x_{min} is the minimum Euclidean distance among all the cities' Euclidean distances, and x_{max} is the maximum Euclidean distance among all the cities' Euclidean distances.

3.3. Epps-Singleton (ES) test

Anticipatory climate change adaptation policies and actions can take place at different scales. To decide whether adaptation measures in one location can be used for neighboring cities or if adaptation and mitigation measures should be planned for each city separately, two factors need to be considered. First, the vulnerability and susceptibility of these cities to climate change and its consequences. Second, determine if the climates of neighboring cities are moving in a similar direction for different climate parameters.

To determine whether two neighboring cities are heading in the same direction, the values of each variable in each city is first assigned an index based on the year and GCM model. The values of the variables are then sorted according to those indices. The absolute change distribution for each variable in each city from the 2020s to the 2080s was then calculated by subtracting the variable value from each GCM model and year in the 2080s from its corresponding variable value in the 2020s. For example, in Calgary, the value of the pr_sum variable based on CanESM5 in 2081 is subtracted from the value of the pr_sum variable based on CanESM5 in 2021. The Epps-Singleton (ES) test statistic is then applied to the results for each of the twenty-eight variables of the considered cities, with the null hypothesis being that the two datasets have the same underlying probability distribution. By comparing the empirical characteristic functions of the two samples, which is the Fourier transform of the observed distribution function of the two samples, the p-value of the ES test provides the probability of incorrectly rejecting the null hypothesis (Goerg and Kaiser, 2009). Two-sample tests are used in statistics to determine whether two samples have been taken from the same population. A commonly used two-sample test in such a case is the Kolmogorov–Smirnov (KS) two-sample test. However, in this study, the Epps-Singleton (ES) test is used because the majority of the climate variables are discrete variables, while an assumption of the KS test is that the data are drawn from a continuous distribution. Moreover, Epps and Singleton (1986) shows that the KS test has lower power than the ES test for continuous data, using computational simulations.

The next step is to interpret the results based on the p-values. Given that the null hypothesis is true, the p-value quantifies the likelihood of observing results at least as extreme as the ones observed. The result is then compared to a predetermined significance level (α). If the reported p-value is less than the significance level, the result is statistically significant. However, critics argue that p-values are frequently misunderstood and misused by many researchers, and that even when correctly understood, they can be an ineffective metric. Colquhoun (2014) stated that the standard significance level of 0.05 produces a minimum false discovery rate of 0.289, meaning that there is a 71.1% probability that a significant result has a real effect. Others contend that p-values encourage

the selective reporting of only positive results, and that they can be used in such a way that show statistical significance when none exists (Head et al., 2015; Vidgen and Yasseri, 2016).

Vidgen and Yasseri (2016) recommended using significance levels as low as 0.01 or 0.001 to prevent selective reporting and p-hacking in scientific research. Therefore, 0.01 is chosen as the significance level (α). When the p-value is lower than 0.01, the null hypothesis that the distributions of the given variable from the two cities are identical can be rejected.

4. Results

The modified Mann-Kendall test, Euclidean distance, and Epps-Singleton test results are presented in this section. The modified Mann-Kendall test results show whether the considered GCMs have an increasing or decreasing trend for a given variable in each city. The magnitude of the changes is then presented in the section 4.2. Given the same time frame for all seventeen cities (2020s-2080s), the Euclidean distance results for the given variable allow us to compare the rate at which change will occur across these cities. Finally, the Epps-Singleton test results provide some information regarding the neighboring cities, which is important for allocating resources and making decisions about adoption measures on a provincial scale.

4.1. Modified Mann-Kendall test

The modified MK test for the precipitation- and temperature-related variables for each city for a p-value of .01 appear in this section. For a given variable in a given city, the number of models that show a trend provides an indicator of the level of model consensus of the trend under the given scenario.

The results of the modified MK test for the precipitation-related variables, under SSP5-8.5 and 2-4.5 can be found in Figure 2 and 3, respectively. Considering the worst-case scenario (SSP5-8.5), most models, across all the cities, show an increasing trend for the total precipitation in a year (Figure 2a), with Iqaluit and Whitehorse having the highest number of models showing an increasing trend and Regina having the lowest number of models showing an increasing trend. Based on the Figure 2b, Iqaluit and Yellowknife are the only cities where several models observe a decreasing trend for dry_day0p2_sum, while models show no trend in the other cities. It can be concluded that under the considered scenario, Iqaluit will be wetter in the future based on the number of models that show an increasing trend for the pr_sum variable (25 models) and the number of models that show a decreasing trend for the dry_day0p2_sum variable (25 models). For the dry_day0p2_max_streak variable (Figure 2c), Iqaluit has the highest number of models showing a decreasing trend (6 models), while Vancouver has the highest number of models showing an increasing trend (4 models).

Except for Calgary where one model shows a decreasing trend for the number of days when the precipitation exceeds 20, all the detected monotonic trends across the considered cities for the number of days when the precipitation exceeds 20, 40, and 76 mm, are increasing trends. However, the number of models showing a trend decreased significantly from the heavy_pr20_sum variable to the heavy_pr76_sum variable. For the heavy_pr20_sum variable (Figure 2d), Quebec City, Montreal, and Fredericton have the highest number of models showing an increasing trend, and Regina, and Yellowknife having the lowest number of models showing an increasing trend. In Calgary and Regina no trend is found for the heavy_pr20_sum variable. For the heavy_pr40_sum variable (Figure 2e), only models in twelve of the cities show a trend, with Fredericton, Halifax, and Quebec City having the highest number of models that show an increasing trend. For the heavy_pr76_sum variable (Figure 2f), only three models in Quebec City, and St. Johns, two models in Fredericton, and one model each in Charlottetown, and Halifax show a trend.

When the results of the two scenarios, SSP5-8.5 and 2-4.5, are compared, it is evident that the number of models exhibiting a monotonic trend is higher in SSP5-8.5 than in SSP2-4.5 for most of the variables and cities. In SSP2-4.5, for example, a trend in the number of days with precipitation exceeding 76 mm was only detected in Montreal. Conversely, in SSP5-8.5, trends were observed in five of the cities under consideration. Moreover, for total annual precipitation SSP2-4.5 shows an average of over 60% less models indicating an upward trend than for SSP5-8.5. The remainder of this work will focus on presenting the results from the SSP5-8.5 scenario, with the data from the SSP2-4.5 scenario available in Appendices C and D.

Figure 3 shows the modified MK test results for six temperature-related variables. Figure2a-c show a selection of variables related to hotter temperatures and Figure2d-f show variables related to colder temperatures. Together these six graphs provide a summary of trends in variables affecting heating and cooling energy demand and the extremes of hot and cold. The evaluation of potential energy costs saving resulting from decreased extreme cold, as well as the assessment of whether such savings offset the costs incurred by extreme heat, is beyond the scope of this study. However, according to Figure 3, it can be observed that the majority of models show an increasing trend across all the cities except for Iqaluit, for days when the maximum temperature exceeds 30 °C, across all the cities except for Iqaluit and St Johns, for heat waves, and across all the cities for cooling degree days, while most of the models show a decreasing trend across all the cities that have historically experienced very cold temperatures as low as - 30°C , for days when the minimum temperature is less than - 30°C, cold waves, and heating degree days.

The results for the entire list of temperature-related variables can be found in Appendix C. The majority of models, across all the cities (except for Iqaluit, and St Johns), show an increasing trend for all the high temperature related variables. Exceptions are for days when the maximum temperature exceeds 40°C and the number of consecutive days when the maximum temperature exceeds 40 °C. The number of models that show an increasing trend is smaller for these cities across the set of cities and Charlottetown, Halifax, Iqaluit, St Johns, Vancouver, Victoria, and Yellowknife show no trend for these two variables.

Considering the variables that can be used as indicators of extreme cold, including below_tmin_30_sum, below_tmin_30_max_streak, and cold_wave_count, most of the models show a decreasing trend across all the cities that have historically experienced very cold temperatures as low as - 20 and - 30°C. Also, for hdd_18_sum, almost all the models across all the cities show a decreasing trend.

For freeze_thaw_day_sum, most models show a decreasing trend across all the cities except for Iqaluit, where seven models observed an increasing trend and seven models observed a decreasing trend, for Yellowknife, where three models observed an increasing trend, and ten models observed a decreasing trend, and for Quebec City, and Winnipeg where one model each observed an increasing trend, and fourteen models observed a decreasing trend. In addition, for freeze_thaw_day_max_streak, the number of models that show a decreasing trend is significantly higher than those that show an increasing trend in all the cities except Charlottetown, Fredericton, Halifax, Quebec City, and Yellowknife, where the number of models observed an increasing trend is higher. Thus, it can be stated that a trend towards fewer freezing thaw days is being observed.

Based on the number of models observed an increasing trend for the comfort_zone_sum variable, St. Johns, Vancouver, Fredericton, Halifax, Victoria, Charlottetown, and Yellowknife, respectively, could have a higher number of days with temperatures within the comfort zone.

In general, under SSP5-8.5 scenario, the modified MK test indicates the cities will be warmer and wetter on an annual basis (seasonal shifts are outside the scope here). Further, the modified MK

test results suggest that within these broad trends there are differences in the extent of changes between the locations.

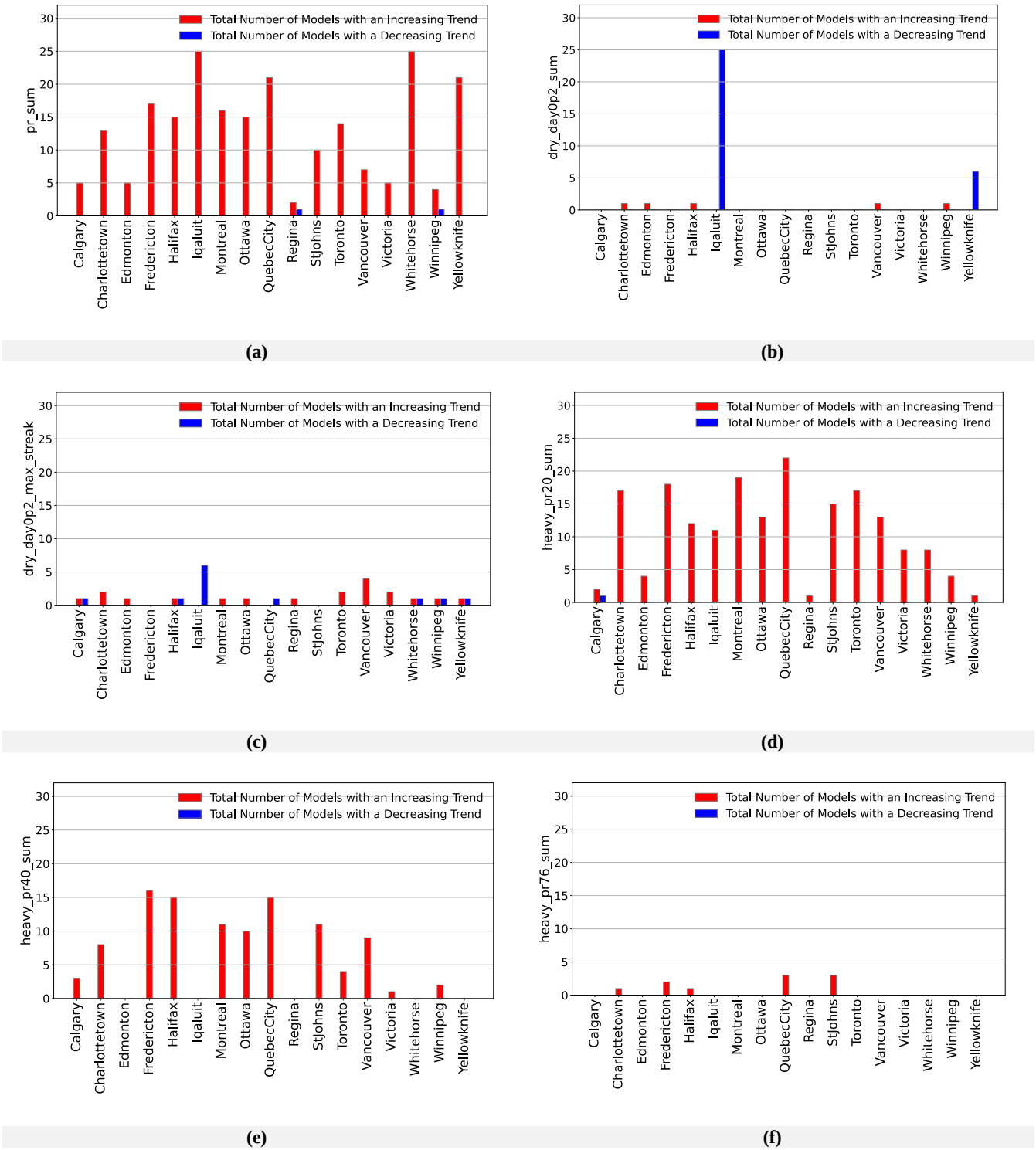

Figure 2. The results of the modified Mann-Kendall Trend test (m-MK test) (SSP5-8.5) for a) pr_sum, b) dry_day0p2_sum, c) dry_day0p2_max_streak, d) heavy_pr20_sum, e) heavy_pr40_sum, and f) heavy_pr76_sum.

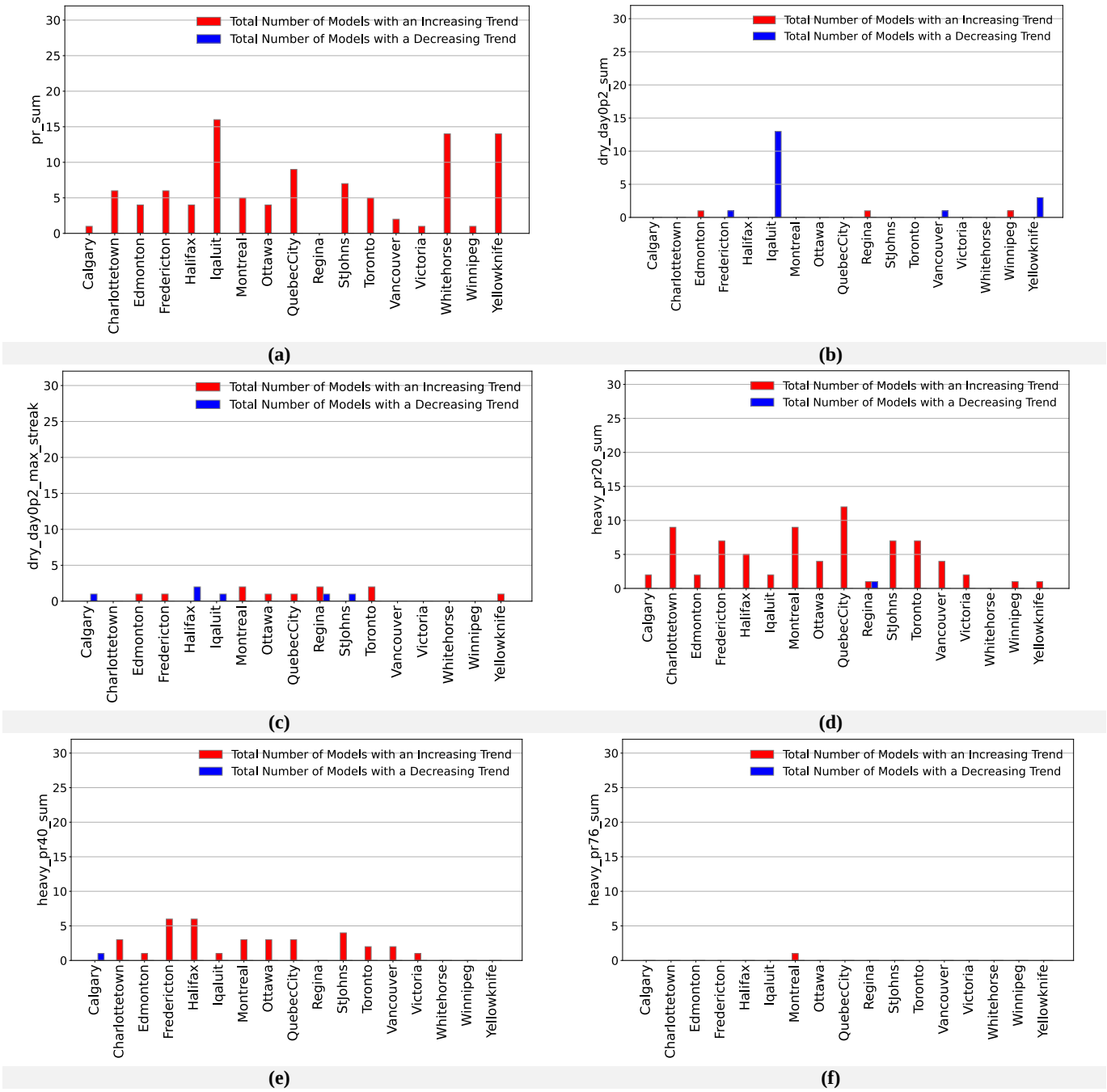

Figure 3. The results of the modified Mann-Kendall Trend test (m-MK test) (SSP2-4.5) for a) pr_sum, b) dry_day0p2_sum, c) dry_day0p2_max_streak, d) heavy_pr20_sum, e) heavy_pr40_sum, and f) heavy_pr76_sum.

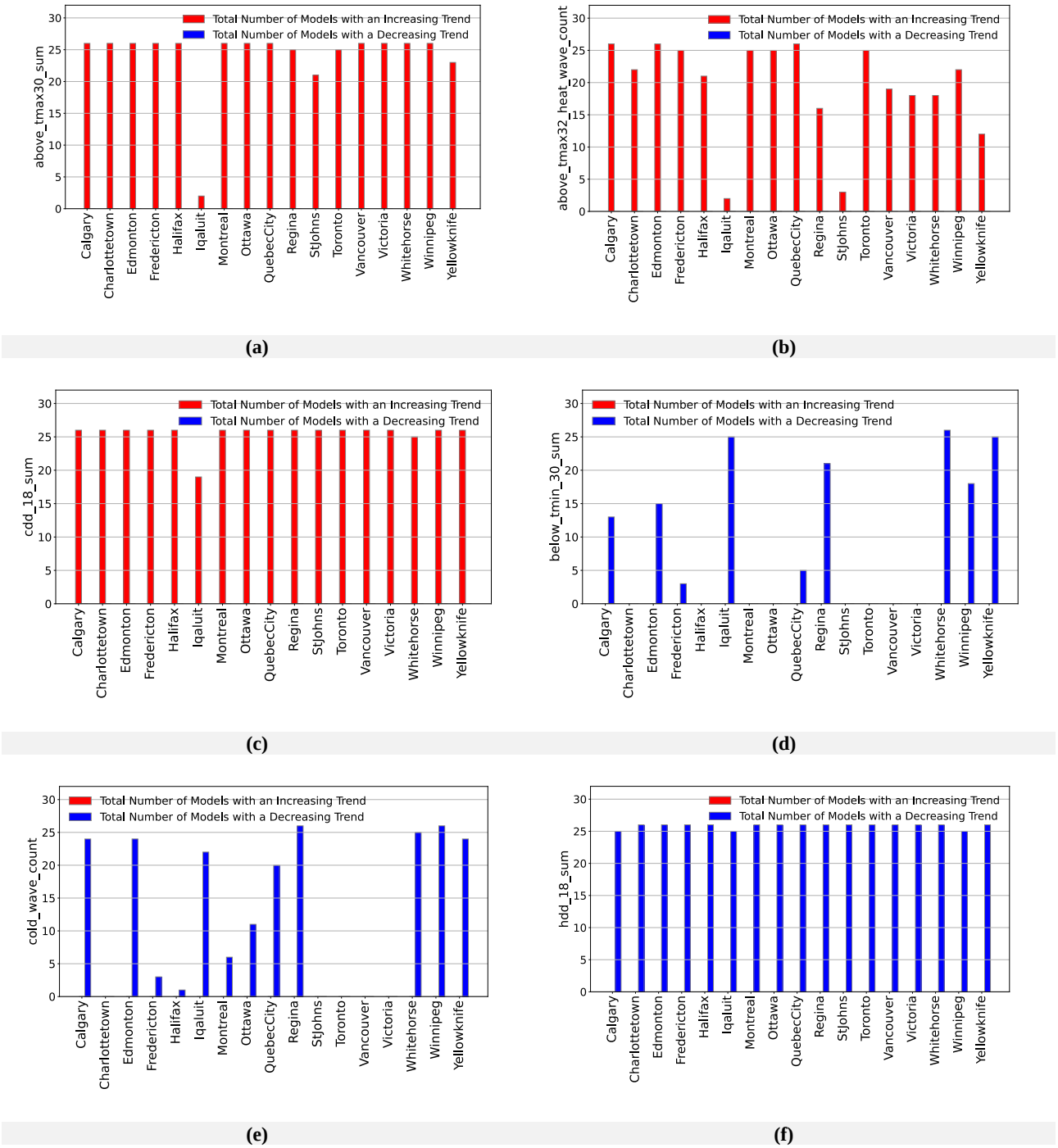

Figure 4. The results of the modified Mann-Kendall Trend test (m-MK test) (SSP5-8.5) for a) above_tmax30_sum, b) above_tmax32_heat_wave_count, c) cdd_sum_18, d) below_tmin_30_sum, e) cold_wave_count, and f) hdd_sum_18.

4.2. Euclidean distance

The Euclidean distance calculation extends the analysis from the modified MK test results to examine the degree of changes in the different cities. The Euclidean distance results provide us with the magnitude of the changes but not whether they are positive or negative. Therefore, the results should be interpreted in conjunction with the MK test results.

Tables 4 and 5 show the normalized Euclidean distance of the variables between the 2020s and 2080s, under SSP5-8.5 scenario. Based on the results Regina, Winnipeg, Ottawa, Montreal, and Toronto are projected to experience the greatest increase in climate variables used as indicators of hot weather under the considered scenario. On the other hand, Iqaluit and St. Johns are expected to experience the smallest increase in these indicators. When considering the climate variables that serve as indicators of cold weather, namely cold_wave_count, below_tmin_30_sum, below_tmin_30_max_streak, and hdd_18_sum, Iqaluit and Yellowknife are projected to show the greatest decrease in these indicators.

In terms of precipitation-related variables, Halifax, St. Johns, Vancouver, and Fredericton are expected to experience the greatest increases, respectively, while Whitehorse and Yellowknife are expected to see the smallest increases.

The consistency in magnitude of changes in precipitation-related variables is evident for the Prairies and Northern Territories, with the exception of Iqaluit. The prairies and cities located in Central Canada show the most consistency among one another in terms of changes in the extreme heat variables. When considering the cooling degree days variable, cities in Central Canada, with the exception of Quebec City, show the highest consistency. Furthermore, cities in Central Canada show a very high degree of consistency when it comes to fluctuations in the number of heat waves per year.

In general, it can be concluded that under the considered scenario, Prairie cities and cities in Central Canada are projected to experience the greatest increase in the number of days with extremely hot temperatures. On the other hand, the Atlantic and West Coast regions are expected to see the largest increase in the frequency of days with heavy precipitation.

Among the cities analyzed, St. Johns, Charlottetown, Toronto, and Vancouver are projected to experience the greatest change in the comfort_zone_day_sum variable, respectively. However, it is important to note that when drawing conclusions about this variable, the trend varies among the models. For Toronto, seven out of the 26 models show a decreasing trend, while only one model shows an increasing trend. On the other hand, St. Johns, Charlottetown, and Vancouver have 25, 7, and 24 models, respectively, that show an increasing trend, with no models showing a decreasing trend for St. Johns and Vancouver, and only one model showing a decreasing trend for Charlottetown. Furthermore, the normalized Euclidean distance of the variables between the 2020s and 2080s, under SSP2-4.5 scenario, as well as difference in Euclidean distance between variables under SSP5-8.5 and SSP2-4.5 can be found in Appendix D. The Difference in Euclidean distance between variables under the two considered scenarios are valid only if the modified MK test indicates a monotonic trend for both SSP2-4.5 and SSP5-8.5 scenarios.

Table 4. Normalized Euclidean distance of the precipitation related variables between 2020s and 2080s (SSP5-8.5). For each variable (row), dark green indicates city with the smallest change (0), and red indicates city with the largest change (1).

City	pr_sum	heavy_pr20_sum	heavy_pr40_sum	heavy_pr76_sum	dry_day0p2_sum	dry_day0p2_max_streak
Calgary	0.21	0.27	0.26	0.23	0.23	0.41
Edmonton	0.17	0.25	0.23	0.21	0.37	0.3
Regina	0.16	0.23	0.22	0.35	0.14	0.48
Winnipeg	0.22	0.32	0.3	0.42	0.13	0.24

Montreal	0.6	0.76	0.55	0.59	0.06	0.05
Ottawa	0.52	0.66	0.45	0.29	0.13	0.06
QuebecCity	0.78	0.93	0.7	0.5	0.03	0.04
Toronto	0.38	0.57	0.4	0.36	0.07	0.1
Vancouver	1	0.97	0.69	0.63	0.63	0.87
Victoria	0.63	0.59	0.5	0.65	0.6	1
Charlottetown	0.51	0.72	0.57	0.59	0.1	0.03
Fredericton	0.73	0.88	0.73	0.9	0.02	0.04
Halifax	0.78	0.93	1	1	0.03	0.05
StJohns	0.79	1	0.85	0.66	0	0
Iqaluit	0.3	0.15	0.1	0.12	1	0.08
Whitehorse	0.02	0	0	0	0.44	0.31
Yellowknife	0	0.05	0.06	0.14	0.36	0.29

Table 5. Normalized Euclidean distance of the temperature related variables (SSP5-8.5) between 2020s and 2080s. For each variable (row), dark green indicates city with the smallest change (0), and red indicates city with the largest change (1).

City	tasmax_max	above_tmax26_sum	above_tmax26_max_streak	above_tmax30_sum	above_tmax30_max_streak	above_tmax32_sum	above_tmax32_max_streak	above_tmax32_heat_wave_count	above_tmax34_sum	above_tmax34_max_streak	above_tmax40_sum	above_tmax40_max_streak	tasmin_min	cold_wave_count	below_tmin_30_sum	below_tmin_30_max_streak	hdd_18_sum	cdd_18_sum	freeze_thaw_day_sum	freeze_thaw_day_max_streak	extreme_tvar_day_sum	comfort_zone_day_sum
Calgary	0.76	0.79	0.58	0.79	0.67	0.79	0.67	0.76	0.73	0.69	0.46	0.44	0.42	0.42	0.12	0.23	0.23	0.67	1	0.62	1	0.02
Edmonton	0.86	0.82	0.59	0.77	0.63	0.75	0.59	0.75	0.66	0.58	0.38	0.4	0.72	0.53	0.18	0.33	0.27	0.71	0.61	0.4	0.34	0.09
Regina	0.94	0.74	0.74	0.86	0.95	0.96	1	0.72	0.99	1	1	1	0.69	0.64	0.27	0.42	0.3	0.91	0.47	0.35	0.72	0.07
Winnipeg	0.89	0.76	0.81	0.92	0.89	0.99	0.87	0.81	1	0.92	0.78	0.74	0.86	0.73	0.22	0.34	0.36	0.95	0.38	0.25	0.26	0.09
Montreal	0.6	0.85	0.9	1	0.92	1	0.82	1	0.87	0.71	0.54	0.46	0.94	0.26	0.01	0.02	0.22	0.98	0.45	0.07	0.08	0.45
Ottawa	0.63	0.84	0.86	1	0.93	1	0.8	0.97	0.9	0.76	0.6	0.59	0.98	0.33	0.02	0.04	0.22	0.96	0.47	0.17	0.12	0.29
QuebecCity	0.63	0.87	0.72	0.83	0.63	0.74	0.52	0.91	0.59	0.46	0.35	0.28	0.82	0.46	0.03	0.06	0.31	0.77	0.35	0.31	0.14	0.29
Toronto	0.52	0.91	1	0.98	1	0.93	0.83	0.94	0.79	0.73	0.42	0.46	0.78	0.01	0	0	0.13	1	0.67	0.22	0	0.65
Vancouver	0.5	1	0.83	0.72	0.72	0.55	0.56	0.51	0.36	0.41	0.06	0.09	0.26	0	0	0	0	0.78	0.19	0.21	0.02	0.61
Victoria	0.48	0.93	0.7	0.5	0.45	0.32	0.29	0.41	0.18	0.16	0.05	0.08	0.01	0	0	0	0	0.64	0	0	0	0.34
Charlottetown	0.2	0.82	0.62	0.66	0.52	0.49	0.34	0.7	0.28	0.22	0.04	0.05	0.5	0.09	0	0.01	0.18	0.7	0.45	0.15	0.04	0.73
Fredericton	0.4	0.79	0.72	0.81	0.67	0.78	0.66	0.89	0.66	0.55	0.4	0.38	0.87	0.25	0.02	0.05	0.23	0.77	0.51	0.37	0.31	0.31
Halifax	0.21	0.85	0.68	0.6	0.48	0.41	0.28	0.57	0.25	0.19	0.06	0.06	0.38	0.05	0	0	0.13	0.64	0.6	0.23	0.08	0.5
StJohns	0	0.57	0.26	0.28	0.17	0.15	0.09	0.26	0.06	0.06	0	0	0	0.01	0	0	0.15	0.42	0.77	0.32	0.01	1

Iqaluit	0.87	0	0	0	0	0	0	0	0	0	0	0	1	1	0.95	1	1	0	0.21	0.18	0.13	0
Whitehorse	1	0.64	0.3	0.4	0.27	0.32	0.24	0.44	0.25	0.24	0.1	0.16	0.62	0.61	0.46	0.55	0.5	0.33	0.71	1	0.47	0.02
Yellowknife	0.4	0.54	0.26	0.34	0.23	0.24	0.18	0.34	0.15	0.14	0.03	0.05	0.74	0.74	1	0.91	0.71	0.39	0.23	0.32	0.04	0.19

4.2.1. Heating and cooling degree days

Figure 5 shows the HDD and CDD with a base temperature of 14°C and the log (electricity demand) based on the temperature response functions suggested by Rivers and Shaffer (2020), over four decades. Since 14°C is used as the base temperature in the proposed functions for calculating log (electricity demand) in Rivers and Shaffer (2020), 14°C is considered as the base temperature while calculating HDD and CDD in Figure 5 to make the results comparable. As shown in the Figure 5, from the 2020s to the 2080s, the CDD and log (electricity demand for cooling) increase while the HDD and log (electricity demand for heating) decrease.

Based on the boxplots of CDD, the cities with the highest energy demand over the considered four decades should be Toronto, Montreal, and Ottawa. However, based on calculations that considered the impact of air conditioner penetration and the residential share of total consumption, Toronto and Ottawa are the cities with the highest energy demand, with Montreal coming in fifth. In addition, St. Johns has the lowest energy demand according to CDD boxplots, but Calgary has the lowest according to boxplots derived from response functions in Rivers and Shaffer (2020). These discrepancies can be attributed to the fact that Ontario has the highest share of households with air conditioners in Canada and Alberta has the lowest residential share of the electricity demand of any province, resulting in a relatively flat temperature response function (Rivers and Shaffer, 2020).

Comparing the boxplots of HDD with those obtained through response functions reveals that Montreal is in the fourth place based on the boxplots of the response functions and is in the seventh place based on the boxplots of the HDD, while Quebec City is in the third place for both HDD and response functions. According to Rivers and Shaffer (2020), Quebec has the highest share of households with electric heat as their primary heating source.

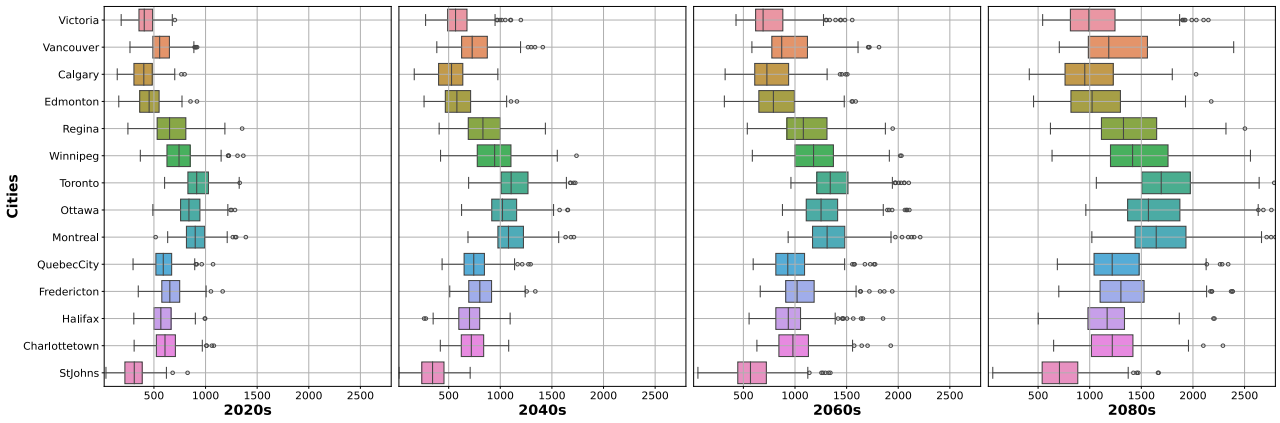

(a) cdd_sum_14

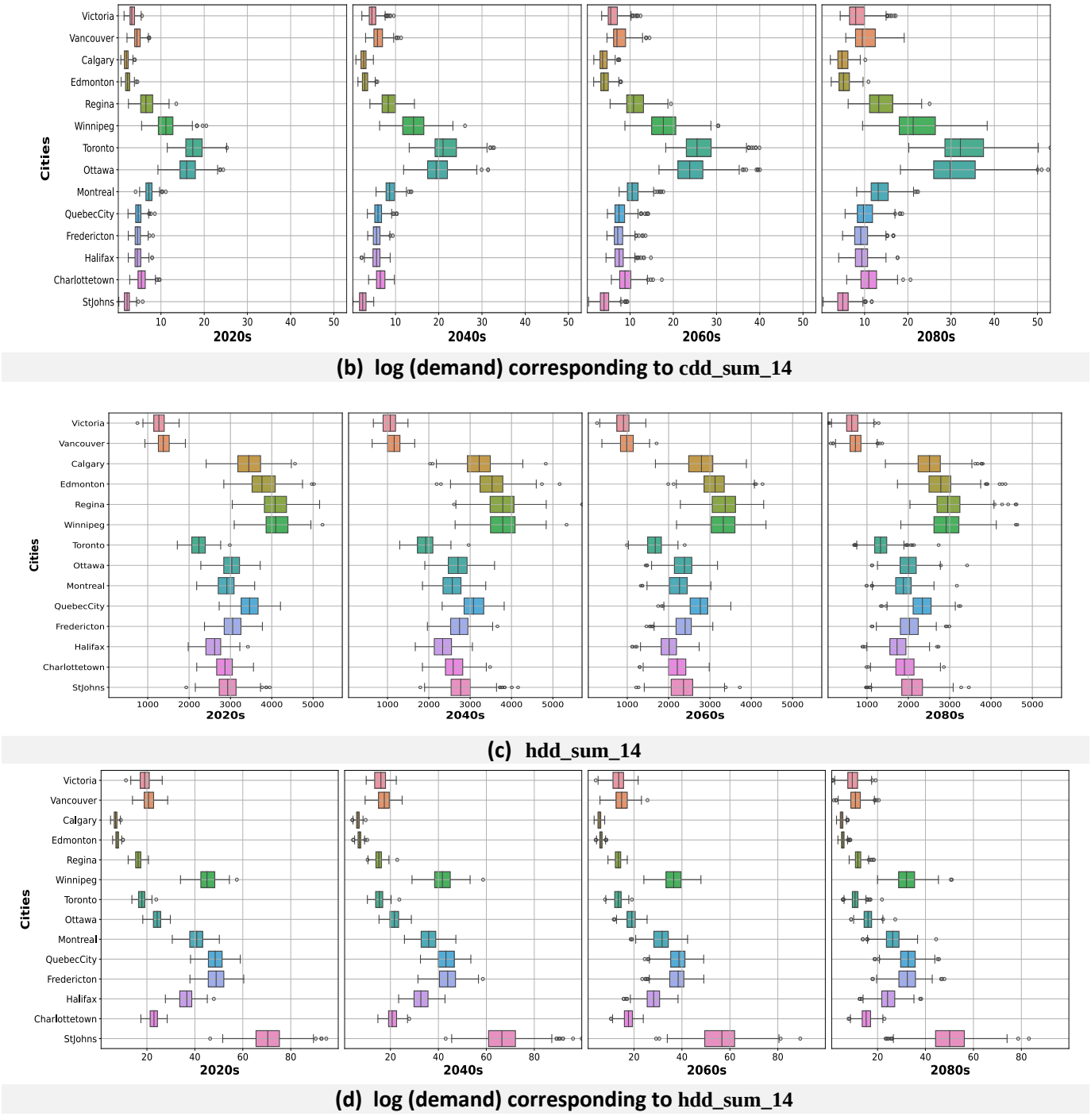

Figure 5. Log (electricity demand) relative to 14°C based temperature, calculated through response function proposed by Rivers and Shaffer (2020), across different cities in Canada in four decades (SSP5-8.5 scenario).

4.3. Epps-Singleton test

Table 8 shows the results of the Epps-Singleton (ES) test for the considered pairs of cities, which were selected because they are neighbors or are located in a relatively short straight-line distance from each other. The empty cells in the table are those where the significance level is below 0.01. Based on the results, coastal cities, even those that are located relatively close to one another (such as Vancouver and Victoria, where only six of the twenty-eight variables pass the ES test and two of these are near the test threshold), follow different trends of change for the majority of their variables. Conversely, where one or both two neighboring cities are inland cities, they have more variables with the probability of having similar trends from the 2020s to the 2080s (such as Montreal and Ottawa,

where twenty-two of the twenty-eight variables pass the ES test, or Calgary and Edmonton, where nineteen of the twenty-eight variables pass the ES test).

To determine whether the similarity in change trends from the 2020s to the 2080s is due to starting from similar situations and ending up at similar points, the variable distributions of each pair of cities in the 2020s (Table 6) and the 2080s (Table 7) were also examined. If a variable passes the ES test for both the 2020s and the 2080s, with p-values that are not close to the test threshold, it suggests that the two considered cities are likely to move in a similar direction with a similar rate of change for that variable from the 2020s to the 2080s. However, a variable does not necessarily pass the test for both the 2020s and the 2080s if it passes the ES test for the change from the 2020s to the 2080s. For example, when comparing change in the cdd_18_sum variable from the 2020s to the 2080s between Regina & Winnipeg, the p-value indicates that there is a high probability that these two cities have a similar trend and rate of change (p-value = 0.844), but when comparing the same variable for the 2020s and 2080s, it reveals that these two cities do not start or end (p-value = 0.068 which is very close to the test threshold) at the same point. The importance of distinguishing between variables that have a similar trend and rate of change from the 2020s to the 2080s but do not have the same starting and ending points and variables that have a similar trend and rate of change from the 2020s to the 2080s due to starting and ending at the same points is that for the first case, we also need to compare the vulnerability of the two considered neighboring cities as well as their current state in regard to the considered variable to detect which city require immediate attention and to prioritize the implementation of adaptation measures and resource allocation.

Table 6. Epps-Singleton (ES) test results for the variables in the 2020s. For a given variable, an empty cell shows two cities have different distributions (p-value < .01), and a non-empty cell indicates strong evidence for the null hypothesis, which is that two cities have similar distributions. The range of p-values is represented by different shades of blue, with the darkest shade indicating .99 and the lightest shade (white) representing .01.

Variables/Cities	Vancouver & Victoria (94 km)	Montreal & Ottawa (161 km)	Halifax & Charlottetown (180 km)	Montreal & QuebecCity (234 km)	Charlottetown & Fredericton (273 km)	Calgary & Edmonton (279 km)	Fredericton & Halifax (281 km)	Toronto & Ottawa (351 km)	Toronto & Montreal (500 km)	Regina & Winnipeg (536 km)
pr_sum					0.117	0.038				
heavy_pr20_sum						0.822		0.144		
heavy_pr40_sum						0.273		0.189	0.014	
heavy_pr76_sum										
dry_day0p2_sum		0.946								
dry_day0p2_max_streak		0.98	0.156	0.049						
tasmax_max						0.125				
above_tmax26_sum		0.602	0.834			0.213				0.532
above_tmax26_max_streak		0.944	0.853			0.099		0.033	0.02	0.441
above_tmax30_sum		0.166	0.47			0.027				0.033
above_tmax30_max_streak	0.05	0.347	0.508			0.281				0.207

above_tmax32_sum	0.621	0.016	0.056			0.225			0.192	
above_tmax32_max_streak	0.662		0.034			0.307			0.293	0.027
above_tmax32_heat_wave_count		0.016				0.269			0.137	
above_tmax34_sum		0.011				0.095			0.316	
above_tmax34_max_streak		0.011				0.383			0.115	
above_tmax40_sum										
above_tmax40_max_streak										
tasmin_min			0.196							
below_tmin_30_sum										0.089
below_tmin_30_max_streak										0.101
cold_wave_count										0.074
comfort_zone_day_sum										
hdd_18_sum	0.108									0.544
cdd_18_sum									0.304	
freeze_thaw_day_sum										
freeze_thaw_day_max_streak							0.139		0.433	
extreme_tvar_day_sum										

Table 7. Epps-Singleton (ES) test results for the variables in the 2080s. For a given variable, an empty cell shows two cities have different distributions (p-value $<$ .01), and a non-empty cell indicates strong evidence for the null hypothesis, which is that two cities have similar distributions. The range of p-values is represented by different shades of blue, with the darkest shade indicating .99 and the lightest shade (white) representing .01.

Variables/Cities	**Vancouver & Victoria (94 km)**	**Montreal & Ottawa (161 km)**	**Halifax & Charlottetown (180 km)**	**Montreal & QuebecCity (234 km)**	**Charlottetown & Fredericton (273 km)**	**Calgary & Edmonton (279 km)**	**Fredericton & Halifax (281 km)**	**Toronto & Ottawa (351 km)**	**Toronto & Montreal (500 km)**	**Regina & Winnipeg (536 km)**
pr_sum						0.04				
heavy_pr20_sum						0.815				
heavy_pr40_sum						0.878		0.46		
heavy_pr76_sum							0.01			
dry_day0p2_sum		0.7								
dry_day0p2_max_streak		0.358	0.111						0.07	
tasmax_max		0.037	0.037			0.031			0.542	
above_tmax26_sum		0.975	0.588			0.112		0.193	0.513	0.691
above_tmax26_max_streak		0.691	0.434			0.083			0.239	0.848
above_tmax30_sum		0.833	0.152			0.021		0.035	0.245	0.542
above_tmax30_max_streak		0.886	0.028			0.289		0.087	0.181	0.132
above_tmax32_sum		0.771	0.014			0.109		0.01	0.137	0.14
above_tmax32_max_streak		0.992	0.075			0.201		0.135	0.17	0.054
above_tmax32_heat_wave_count		0.538				0.081			0.129	0.535

above_tmax34_sum		0.604	0.076			0.118			0.053	0.053
above_tmax34_max_streak		0.704	0.474			0.111			0.043	0.113
above_tmax40_sum		0.377				0.77		0.099	0.585	
above_tmax40_max_streak		0.109				0.942			0.108	
tasmin_min			0.678			0.26				
below_tmin_30_sum										
below_tmin_30_max_streak										
cold_wave_count						0.415				0.08
comfort_zone_day_sum				0.018						
hdd_18_sum	0.162				0.101					0.153
cdd_18_sum		0.288			0.011	0.299			0.411	0.068
freeze_thaw_day_sum										
freeze_thaw_day_max_streak										
extreme_tvar_day_sum										

Table 8. Epps-Singleton (ES) test results for absolute change of the variables from the 2020s to the 2080s. For a given variable, an empty cell shows two cities have different distributions (p-value $<$. 01), and a non-empty cell indicates strong evidence for the null hypothesis, which is that two cities have similar distributions. The range of p-values is represented by different shades of blue, with the darkest shade indicating .99 and the lightest shade (white) representing .01.

Variables/Cities	**Vancouver & Victoria (94 km)**	**Montreal & Ottawa (161 km)**	**Halifax & Charlottetown (180 km)**	**Montreal & Quebec City (234 km)**	**Charlottetown & Fredericton (273 km)**	**Calgary & Edmonton (279 km)**	**Fredericton & Halifax (281 km)**	**Toronto & Ottawa (351 km)**	**Toronto & Montreal (500 km)**	**Regina & Winnipeg (536 km)**
pr_sum		0.735		0.026	0.017	0.493	0.564	0.148		0.176
heavy_pr20_sum		0.433			0.123	0.695	0.349	0.252		0.013
heavy_pr40_sum		0.234		0.016	0.01	0.898		0.666		
heavy_pr76_sum							0.027			
dry_day0p2_sum	0.896	0.733	0.7	0.4	0.64	0.457	0.814	0.777	0.775	0.969
dry_day0p2_max_streak	0.812	0.439	0.145	0.059	0.876		0.646	0.245		
tasmax_max	0.52	0.808	0.089	0.818	0.113	0.105	0.113	0.249	0.135	0.682
above_tmax26_sum	0.016	0.984	0.76	0.544	0.769	0.806	0.1	0.157	0.37	0.712
above_tmax26_max_streak		0.734	0.562		0.067	0.706	0.627		0.014	0.364
above_tmax30_sum		1	0.087			0.483		0.628	0.625	0.401
above_tmax30_max_streak		0.951	0.078		0.012	0.601		0.741	0.662	0.294
above_tmax32_sum		0.997				0.37		0.272	0.278	0.687
above_tmax32_max_streak		0.917	0.014			0.394		0.648	0.316	0.167
above_tmax32_heat_wave_count		0.807		0.217		0.157		0.278	0.245	
above_tmax34_sum		0.911	0.085			0.277		0.012	0.097	0.49
above_tmax34_max_streak		0.907	0.481			0.26		0.035	0.078	0.575
above_tmax40_sum		0.349				0.794		0.074	0.503	

above_tmax40_max_streak		0.131				0.964			0.119	
tasmin_min	0.022	0.982	0.395	0.151				0.128	0.292	0.313
below_tmin_30_sum										0.111
below_tmin_30_max_streak										0.08
cold_wave_count										
comfort_zone_day_sum			0.01							
hdd_18_sum	0.743	0.991	0.132		0.186	0.611				0.486
cdd_18_sum		0.958	0.179		0.208	0.557		0.672	0.909	0.844
freeze_thaw_day_sum		0.454			0.082					0.203
freeze_thaw_day_max_streak		0.285	0.05			0.038	0.115			0.044
extreme_tvar_day_sum										

5. Discussion

In this study the SSP5-8.5 scenario, which is commonly referred to as the worst-case scenario, as well as SSP2-4.5 are considered. According to Schwalm et al. (2020), without significant near-term global mitigation measures, this SSP5-8.5 scenario, to the extent that it accords with RCP 8.5, remains quite plausible.

The findings of this study are consistent with earlier research on the impact of climate change in Canada. For instance, Berardi & Jafarpur, (2020) have studied the impact of climate change on building energy demand in Toronto, Ontario. Their research shows that under the RCP 8.5 scenario, Toronto is projected to experience an average decrease of 18%–33% in heating energy use intensity and an average increase of 15%–126% in cooling energy use intensity by 2070. These findings align with the results of this study, which also indicate a significant increase in cdd_18_sum and a decrease in hdd_18_sum for Toronto. Also, Ogden & Gachon, (2019) have studied the infectious disease risks associated with climate change in Canada and states that under RCP 8.5, northeastern Canada is expected to experience the greatest increase in temperature by the 2070s. Their finding is consistent, to some extent, with the results of this study, which show the highest increase in temperature occurring in Central Canada in addition to Prairie cities. Furthermore, they predict changes in annual total precipitation, which will include slight increases in precipitation in the Prairie provinces. This prediction is consistent with the findings of this study, which also suggest insignificant increase in total precipitation for those regions.

From the results, and with reference to vulnerabilities of the Canadian built environment and population many observations are drawn in the following sections.

5.1. Precipitation and flooding

Floods are already the most frequent and costliest natural disasters in Canada, according to the Canadian Disaster Database, with 241 flood disasters occurring between 1900 and 2005(Sandink et al., 2010). There are several causes of flooding in Canada, ranging from spring snowmelt to tsunamis in coastal areas, of which, as stated by Burrell (2012), over 65 percent are caused by snowmelt runoff, storm rainfall, or rain on snow. Increasing precipitation and temperature, as well as deterioration of intra-urban (situated within the city) assets, are all factors that contribute to an increase in flood risk in urban areas (O'Donnell and Thorne, 2020). This study is restricted to considering pluvial events. For these, an increase in flood risk in the cities studied here should be expected under SSP5-8.5 (and to a lesser extent for SSP4-2.5), particularly in Halifax, St Johns, Fredericton, Quebec City, and

Vancouver where the results show a significant increase in the frequency of days with heavy precipitation.

Considering the projected increase in the frequency of days with heavy precipitation under the considered scenario, the vulnerability of at-grade and underground infrastructure assets will also be expected to increase in the future. Therefore, establishing sustainable stormwater management systems is essential for cities to meet their aims of reducing potential flood damage and achieving climate change adaptation. The City of Victoria is now working on implementing such a system through stormwater utility.

5.2. Drought, heat, and wildfire

The second most common disaster in Canada is wildfire (Sandink et al., 2010). Considering the precipitation-related variables, under the SSP5-8.5 scenario, we can conclude that the amount and intensity of precipitation will increase in Vancouver from the 2020s to the 2080s, while the maximum number of consecutive days without rain (dry_day0p2_max_streak) or drought length will also increase. Although the City of Vancouver is likely to be relatively safe from wildfire, worsening drought and increased extreme heat raise the risk of wildfire in Metro Vancouver and surrounding rural regions and consequently increasing the risk of air pollution in the City of Vancouver. While under the SSP5-8.5 scenario, Vancouver will experience an increasing trend in the maximum number of consecutive days without rain, under the SSP2-4.5 scenario, no trend is observed for this variable. Moreover, under the SSP2-4.5 scenario, one of the models shows a decreasing trend for the total number of days without rain in a year variable in this city. This emphasizes the importance of the scenario selection in the risk perception and, subsequently, the decisions regarding the adaptation measures.

Except for Iqaluit, under both considered scenarios, all the cities included in this study are predicted to experience an increase in the frequency of days with extremely high temperatures as well as the number of consecutive days with extremely high temperatures. In Regina, Winnipeg, Montreal, Ottawa, and Toronto, this could be more severe. Increasing number of days with temperatures above the minimum mortality temperature (i.e., the temperature at which mortality is minimized in the estimated temperature-mortality association curve (Lee et al., 2017)) contributes to an increase in heat-related mortality and morbidity.

Moreover, extreme weather conditions reduce infrastructure reliability (Ouyang et al., 2023).The main question regarding increasing the number of days with extreme hot temperatures or heat waves in the cities considered in this study is whether Canadian infrastructure at present can accommodate the increase in peak electricity demand and the expansion of the diurnal range of hourly consumption corresponding to the projected change in temperature. Due to the compounding effect of high energy demand for cooling and high temperatures on power transformer capacity and electrical transmission efficiency, extreme heat will cause issues for the distribution system (AECOM Consultants Inc., 2015). Even if we only look at the residential sector, taking into account the anticipated rise in air conditioner installation, as we have already seen in a city like Vancouver where builders will be required to install mechanical air cooling equipment in all new multi-family homes starting in 2025, and considering the fact that the residential sector accounted for the second-largest share (30%) of the electricity demand in Canada after the industry sector (33%) (IEA, 2022), a huge increase in energy demand during the summer should be expected. The largest increases in energy demand (CDD) from the 2020s to the 2080s under the considered scenario, will be in Toronto, Montreal, Ottawa, Winnipeg, and Regina, respectively. According to Rivers and Shaffer (2020), Ontario already has the largest share of households with air conditioners in Canada. As a result, by

increasing the extreme heat in the future, Montreal, Winnipeg, and Regina should experience a greater rate of change in the share of houses with air conditioners than Toronto and Ottawa. The findings in this study suggest that projecting future energy demand solely based on climate parameters can be misleading, and there are other factors that must be considered when prioritizing adaptation and mitigation measures regarding the changes in energy demand across the cities.

Furthermore, much of the infrastructure in Canada was not designed to withstand extremely hot weather conditions. For instance, 32.2°C has historically been the preferred rail laying temperature (PRLT) across Canada (Chiotti et al., 2017). To lessen the risk of track bending or buckling in hot weather, Metrolinx, an agency of the Ontario government responsible for coordinating and integrating transportation in the Greater Toronto and Hamilton Area, recently raised its PRLT to 37.7°C for all replaced or new track (Chiotti et al., 2017). Currently, Manitoba Infrastructure and Transportation mandates that materials used to build large culverts and bridges be able to resist temperatures between -40°C and +40°C (Palko and Lemmen, 2017). Those are two examples of adoption measures that have already been implemented, considering the anticipated rise in temperatures.

In addition, what level of heat constitutes a problem for the built environment varies in Canada. An increase in permafrost thawing is anticipated as a result of the forecasted decrease in the frequency of extreme cold days and cold waves in Iqaluit and an increase in the frequency of extreme heat days in Whitehorse and Yellowknife. Thus, the infrastructure that was constructed on permafrost in these three cities, could need additional maintenance or replacement. As highlighted by Suter et al. (2019), supporting current infrastructure into the future may require additional annual investment in the regions of Northern Canada and Western Siberia of more than 1% of annual GRP.

5.3. Similarity of climate stresses

The Epps-Singleton (ES) test results show that the neighboring inland cities could have more similar conditions in the 2080s, considering the climate variables in this study. This means that essential services such as health, water sanitation, transportation infrastructure, and utilities could face increased pressure in the event of a heat wave or extreme precipitation on a provincial or regional scale, affecting multiple cities.

Furthermore, keeping up with climate change adaptation in even nearby cities may require different degrees of action. For example, Montreal and Ottawa are neighboring cities, but the change in the number of days with at least 40 mm of precipitation from the 2020s to the 2080s is not that similar in these two cities (the p-value from the ES test on the absolute change of the considered variable from the 2020s to the 2080s is 0.234). For this variable, Montreal could experience a greater change than Ottawa. But for example, the change in the number of days with at least 40 mm of precipitation from the 2020s to the 2080s is very similar in Calgary and Edmonton (the p-value from the ES test is equal to 0.898), and these two cities could have very similar situations in the 2080s (the p-value from the ES test in the 2080s is equal to 0.878). As a result, for these two cities the level of vulnerability should be the main factor in prioritizing the adaptation measures.

5.4. Summary

To address the objective of this study, which is to examine the potential impacts of climate change on major Canadian cities, a comprehensive approach was taken, incorporating all twenty-six GCMs suggested by PCIC to maximize the ability to capture the variability of climate projections across Canada. However, since a large number of GCMs were considered, the common approach (Sen's slope estimator) for comparing the magnitude and direction of changes across cities and variables is

no longer valid. To address the issue, the modified Mann-Kendall test and the Euclidean distance were used to capture both the direction and magnitude of changes for a given variable across cities.

Under both SSP5-8.5 and SSP2-4.5 scenarios, Canadian cities will experience more extreme heat and heavy rainfall, as well as less extreme cold, in the future. In particular, Atlantic provinces and Central Canada would be subject to more extreme pluvial events. Moreover, cities such as Regina, Winnipeg, Montreal, Ottawa, and Toronto are expected to face significant increase in extreme heat which could lead to elevated mortality rates in the absence of adequate adaptation measures, high energy demand for cooling, and reduction in infrastructure reliability.

The results of this study show the risk posed by climate change and the associated uncertainty with the findings to decision makers and non-experts. The number of models with an increasing or declining trend indicates our level of confidence in the results. For example, we can confidently say that under the SSP5-8.5 scenario, cities in this study will experience an increase in cdd_sum_18 (With the exception of Iqaluit and Whitehorse, where 19 and 25 of the models, respectively, show an increasing trend, all the GCMs show an increasing trend in the remaining cities). However, the level of uncertainty in the projected trend for heavy_pr40_sum is very high, with less than half of the examined models showing a significant trend. Furthermore, for regional planning or if the magnitude of changes in a specific city needs to be considered, the Euclidean distance results can be denormalized to see the magnitude of changes for different variables under consideration as a single number, and for national planning or comparing different cities, the normalized Euclidean distances between the 2020s and the 2080s can be used.

It is important to acknowledge that the performance of the GCMs in predicting future climate conditions may vary among cities. Future research could include a historical comparison of projected and observed data to enhance the selection process of GCMs for each of the seventeen cities.

Furthermore, as reported by Tam et al. (2015), urban climate change caused by urbanization has had a more immediate impact on the urban thermal environment compared to global climate change. This impact is evident through the emergence of various phenomena such as the urban heat island (UHI) effect i.e. where the air temperature in urban areas is significantly higher than in the surrounding rural areas, urban cool island (UCI) effect i.e. where the air temperature of the surrounding rural area is warmer than that of the urban area (X. Yang et al., 2017), and urban dry island (UDI) effect, closely linked to the UHI, where the relative humidity in urban areas is lower than in the rural zones (Lokoshchenko, 2017). According to Y. Wang et al. (2016), a UHI intensity of 2-3°C results in a 4-7% increase in the mortality rate in Canada. Considering the fact that climate model projections currently do not incorporate the influence of urbanization, it is probable that the frequency of days with extremely high temperatures in Canadian cities will be even greater than what is indicated by the findings of this study and will also be varies for different areas within the cities based on urban surface properties such as population density (Fischer et al., 2012). Future research should further investigate the UHI effects in conjunction with the findings of this study to obtain a more detailed insight into the future of the cities under consideration.

Data source

"Pacific Climate Impacts Consortium, University of Victoria, (Dec. 2021). Statistically Downscaled Climate Scenarios. Downloaded from https://data.pacificclimate.org/portal/downscaled_cmip6/map/ between 20 and 25 March 2022. Method: BCCAQ v2. GCMs: ACCESS-CM2, ACCESS-ESM1-5, BCC-CSM2-MR, CanESM5, CMCC-ESM2, CNRM-CM6-1, CNRM-ESM2-1, EC-Earth3, EC-Earth3-Veg, FGOALS-g3, GFDL-ESM4, HadGEM3-GC31-LL, INM-CM4-8, INM-CM5-0,

IPSL-CM6A-LR, KACE-1-0-G, KIOST-ESM, MIROC-ES2L, MIROC6, MPI-ESM1-2-HR, MPI-ESM1-2-LR, MRI-ESM2-0, NorESM2-LM, NorESM2-MM, TaiESM1, UKESM1-0-LL. SSPs: 5-8.5. Downloaded variables: Total precipitation per day (mm), maximum temperature per day (°C), and minimum temperature per day (°C).

Appendix

Appendix A (Comparing rainfall and precipitation data)

A comparison between the median of the sum of precipitation per year (mm per year) and rainfall per year (mm per year) across the 2020s, 2040s, 2060s, and 2080s can be found in Table 9, where the maximum daily temperature is used to derive rainfall data from precipitation data. The largest differences between the medians of the sum of daily precipitation per year (mm per year) and the sum of daily rainfall per year (mm per year) belong to Quebec City and Iqaluit. For Victoria and Vancouver, there is almost no difference between them across the four decades. The difference between the total number of days with precipitation > 20, 40, and 76 mm per year and rainfall > 20, 40, and 76 mm per year is insignificant.

The total number of models that show an increasing or decreasing trend for none of the precipitation-related variables changes if this rainfall data is used in place of precipitation data. Additionally, if the cities are sorted based on the Euclidean distance between the 2020s and the 2080s of their total number of days with precipitation exceeding 20, 40, and 76 mm per year, considering rainfall rather than precipitation does not change the order of the cities. However, the order of the first nine cities with the largest Euclidean distance between the 2020s and the 2080s for the total precipitation per year (pr_sum) changes from Vancouver, St. Johns, Halifax, Quebec City, Fredericton, Victoria, Montreal, Ottawa, and Charlottetown to Quebec City, Vancouver, St. Johns, Fredericton, Halifax, Montreal, Charlottetown, Ottawa, and Victoria (Tables 10 and 11) when considering rainfall instead of precipitation.

Table 9. Median of the sum of daily precipitation per year (mm per year) and daily rainfall per year (mm per year) across the 2020s, 2040s, 2060s, and 2080s, under SSP5-8.5 scenario.

	Precipitation				**Rainfall**			
City	Median_20	Median_40	Median_60	Median_80	Median_20	Median_40	Median_60	Median_80
Calgary	418	433	438	459	378	392	402	417
Charlottetown	1153	1180	1201	1238	1054	1090	1137	1181
Edmonton	447	460	469	478	382	394	415	423
Fredericton	1174	1202	1256	1299	1064	1110	1194	1258
Halifax	1425	1427	1479	1538	1343	1377	1446	1492
Iqaluit	470	495	530	594	302	334	379	437
Montreal	1048	1096	1134	1161	940	1012	1053	1103
Ottawa	938	979	989	1041	839	893	917	983
QuebecCity	1253	1319	1367	1415	1084	1173	1237	1315
Regina	398	386	402	401	331	324	344	352
StJohns	1448	1476	1521	1543	1328	1371	1451	1498
Toronto	825	837	847	895	789	816	828	891
Vancouver	1286	1298	1381	1376	1286	1298	1381	1376
Victoria	835	826	904	902	832	826	904	902
Whitehorse	325	330	375	392	259	276	321	344
Winnipeg	537	533	551	567	452	459	481	492
Yellowknife	311	328	345	357	206	221	237	267

Table 10 Normalized Euclidean distance of the precipitation variables between 2020s and 2080s under SSP5-8.5 scenario. For each variable (row), dark green indicates city with the smallest change (0), and red indicates city with the largest change (1).

City	pr_sum	heavy_pr20_sum	heavy_pr40_sum	heavy_pr76_sum
Calgary	0.21	0.27	0.26	0.23
Charlottetown	0.51	0.72	0.57	0.59
Edmonton	0.17	0.25	0.23	0.21
Fredericton	0.73	0.88	0.73	0.9
Halifax	0.78	0.93	1	1
Iqaluit	0.3	0.15	0.1	0.12
Montreal	0.6	0.76	0.55	0.59
Ottawa	0.52	0.66	0.45	0.29
Quebec City	0.78	0.93	0.7	0.5
Regina	0.16	0.23	0.22	0.35
St Johns	0.79	1	0.85	0.66
Toronto	0.38	0.57	0.4	0.36
Vancouver	1	0.97	0.69	0.63
Victoria	0.63	0.59	0.5	0.65
Whitehorse	0.02	0	0	0
Winnipeg	0.22	0.32	0.3	0.42
Yellowknife	0	0.05	0.06	0.14

Table 11. Normalized Euclidean distance of the rainfall variables between 2020s and 2080s under SSP5-8.5 scenario. For each variable (row), dark green indicates city with the smallest change (0), and red indicates city with the largest change (1).

City	rainfall	heavy_rainfall20	heavy_rainfall40	heavy_rainfall76
Calgary	0.2	0.26	0.26	0.23
Charlottetown	0.64	0.7	0.58	0.61
Edmonton	0.16	0.24	0.23	0.22
Fredericton	0.89	0.87	0.74	0.92
Halifax	0.86	0.92	1	1
Iqaluit	0.33	0.14	0.1	0.13
Montreal	0.73	0.72	0.55	0.61
Ottawa	0.62	0.64	0.45	0.3
Quebec City	1	0.88	0.7	0.52
Regina	0.15	0.22	0.22	0.36
St Johns	0.92	1	0.84	0.68
Toronto	0.42	0.55	0.4	0.37
Vancouver	0.98	0.93	0.69	0.65
Victoria	0.61	0.56	0.5	0.67
Whitehorse	0.04	0	0	0
Winnipeg	0.22	0.3	0.3	0.43
Yellowknife	0	0.05	0.06	0.15

Appendix B (Fitting linear and non-linear models to data)

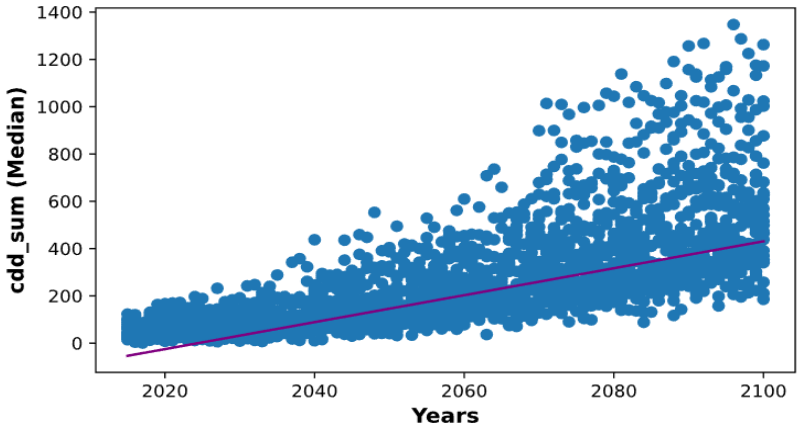

(a)

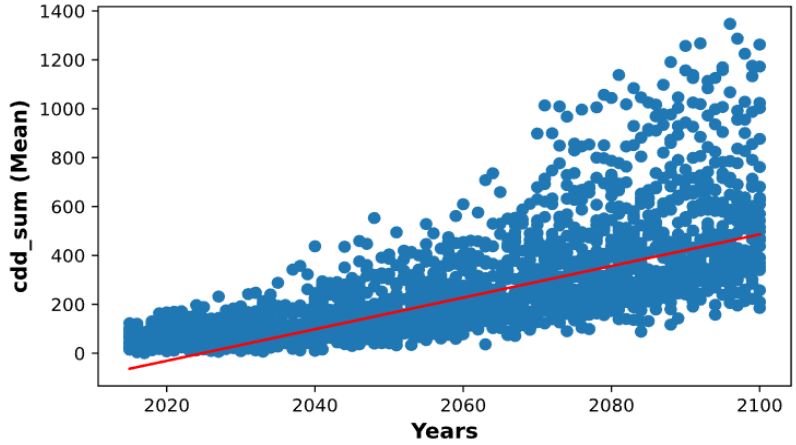

(b)

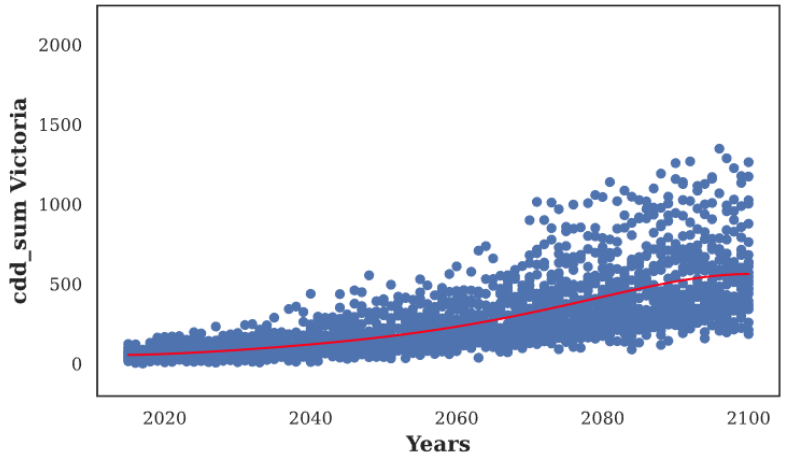

(c)

Figure 6. a) Fitting a linear model to the data, using the median of slopes and intercepts obtained by applying Sen's Slope Estimator to each model where median of the slopes is 5.7, and median of the intercepts is -53.75 (°C per year), b) Fitting a linear model to the data, using the mean of slopes and intercepts obtained by applying Sen's Slope Estimator to each model where mean of the slopes is 6.46, and mean of the intercepts is -63.32 (°C per year), and c) Fitting a non-linear (five-order polynomial) model to the data for the cdd_sum variable in Victoria.

Appendix C (The m-MK test results for the entire list of variables)

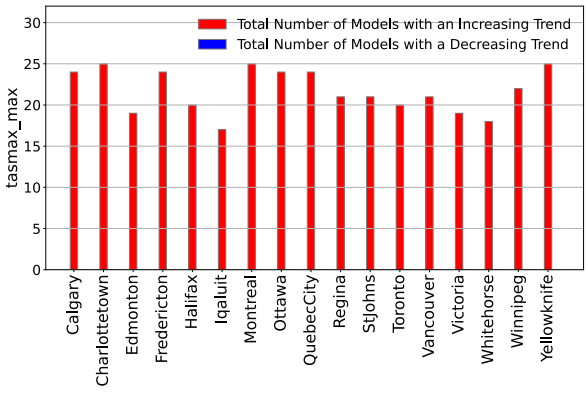

(a)

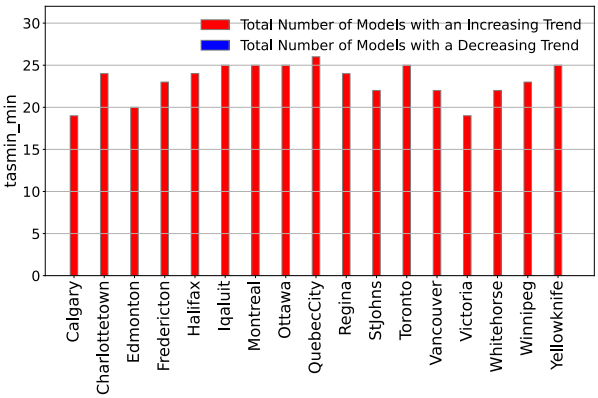

(b)

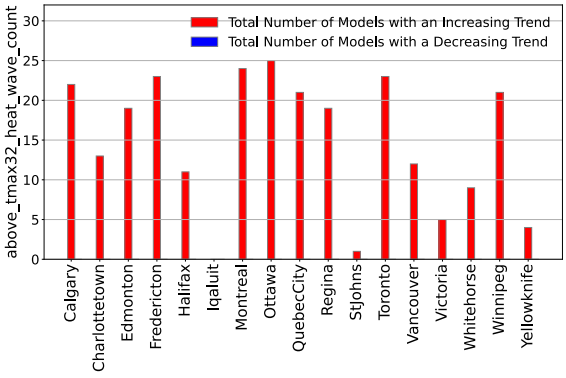

(c)

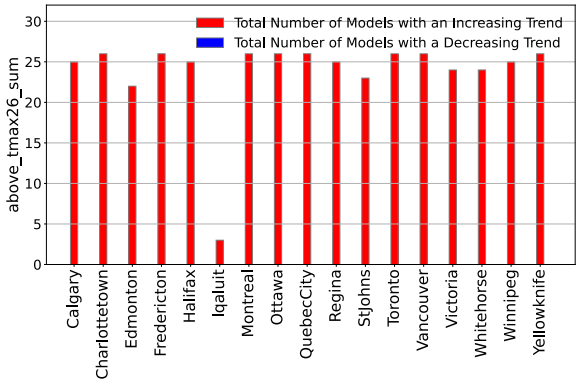

(d)

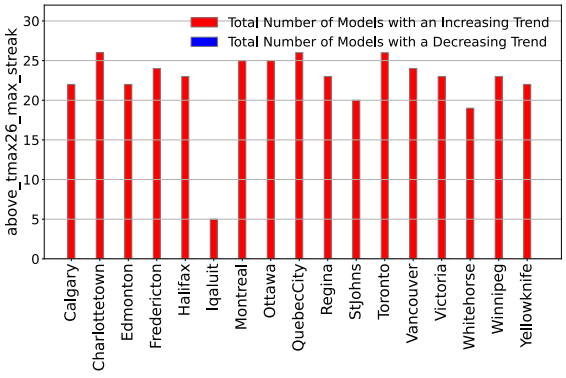

(e)

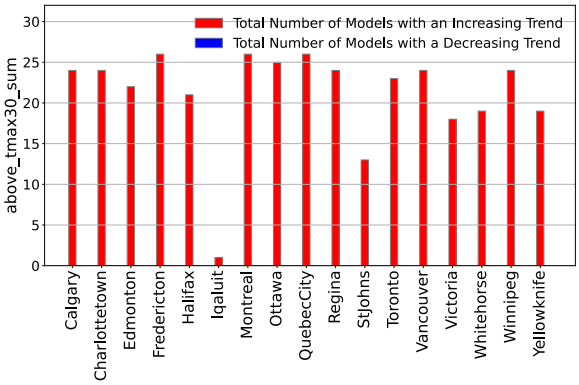

(f)

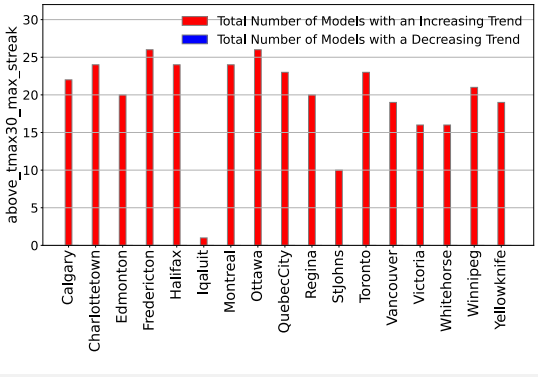

(g)

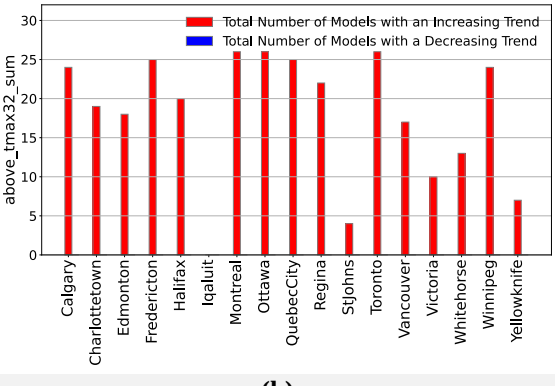

(h)

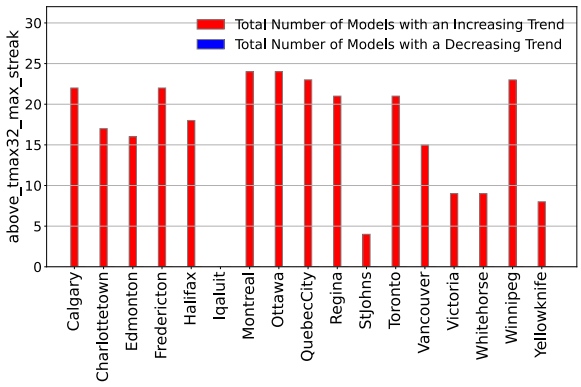
Total Number of Models with an Increasing Trend
Total Number of Models with a Decreasing Trend
above_tmax32_max_streak
Calgary
Charlottetown
Edmonton
Fredericton
Halifax
Iqaluit
Montreal
Ottawa
QuebecCity
Regina
StJohns
Toronto
Vancouver
Victoria
Whitehorse
Winnipeg
Yellowknife

(i)

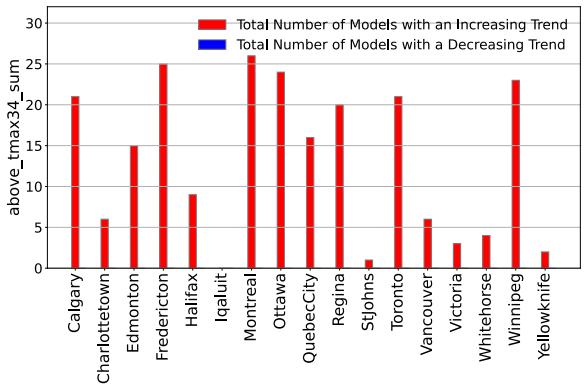
Total Number of Models with an Increasing Trend
Total Number of Models with a Decreasing Trend
above_tmax34_sum
Calgary
Charlottetown
Edmonton
Fredericton
Halifax
Iqaluit
Montreal
Ottawa
QuebecCity
Regina
StJohns
Toronto
Vancouver
Victoria
Whitehorse
Winnipeg
Yellowknife

(j)

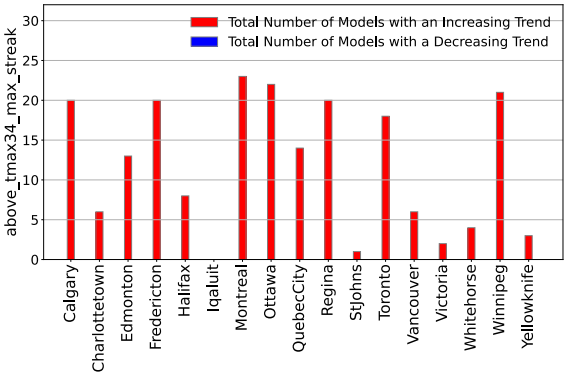
Total Number of Models with an Increasing Trend
Total Number of Models with a Decreasing Trend
above_tmax34_max_streak
Calgary
Charlottetown
Edmonton
Fredericton
Halifax
Iqaluit
Montreal
Ottawa
QuebecCity
Regina
StJohns
Toronto
Vancouver
Victoria
Whitehorse
Winnipeg
Yellowknife

(k)

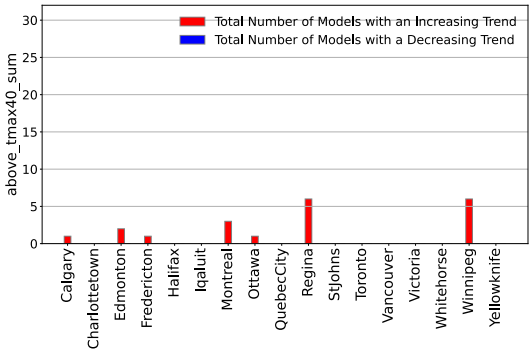
Total Number of Models with an Increasing Trend
Total Number of Models with a Decreasing Trend
above_tmax40_sum
Calgary
Charlottetown
Edmonton
Fredericton
Halifax
Iqaluit
Montreal
Ottawa
QuebecCity
Regina
StJohns
Toronto
Vancouver
Victoria
Whitehorse
Winnipeg
Yellowknife

(l)

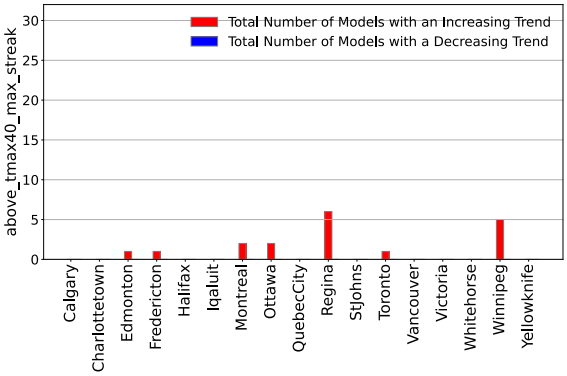
Total Number of Models with an Increasing Trend
Total Number of Models with a Decreasing Trend
above_tmax40_max_streak
Calgary
Charlottetown
Edmonton
Fredericton
Halifax
Iqaluit
Montreal
Ottawa
QuebecCity
Regina
StJohns
Toronto
Vancouver
Victoria
Whitehorse
Winnipeg
Yellowknife

(m)

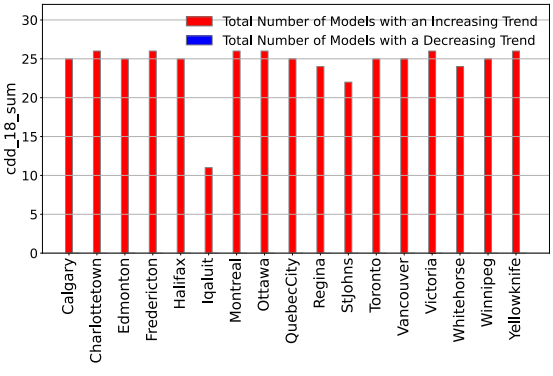
Total Number of Models with an Increasing Trend
Total Number of Models with a Decreasing Trend
cdd_18_sum
Calgary
Charlottetown
Edmonton
Fredericton
Halifax
Iqaluit
Montreal
Ottawa
QuebecCity
Regina
StJohns
Toronto
Vancouver
Victoria
Whitehorse
Winnipeg
Yellowknife

(n)

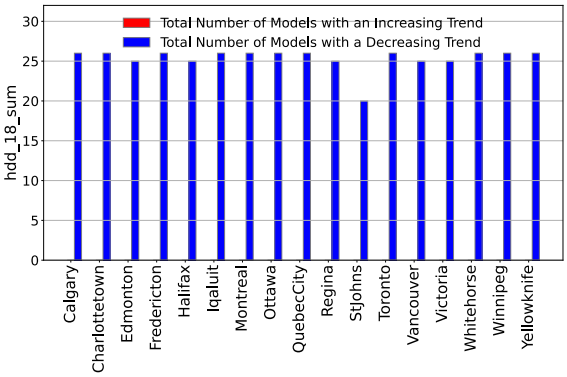
Total Number of Models with an Increasing Trend
Total Number of Models with a Decreasing Trend
hdd_18_sum
Calgary
Charlottetown
Edmonton
Fredericton
Halifax
Iqaluit
Montreal
Ottawa
QuebecCity
Regina
StJohns
Toronto
Vancouver
Victoria
Whitehorse
Winnipeg
Yellowknife

(o)

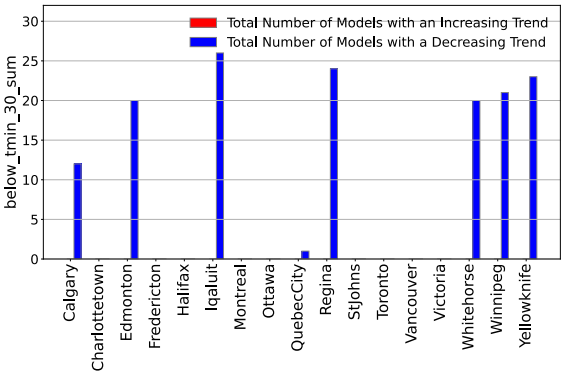
Total Number of Models with an Increasing Trend
Total Number of Models with a Decreasing Trend
below_tmin_30_sum
Calgary
Charlottetown
Edmonton
Fredericton
Halifax
Iqaluit
Montreal
Ottawa
QuebecCity
Regina
StJohns
Toronto
Vancouver
Victoria
Whitehorse
Winnipeg
Yellowknife

(p)

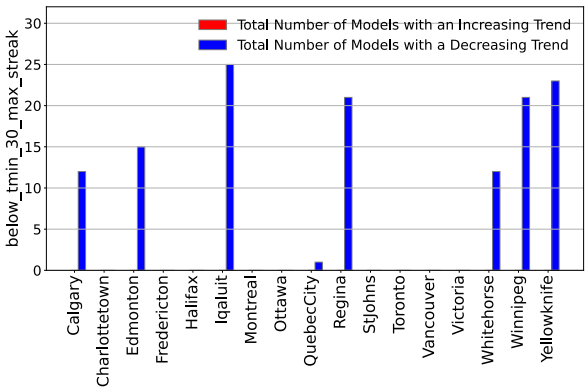

(q)

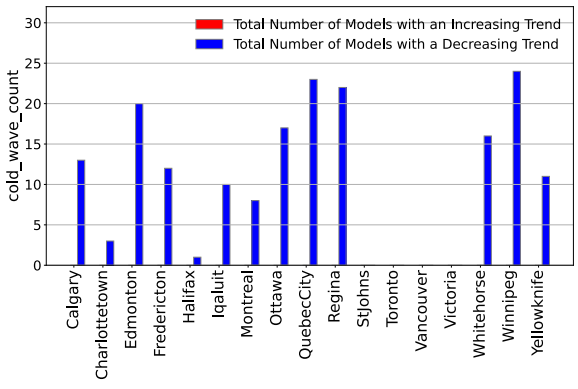

(r)

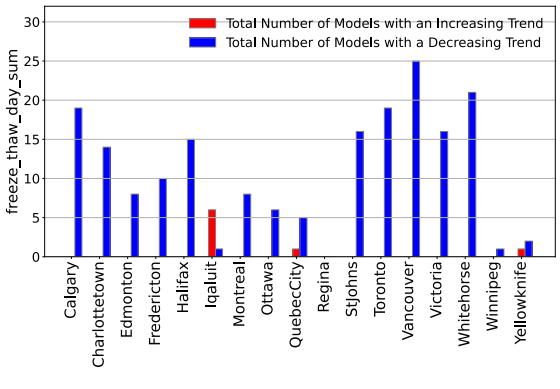

(s)

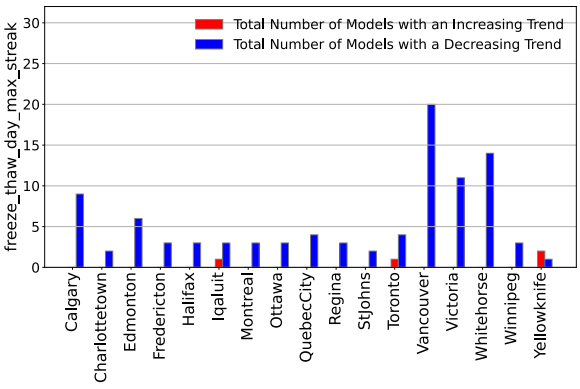

(t)

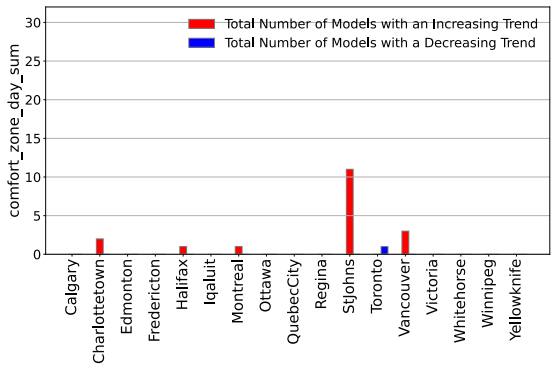

(u)

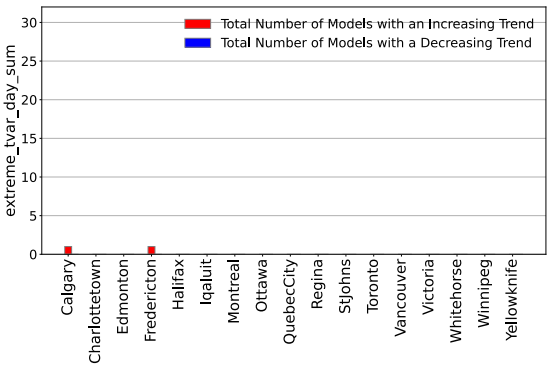

(v)

Figure 7. The results of the modified Mann-Kendall Trend test (m-MK test) (SSP2-4.5) for a) tasmax_max , b) tasmin_min, c) above_tmax32_heat_wave_count , d) above_tmax26_sum, e) above_tmax26_max_streak, f) above_tmax30_sum, g) above_tmax30_max_streak, h) above_tmax32_sum, i) above_tmax32_max_streak, j) above_tmax34_sum, k) above_tmax34_max_streak, l) above_tmax40_sum, m) above_tmax40_max_streak, n) cdd_sum_18, o) hdd_sum_18, p) below_tmin_30_sum, q) below_tmin_30_max_streak, r) cold_wave_count, s) freeze_thaw_day_sum, t) freeze_thaw_day_max_streak, u) comfort_zone_sum, and v) extreme_tvar_day_sum.

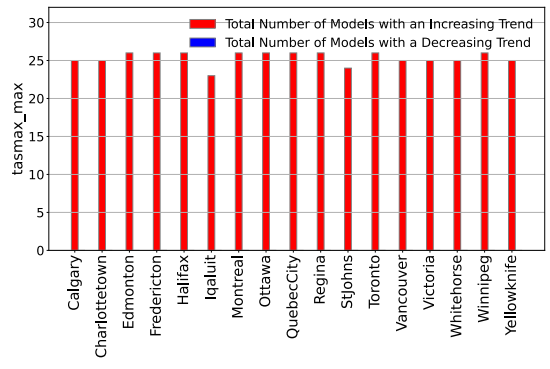

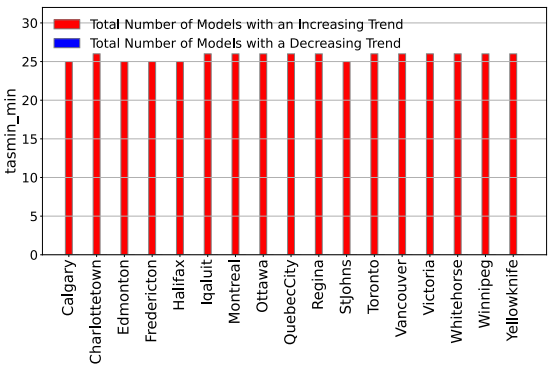

(a)

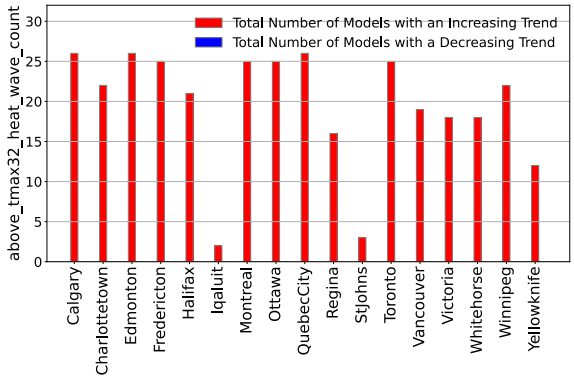
above_tmax32_heat_wave_count
Total Number of Models with an Increasing Trend
Total Number of Models with a Decreasing Trend
Calgary
Charlottetown
Edmonton
Fredericton
Halifax
Iqaluit
Montreal
Ottawa
QuebecCity
Regina
StJohns
Toronto
Vancouver
Victoria
Whitehorse
Winnipeg
Yellowknife

(b)

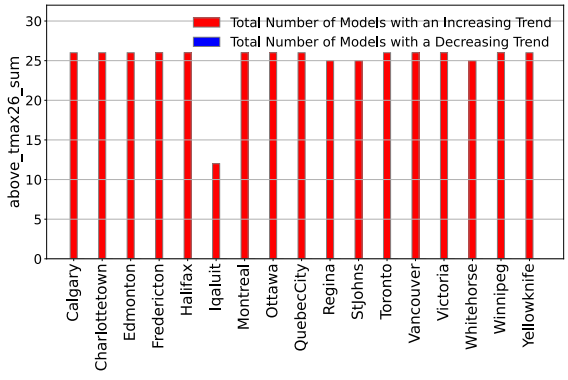
above_tmax26_sum
Total Number of Models with an Increasing Trend
Total Number of Models with a Decreasing Trend
Calgary
Charlottetown
Edmonton
Fredericton
Halifax
Iqaluit
Montreal
Ottawa
QuebecCity
Regina
StJohns
Toronto
Vancouver
Victoria
Whitehorse
Winnipeg
Yellowknife

(c)

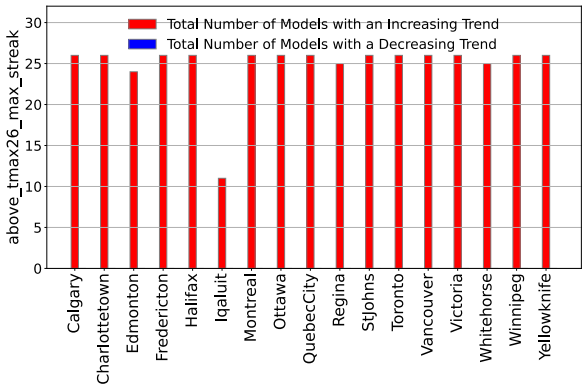
above_tmax26_max_streak
Total Number of Models with an Increasing Trend
Total Number of Models with a Decreasing Trend
Calgary
Charlottetown
Edmonton
Fredericton
Halifax
Iqaluit
Montreal
Ottawa
QuebecCity
Regina
StJohns
Toronto
Vancouver
Victoria
Whitehorse
Winnipeg
Yellowknife

(d)

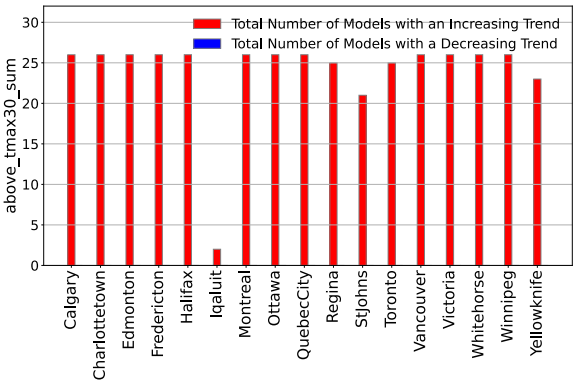
above_tmax30_sum
Total Number of Models with an Increasing Trend
Total Number of Models with a Decreasing Trend
Calgary
Charlottetown
Edmonton
Fredericton
Halifax
Iqaluit
Montreal
Ottawa
QuebecCity
Regina
StJohns
Toronto
Vancouver
Victoria
Whitehorse
Winnipeg
Yellowknife

(e)

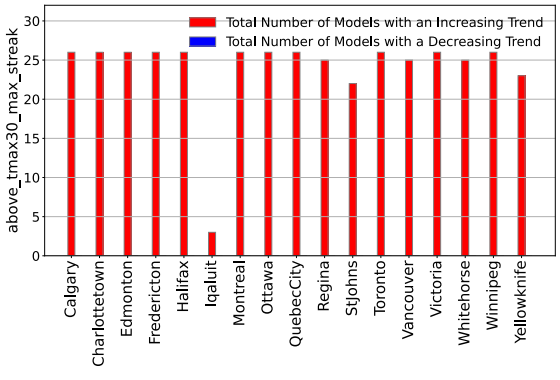
above_tmax30_max_streak
Total Number of Models with an Increasing Trend
Total Number of Models with a Decreasing Trend
Calgary
Charlottetown
Edmonton
Fredericton
Halifax
Iqaluit
Montreal
Ottawa
QuebecCity
Regina
StJohns
Toronto
Vancouver
Victoria
Whitehorse
Winnipeg
Yellowknife

(f)

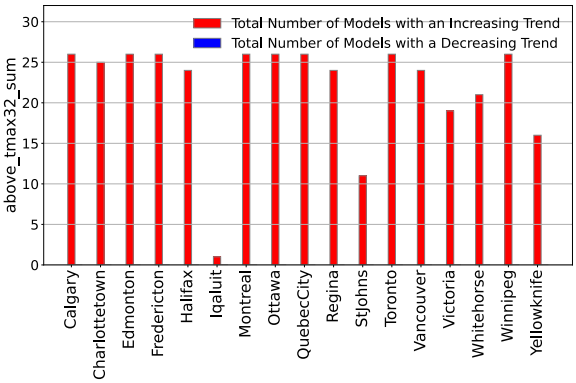
above_tmax32_sum
Total Number of Models with an Increasing Trend
Total Number of Models with a Decreasing Trend
Calgary
Charlottetown
Edmonton
Fredericton
Halifax
Iqaluit
Montreal
Ottawa
QuebecCity
Regina
StJohns
Toronto
Vancouver
Victoria
Whitehorse
Winnipeg
Yellowknife

(g)

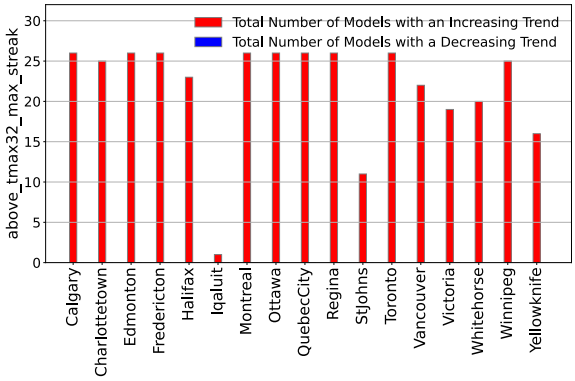
above_tmax32_max_streak
Total Number of Models with an Increasing Trend
Total Number of Models with a Decreasing Trend
Calgary
Charlottetown
Edmonton
Fredericton
Halifax
Iqaluit
Montreal
Ottawa
QuebecCity
Regina
StJohns
Toronto
Vancouver
Victoria
Whitehorse
Winnipeg
Yellowknife

(h)

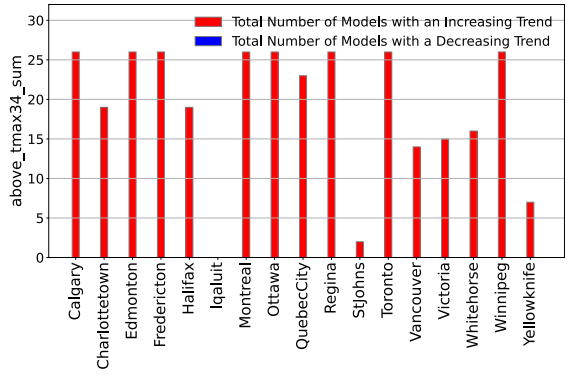
above_tmax34_sum
Total Number of Models with an Increasing Trend
Total Number of Models with a Decreasing Trend
Calgary
Charlottetown
Edmonton
Fredericton
Halifax
Iqaluit
Montreal
Ottawa
QuebecCity
Regina
StJohns
Toronto
Vancouver
Victoria
Whitehorse
Winnipeg
Yellowknife

(i)

(j)

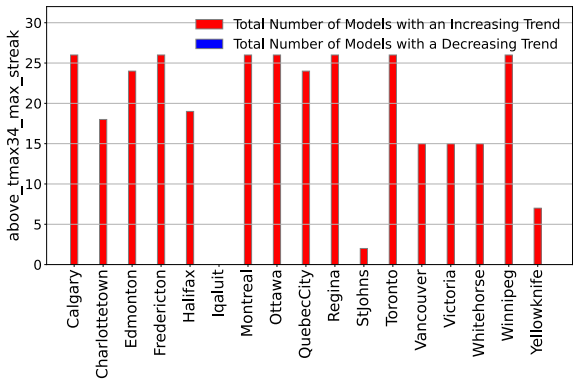
above_tmax34_max_streak
Total Number of Models with an Increasing Trend
Total Number of Models with a Decreasing Trend
Calgary
Charlottetown
Edmonton
Fredericton
Halifax
Iqaluit
Montreal
Ottawa
QuebecCity
Regina
StJohns
Toronto
Vancouver
Victoria
Whitehorse
Winnipeg
Yellowknife

(k)

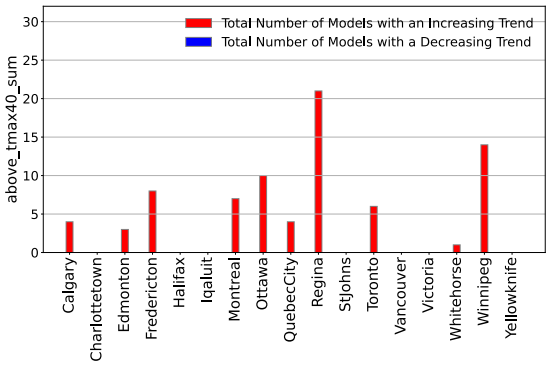
above_tmax40_sum
Total Number of Models with an Increasing Trend
Total Number of Models with a Decreasing Trend
Calgary
Charlottetown
Edmonton
Fredericton
Halifax
Iqaluit
Montreal
Ottawa
QuebecCity
Regina
StJohns
Toronto
Vancouver
Victoria
Whitehorse
Winnipeg
Yellowknife

(l)

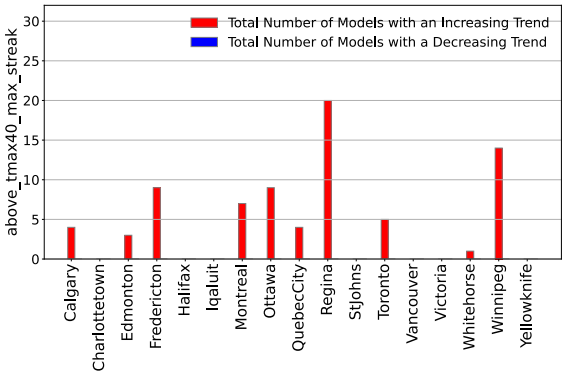
above_tmax40_max_streak
Total Number of Models with an Increasing Trend
Total Number of Models with a Decreasing Trend
Calgary
Charlottetown
Edmonton
Fredericton
Halifax
Iqaluit
Montreal
Ottawa
QuebecCity
Regina
StJohns
Toronto
Vancouver
Victoria
Whitehorse
Winnipeg
Yellowknife

(m)

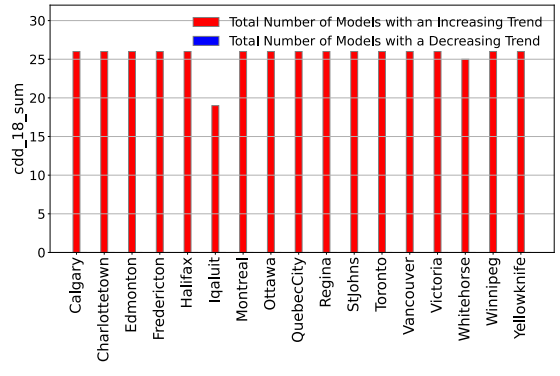
cdd_18_sum
Total Number of Models with an Increasing Trend
Total Number of Models with a Decreasing Trend
Calgary
Charlottetown
Edmonton
Fredericton
Halifax
Iqaluit
Montreal
Ottawa
QuebecCity
Regina
StJohns
Toronto
Vancouver
Victoria
Whitehorse
Winnipeg
Yellowknife

(n)

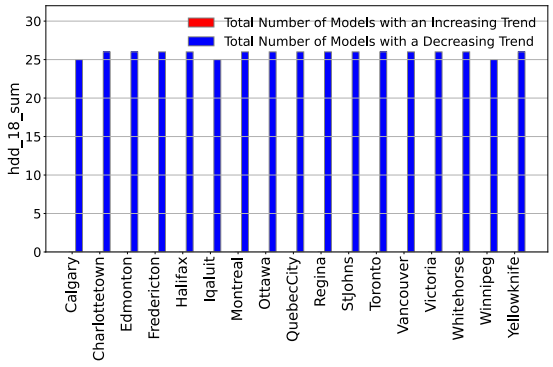
hdd_18_sum
Total Number of Models with an Increasing Trend
Total Number of Models with a Decreasing Trend
Calgary
Charlottetown
Edmonton
Fredericton
Halifax
Iqaluit
Montreal
Ottawa
QuebecCity
Regina
StJohns
Toronto
Vancouver
Victoria
Whitehorse
Winnipeg
Yellowknife

(o)

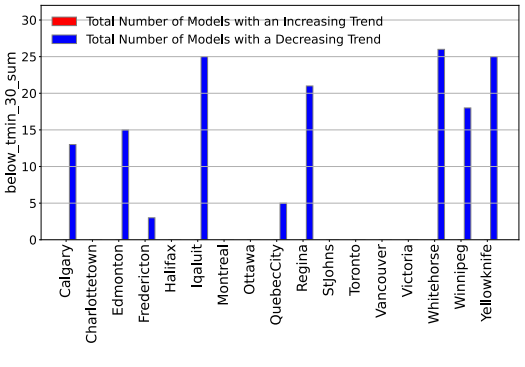
below_tmin_30_sum
Total Number of Models with an Increasing Trend
Total Number of Models with a Decreasing Trend
Calgary
Charlottetown
Edmonton
Fredericton
Halifax
Iqaluit
Montreal
Ottawa
QuebecCity
Regina
StJohns
Toronto
Vancouver
Victoria
Whitehorse
Winnipeg
Yellowknife

(p)

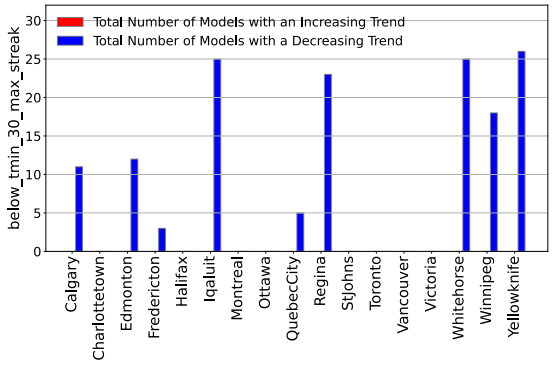
below_tmin_30_max_streak
Total Number of Models with an Increasing Trend
Total Number of Models with a Decreasing Trend
Calgary
Charlottetown
Edmonton
Fredericton
Halifax
Iqaluit
Montreal
Ottawa
QuebecCity
Regina
StJohns
Toronto
Vancouver
Victoria
Whitehorse
Winnipeg
Yellowknife

(q)

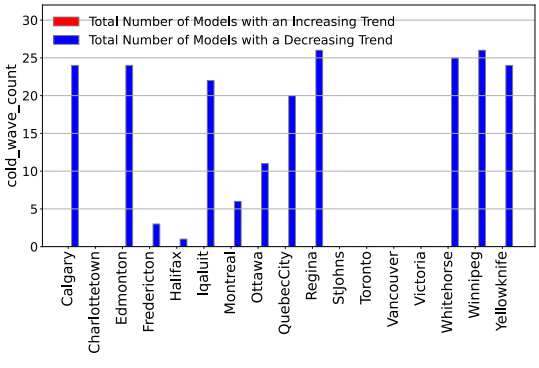
cold_wave_count
Total Number of Models with an Increasing Trend
Total Number of Models with a Decreasing Trend
Calgary
Charlottetown
Edmonton
Fredericton
Halifax
Iqaluit
Montreal
Ottawa
QuebecCity
Regina
StJohns
Toronto
Vancouver
Victoria
Whitehorse
Winnipeg
Yellowknife

(r)

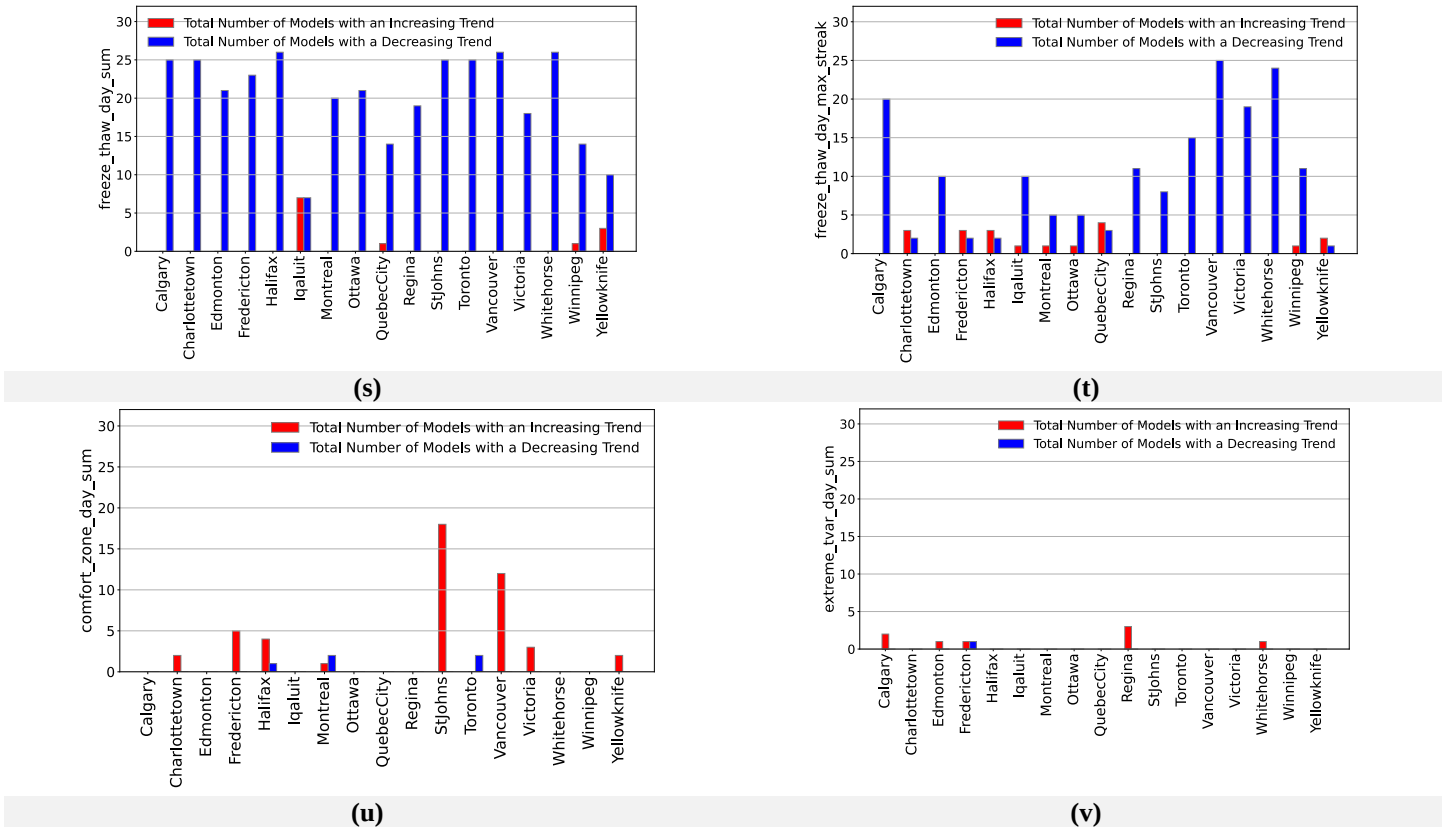

Figure 8. The results of the modified Mann-Kendall Trend test (m-MK test) (SSP5-8.5) for a) tasmax_max , b) tasmin_min, c) above_tmax32_heat_wave_count , d) above_tmax26_sum, e) above_tmax26_max_streak, f) above_tmax30_sum, g) above_tmax30_max_streak, h) above_tmax32_sum, i) above_tmax32_max_streak, j) above_tmax34_sum, k) above_tmax34_max_streak, l) above_tmax40_sum, m) above_tmax40_max_streak, n) cdd_sum_18, o) hdd_sum_18, p) below_tmin_30_sum, q) below_tmin_30_max_streak, r) cold_wave_count, s) freeze_thaw_day_sum, t) freeze_thaw_day_max_streak, u) comfort_zone_sum, and v) extreme_tvar_day_sum.

Appendix D (The Euclidean distance results under SSP2-4.5 and comparison between the results under SSP2-4.5 and SSP5-8.5)

Table 12. Normalized Euclidean distance of the precipitation related variables (SSP2-4.5) between 2020s and 2080s. For each variable (row), dark green indicates city with the smallest change (0), and red indicates city with the largest change (1).

City	pr_sum	heavy_pr20_sum	heavy_pr40_sum	heavy_pr76_sum	dry_day0p2_sum	dry_day0p2_max_streak
Calgary	0.24	0.31	0.27	0.26	0.32	0.56
Edmonton	0.29	0.3	0.28	0.23	0.71	0.37
Regina	0.23	0.28	0.25	0.45	0.54	0.51
Winnipeg	0.34	0.41	0.41	0.46	0.36	0.43
Montreal	0.54	0.66	0.51	0.59	0.18	0.11
Ottawa	0.44	0.59	0.39	0.33	0.25	0.07
QuebecCity	0.7	0.87	0.67	0.55	0.21	0.08
Toronto	0.47	0.58	0.43	0.4	0.24	0.17

Vancouver	1	1	0.68	0.59	0.88	0.88
Victoria	0.66	0.61	0.53	0.67	0.81	1
Charlottetown	0.59	0.75	0.62	0.69	0.06	0.04
Fredericton	0.7	0.77	0.69	0.87	0.11	0.06
Halifax	0.83	0.99	1	1	0.02	0.04
StJohns	0.65	0.92	0.74	0.66	0	0
Iqaluit	0.2	0.16	0.12	0	1	0.17
Whitehorse	0	0	0	0	0.55	0.39
Yellowknife	0	0.07	0.08	0	0.52	0.41

Table 13. Normalized Euclidean distance of the temperature related variables (SSP2-4.5) between 2020s and 2080s. For each variable (row), dark green indicates city with the smallest change (0), and red indicates city with the largest change (1).

City	tasmax_max	above_tmax26_sum	above_tmax26_max_streak	above_tmax30_sum	above_tmax30_max_streak	above_tmax32_sum	above_tmax32_max_streak	above_tmax32_heat_wave_count	above_tmax34_sum	above_tmax34_max_streak	above_tmax40_sum	above_tmax40_max_streak	tasmin_min	cold_wave_count	below_tmin_30_sum	below_tmin_30_max_streak	hdd_18_sum	cdd_18_sum	freeze_thaw_day_sum	freeze_thaw_day_max_streak	extreme_tvar_day_sum	comfort_zone_day_sum
Calgary	0.23	0.88	0.53	0.72	0.57	0.61	0.55	0.73	0.52	0.55	0.38	0.44	0.74	0.65	0.17	0.27	0.28	0.61	1	0.57	0.67	0
Edmonton	0.31	0.89	0.51	0.67	0.45	0.55	0.46	0.65	0.44	0.5	0.27	0.36	0.96	0.73	0.23	0.32	0.31	0.65	0.67	0.41	0.34	0.09
Regina	0.41	0.89	0.77	0.98	1	1	1	0.95	1	1	1	1	0.87	0.83	0.32	0.4	0.33	0.94	0.68	0.45	1	0.1
Winnipeg	0.35	0.92	0.8	1	0.84	0.98	0.88	1	0.93	0.83	0.54	0.64	0.95	0.89	0.27	0.36	0.36	1	0.49	0.23	0.38	0.16
Montreal	0.21	0.85	0.81	0.89	0.7	0.76	0.65	0.94	0.59	0.51	0.22	0.35	0.88	0.41	0.01	0.03	0.2	0.93	0.4	0.08	0.06	0.71
Ottawa	0.25	0.83	0.79	0.88	0.71	0.81	0.66	0.94	0.67	0.59	0.34	0.48	1	0.55	0.02	0.05	0.22	0.9	0.38	0.18	0.16	0.47
QuebecCity	0.12	0.84	0.56	0.65	0.39	0.47	0.33	0.68	0.32	0.33	0.09	0.19	0.71	0.65	0.03	0.07	0.28	0.71	0.4	0.3	0.12	0.42
Toronto	0.2	0.88	1	0.85	0.67	0.72	0.59	0.89	0.56	0.49	0.32	0.43	0.79	0.03	0	0	0.1	0.94	0.69	0.14	0.07	0.86
Vancouver	0.21	1	0.67	0.4	0.31	0.25	0.26	0.34	0.17	0.24	0.02	0.03	0.53	0	0	0	0	0.72	0.3	0.21	0	0.46
Victoria	0.3	0.77	0.41	0.22	0.15	0.14	0.16	0.26	0.09	0.14	0.02	0.03	0.35	0	0	0	0	0.53	0	0	0.03	0.18
Charlottetown	0.01	0.79	0.57	0.51	0.3	0.27	0.25	0.43	0.12	0.15	0.01	0.03	0.6	0.13	0	0.01	0.15	0.72	0.44	0.2	0.15	1
Fredericton	0.09	0.78	0.62	0.7	0.53	0.61	0.47	0.84	0.46	0.43	0.18	0.31	0.95	0.37	0.02	0.05	0.2	0.74	0.47	0.26	0.39	0.46
Halifax	0.04	0.82	0.54	0.43	0.28	0.23	0.18	0.36	0.12	0.16	0.04	0.1	0.45	0.07	0	0	0.1	0.65	0.55	0.25	0.1	0.72
StJohns	0	0.59	0.21	0.17	0.09	0.05	0.07	0.08	0.01	0.02	0	0	0	0.02	0	0	0.17	0.45	0.76	0.35	0.04	0.93
Iqaluit	1	0	0	0	0	0	0	0	0	0	0	0	0.83	1	1	1	1	0	0.36	0.3	0.18	0
Whitehorse	0.61	0.58	0.23	0.27	0.24	0.2	0.27	0.27	0.16	0.27	0.07	0.14	0.77	0.77	0.49	0.54	0.59	0.25	0.8	1	0.58	0
Yellowknife	0.31	0.48	0.2	0.23	0.2	0.13	0.18	0.2	0.09	0.16	0.02	0.05	0.56	0.79	0.96	0.75	0.71	0.37	0.35	0.46	0.11	0.16

Table 14. Difference in Euclidean distance between precipitation-related variables under SSP5-8.5 and SSP2-4.5.

City	pr_sum	heavy_pr20_sum	heavy_pr40_sum	heavy_pr76_sum	dry_day0p2_sum	dry_day0p2_max_streak
Calgary	197.6	2.0	1.6	0.0	4.7	-10.5
Edmonton	-114.2	0.4	-0.1	0.2	-17.9	0.1
Regina	33.7	0.4	0.4	-0.6	-47.5	11.8
Winnipeg	-157.9	-1.9	-2.8	0.2	-23.7	-23.9
Montreal	508.7	19.9	5.3	1.0	-16.1	-4.3
Ottawa	563.3	17.2	6.0	0.1	-9.9	4.6
Quebec City	575.4	19.0	5.5	0.3	-25.7	-2.6
Toronto	-24.3	7.7	1.1	0.1	-21.7	-5.4
Vancouver	310.4	10.9	4.8	1.6	18.1	27.9
Victoria	183.7	7.0	1.4	0.9	21.1	33.2
Charlottetown	24.4	7.8	1.0	-0.2	9.5	4.1
Fredericton	409.8	23.3	6.5	2.0	-15.5	3.0
Halifax	122.7	7.3	5.2	1.7	-1.2	7.9
StJohns	789.4	21.4	10.1	1.2	-4.6	5.1
Iqaluit	643.5	3.4	0.6	1.7	86.0	-9.8
Whitehorse	333.8	1.9	1.1	0.0	19.2	-0.6
Yellowknife	273.1	0.5	0.1	2.0	4.4	-9.9

Table 15. Difference in Euclidean distance between temperature-related variables under SSP5-8.5 and SSP2-4.5.

City	tasmax_max	above_tmax26_sum	above_tmax26_max_streak	above_tmax30_sum	above_tmax30_max_streak	above_tmax32_sum	above_tmax32_max_streak	above_tmax32_heat_wave_count	above_tmax34_sum	above_tmax34_max_streak	above_tmax40_sum	above_tmax40_max_streak	tasmin_min	cold_wave_count	below_tmin_30_sum	below_tmin_30_max_streak	hdd_18_sum	cdd_18_sum	freeze_thaw_day_sum	freeze_thaw_day_max_streak	extreme_tvar_day_sum	comfort_zone_day_sum
Calgary	46.5	327.8	296.6	377.9	223.4	372.0	191.2	26.7	325.9	154.7	106.3	45.4	37.9	3.3	-6.7	-4.5	7568.3	4294.9	234.4	16.5	21.4	2.6
Edmonton	48.1	342.3	325.3	384.0	235.7	363.3	171.8	32.1	307.9	127.2	91.2	42.3	52.0	9.7	0.3	5.9	8155.6	4497.5	125.1	5.6	3.8	2.7
Regina	47.7	268.7	330.8	302.9	258.9	323.5	240.0	7.6	330.6	193.4	212.5	103.5	54.5	14.6	7.9	8.6	8648.4	5093.2	43.1	-3.7	-2.5	1.6
Winnipeg	47.6	272.5	375.5	344.2	270.4	358.8	210.1	12.9	361.7	190.9	186.5	80.0	64.4	21.6	3.3	1.3	9667.3	5182.6	51.0	6.3	-0.7	0.4
Charlottetown	30.0	394.3	321.9	360.0	214.4	278.6	107.5	42.1	163.1	60.0	9.9	5.6	51.4	1.5	-0.4	-0.4	7875.7	4076.0	105.9	-2.3	-2.3	0.7
Fredericton	36.2	383.2	377.6	405.0	236.2	356.2	199.7	32.9	298.8	126.7	103.9	42.2	64.7	3.5	0.4	0.2	8536.7	4679.4	129.0	17.2	1.0	0.3
Halifax	29.3	410.1	386.6	353.0	200.2	238.7	97.7	34.5	140.5	49.9	13.8	5.2	49.7	0.6	0.0	0.0	7282.3	3794.9	157.2	3.0	1.0	0.0

StJohns	21.5	272.8	161.8	189.1	78.8	110.4	39.5	22.8	53.1	28.5	0.0	0.0	40.3	0.4	0.0	0.0	7055.1	2487.6	181.3	3.5	0.0	15.5
Montreal	40.5	396.2	454.5	479.5	325.2	462.5	233.9	36.5	394.6	167.6	142.7	51.6	74.3	1.3	-0.2	-1.1	8168.2	5900.9	119.7	1.4	2.1	-2.0
Ottawa	40.2	393.3	433.0	483.4	329.7	444.3	221.2	33.5	390.5	174.1	152.2	65.1	71.8	-0.1	-1.8	-1.8	8094.6	5820.0	136.9	2.4	0.8	-1.1
Quebec City	45.0	422.4	410.9	445.5	251.0	394.7	169.8	45.3	300.2	112.4	100.0	32.3	72.8	7.4	2.3	0.0	9437.1	4872.4	63.5	6.9	2.9	0.3
Toronto	37.0	432.4	451.4	483.6	378.1	427.5	246.6	34.5	353.5	174.9	96.7	49.1	65.6	-0.6	0.0	0.0	7316.0	6028.9	152.0	11.7	-1.4	2.1
Vancouver	35.9	456.0	461.1	481.1	326.1	346.4	200.3	30.6	200.8	110.1	16.5	11.2	35.3	0.0	0.0	0.0	5537.5	4846.3	6.9	3.5	2.0	14.1
Victoria	31.4	516.3	469.4	363.4	216.4	208.1	104.2	26.1	106.6	41.4	12.4	10.3	24.2	0.0	0.0	0.0	5480.5	4356.1	-3.7	0.3	0.0	11.0
Iqaluit	21.6	57.0	25.6	22.2	12.8	17.7	14.1	3.4	13.7	10.2	0.0	0.0	81.4	42.3	86.7	13.4	16969.1	475.1	0.6	-9.8	0.4	1.7
Whitehorse	42.8	345.8	191.5	248.0	97.1	181.4	61.8	28.0	128.8	49.8	25.3	17.8	53.3	15.9	37.9	9.3	10242.7	2635.2	138.4	16.9	1.5	2.4
Yellowknife	27.8	308.4	168.4	215.6	82.7	145.7	52.4	23.1	84.9	33.1	6.1	4.6	72.8	28.2	133.8	37.6	13668.3	2650.9	15.8	-8.5	-1.1	5.2

Chapter 3: Residential Flood Risk in Metro Vancouver due to Climate Change using Probability Boxes

Abstract

To enhance the decision-making process and reduce economic losses caused by future flooding, it is critical to quantify uncertainty in each step of flood risk analysis. To address the often-missing uncertainty quantification, we propose a new methodology that combines damage functions and probability bounds analysis. We estimate the likely direct tangible damage to 375,973 residential buildings along the Fraser River through Metro Vancouver, Canada, for a range of climate change driven flood scenarios, while transparently representing the associated uncertainties caused by sampling error, imprecise measurement, and uncertainty in building height and basement conditions. Furthermore, for the purposes of developing effective management strategies, uncertainties in this study are classified into two categories, namely aleatory and epistemic. According to our findings and absent significant action, we should expect an enormous increase in flood damage to the four categories of residential buildings considered in this study by the year 2100. Moreover, the results show that second-order Monte Carlo simulation cannot adequately represent epistemic uncertainty for small sample sizes. In such a case, we recommend employing a probability box to delineate the epistemic uncertainty.

1. Introduction

Estimating the probability and consequences of a flood event is very challenging. Flood analysis is often undertaken using models and expert judgment as a result of scarcity and unavailability of statistical information on the probability and consequences of a flood event (Gouldby et al. 2009). Models are imperfect depictions of the real system, resulting in intrinsically uncertain findings. Human expert judgment is also subjective and inherently uncertain (Gouldby et al. 2009). As a result, every flood risk assessment is accompanied by uncertainty while climate change, and anthropogenic changes to basin water supplies, have also greatly exacerbated these uncertainties in recent years. The resulting discrepancies between the modelled variables and their "real" values are mostly caused by uncertainty in the input data, parameters, and model structure. However, as highlighted by Dimitriadis et al. (2016), the uncertainty associated with an input variable can sometimes be more significant than the overall uncertainty associated with each model. Furthermore, depending on the modelled variable, the sources of uncertainty and their significance could be varied. For example, as reported by Dimitriadis et al. (2016), in flood hazard maps extracted from hydraulic simulation, increasing the floodplain friction, the lateral gradient, and the grid cell size increases flood volume uncertainty, whereas increasing the input discharge, the longitudinal gradient, and the channel friction decreases flood volume uncertainty.

As reported by Tate et al. (2015), most of the assessed sources of uncertainty are flood hazard-related, such as flood frequency analysis, and stage-discharge rating curves. There are not many studies in which uncertainty is factored into flood damage estimates, and the limited existing ones mostly focus on the hydrological and hydraulic components. For instance, Apel et al. (2004) derives uncertainty bounds associated with economic risks. While they consider many sources of uncertainty, all of them are related to hydrological components. De Moel et al. (2012) evaluates the contribution of inundation depth, land use, value of elements at risk and depth–damage curves on uncertainty in the flood damage estimates for a single dike ring in the Netherlands. Egorova et al. (2008) and Wagenaar et al. (2016) quantify the uncertainty in the damage estimates, focusing on different flood damage functions as well as maximum damages. Nofal et al. (2020) propagate uncertainties in flood depth and component repair/replacement costs in their 2D and 3D flood fragility and loss functions for one-story single-family residential buildings. Merz et al. (2004) quantifies the variability associated with damage estimates by categorizing buildings in the study area as "private housing" or "manufacturing," with both sectors further classified as "flooded cellar only" or "flooded stories". Freni et al. (2010) and Bubeck et al. (2011) conclude that depth-damage functions are the main source of uncertainty. Although depth-damage functions play a significant role in the uncertainty associated with flood damage estimates, failure to account for other sources of uncertainty can result in miscalculation and massive economic losses. Therefore, in this study, we intend to provide a framework for understanding and anticipating potential flood damage and its associated uncertainties, other than uncertainties caused by depth-damage functions.

Using sample data in flood damage assessment is a common approach. However, small sample size, as well as imprecise measurements and the use of subjective information complicate modelling and estimation and bring into question whether the available information is adequate for probabilistic modelling. Therefore, we need to assess and communicate the uncertainty caused by using sample data to decision makers in a transparent manner. This is one of the objectives of this research. Another important goal of this research is to distinguish between aleatory and epistemic uncertainty in flood damage analysis, and present both simultaneously. While epistemic uncertainty contributes significantly to the uncertainty associated with damage estimation, most previous studies have focused on aleatory (natural variability) uncertainty, with only a few studies presenting both aleatory and epistemic uncertainty using different depth-damage-functions as well as flood loss estimation models (Merz & Thieken 2009) or using two-layer Monte Carlo simulation (Apel et al. 2004). The problem with using several depth-damage-functions and flood loss estimation models to drive uncertainty estimation is that such damage functions and models are not available for all regions; additionally, depth damage functions and loss estimation models cannot be directly compared due to different methodologies used for various damage models, as well as different architectural and structural design in different countries. Furthermore, using the second order Monte Carlo simulation is both time-consuming and computationally intensive. Our proposed method is an alternative to the above-mentioned methods for representing aleatory and epistemic uncertainty, accounts for sampling and measurement error and runs in seconds on desktop computers.

The remainder of this paper is organised as follows. First, the fundamentals of probability box theory and the construction of the probability box are introduced. Thereafter is a brief review of the various types of damage caused by flooding, as well as the various types of flood depth-damage functions in section 3. The methodology and case study follows in section 4. Finally, the results, as well as a comparison of probability box and second order Monte Carlo simulation are presented in section 5.

2. P-box

A probability box, or a p-box is a computationally practical calculation of the theory of imprecise probabilities (Walley 1991) which combines standard interval analysis with traditional probability theory (Ferson and Tucker 2008, Beer et al. 2013).

$[\overline{F}_X, \underline{F}_X]$ is a "probability box" or "p-box" of the imprecisely known cumulative distribution function F_X, when the non-decreasing functions $\overline{F}_X$ and $\underline{F}_X$ circumscribe it such that $\underline{F}_X(x) \leq F_X(x) \leq \overline{F}_X(x)$ for supported values of x. $\underline{F}_X(x)$, which is the probability that the random variable X is smaller than x, represents a lower bound on probabilities and an upper bound on quantiles, and $\overline{F}_X(x)$ which is the probability that the random variable X is not larger than *x*, is an upper bound on probabilities and a lower bound on quantiles (Ferson et al. 2003). Upper and lower bounds on distribution functions can be calculated using a lower probability measure $\underline{P}$ for a random variable X as in equations (1) and (2) (Walley 1991) where $\underline{P}$ is measure of evidence in favor of X or measure of belief in X.

$$\underline{F}_X(x) = \underline{P}(X \leq x) \tag{1}$$

$$\overline{F}_X(x) = \overline{P}(X \leq x) = 1 - \underline{P}(X > x) \tag{2}$$

The probability bounding method enables analysts to perform calculations even if there is doubt about the distribution parameters, shape of the probability distribution, and dependencies between variables (Beer et al. 2013).

Another important advantage of using probability boxes is distinguishing between the two essentially distinct types of uncertainty, namely "variability" and "incertitude". Variability, also known as aleatory uncertainty, is caused by heterogeneity, environmental stochasticity, temporal fluctuations, spatial variation, or other variations among components or individuals (Ferson et al. 2003). Incertitude, also known as epistemic uncertainty, is caused by lack of knowledge or inadequate information as a result of measurement inaccuracy, potential biases in empirical design, small sample sizes, and surrogate data (Ferson et al. 2010). Probability box separates aleatory and epistemic uncertainty and propagates them through different mathematical expressions, allowing each to retain its own characteristic. Aleatory uncertainty is propagated according to probability theory rules, whereas epistemic uncertainty is propagated using interval analysis rules (Ferson & Tucker 2008).

Five techniques are available for presenting empirical and theoretical data in a p-box (Ferson et al. 2003) as follows. First, direct assumption: Sometimes analysts may have knowledge of a system that includes at least a partial mechanical understanding of how variation emerges in a certain quantity; This knowledge, however, may be limited in a way that enables the analyst to specify the shape or family of the distribution but not exactly what the parameters of the distribution are. In this situation, it is easy to build a p-box that encloses all possible cumulative distribution functions (CDFs). Second, modeling: The modeling technique breaks the estimation problem down into sub-problems that are expected to be easier to solve, and then reconstructs the desired estimate from those parts. Third, robust Bayes methods: Finding an accurate prior distribution and an appropriate likelihood function, which are used in a standard application of Bayes' rule to obtain a posterior distribution, might be challenging in some cases. In this instance, the robust Bayes technique, which applies standard Bayesian analysis to all possible combinations of prior distributions and likelihood functions, can be utilised. The analyst chooses the mentioned combinations from empirically plausible classes of priors and likelihoods. Fourth, constraint specification: This approach generates p-boxes by utilizing available information about a distribution or its underlying random variable as

constraints. Information about summary statistics, quantile bounds, and qualitative information about distribution shape are all examples of information that can be used to circumscribe the distribution of a random variable in this technique. Fifth, observation of measurements: This approach can be used to deal with measurement uncertainty and/or sampling uncertainty associated with empirical data. The observation of measurements technique was used in this study to implement our data in p-boxes. This technique is explained in further detail in the methodology section.

3. Flood Damage

Flood damages are broadly divided into two classes: tangible damage and intangible damage. Tangible damages are those which can be quantified in monetary terms such as damage to buildings, powerlines, roads, etc. While intangible damages are ones where their monetary values are difficult to determine such as loss-of-life, flood damage to environmental quality and social wellbeing, etc. (Kang et al. 2005). Each of these two groups is subdivided further into direct and indirect classifications. Direct damage is caused by physical contact with floodwater; indirect flood damage occurs as a result of interruption and disruption of economic and social activities induced by direct flood damage (Dutta et al. 2001). Indirect damage can be calculated as a percentage of the direct damage (Breaden 1971). In this study, we focus on direct tangible damage, which is the major class of flood damages, as realised from the review of previous works on this subject (Merz et al. 2004).

According to Thieken et al. (2005), the severity of flood damage is affected by two types of factors: impact parameters and resistance parameters. The flood impact parameters which reflect the unique characteristics of a flood event include hydrological load (water level, flow velocity, and flood duration), as well as contamination. The resistance parameters, that capture the characteristics of the affected building, are divided into permanent resistance (building type, building material, and precautionary measures), and temporal resistance (flood warning and preparedness).

The stage-damage curves and damage-frequency curves are the two main methodologies for evaluating direct tangible damage to buildings caused by flooding (Federal Flood Damage Estimation Guidelines for Buildings and Infrastructure 2021). Damage-frequency curves show how damage varies as a function of flood frequency or return period. Stage-damage curves, which are the most frequent and widely accepted technique for assessing direct tangible damage at urban scales, represent the relationship between flood parameters and possible damage. Since water depth is the major damage variable, the stage damage curves usually represent damage as a function of water depth. Stage-damage functions are established separately for structure and content (movable inventory within the structure) damage.

There are two types of stage-damage functions: relative and absolute. The absolute damage functions give the absolute monetary amounts of damage to a building (Pistrika et al. 2014); thus, these types of functions have a short lifespan. The relative damage functions give damage in the percentage of the value of an asset (Thieken et al. 2005, Pistrika et al. 2014). The depth-damage functions used in this study are relative functions. As a result, the p-boxes generated almost never need to be updated by changes in property market values.

In addition to the distinction between absolute and relative damage functions, there is also the distinction between empirical and synthetic damage functions. The empirical method is based on damage data collected aftermath of a flood event, and the synthetic method, is based on expert knowledge, interview survey, or questionnaire (Thieken et al. 2005, Merz et al. 2010). Each method has its own set of advantages. Empirical functions, for example, can better reflect variability within a single building category (Merz et al. 2004), while synthetic functions can be used in any area

because they are based on hypothetical analyses rather than information from a real flood event (Smith 1994).

4. Methodology

The methodology assesses potential damage to detached homes as follows. A spatial inventory of buildings data is overlapped with flood inundation map for each scenario of interest to exclude the buildings without flood exposure and to derive flood elevation at the location of each building for the remaining ones. For each of the scenarios the flooded buildings are classified based on the number of stories and foundation type as follows: one-story with basement, one-story without basement, two-story with basement, and two-story without basement. The rationale for this selection is because in flood damage assessment, the type of foundations and main floor height are the most significant predictors of vulnerability. As emphasised by Bryant (2019), the majority of damages from small events (5 to 35 annual recurrence interval) are caused by groundwater and basement damage, particularly in homes with fully developed and furnished basements. Also, Abboud et al. (2018) showed the severity of flooding and basement floor elevation are highly correlated. Furthermore, the type of foundation has a considerable influence on the vulnerability of the building to flood. That is the reason flood insurance premiums differ across structures with basement foundations, crawl spaces, and slab foundations. Elevated structures often pay a lower premium in comparison to those that do not have a space between the dwelling and the ground level.

The damage functions used in this study calculate damage according to the input inundation depth. To calculate inundation depth for each building we use sample data since, as is common, we do not have the first story height for all the buildings in the study area. Moreover, the data have uncertainties from imprecise measurements. Therefore, two key factors that need to be considered here are measurement and sampling errors.

Measurement is an experimental procedure, and hence measurement findings cannot be guaranteed to be entirely accurate. According to the postulates of measurement theory (Rabinovich 2005): The true value of the measure exists and is constant. However, it cannot be found. Ferson et al. (2003), depicted how we can establish a p-box while considering the measurement error. Assume we have some sample data for a variable. We can consider these samples as triangles distributed along an x-axis. The bases of these triangles show the interval range associated with the measurements and the peaks of the triangles represent the best estimates as point values. As depicted in Figure 1, the corresponding p-box of these values is composed of two cumulative distribution functions. The Upper bound of this p-box is based on the left endpoints of the triangle bases and increments by a step function by 1/ (numbers of samples). The lower bound is based on the right endpoints of the triangle bases and increments in the same way as the upper bound. When the measurement uncertainties associated with the samples are negligible, the p-box degenerates to the cumulative empirical distribution function (EDF) (Ferson et al. 2003), while significant measurement uncertainties lead the p-box to be wide.

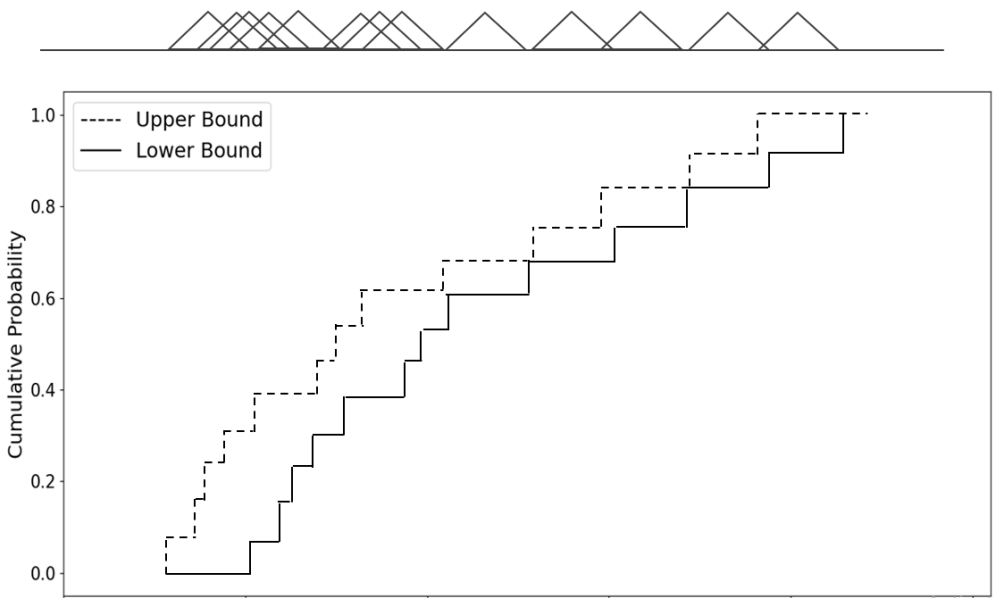

Figure 1. P-box (below) represents the data set (above). Triangles depict the data set, with the bases of these triangles illustrating the intervals around the best estimates (triangle peaks). Adapted from Ferson et al. (2003).

However, measuring all the members in a population of interest is not always feasible. In most cases, the available data represents only a small sample from a much larger population. This results in incertitude about the distribution function which is referred to as "sampling uncertainty" (Ferson et al. 2003). To account for the sampling uncertainty in the input data and propagate it consistently through the other steps of the analysis, as indicated by Ferson et al. (2003), we can apply Kolmogorov-Smirnov (KS) confidence limits to the measurement uncertainty bounds. Figure 2 shows bounds for expected damage for one of the scenarios studied here. The 95% Kolmogorov-Smirnov confidence limits applied to the sample data (solid lines) which means that the true distribution has a 95% chance of being inside the bounds. The dashed bounds show the expected damage distribution considering the measurement errors. The 95% KS confidence bounds convergence to the bounds prescribed for measurement errors as the number of samples increases. However, even for extremely large sample sizes, the breadth between confidence limits cannot get smaller than the breadth between bounds representing incertitude from measurement error (Ferson et al. 2010). Therefore, considering incertitude arises from sampling errors would circumscribe the measurement errors as well.

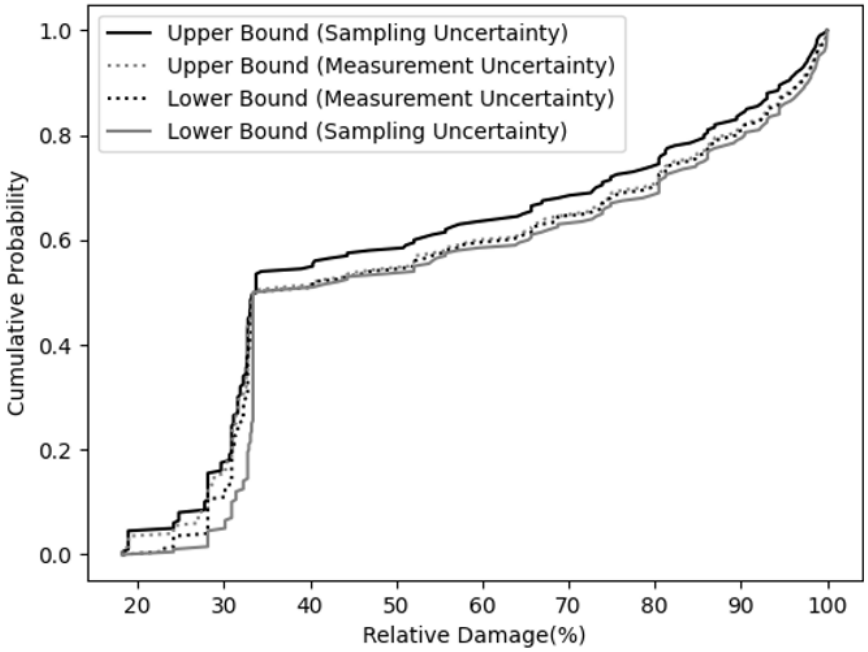

Figure 2. Expected relative damage to one-story residential buildings with finished basement in Metro Vancouver in case of the CMIP6 ensemble SSP2.45 (2020 - 2060) flood scenario. Solid bounds show the 95% Kolmogorov-Smirnov confidence limits applied to the sample data and the dashed bounds show the expected damage considering imprecision in the measurement.

To account for sampling uncertainties, for each flood scenario, we establish p-boxes for both flood elevation (considering the flood elevation at the location of each sample building) and main floor height for the four building categories. Afterward inundation p-boxes are calculated through the following formula, which was then used as an input in the relevant damage functions:

$$\text{Inundation P-box} = \text{Flood Elevation P-box} - \text{Main Floor Height P-box} \quad (3)$$

We use independent subtraction in Equation 3 because, according to Table 1, there is no significant correlation between first floor height of a building and flood elevation at its location. Therefore, building location in flood-prone areas does not imply elevated main floor height. However, if there is any doubt about the type of dependency between variables, we can use Fréchet subtraction, which can be calculated using the following formula, where $[\overline{F}_X , \underline{F}_X]$ is the p-box for quantity X and $[\overline{F}_Y , \underline{F}_Y]$ is the p-box for quantity Y (Oberkampf et al. 2004):

$$\overline{F}_{X-Y}(Z) = 1 + \inf_{z=x-y}\min(\overline{F}_X(x) - \underline{F}_Y(y), 0) \quad (4)$$

$$\underline{F}_{X-Y}(Z) = \sup_{z=x-y}\max(\underline{F}_X(x) - \overline{F}_Y(y), 0) \quad (5)$$

Table 2. Correlation between the first-floor height and flood elevation at the location of each building for different flood scenario.

Scenario	Pearsons Correlation	Spearmans Correlation
$\mathbf{FS_{Coastal}}$	-0.026	0.008
$\mathbf{FS_{Historic}}$	-0.244	-0.222
$\mathbf{FS_{2100}}$	0.027	0.025
$\mathbf{FS_{SSP5\ 8.5}}$	0.008	0.014

To avoid bias in the inference, samples are chosen in such a way that they are distributed across the entire population of flooded buildings for each flood scenario. Figures 10, 11, 12, and 13 in Appendix A depict the samples and total population for the 2100 Fraser River freshet flood scenario for the four building classes. Because the depth-damage functions used in this study calculate the relative damage based on the inundation depth, number of stories, and the presence or absence of a basement, we did not consider other flood damage influential factors such as construction materials or the social vulnerability of the area in which flooded buildings are located. For example, Figure 14 in Appendix B shows different social vulnerability class in British Columbia, Canada (data source: Chakraborty et al. 2020). In case of 2100 Fraser River freshet flood scenario, we expect that a greater proportion of buildings will be flooded in areas with very low, low, and medium low social vulnerability (Figure 15). In this case, we recommend selecting a higher proportion of samples from these three classes to obtain more representative samples.

The relative damage is then determined for each inundation p-box and reported as a number ranging from 0 to 100, with 0 representing no damage and 100 representing 100 percent damage (the methodology algorithm can be found in Figure 3). To calculate the absolute damage, the relative damage p-box could be multiplied by the property value assigned to each building (excluding the value of the land). Alternatively, we could establish the property value p-box for each building class in the study area and then multiply them by the relative damage p-boxes.

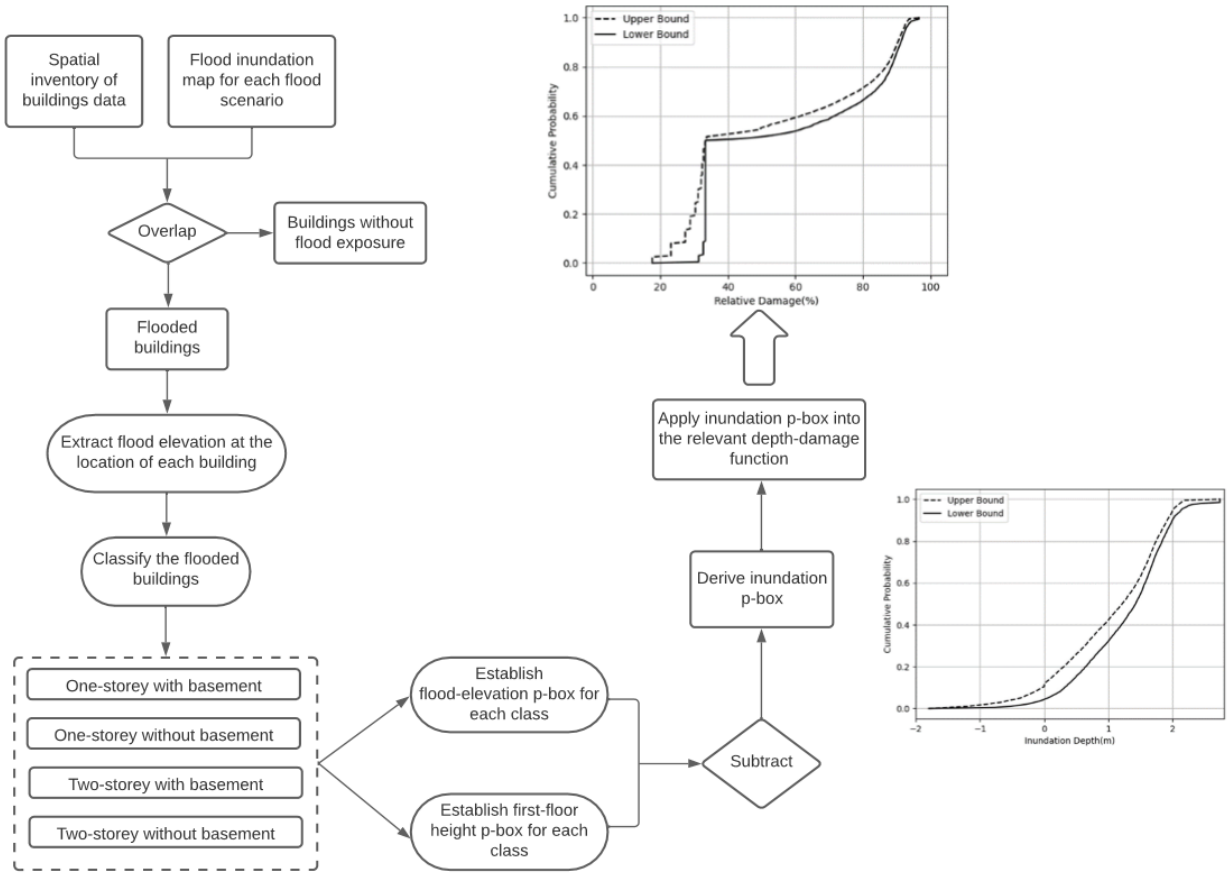

Figure 3. Methodology algorithm.

4.1. Case Study

Currently, flooding is the main source of property insurance claims in Canada. Insurance claims associated with water damage have reached all-time highs in recent years. As a result, insurers have started to charge higher deductibles, limit coverage for sewer backups, restrict overland flood insurance in high-risk areas, and exclude properties that are the subject of multiple claims (Henstra & Thistlethwaite 2017). Furthermore, the Fraser River Basin which is the largest Pacific watershed (240,000 km2) in Canada, is expected to experience extreme flood events with unprecedented frequency by the end of the twenty-first century (Curry et al. 2019).

For this study, we use a geospatial dataset generated by IBI Group and Golder Associates (2020) that contains the main floor height of approximately 15,000 buildings in the Lower Mainland of British Columbia, of which 12,972 are one- and two-story residential buildings. This dataset was integrated with another geospatial dataset that was originally developed for earthquake damage assessment. The latter includes construction year, foundation type, number of stories, number of units, building area, land use, construction material type (wood, concrete, steel, masonry), and the asset value of the 450,000 buildings in Metro Vancouver, Canada. About 83.5 percent (375,973) of these 450,000 buildings are residential buildings. 40.37 percent of these residential buildings are one-story buildings with basement, 14.95 percent are one-story buildings without basement, 20.25 percent are two-story buildings with basement, and 24.43 percent are two-story buildings without basement.

In this study, five flood scenarios (Table 1) are considered to assess how climate change will affect the likely flood damage.

Table 2. Considered scenarios and the number of buildings exposed to flood in each scenario.

Scenario	Description of each scenario	Annual Exceedance Probability (%)	Flooded Buildings in the Sample Data	
			Number	Percent
$\mathbf{FS_{Coastal}}$	Coastal flood (0 m sea level rise)	2	5,462	42.1
$\mathbf{FS_{Historic}}$	Historic Fraser River Freshet Flood Scenarios	2	594	4.6
$\mathbf{FS_{2100}}$	2100 Fraser River Freshet Flood Scenarios (1 m sea level rise)	2	10,611	81.8
$\mathbf{FS_{SSP2.45}}$	Coupled Model Intercomparison Project 6 (CMIP6) ensemble SSP 2.45 (2020 - 2060)	1	3,768	29
$\mathbf{FS_{SSP5\ 8.5}}$	Coupled Model Intercomparison Project 6 (CMIP6) ensemble SSP5 8.5 (2020 - 2060)	1	3,799	29.3

For scenarios $FS_{Coastal}$, $FS_{Historic}$, and FS_{2100} in Table 2, we utilise 1-in-50 year floodplain maps, developed by IBI Group and Golder Associates (2020) along the Fraser River through Metro Vancouver, Canada. These are scenarios commissioned by the Fraser Basin Council (FBC) and serve as planning scenarios created for and used by decision makers in the region. We add additional scenarios ($FS_{SSP2.45}$ and $FS_{SSP5\ 8.5}$) to argument those ones since they have a shorter timeframe and hence augment what is being examined in the region by showing what might happen in the nearer term and for a higher level of severity. For scenarios $FS_{SSP2.45}$ and $FS_{SSP5\ 8.5}$ in Table 2, we use high-resolution Canada-wide floodplain maps for 1-in-100 years, developed by Mohanty and Simonovic (2021), where the most recent Coupled Model Intercomparison Project (CMIP6) was used to project future changes in floodplain regimes across Canada.

Hazard United States Multi-Hazards (HAZUS-MH) developed by FEMA, provides damage functions associated with each specific occupancy class (e.g., residential) and subclass (e.g., two-story, with no basement). These functions estimate building replacement costs at different water depths (FEMA, 2018). However, since most of these depth-damage functions were developed based on the data from various districts of the United States and to account for differences in architectural and structural design in Canada and the United States, the depth-damage functions developed by Bonnifait (2005) (Table 3) based on empirical data from flood observations in Quebec, Canada, were used in this study. These curves include only damage to the structural (load bearing) system, architectural, electrical components, and building finishes and excluding content damage (damage to furniture and property within the residence). Since the functions used are based on data from the region investigated (Quebec, Canada), applying them to another province or region may result in over or under estimation of damage. This uncertainty is not considered in this study since the construction practices can be assumed to be similar.

Table 3. Damage functions are based on empirical data driven from Bonnifait (2005).

Building Class	Flood Depth from the first floor (m)	Relative Damage
One-story with Finished Basement	$H < -0.4$	$0.36 \exp(-0.04 \exp(-1.6 H))$
	$H \geq -0.4$	$\exp(-0.7 \exp(-1.1 H))$
One-story with Unfinished Basement	$H < 0$	$0.3 \exp(1.7 H)$
	$H \geq 0$	$\exp(-1.2 \exp(-1.7 H))$
One-story without Basement	$H < 0$	$0.08 \exp(1.3 H)$
	$H \geq 0$	$\exp(-2.4 \exp(-1.8 H))$
Two-story with Finished Basement	$H < -0.4$	$0.27 \exp(-0.04 \exp(-1.6 H))$
	$-0.4 \leq H < 2.5$	$0.81 \exp(-0.7 \exp(-1.3 H))$
	$H \geq 2.5$	$\exp(-0.7 \exp(-2.1(H-2)))$
Two-story with Unfinished Basement	$H < -0.1$	$0.15 \exp(1.4H)$
	$-0.1 \leq H < 2.5$	$0.82 \exp(-1.5 \exp(-1.5 H))$
	$H \geq 2.5$	$\exp(-0.7 \exp(-2.1 (H-2)))$
Two-story without Basement	$H < 0$	$0.06 \exp(1.2 H)$
	$0 \leq H < 2.5$	$0.82 \exp(-2.5 \exp(-1.9 H))$
	$H \geq 2.5$	$\exp(-0.8 \exp(-2.4(H-2)))$

5. Results

The following figures and tables show the relative flood damage p-box as well as the mean and variance interval of the expected damage for each building category and scenario. Since we did not find much difference between damage p-boxes of SSP2.45 and SSP8.5 before 2060, suggesting the major flood risk differences in these scenarios will not be realised yet by 2060, only the p-boxes belonging to SSP8.5 are presented.

In the following figures, the vertical axis represents the cumulative probability of the corresponding relative damage given on the horizontal axis. There are two ways to read the presented p-boxes. The first is to read the probability range of a given level of damage, and the second is to read the damage range for a given probability.

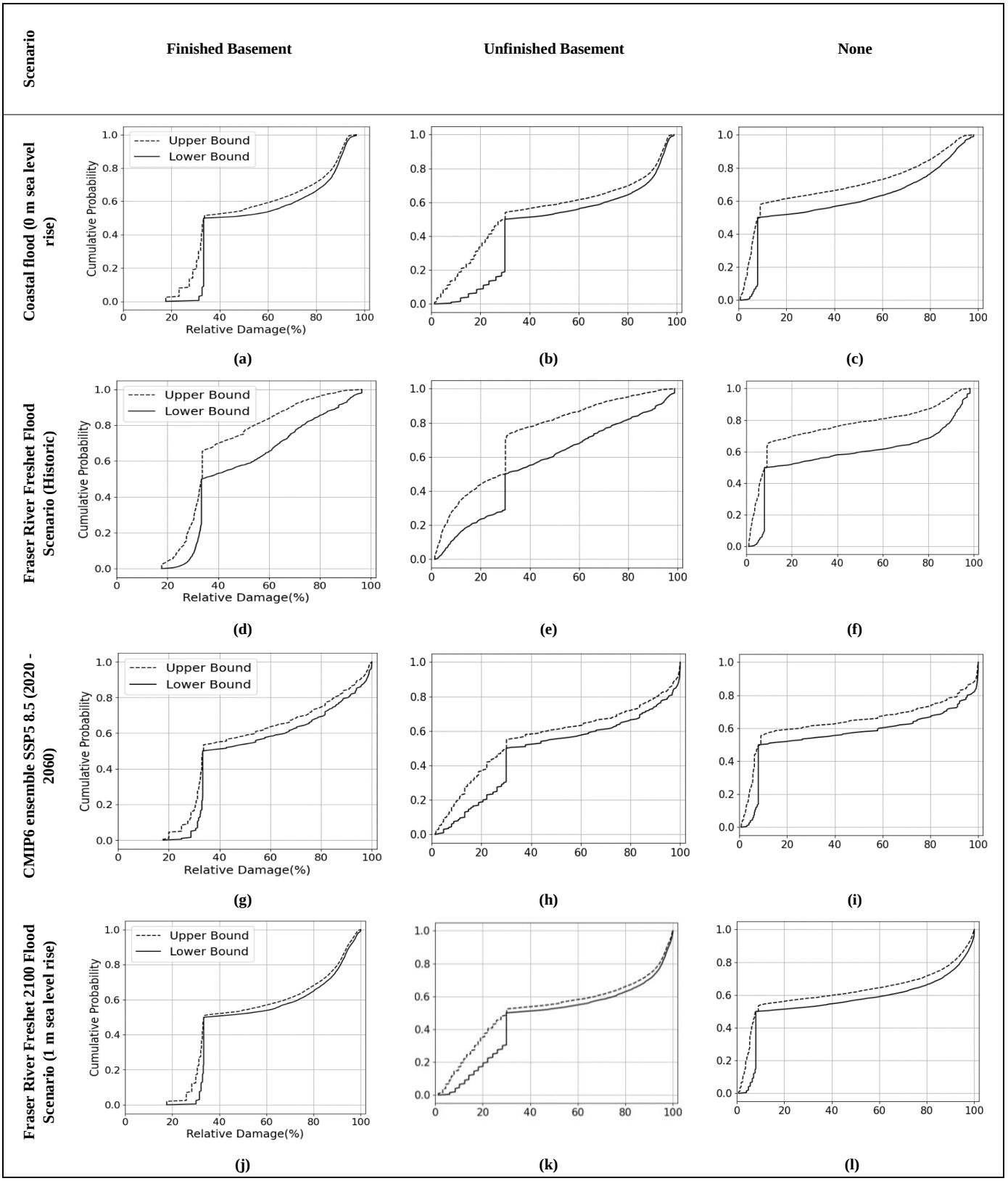

Figure 4. Relative flood damage to one-story buildings a) with finished basement, in case of $FS_{Coastal}$, b) with unfinished basement, in case of $FS_{Coastal}$, c) without basement, in case of $FS_{Coastal}$, d) with finished basement, in case of $FS_{Historic}$, e) with unfinished basement, in case of $FS_{Historic}$, f) without basement, in case of $FS_{Historic}$, g) with finished basement, in case of $FS_{SSP5\ 8.5}$, h) with unfinished basement, in case of $FS_{SSP5\ 8.5}$, i) without basement, in case of $FS_{SSP5\ 8.5}$, j) with finished basement, in case of FS_{2100}, k) with unfinished basement, in case of FS_{2100}, and l) without basement, in case of FS_{2100}.

Table 4. Mean and variance of expected relative damage to one-story buildings with basement in Metro Vancouver, in case of four different flood scenarios.

Scenario	Relative Damage to One Story Buildings (%)				Population	Number of Samples	Sampling Fraction (%)
	Finished Basement		Unfinished Basement				
	Mean	Variance	Mean	Variance			
Fraser River Freshet 2100 Flood Scenario (1 m sea level rise)	[55,58]	[7,8]	[48,54]	[11,15]	9981	5120	0.51
Coastal flood (0 m sea level rise)	[53,57]	[6,7.8]	[46,55]	[8.5,13]	8155	2807	0.34
CMIP6 ensemble SSP5 8.5 (2020 - 2060)	[52,57]	[6,8]	[44,53]	[10,14.4]	5944	1717	0.29
Historic Fraser River Freshet Flood Scenario	[40,50]	[2,6]	[28,45]	[4,11]	798	252	0.32

Table 5. Mean and variance of expected relative damage to one-story buildings without basement in Metro Vancouver, in case of four different flood scenarios.

Scenario	Relative Damage to One Story Buildings Without Basement (%)		Population	Number of Samples	Sampling Fraction (%)
	Mean	Variance			
Fraser River Freshet 2100 Flood Scenario (1 m sea level rise)	[38,44.22]	[14.3,17.7]	3196	1605	0.50
CMIP6 ensemble SSP5 8.5 (2020 - 2060)	[36,44]	[14,18.2]	2862	811	0.28
Coastal flood (0 m sea level rise)	[30,39.5]	[9.6,14.3]	3440	686	0.20
Historic Fraser River Freshet Flood Scenario	[24,41.5]	[8,16.68]	500	129	0.26

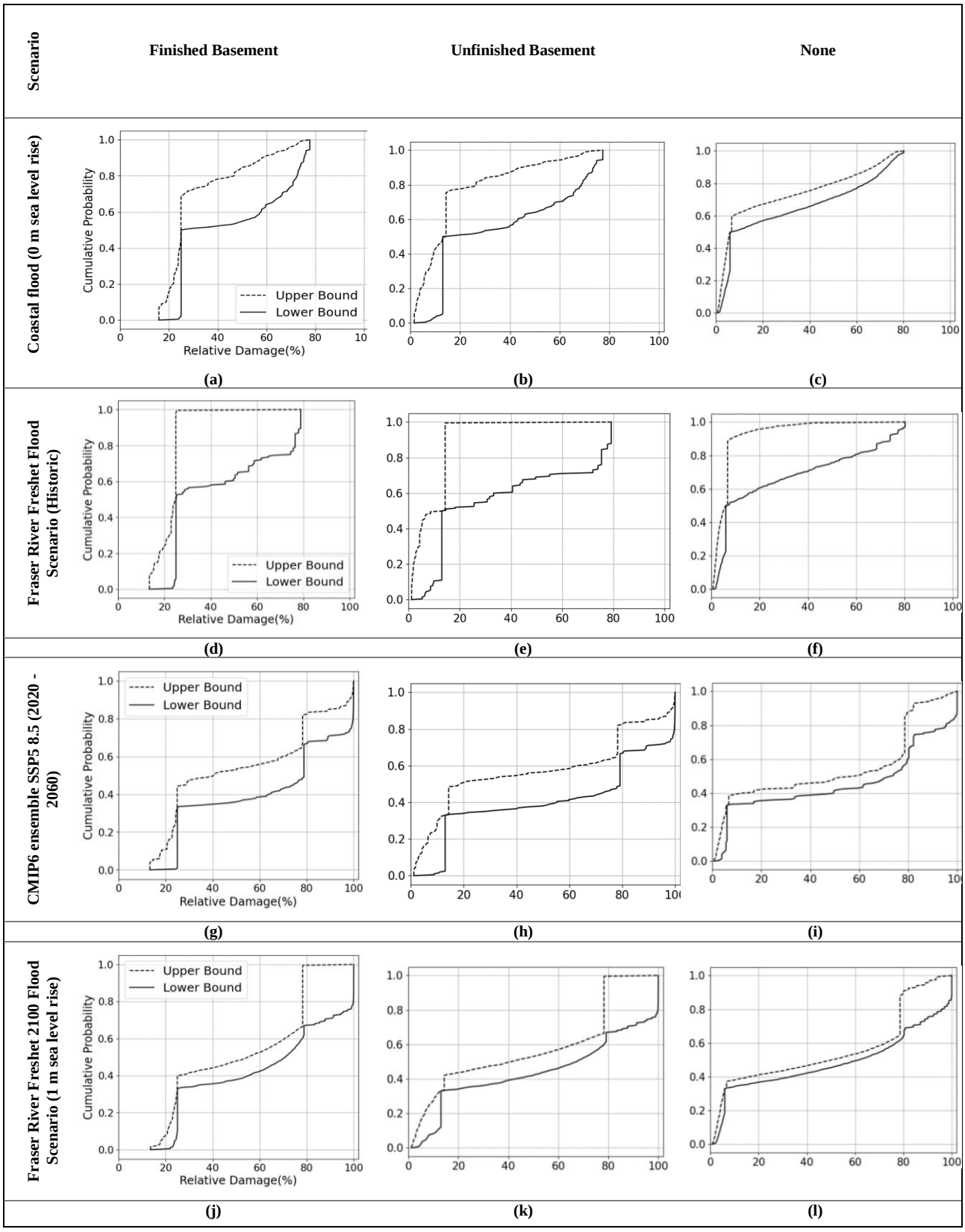

Figure 5. Relative flood damage to two-story buildings a) with finished basement, in case of $FS_{Coastal}$, b) with unfinished basement, in case of $FS_{Coastal}$, c) without basement, in case of $FS_{Coastal}$, d) with finished basement, in case of $FS_{Historic}$, e) with unfinished basement, in case of $FS_{Historic}$, f) without basement, in case of $FS_{Historic}$, g) with finished basement, in case of $FS_{SSP5\ 8.5}$, h) with unfinished basement, in case of $FS_{SSP5\ 8.5}$, i) without basement, in case of $FS_{SSP5\ 8.5}$, j) with finished basement, in case of FS_{2100}, k) with unfinished basement, in case of FS_{2100}, and l) without basement, in case of FS_{2100}.

Table 6. Mean and variance of expected relative damage to two-story buildings with basement in Metro Vancouver, in case of four different flood scenarios.

Scenario	Relative Damage to Two Story Buildings (%)				Population	Number of Samples	Sampling Fraction (%)
	Finished Basement		Unfinished Basement				
	Mean	Variance	Mean	Variance			
CMIP6 ensemble SSP5 8.5 (2020 - 2060)	[51,64.7]	[7,12.4]	[42.5,59.7]	[10,17.8]	964	106	0.11
Fraser River Freshet 2100 Flood Scenario (1 m sea level rise)	[50.4,62.7]	[5,11]	[41.8,56.5]	[8,16.8]	591	230	0.39
Historic Fraser River Freshet Flood Scenario	[41,58]	[6,10]	[32,53]	[9.2,15.4]	41	17	0.41
Coastal flood (0 m sea level rise)	[31,46]	[1.9,5.9]	[17,36]	[2,8.8]	181	53	0.29

Table 7. Mean and variance of expected relative damage to two-story buildings without basement in Metro Vancouver, in case of four different flood scenarios.

Scenario	Relative Damage to Two Story Buildings Without Basement (%)		Population	Number of Samples	Sampling Fraction (%)
	Mean	Variance			
CMIP6 ensemble SSP5 8.5 (2020 - 2060)	[44.6,54.4]	[11.3,17]	1947	580	0.30
Fraser River Freshet 2100 Flood Scenario (1 m sea level rise)	[43.6,51.8]	[11.2,16.6]	21236	1729	0.08
Coastal flood (0 m sea level rise)	[20.8,28.2]	[5.7,8.6]	20496	760	0.04
Historic Fraser River Freshet Flood Scenario	[6,26]	[0.3,8.4]	304	95	0.31

As mentioned earlier, probability bounds analysis distinguishes between variability and incertitude. The breadth of a probability box between the left and right sides represents epistemic uncertainty, while the overall range and steepness of the probability box represents variability (Ferson et al. 2003). Aleatory uncertainty is related to the variability or heterogeneity within a population. Comparing the relative damage p-boxes of different building classes under different scenarios, two-story buildings with finished basement in case of $FS_{Coastal}$ has the smallest aleatory uncertainty (the overall range of relative damage is between 15% and 77%). Since the variability or aleatory uncertainty cannot be reduced, here only the epistemic uncertainty associated with the relative damage p-boxes will be discussed.

As the information about a distribution's parameters becomes more precise, the bounds will approach a precise distribution. Conversely, when the information is limited or poor, the bounds tend to be much wider, indicating a lack of confidence in the specification of this distribution (Beer et al., 2013). This is what we see when we compare the p-boxes of the $FS_{Historic}$ flood scenario to the other flood scenarios in Figures 4 and 5. The total number of inundated buildings in the $FS_{Historic}$ flood scenario is significantly lower than the other flood scenarios in this study. As a result, we have a smaller sample pool from which to form empirical bounding cumulative histograms of first-floor height and flood depth to assess the relevant damage for the entire population. Take as an example one-story buildings with basement in the $FS_{Historic}$ flood scenario with a total population of 798

(Table 4). According to the following formula (Equation. 6, where n is the sample size and N is the population size) proposed by Yamane (1967), assuming 95% confidence interval, maximum variability (p=.5), and ±5% precision, appropriate sample size, in this case, would be 266 which is slightly larger than the sample size used here (252). While 384 would be an acceptable sample size for the one-story buildings with basement in the FS_{2100} flood scenario with a total population of 9981, where we used a sample size greater than 384.

$$n = \frac{N}{1 + N(.05)^2} \tag{6}$$

The FS_{Historic} flood scenario has the widest p-boxes or greatest epistemic uncertainty among the four scenarios considered in this study. The best-possible or simply tightest p-boxes are for the FS_{2100} flood scenario with the largest sample size. Comparing the various building classes in the study area, two-story buildings with basement have the highest epistemic uncertainty because the total number of flooded buildings in this class is significantly smaller than the other building classes.

The relative damage p-boxes in Figures 4 and 5 are made up of two (for one-story buildings) or three (for two-story buildings) parts, each with a different tilt and breadth between the left and right edge of the p-box. This is because different damage functions have different criteria, implying different sample sizes.

When the damage p-boxes of the $FS_{SSP5\ 8.5}$ and FS_{2100} flood scenarios are compared to the FS_{Historic}, we can see that we should expect significantly higher damage in Metro Vancouver in the future, all else being the same. Considering two-story buildings in the FS_{Historic} and FS_{2100} flood scenarios (Figure 5). The water depth inside the buildings does not exceed 2.5 meters in the FS_{Historic} flood scenario. Therefore, the input inundation p-boxes for this scenario do not meet the third criterion of the relevant depth-damage functions ($H \geq 2.5$). Consequently, the resulting damage p-boxes are made up of two parts in this scenario. While damage p-boxes of the FS_{2100} flood scenario, are made up of three parts, that means the input inundation p-boxes satisfy all the three criteria in the relevant depth-damage functions.

For the FS_{Coastal} scenario, one-story buildings with basement (finished and unfinished) sustain the highest inundation depth and damage compared to other buildings' categories. Figure 6 shows the inundation depth p-box and its corresponding damage p-box for different building categories in the FS_{Coastal} flood scenario. The probability that inundation depth is 1.5 meters or less is between 54.5% and 63.5% in one-story buildings with basement, between 66% and 81% in one-story buildings without basement, between 68% and 97.5% in two-story buildings with basement, and between 78.5% and 89% in two-story buildings without basement. In the remaining scenarios, one-story buildings with finished basement and in the second place, two-story buildings with finished basements are expected to sustain the highest damage. This reveals the impact of finished basements on total flood damage as well as the efficacy of structural (e.g., filling in the existing basement) and non-structural (e.g., restricting the construction of buildings with basements in floodplains) mitigation measures aimed at finished basements. For each building class and flood scenario, relative damage values for the 50th and 95th percentiles, as well as uncertainty, are reported in Appendix A.

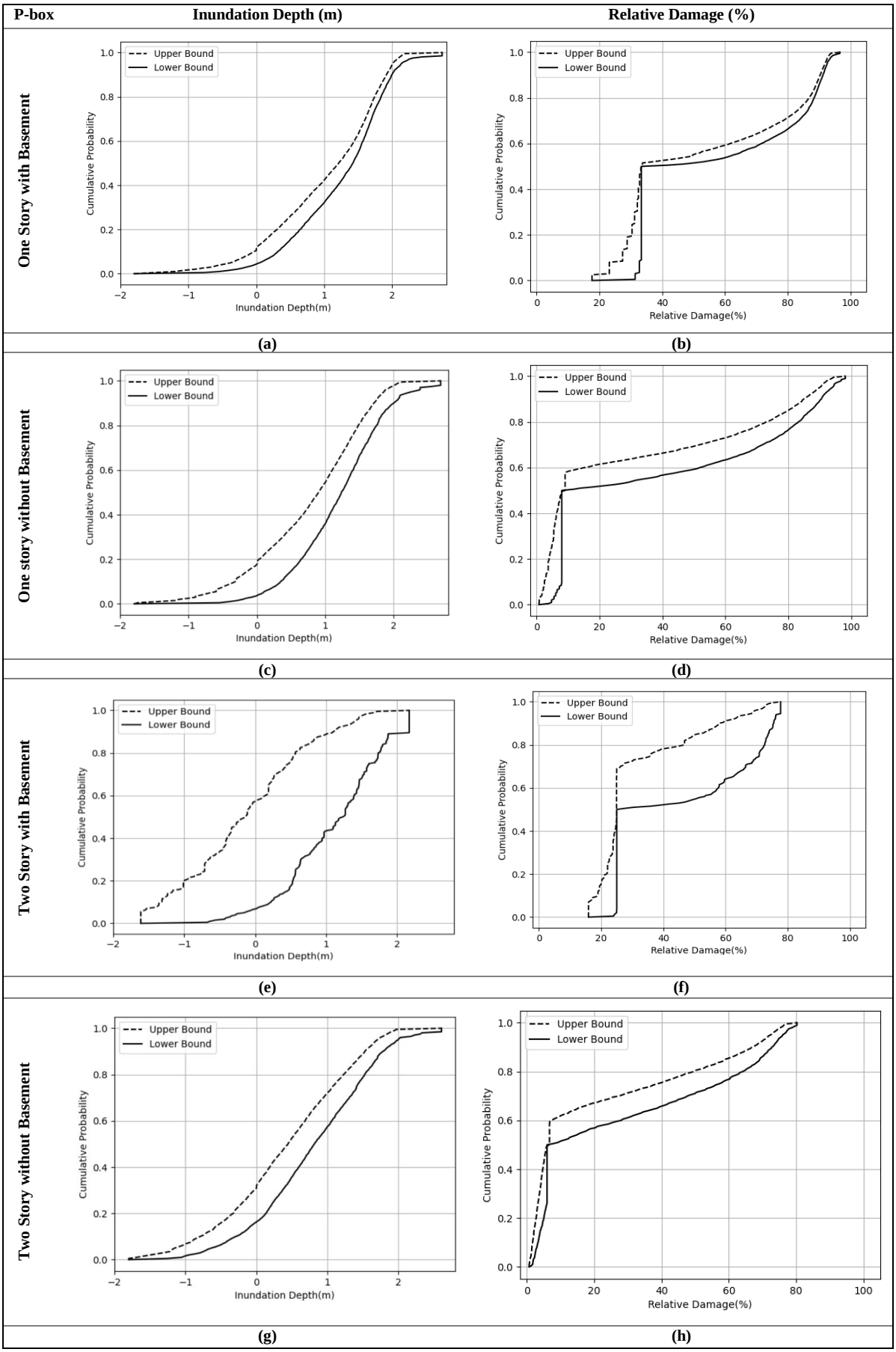

Figure 6. a) Inundation depth p-box of one one-story buildings with basement, b) relative damage p-box of one one-story buildings with basement, c) inundation depth p-box of one one-story buildings without basement, d) relative damage p-box of one one-story buildings without basement, e) inundation depth p-box of two-story buildings with basement, f) relative damage p-box of two-story

buildings with basement, g) inundation depth p-box of two-story buildings without basement, and h) relative damage p-box of two-story buildings without basement, in case of $FS_{Coastal}$ flood scenario.

Another factor to consider is that we do not know whether the basements of the buildings in our sample are finished or unfinished. To answer the question of what the probability box for relative damage is given that we do not know if the basement is finished or unfinished, we could mix the relative damage p-boxes of the finished and unfinished basements. We assign equal weights to both finished and unfinished basements because there is no information about the proportion of buildings' finishes in the study area. In Figure 7, the mean relative damage and uncertainty of two-story buildings with finished, unfinished, and a mixture of both are depicted in case of FS_{2100} flood scenario.

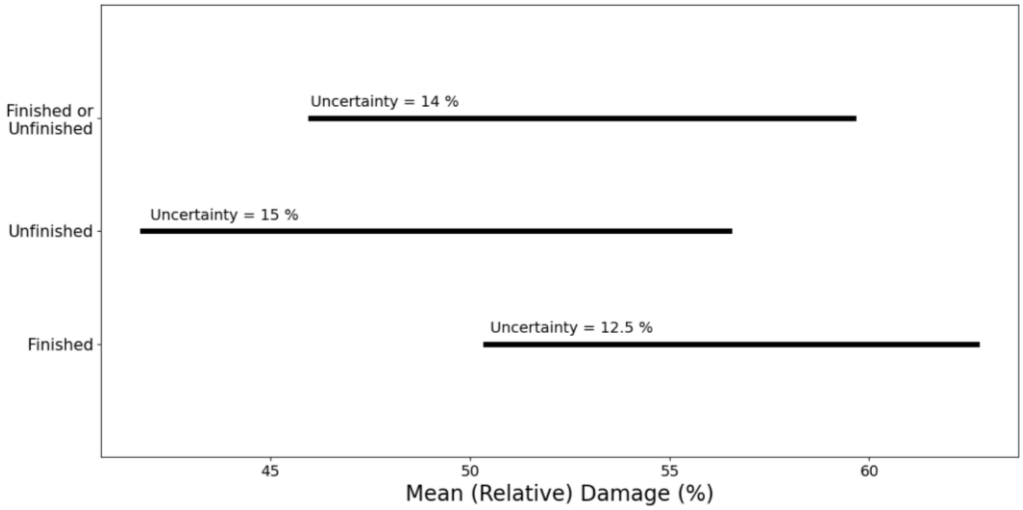

Figure 7. The expected mean relative damage interval for two-story buildings when we do not know if the basement is finished or unfinished in case of FS_{2100} flood Scenario.

In addition, we increased the first-floor height of the buildings with the height from the adjacent ground less than 1 meter by 1 meter to explore the impact of first-floor height on the resultant damage in each building category, as well as the applicability of the proposed method for evaluating the impact of various mitigation measures. Table 8 shows the mean relative flood damage interval in case of FS_{2100} flood scenario before and after raising the first-floor height. The greatest change in resultant damage belongs to one-story buildings without basement.

Table 8. Mean relative flood damage interval of different building categories, for FS_{2100} flood Scenario, before and after raising the first-floor height by 1 meter.

Story	Basement	Before altering the first-floor height	After altering the first-floor height
1	Finished	[55,58]	[50,52.8]
1	Unfinished	[48,54]	[42.4,47]
1	None	[38,44.22]	[30,36]
2	Finished	[51,64.7]	[48,61.2]
2	Unfinished	[42.5,59.7]	[38.7,54]
2	None	[43.6,51.8]	[38.7,49]

One of the other applications of probability bounds analysis is providing an alternative to second-order or nested Monte Carlo simulation, which is generally implemented to address uncertainty in flood damage assessment (Apel et al. 2004, Apel et al. 2008).

We use second-order Monte Carlo simulation to estimate the uncertainty in the input parameters, first-floor height, and flood depth, to make up the distribution of possible inundation depth and calculate the involved uncertainty by running the simulation 500^2 times. Figure 8 shows the results for one-story buildings with basement in the event of FS_{2100} flood scenario. The probability box, as shown in Figure 8, encloses the Monte Carlo simulation result, whereas the time required to complete the p-box is significantly less than that of the Monte Carlo simulation. The same procedure is repeated for two-story buildings with basement (Figure 9). The Monte Carlo simulation almost completely fills the b-box for one-story buildings where we have a large sample size (5120). In other words, both methodologies can be used to represent epistemic uncertainty for large sample sizes. However, even with an 80 percent confidence interval (Figure 9. b), the results of the Monte Carlo simulation do not fill the p-box for the two-story buildings for which we have a small sample size (230). Therefore, for small sample size, using second order Monte Carlo simulation can result in an ignorance of the associated epistemic uncertainty.

In addition, probability bounds analysis is not computationally intensive, and it does not have parameterization and interpretation issues associated with the second-order Monte Carlo simulation.

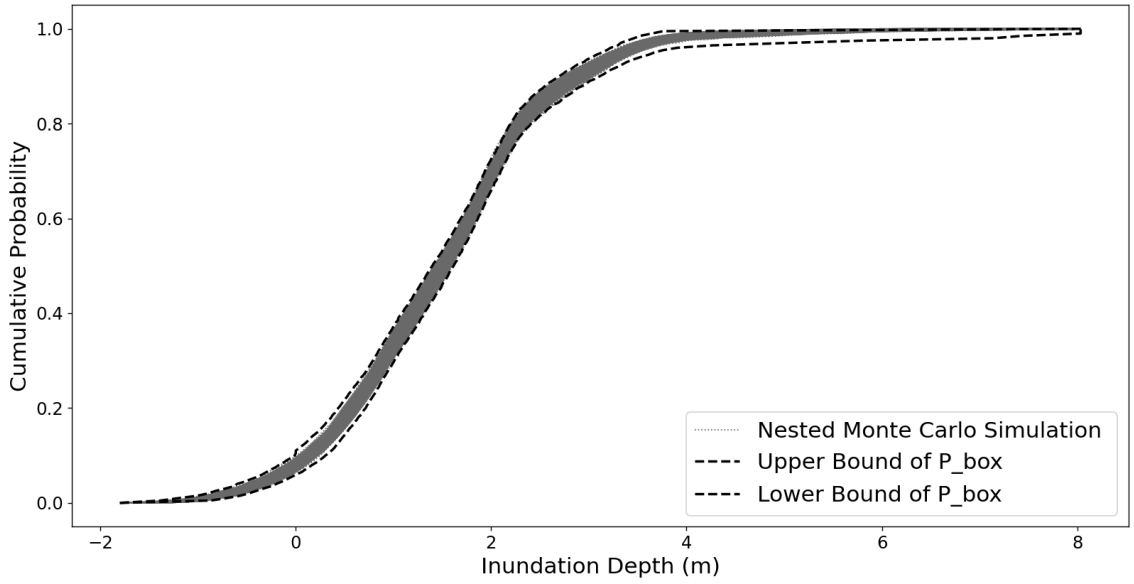

Figure 8. Inundation p-box (99% confidence interval) of one-story buildings with basement in case of FS_{2100} flood scenario bounds the results of second-order Monte Carlo simulation with sample size equal to 5000 and 500 iterations in each step.

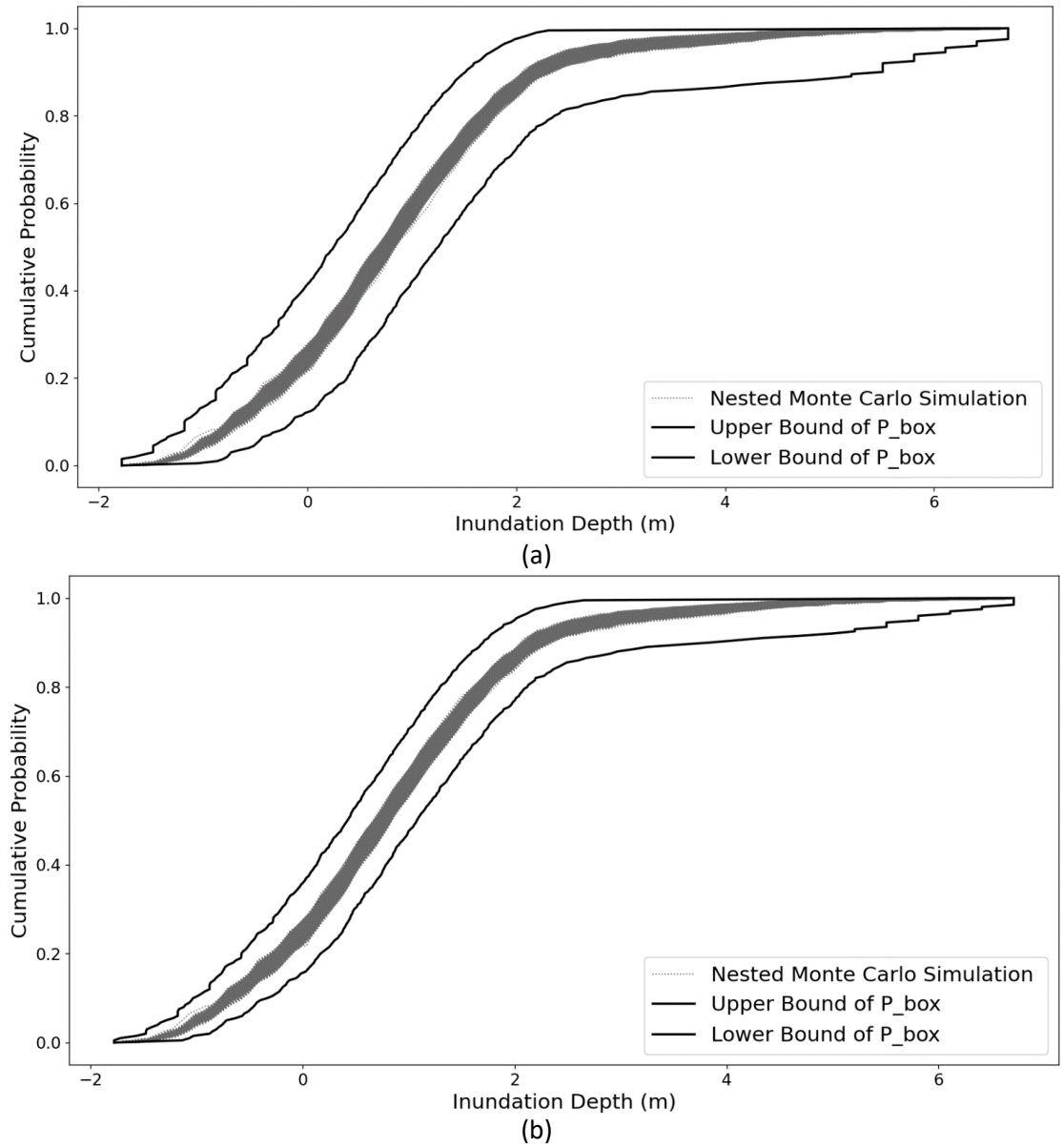

Figure 9. Inundation p-box with 99% confidence interval (a) and 80% confidence interval (b) of two-story buildings with basement in case of FS_{2100} flood scenario bounds the results of second-order Monte Carlo simulation with sample size equal to 5000 and 500 iterations in each step.

6. Conclusion

Climate change projections, as well as rapid growth in urbanization, indicate we will confront enormous increases in both flood hazard and exposure. As a result, flood risk mitigation techniques, both structural (e.g., flood walls and dikes) and non-structural (e.g., zoning regulations, flood construction level regulations), are essential to avoid prohibitive response and recovery costs. However, in order to make any type of choice about preventative measures, we need to know about the probable damage and the uncertainty involved in order to select measures that optimise protection from flood damage while minimizing cost. Ignorance of the uncertainty in damage estimates can lead to misjudgment and massive economic losses.

The results show that in the absence of major flood risk management measures, we should expect a significant increase in direct tangible losses due to flooding in Metro Vancouver by the end of this century. The proposed method in this study will assist decision makers, planners, and insurance companies examine the efficacy of various measures while accounting for ranges of uncertainty. It is

also a useful tool for dealing with uncertainty brought on by a diversity of beliefs and interests, in cases such as management of transboundary flood risk (Heinrich & Penning-Rowsell, 2022).

We can use the generated p-boxes to calculate indirect damage p-boxes or use the same method to generate damage p-boxes caused by the flow velocity and add the resulting p-boxes to ones in this study to get more comprehensive insights into potential losses while considering the associated uncertainties. In addition, since the depth-damage functions used in this study are relative functions, the p-boxes generated almost never need to be updated by changes in the property market values.

Although the scope of this study is limited to flood damage estimation, the proposed methodology could be extended to all the steps of flood risk analysis.

Here, we do not consider flood damage to moveable content within the buildings. For the future studies, it is worth nothing if we use the same methodology to establish p-boxes for different groups of inventories inside the buildings and add the resultant p-boxes to the ones in this study to gain a more comprehensive insight into the expected flood damage.

Data Availability

The building datasets generated during and/or analyzed for this study were made available from DRR-Pathways project partners via a data sharing agreement. The flood plain maps for the Historic and year 2100 Fraser River freshet flood scenarios, as well as Coastal flood scenario, can be requested from the Fraser Basin Council. The flood maps for the CMIP6 floods can be downloaded from: https://www.floodmapviewer.com.

Appendix

Appendix A

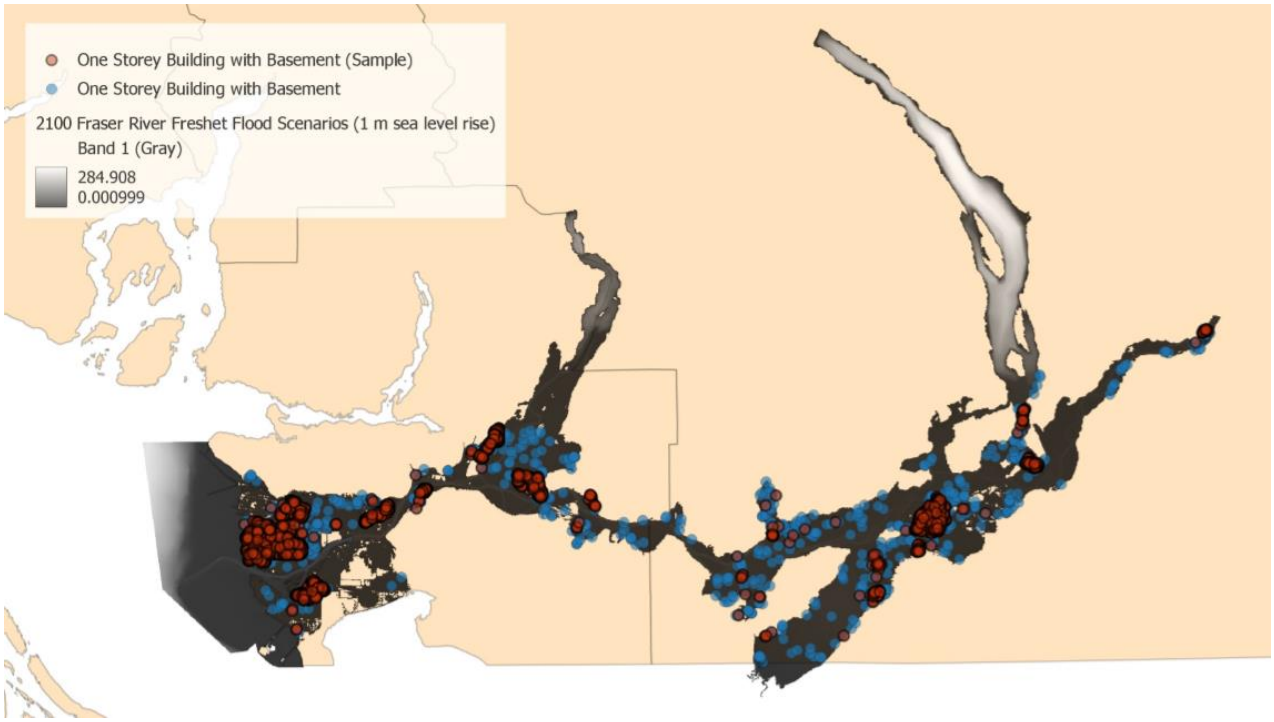

Figure 10. Samples and entire population of flooded one story buildings with basement in case of FS_{2100} flood scenario.

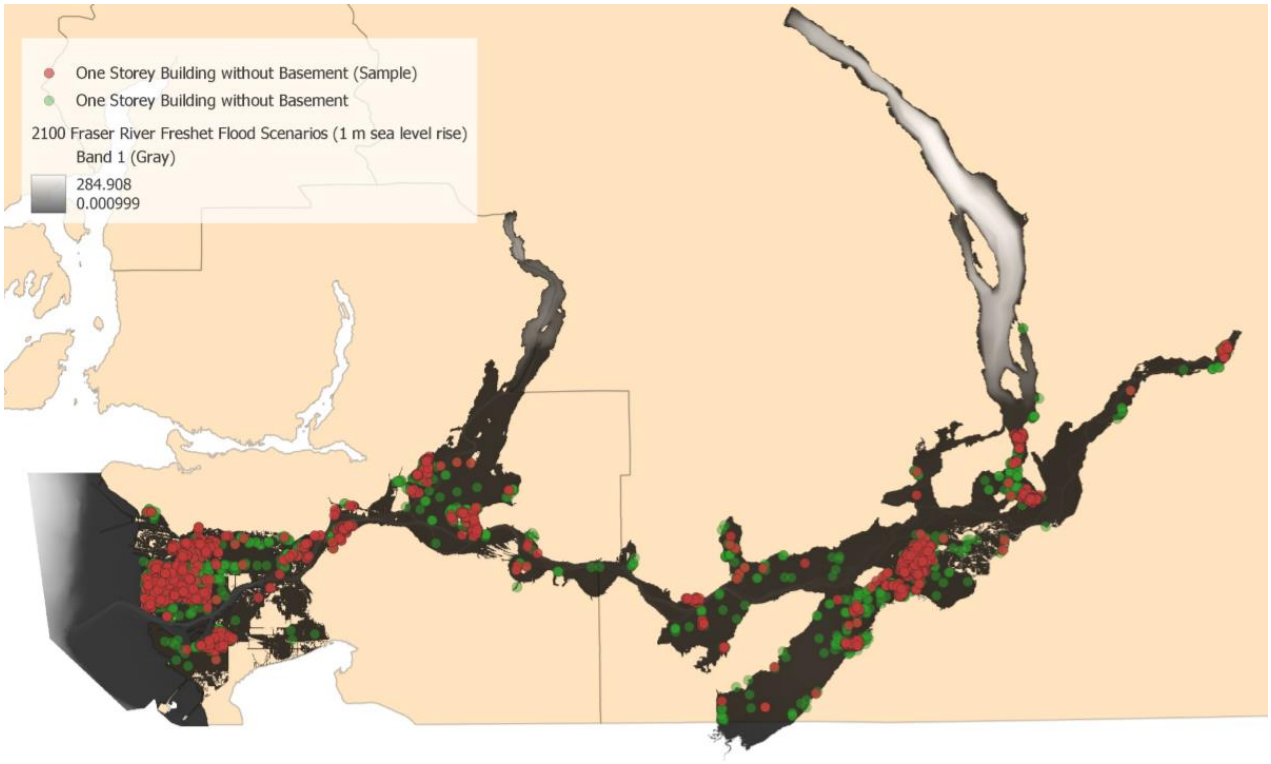

Figure 11. Samples and entire population of flooded one story buildings without basement in case of FS_{2100} flood scenario.

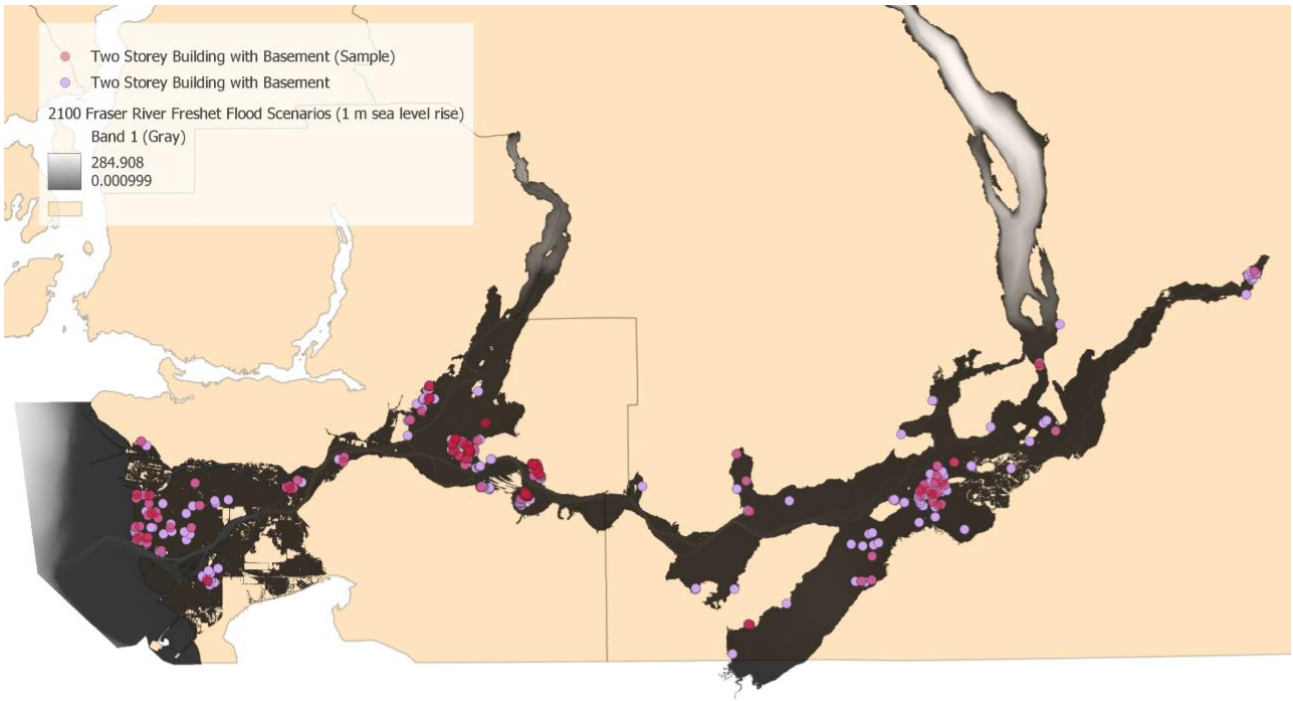

Figure 12. Samples and entire population of flooded two story buildings with basement in case of FS_{2100} flood scenario.

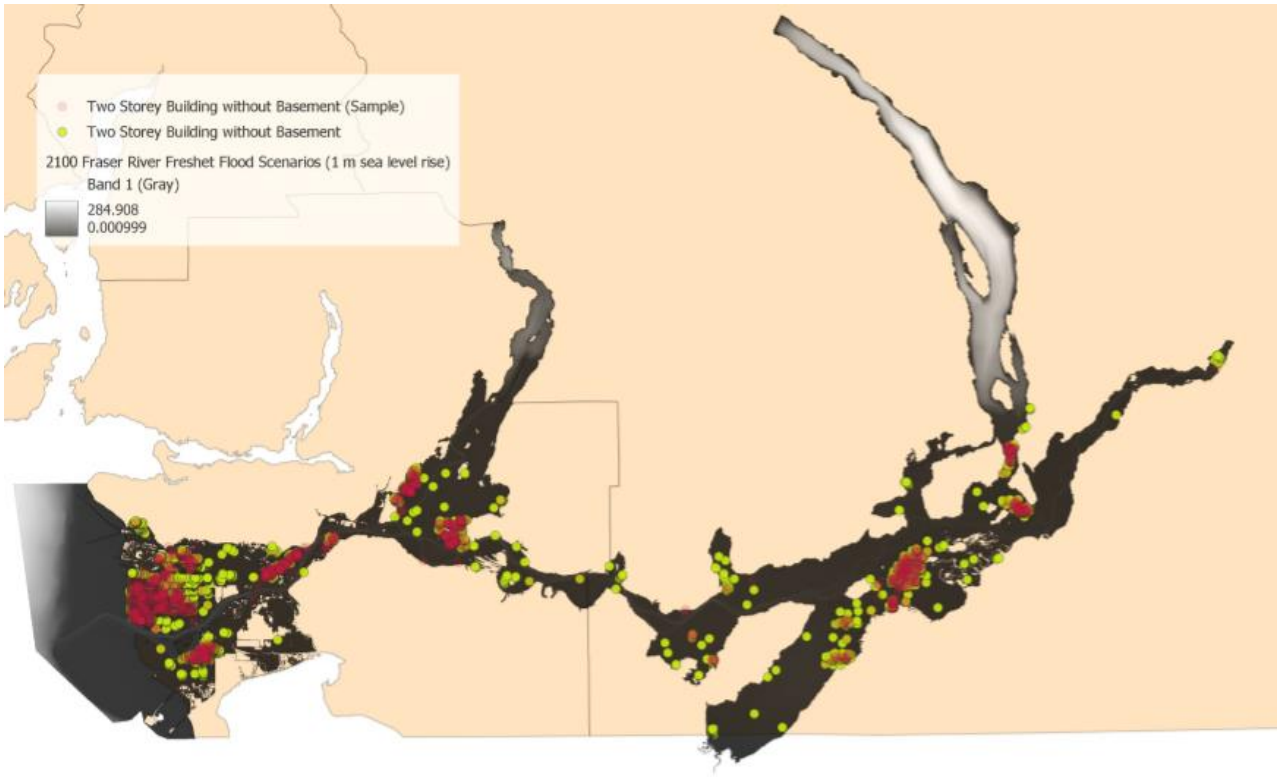

Figure 13. Samples and entire population of flooded two story buildings without basement in case of FS_{2100} flood scenario.

Appendix B

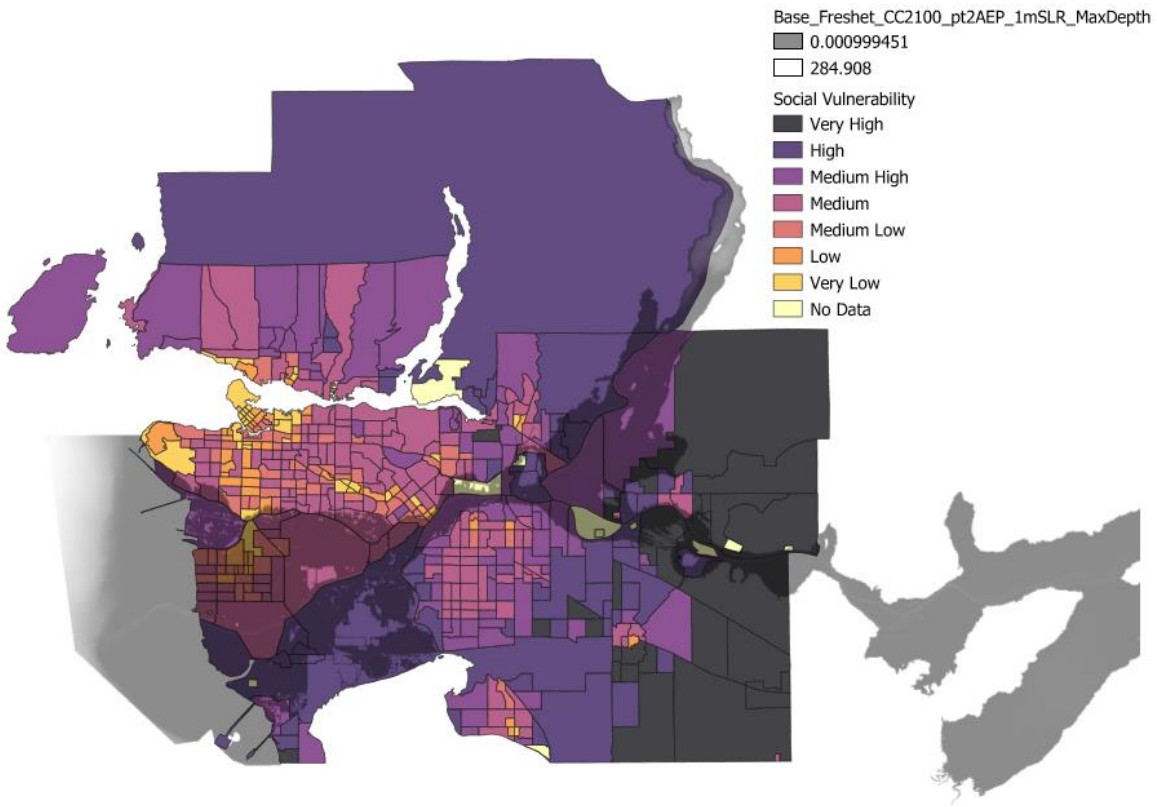

Figure 14. Social vulnerability classes of British Colombia, Canada.

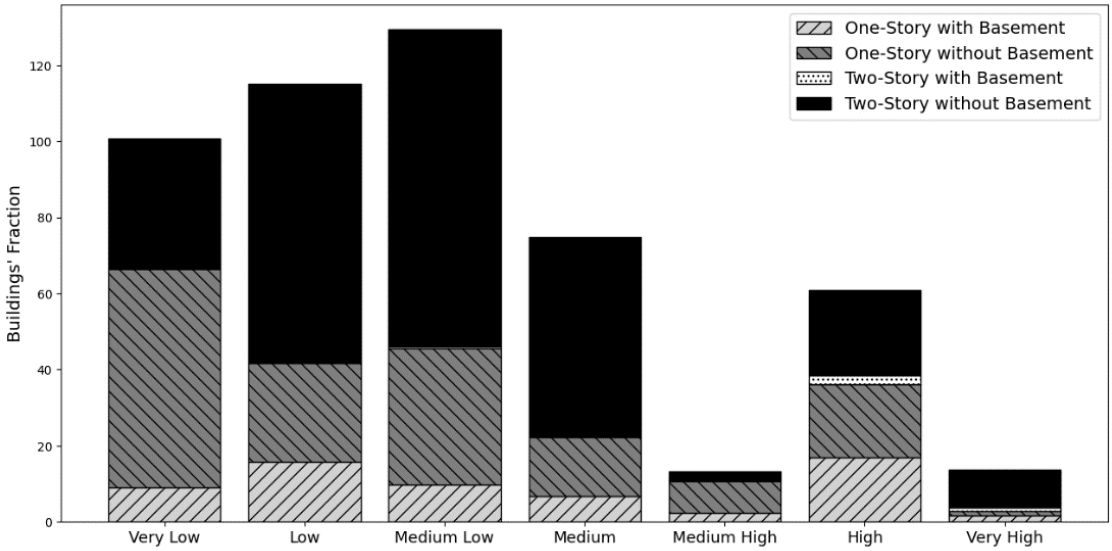

Figure 15. Fraction of flooded buildings for each social vulnerability class in case of FS_{2100} flood scenario.

Appendix C

Table 9. Relative damage to the four building categories in case of $FS_{Coastal}$ flood scenario.

Building Class	Type of Basement	Flood Depth from the first floor (m)	Relative Damage (%)					Number of Samples
			50 Percentile		95 Percentile		Uncertainty (%)	
			Lower Bound	Upper Bound	Lower Bound	Upper Bound		
One-story with Basement	Finished	H < - 0.4	31.22	33.37	33.22	33.37	3.90	2807
		H ≥ - 0.4	83.39	86.59	92.62	93.54	5.30	
	Unfinished	H < 0	15.99	30.00	27.19	30.00	11.13	
		H ≥ 0	86.96	90.37	96.14	96.87	7.08	
One-story without Basement		H < 0	4.85	8.00	7.47	8.00	3.10	686
		H ≥ 0	64.00	78.62	91.87	95.89	16.12	
Two-story with Basement	Finished	H < - 0.4	22.07	25.03	24.99	25.03	3.50	53
		- 0.4 ≤ H < 2.5	36.04	70.82	72.45	77.69	25.46	
	Unfinished	H < - 0.1	5.53	13.04	12.82	13.04	6.66	
		- 0.1 ≤ H < 2.5	14.35	65.59	68.48	77.39	31.79	
Two-story without Basement		H < 0	3.21	5.74	5.55	6.00	1.63	760
		0 ≤ H < 2.5	38.81	57.16	74.59	77.78	13.18	

Table 10. Relative damage to the four building categories in case of $FS_{Historic}$ flood scenario.

Building Class	Type of Basement	Flood Depth from the first floor (m)	Relative Damage (%)					Number of Samples
			50 Percentile		95 Percentile		Uncertainty (%)	
			Lower Bound	Upper Bound	Lower Bound	Upper Bound		
One-story with Basement	Finished	H < - 0.4	29.49	33.35	33.06	33.37	3.77	252
		H ≥ - 0.4	49.91	68.33	82.98	94.72	17.77	
	Unfinished	H < 0	7.29	22.41	24.79	30.00	10.40	
		H ≥ 0	34.30	68.13	86.95	98.77	23.13	
One-story without Basement		H < 0	3.75	8.00	7.40	8.00	3.59	129
		H ≥ 0	37.50	86.37	92.49	98.28	31.40	
Two-story with Basement	Finished	H < - 0.4	20.58	25.03	24.25	25.03	5.52	17
		- 0.4 ≤ H < 2.5	24.95	74.47	24.95	78.83	37.44	
	Unfinished	H < - 0.1	2.87	13.04	6.84	13.04	8.63	
		- 0.1 ≤ H < 2.5	14.35	73.98	14.35	79.16	45.61	
Two-story without Basement		H < 0	2.27	6.00	5.18	6.00	2.34	95
		0 ≤ H < 2.5	6.73	49.22	26.48	80.25	37.64	

Table 11. Relative damage to the four building categories in case of $FS_{SSP2.45}$ flood scenario.

Building Class	Type of Basement	Flood Depth from the first floor (m)	Relative Damage (%)					Number of Samples
			50 Percentile		95 Percentile		Uncertainty (%)	
			Lower Bound	Upper Bound	Lower Bound	Upper Bound		
One-story with Basement	Finished	H < - 0.4	31.12	33.22	33.09	33.33	2.71	1701
		H ≥ - 0.4	80.46	85.69	98.77	99.89	6.63	
	Unfinished	H < 0	12.04	23.77	26.55	30.00	8.14	
		H ≥ 0	83.20	89.72	99.76	99.99	8.07	
One-story without Basement		H < 0	5.20	8.00	7.68	8.00	2.79	808
		H ≥ 0	83.37	91.27	99.81	100.00	13.27	
Two-story with Basement	Finished	H < - 0.4	22.34	25.03	24.81	25.03	3.90	103
		- 0.4 ≤ H < 2.5	44.19	78.83	78.40	78.83	25.14	
		H ≥ 2.5	84.93	99.90	99.91	100.00	9.85	
	Unfinished	H < - 0.1	5.35	13.04	11.87	13.04	7.11	
		- 0.1 ≤ H < 2.5	23.04	79.16	78.49	79.16	33.47	
		H ≥ 2.5	84.93	99.90	99.91	100.00	9.85	

Two-story without Basement		H < 0	3.19	6.00	5.09	6.00	2.46	576
		0 ≤ H < 2.5	55.75	72.38	79.98	80.25	14.79	
		H ≥ 2.5	78.59	98.59	96.34	100.00	12.43	

Table 12. Relative damage to the four building categories in case of $FS_{SSP5\ 8.5}$ flood scenario.

Building Class	Type of Basement	Flood Depth from the first floor (m)	Considering Sampling Error					Number of Samples
			Relative Damage (%)					
			50 Percentile		95 Percentile		Uncertainty (%)	
			Lower Bound	Upper Bound	Lower Bound	Upper Bound		
One-story with Basement	Finished	H < - 0.4	31.34	33.31	33.04	33.33	2.76	1717
		H ≥ - 0.4	80.60	85.63	98.84	99.88	6.59	
	Unfinished	H < 0	13.32	26.30	27.77	30.00	8.08	
		H ≥ 0	83.70	90.50	99.79	99.99	8.11	
One-story without Basement		H < 0	5.16	8.00	7.54	8.00	2.78	811
		H ≥ 0	81.89	92.12	99.78	100.00	13.16	
Two-story with Basement	Finished	H < - 0.4	22.29	25.03	24.66	25.03	4.40	106
		- 0.4 ≤ H < 2.5	40.48	78.83	77.97	78.83	26.22	
		H ≥ 2.5	80.38	99.86	99.88	100.00	9.95	
	Unfinished	H < - 0.1	5.79	13.04	11.18	13.04	7.08	
		- 0.1 ≤ H < 2.5	18.59	79.16	77.82	79.16	34.41	
		H ≥ 2.5	80.38	99.86	99.88	100.00	9.95	
Two-story without Basement		H < 0	3.38	6.00	5.62	6.00	2.09	580
		0 ≤ H < 2.5	57.51	72.77	79.37	80.25	15.36	
		H ≥ 2.5	78.59	98.05	96.91	100.00	11.85	

Table 13. Relative damage to the four building categories in case of FS_{2100} flood scenario.

Building Class	Type of Basement	Flood Depth from the first floor (m)	Relative Damage (%)					Number of Samples
			50 Percentile		95 Percentile		Uncertainty (%)	
			Lower Bound	Upper Bound	Lower Bound	Upper Bound		
One-story with Basement	Finished	H < - 0.4	31.32	33.37	33.32	33.37	2.64	5120
		H ≥ - 0.4	86.89	89.08	97.86	98.69	3.51	
	Unfinished	H < 0	14.89	24.26	27.71	30.00	7.83	
		H ≥ 0	91.24	93.26	99.49	99.76	4.39	
		H < 0	5.15	8.00	7.39	8.00	2.90	1605

One-story without Basement		H ≥ 0	85.78	90.88	99.44	99.99	9.62	
Two-story with Basement	Finished	H < - 0.4	22.95	25.03	24.88	25.03	2.98	230
		- 0.4 ≤ H < 2.5	54.94	70.95	76.30	78.83	14.96	
		H ≥ 2.5	78.27	99.96	78.27	100.00	18.93	
	Unfinished	H < - 0.1	5.23	13.04	11.96	13.04	5.31	
		- 0.1 ≤ H < 2.5	41.08	67.42	75.12	79.16	19.92	
		H ≥ 2.5	78.27	99.96	78.27	100.00	18.93	
Two-story without Basement		H < 0	3.63	5.64	5.74	6.00	1.42	1729
		0 ≤ H < 2.5	50.30	61.52	78.68	80.25	9.57	
		H ≥ 2.5	78.59	98.17	93.48	100.00	13.67	

Chapter 4: Probability Box Method for Assessing Networked Reliability of Infrastructure and Buildings

Abstract

Assessing reliability is a critical concept that has attracted increasing attention as the reliance of cities on complex systems (e.g., power supply) and networks (e.g., electric transmission network, or the network of components in modern buildings) has grown. However, the associated uncertainty with the reliability analysis caused by lack of information as well as limited time and resource for detailed analysis casts doubt on the comprehensive characterization of uncertainty and its impact evaluation along with the practical applicability of reliability analysis. Using imprecise probability analysis in a probability box approach, we introduce a novel, straightforward method to evaluate the reliability of complex systems and networks when dealing with uncertainty in input parameters as well as indeterminant dependency between functions or components of the systems that are often either ignored or previously required a great deal of knowledge and effort to define and compute. The proposed approach can assist in making full use of the available data while transparently presenting the aleatory and epistemic uncertainties in the results and preventing the errors caused by neglecting both functional and random variate dependency. In addition to demonstrating the applicability of the method, it is used to quantify the time to failure and repair time of four real-world networks including power grid, municipal water, and wastewater as well as a building that relies on them.

1. Introduction

Assessing the risks to infrastructure or buildings due to failures in operations requires risk assessment that extends beyond the limits of individual assets to those external operations that enable the functioning of the asset. The complement of risk is reliability (Singh et al., 2007) which is defined as the probability that a system will perform its intended function under stated conditions without failure for a given time interval (Birolini, 2014). However, the uncertainty associated with reliability, makes the complementary relationship questionable. Ignoring uncertainty in reliability assessment may lead to overestimation/underestimation of the results and consequently poor decision making in design, maintainability, and logistic support allocation.

Uncertainty in reliability analysis is caused by inaccuracy in estimate of the precise value of the variables, as well as unknown dependency. This study provides a comprehensive framework for evaluating the reliability of complex systems with imprecise variables and non-deterministic functional dependency using probability bounds (p-boxes) and considers uncertainty in dependency between random variates.

Various effective system reliability analysis methods based on probability bounds analysis have been proposed in recent years. Crespo et al., (2013) introduce a framework for reliability analysis applicable to systems subject to a set of design polynomial inequality requirements dependent on an uncertain parameter, represented by a p-box. They also look for elements of the p-

box that minimize and maximize the probability of the failure domain's bounding sets. P-box is used in (Zhang et al., 2017) to handle epistemic uncertainty in the parameters of the multiple dependent competing failure processes (MDCFP) models. Liu et al., (2017) propose a reliability analysis method that can be used to obtain the upper and lower bounds of the reliability index by solving a two-layer nesting optimization problem with independent uncertainty variables. Simon & Bicking, (2017) assess system reliability while representing epistemic and aleatory uncertainties caused by input parameters. They do this by integrating p-boxes with belief functions. To handle hybrid (epistemic and aleatory) uncertainty and non-deterministic dependency, Song et al., (2020) propose a reliability assessment model based on affine arithmetic and probability box. Yang et al., (2019) introduce a method for analyzing the reliability of complex systems with a limited number of samples, while the uncertainty in limited samples is handled using the probability box.

There are many approaches that seek to handle uncertainty due to undetermined dependency in reliability assessment. Such approaches can be classified into four categories. First, assuming events, variables, or system components are independent (e.g. Yang et al. 2019, Liu et al. 2017, and Feng et al. 2016) without any justification for doing so, for reasons such as mathematical convenience, lack of information, and lack of feasible and practical alternative strategies (Oberkampf et al. 2004). Second, using Monte Carlo simulation (e.g. (Lei & Singh, 2016)). However, as stated by Tucker & Ferson, (2003), there are two major challenges to dealing with correlations and dependencies in Monte Carlo simulation including the potential complexity of dependencies and lacking empirical data. Third, using copula for analysing dependency bounds (e.g. Wang and Pham, 2012). The problem with this method is that in many real-world applications, we do not have sufficient information to determine dependent parameters. Fourth, integrating other methods such as affine arithmetic (Song et al., 2020), belief functions (Simon & Bicking, 2017), and Monte Carlo simulation (Iqbal & Öberg, 2013) with p-box. To our knowledge, except for Karanki et al. (2009) no prior studies on reliability assessment have examined the non-deterministic dependency through the p-box. Karanki et al. combined fault tree analysis with the second order Monte Carlo simulation as well as probability bound analysis to evaluate the unavailability of the main control power supply system (MCPS) of a nuclear power plant. For the Monte Carlo simulation, they used the same random variate for identical basic events, while for the p-boxes, they used Fréchet dependency between the variables of identical basic events, on the premise that the data of identical basic events are entirely correlated. The focus of this study is on uncertainty caused by imprecise failure rate, which is an important factor of reliability analysis during the design and development of complex systems, as well as unknown dependency between downtime of functions. However, the proposed method can be applied to other variables or other types of dependency. In addition, we investigate how dependence assumptions affect the quantitative results of reliability analysis, as well as whether investigating the precise value of the variables or the dependency between variables and components in a complex system is worthwhile in all scenarios.

This paper is organized as follows: sections 2.1 and 2.2 introduce the fundamentals of reliability assessment and probability boxes, respectively. Section 3 presents the methodology and three demonstration examples. Section 4 includes three practical case applications of the proposed method. The paper concludes with a discussion of some related aspects in section 5 and a conclusion in section 6.

2. Background

2.1. Reliability

IEEE standard (IEEE, 1991) defines reliability as "the ability of a system or component to perform its required functions under stated conditions for a specified period of time". Mathematically, we can derive measures of reliability and repair times as follows (P. Lees, 2005). Let the probability of survival (also called reliability) be $R(t) = \Pr[T \geq t]$ where reliability is measured as the probability Pr that failure will not occur until $T \geq t$, where t is the mission time. Then, for a constant rate of failure or hazard, λ, we have:

$$\lambda = -\frac{1}{R(t)}\frac{dR(t)}{dt} \quad (1)$$

Such that

$$R(t) = e^{-\lambda t} \quad (2)$$

We are also interested in the failure probability or unreliability, $F_q(t) = \Pr[T < t]$, which is the probability that failure occurs before the mission time t. $F_q(t)$ is a cumulative distribution function and takes the form

$$F_q(t) = 1 - R(t) = 1 - e^{-\lambda t} \quad (3)$$

It is sometimes convenient to also define a failure density function $f_q(t)$:

$$f_q(t) = \frac{dQ(t)}{dt} = \lambda e^{-\lambda t} \quad (4)$$

Further, length (l) of repair time, which is central to questions of resilience, can fit a variety of distributions, such as lognormal. The most common assumption is that the repair time density function follows an exponential:

$$F_l(t) = 1 - \exp\left(-\frac{t}{m}\right) \quad (5)$$

where m is the mean repair time.

2.2. Probability boxes

Even for the application of the standard reliability equations shown above there can be challenges when assessing large systems. Probability boxes (p-boxes) are an increasingly popular method for implementing imprecise probability assessments in such cases that work quickly on standard computer hardware and can account for a range of dependence relationships between random variates. A p-box ($[\overline{F}(x), \underline{F}(x)]$) of a random variable x whose distribution $F(x)$ is unknown except that it is within the p-box, expressed by a lower bound and an upper bound on the cumulative distribution function (CDF), where $\underline{F}(x) \leq \overline{F}(x)$ for all $x \in R$ (Tucker & Ferson 2003, Ferson et al. 2003).

A p-box can be defined through the lower probability $\underline{P}$ and upper probability $\overline{P}$ where $\underline{F}_X(x) = \underline{P}(X \leq x)$ and $\overline{F}_X(x) = \overline{P}(X \leq x) = 1 - \underline{P}(X > x)$ (Walley 1991).

Williamson and Downs (1990) present algorithms for performing probabilistic arithmetic on random variables that are represented by upper and lower bounds on their distribution when they are independent or when the dependency structure of the variables is unknown. These algorithms were later extended to include additional convolutions, transformations, and dependency types, and they were implemented in software (Gray et al. 2022, Ferson 2020).

In general, in convolutions involving probability boxes, four assumptions can be made regarding the dependency type between variables, including independence, perfect, and opposite dependence associated with maximum correlation and minimum correlation, respectively, for the given marginal distribution shapes. And, finally, if there is no information about the nature of dependencies between variables, we can use Fréchet, whose bounds enclose all the other dependencies (Oberkampf et al., 2004). In this study, we implement three functional dependency types, including independence, perfect dependency, and Fréchet. In the following section, we examine the impact of each of them on the estimated reliability and associated uncertainty.

3. Methodology

We are concerned with assessing the reliability function of a system under imprecise conditions that is comprised of a set of functions $S = \{ i : i > 0, i \in Z\}$. For each function i, we can establish the sets S_i and E_i that specify the direct functional dependencies, not to be confused with random variates that can be probabilistically dependent, of function i from the set of all functions, where $S_i \subseteq S$ is drawn from entities in the same system as i and $E_i \subseteq E = \{j: j > 0, j \in Z\}$ is drawn from the surrounding environment. Functional dependencies are those things whose failure cause a failure in the function. For convenience we can also define each function's set of functional dependencies $D_i = S_i \cup E_i$. For any subset (i.e., group) of functions $G \subseteq S$ we can also establish a set of dependencies from the dependencies of the comprising functions of G, such as:

$$S_G = \bigcup_{i \in G} S_i \tag{6}$$

With these definitions we can establish expressions for reliability of system functions or sets of system functions subject to imprecise probabilities. Here we are using the time to failure expression from equation 3 as an illustration. First, we must establish an expression for time to failure (i.e., unreliability, q) as a p-box. For the *i*th function we can say that this is:

$$\overline{\underline{F}}_{q,i}(t) = 1 - \exp(-\overline{\underline{\lambda}}(t)) \tag{7}$$

where $\overline{\underline{F}}_{q,i}(t)$ is the time to failure p-box for function i; and $\overline{\underline{\lambda}}$ could be a point-value, an interval, or a p-box. If it is a point-value (a scalar) then $\overline{\underline{F}}_{q,i}(t)$ becomes $F_{q,i}(t)$, a precisely defined cumulative distribution function. We do not account for i's dependencies in equation 7. Depending on how the functional dependencies are configured, equation 8 or 9 can be used to account for i's dependencies. We can use equation 8 for series functional dependencies and equation 9 for parallel functional dependencies.

$$\overline{\underline{F}}^{*}_{q,i}(t) = \min_{\substack{k \\ i' \in D_i}} \overline{\underline{F}}_{q,i'}(t) \tag{8}$$

$$\overline{\underline{F}}^{*}_{q,i}(t) = \max_{\substack{k \\ i' \in D_i}} \overline{\underline{F}}_{q,i'}(t) \tag{9}$$

where $\underline{\overline{F}}^{*}_{q,i}(t)$ is the time to failure p-box for function i when the potential failure of their functional dependencies are taken into account.; $\min_k$ and $\max_k$ are the minimum and maximum operators respectively; k could be Fréchet, perfect, and independent (e.g. $\min_{\text{Fréchet}}$ is the Fréchet minimum operator); $\underline{\overline{F}}_{q,i'}(t)$ is the p-box of time to failure of function i when accounting for just its own potential for failure (not including the potential of its dependencies to fail). It follows from equations 3, 8, and 9 that the reliability of i is $\underline{\overline{R}}^{*}_{i}(t) = 1 - \underline{\overline{F}}^{*}_{q,i}(t)$.

Complex systems typically feature hybrid series-parallel arrangements. In such instances, each series and parallel subset can be assessed using Equations 10 and 11 respectively, where $p \subset D_i$ is a subset of the system or environment functions that forms a series or parallel configuration. In case of parallel configuration, all elements of p must fail for a failure to register on any functions that rely on it. The next step would be to combine $\underline{\overline{F}}^{*}_{q,ip}(t)$ of all subsets in the system using the appropriate min and max operations to determine the time to failure of the entire system.

$$\underline{\overline{F}}^{*}_{q,ip}(t) = \min_{k}_{i' \in p \subset D_i} \underline{\overline{F}}_{q,i'}(t) \quad (10)$$

$$\underline{\overline{F}}^{*}_{q,ip}(t) = \max_{k}_{i' \in p \subset D_i} \underline{\overline{F}}_{q,i'}(t) \quad (11)$$

Similarly, the time to failure of a subset of functions in series, G, becomes:

$$\underline{\overline{F}}^{*}_{q,G}(t) = \min_{F}_{i' \in D_G} \underline{\overline{F}}_{q,i'}(t) \quad (12)$$

If G contains all functions, then this expression provides the p-box for the time until the entire system fails. Or, if G includes functions within just one type of subsystem, such as power, then it describes the time until a fault occurs in that sub-system.

The methodology described above can account for many complexities in reliability assessment. Before moving on to more detailed cases, it is worth examining the application of the above equations with three demonstration examples.

3.1. Demonstration Example 1

Assume an expert is asked about the failure rates (λ) of the system components in Figure 1.a, and they provide us with the precise values of λ in an ideal situation with no epistemic uncertainty as follows: $\lambda_A = 0.01$, $\lambda_B = 0.003$, $\lambda_C = 0.015$, and $\lambda_D = 0.07$. Time to failure p-boxes corresponding to these precise failure rates collapse into cumulative distribution functions (Figure 1.b).

If we consider redundancy without repair, and it is assumed that failed redundant units remain failed until the whole system fails then the time to failure of A in the system ($\underline{\overline{F}}^{*}_{q,A}$) can be calculated through the following formula:

$$\underline{\overline{F}}^{*}_{q,A} = \min_k ((\max_k (F_{q,B}, F_{q,C}, F_{q,D}), F_{q,A}) \quad (13)$$

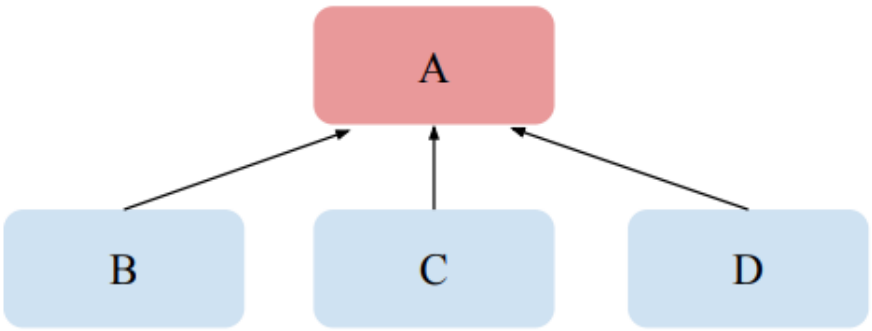
A
B
C
D

(a)

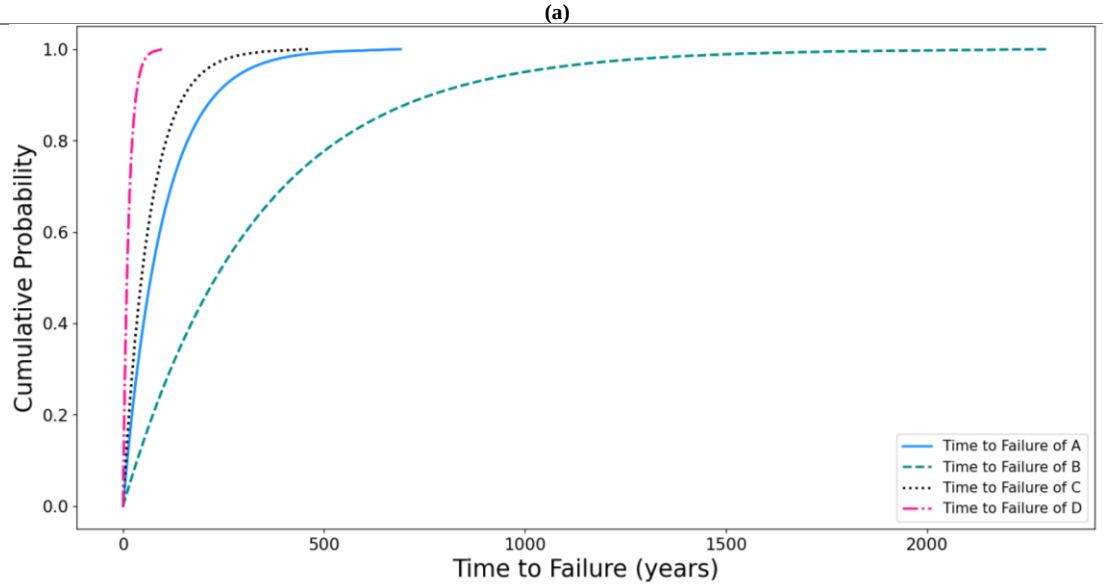
Cumulative Probability
Time to Failure (years)
Time to Failure of A
Time to Failure of B
Time to Failure of C
Time to Failure of D

(b)

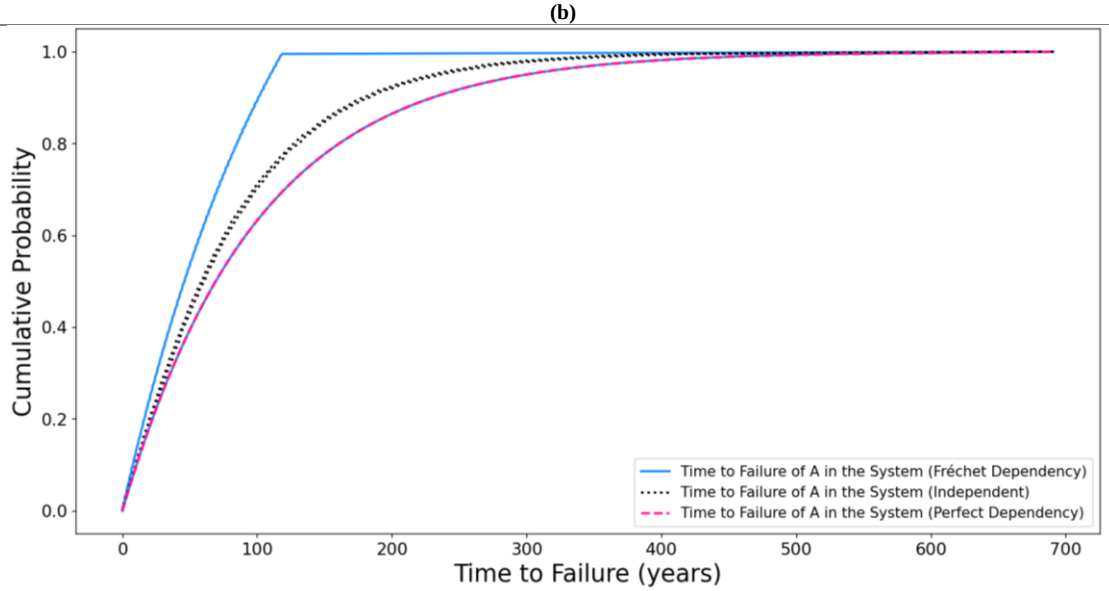
Cumulative Probability
Time to Failure (years)
Time to Failure of A in the System (Fréchet Dependency)
Time to Failure of A in the System (Independent)
Time to Failure of A in the System (Perfect Dependency)

(c)

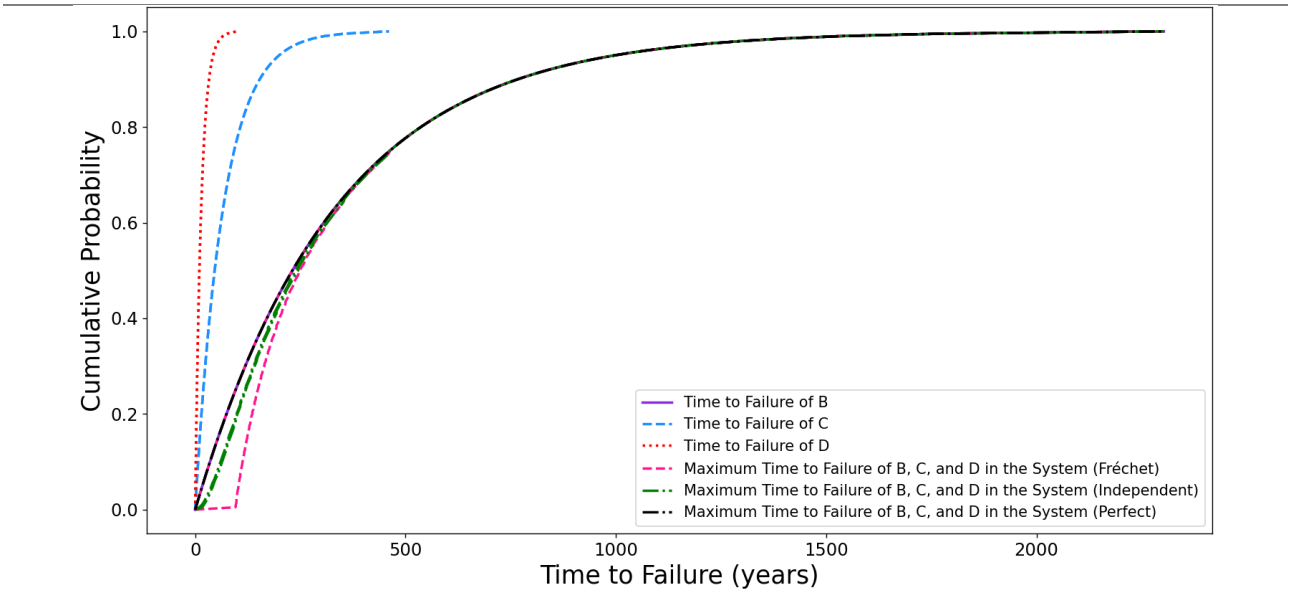

(d)

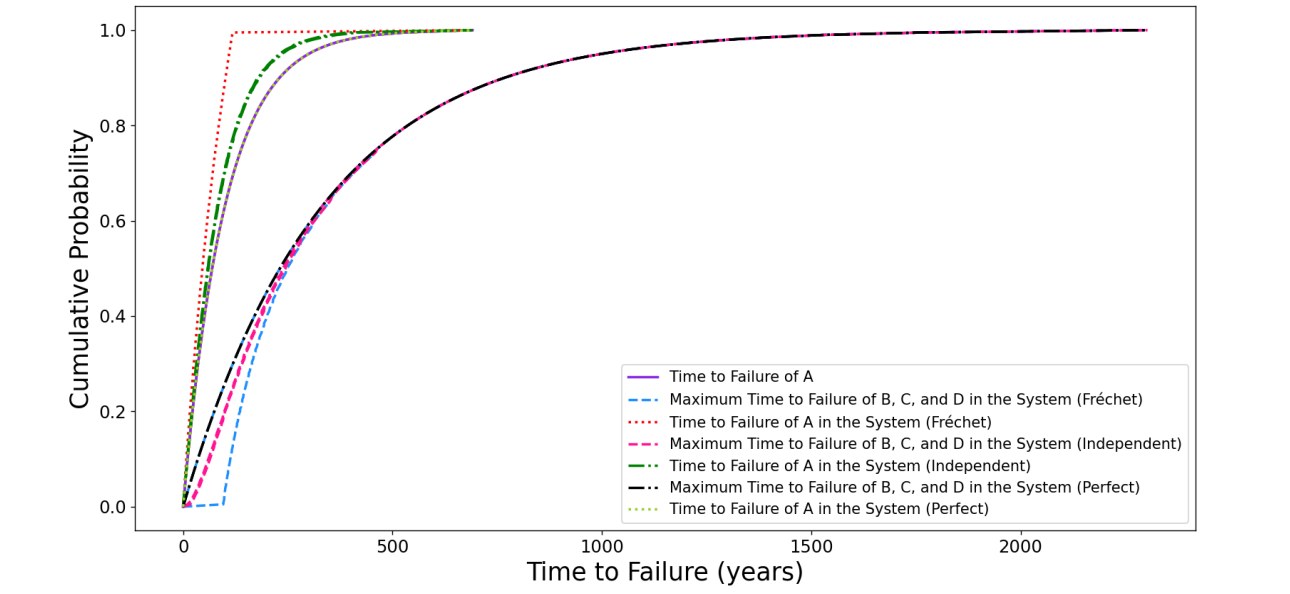

(e)

Figure 1. a) Redundant system composed of unit A with failure rate λ_A= 0.01, B with failure rate λ_B= 0.003, C with failure rate λ_C= 0.015, and D with failure rate λ_D= 0.07 (failures/year). b) Time to failure of system units in Figure 1.a. c) Time to failure of the system (unit A in the system) in Figure 1.a, for different type of probabilistic dependency between time to failure of units A, B, C, and D. d) Time to failure of B, C, and D, and $\max_k$ ($F_{q,B}$, $F_{q,C}$, $F_{q,D}$), for different probabilistic dependency type. e) Time to failure of A, $\max_k$ ($F_{q,B}$, $F_{q,C}$, $F_{q,D}$), and minimum time to failure of A and $\max_k$ ($F_{q,B}$, $F_{q,C}$, $F_{q,D}$) for different types of dependency.

Figure 1.c depicts the time to failure of unit A in the system ($\overline{F}^{*}_{q,A}$) in Figure 1.a for various types of probabilistic dependency between time to failure of units A, B, C, and D. In case of perfect probabilistic dependency between time to failure of systems units, the uncertainty in the estimated time to failure of the system, which is reflected in the breadth between the left and right bounds of the p-box, is 3.5 years. We have a 5.9 years uncertainty in the estimated time to failure of the system if we assume there is no probabilistic dependency between the time to failure of the system units. And finally, the maximum uncertainty is caused by not making any assumptions about the probabilistic relationship between the time to failure of system units (Fréchet), which results in 51.6 years.

As shown in Figure 1.c, the independent case leads to higher probability of failure or smaller time to failure than the perfect case, and that there are regions of the Fréchet, that still include higher probabilities than the perfect case for a given time. To further investigate the role of stochastic dependence, we will first focus on the maximum part of the Equation 13. As stated by Oberkampf et al. (2004), if one random variable is almost certainly a non-decreasing function of the other, they have perfect dependence. Therefore, when there is perfect dependency between time to failure of the units, the presence of high (low) failure time for one unit of the system implies that the others will also take high (low) values. Figure 1.d shows that the maximum time to failure probability or minimum probability of failure of units B, C, and D when they are perfectly dependent is equal to the probability of failure of unit B, which has the smallest failure probability or longest time to failure among the other units.

Variables or events on the other hand are independent if the occurrence of a specific value of the one has no impact on the probability of occurrence of any value of the other. The maximum time to failure probability of units B, C, and D when they are independent, would be the multiplication of time to failure probability of each of them. Since the probabilities are in the range [0,1], multiplying them yields a lower probability than each of them separately. That is the reason independent scenario leads to lower failure probability or longer time to failure probability than the perfect scenario in Figure 1.d.

The next step would be to calculate minimum of ($\max_k$ ($F_{q,B}$, $F_{q,C}$, $F_{q,D}$)) and $F_{q,A}$. In case of perfect dependency, minimum of ($\max_k$ ($F_{q,B}$, $F_{q,C}$, $F_{q,D}$)) and $F_{q,A}$ will be the smaller one which is $F_{q,A}$ (Figure 1.e). In case of Independence assumption, the minimum time to failure probability of ($\max_k$ ($F_{q,B}$, $F_{q,C}$, $F_{q,D}$)) and $F_{q,A}$, would be multiplication of time to failure probability of each of them. Therefore, the resultant time to failure p-box will be smaller than perfect dependency scenario. Finally, the p-box that results when no assumptions are made regarding the probabilistic relationship between the time to failure of ($\max_k$ ($F_{q,B}$, $F_{q,C}$, $F_{q,D}$)) and $F_{q,A}$ (Fréchet), encloses the bounds of perfect and independent p-boxes.

As we can see the assumption about the nature of the dependency between the time to failure of system units significantly affects the estimated time to failure of the system and its associated uncertainty. For example, assuming perfect dependency between time to failure of the systems units leads to larger time to failure of the system in comparison to independence assumption. Therefore, assuming independence when it is not justified, may lead to overestimation of the reliability. Accordingly, when we do not have enough information regarding the type of dependency between the system components, we should make no assumption (Fréchet), rather than an independence assumption.

3. 2. Demonstration Example 2

Often, due to time and resource constraints, we just have an interval representing the possible values of the failure rate (λ). This interval can be used to establish the corresponding time to failure P-box.

Considering the system in Figure 1.a but with interval values for the failure rates such that λ_A= [0.01,0.02], λ_B= [0.003,0.004], λ_C= [0.015,0.02], λ_D= [0.07,0.08]. The corresponding time to failure p-boxes of these intervals are presented in Figure 2.a.

We are considering redundancy without repair, and it is assumed that failed redundant units remain failed until the whole system fails. Time to Failure of A in the system ($\overline{\underline{F}}^{*}_{q,A}$) is calculated through the Equation 14 and resultant p-boxes are presented in Figure 2.b.

$$\overline{\underline{F}}^{*}_{q,A} = \min_k \left((\max_k \left(\overline{\underline{F}}_{q,B}, \overline{\underline{F}}_{q,C}, \overline{\underline{F}}_{q,D} \right), \overline{\underline{F}}_{q,A} \right) \quad (14)$$

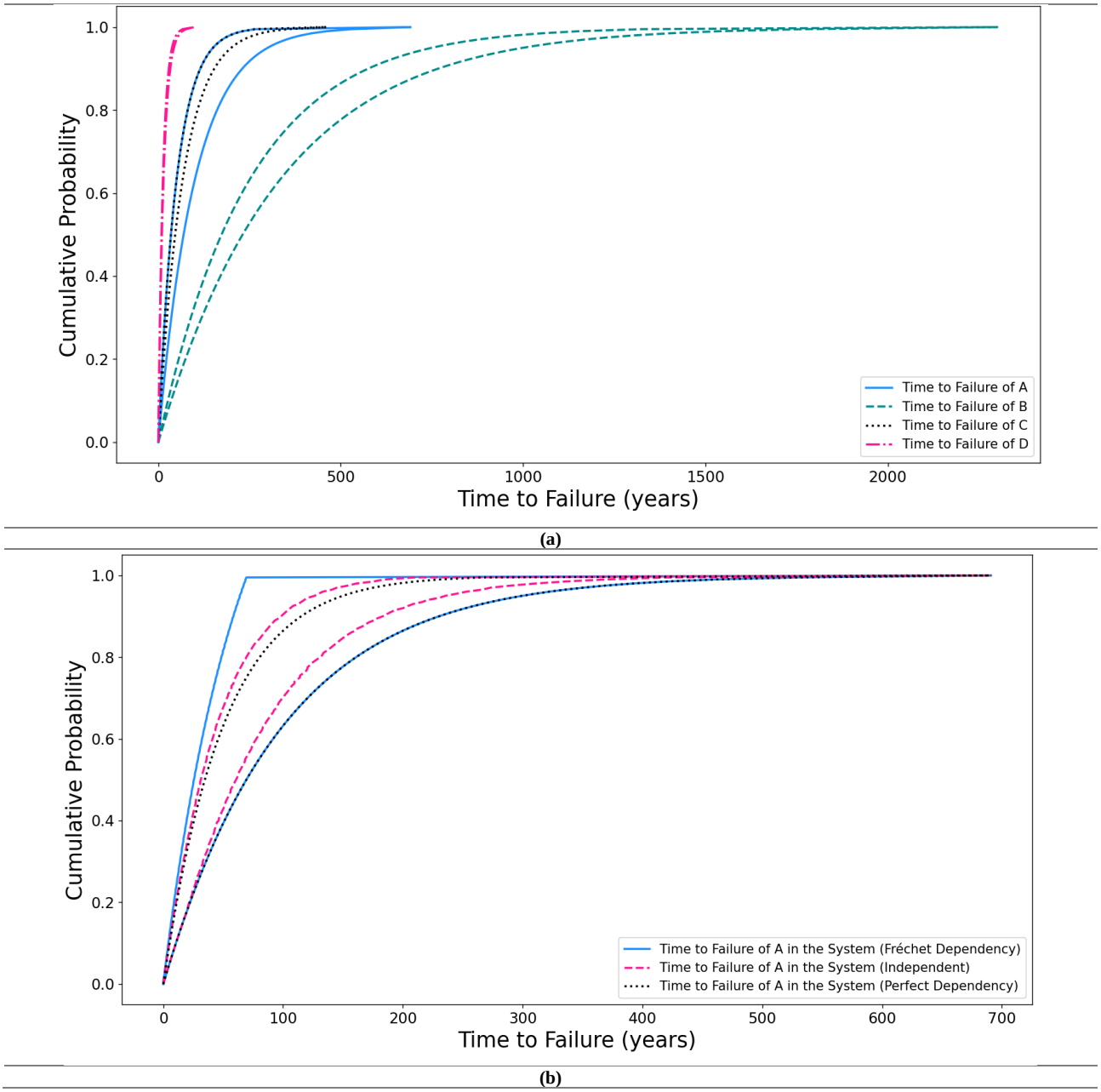

Figure 2. a) Time to failure p-boxes of units A, B, C, and D in the Figure 1.a where the time to failure of each unit represents by an interval to emphasize the commonness of epistemic uncertainty as follow: λ_A= [0.01,0.02], λ_B= [0.003,0.004], λ_C= [0.015,0.02], λ_D= [0.07,0.08]. b) Time to failure of unit A in the system ($\overline{\underline{F}}^{*}_{q,A}$) for different type of dependency between time to failure of units A, B, C, and D.

We widen λ_A by increasing the right end point of the λ_A interval to investigate how the precision of the hazard rate affects the estimated time to failure of the system and whether the effects are the same for different types of dependency between the systems components. Figure 3.a shows

how uncertainty changes by widening λ_A. As the interval increases, the uncertainty in the case of perfect dependency approaches asymptotically to Fréchet's uncertainty. Furthermore, we can see that the uncertainty for the independent case is lower than that of the perfect dependent and Fréchet cases.

In conclusion, regardless of the type of dependency we have between system components, the uncertainty of the estimated time to failure increases as λ_A widens. We can also see that for large hazard rate intervals, it is not worthwhile to investigate the precise dependency between system units, and it is more practical to focus on investigating the precise hazard rate (λ_A). Figure 3.a also shows that the difference between uncertainty in Fréchet and perfect case is less than the difference between uncertainty in Fréchet and independent scenario. This is because positive perfect dependency is equal to either one of the Fréchet bounds. As shown in Figure 2.b, the lower bound of $\underline{\overline{F}}^{*}_{q,A}$ for perfect dependency coincides with the lower bound of $\underline{\overline{F}}^{*}_{q,A}$ in case of Fréchet dependency. As the λ_A's right endpoint is increased, the uncertainty in the perfect dependent case grows, and the upper bound of the perfect dependent case approaches the upper bound of the Fréchet scenario.

Furthermore, to investigate how the position of the unit in the system can change our above conclusion, we widen λ_B by increasing the right end point of the λ interval and fix the hazard rate of units A, C, and D as reported in Figure 3.b and 3.c. We also repeat the same procedure for λ_D, (Figure 3.d and 3.e). We see that for λ_B, by increasing interval breadth, the uncertainty increases for Fréchet and independent cases and then it becomes constant. For λ_B, dependency appears to have a greater influence on the uncertainty of the estimated time to failure. Also, we see that increasing λ_B has no effect on the associated uncertainty with the perfect dependency. Because unit B has the lowest hazard rate and failure probability in comparison to the others system components. Therefore, no matter what the right endpoint of its interval is, in Equation 14, the results of $\max_k (\underline{\overline{F}}_{q,B}, \underline{\overline{F}}_{q,C}, \underline{\overline{F}}_{q,D})$ would always be $\underline{\overline{F}}_{q,B}$, but in the minimum part of the Equation 14, the $\underline{\overline{F}}_{q,A}$ would be effective since it has the higher failure probability. That is why, for perfect dependency, changing λ_B has no effect on the uncertainty in the estimated time to failure. Instead, in case of perfect dependency, the rate of change in uncertainty by changing A is greater than the others.

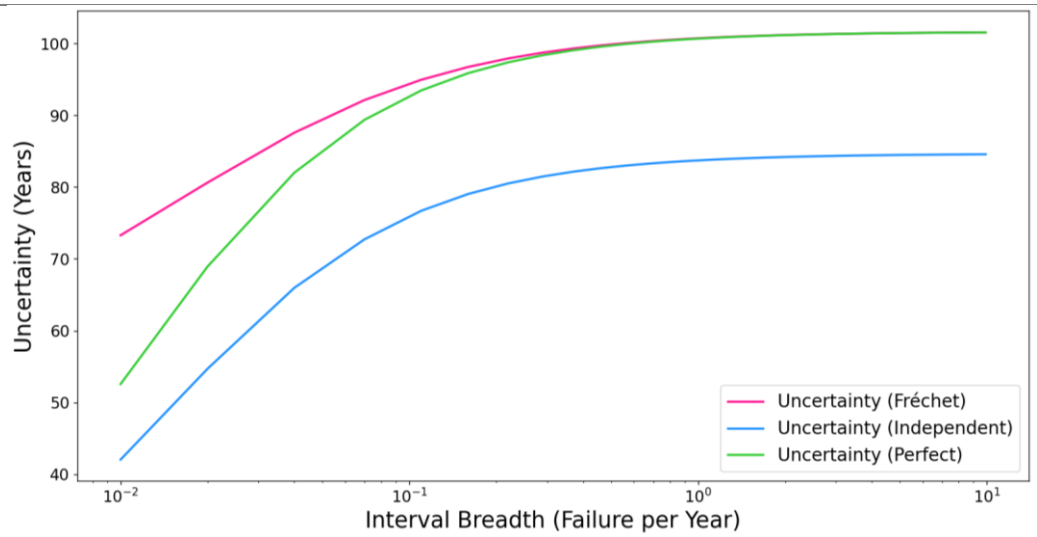

(a)

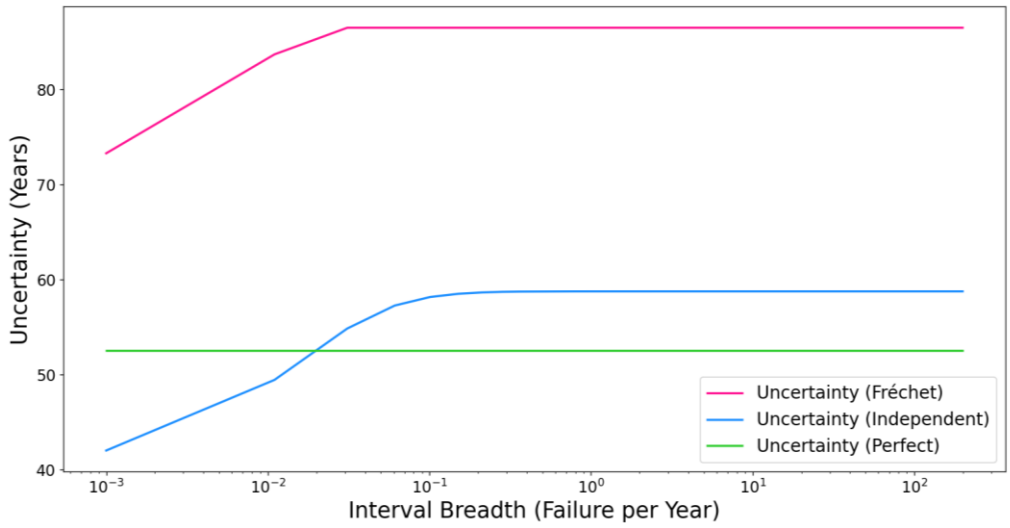
Uncertainty (Years)
80
70
60
50
40
10^{-3}
10^{-2}
10^{-1}
10^{0}
10^{1}
10^{2}
Interval Breadth (Failure per Year)
Uncertainty (Fréchet)
Uncertainty (Independent)
Uncertainty (Perfect)

(b)

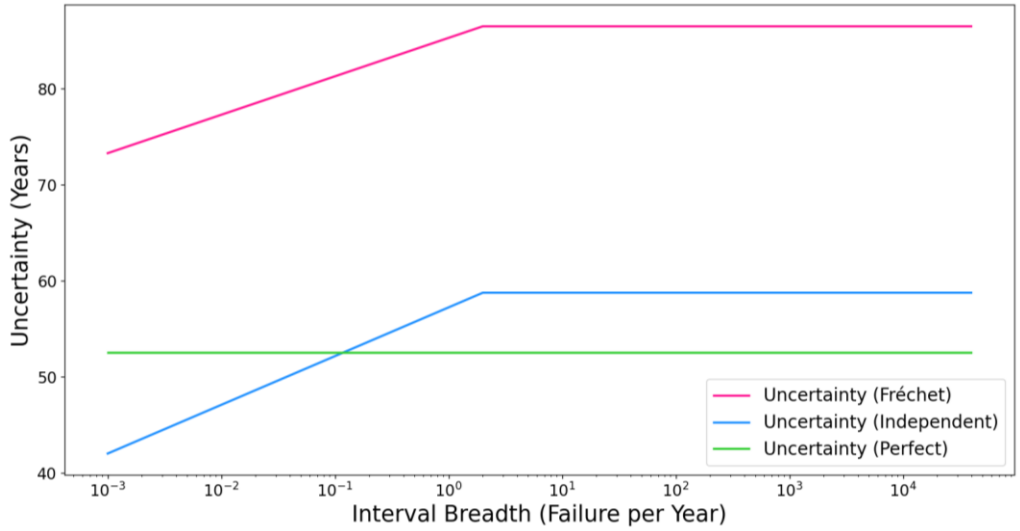
Uncertainty (Years)
80
70
60
50
40
10^{-3}
10^{-2}
10^{-1}
10^{0}
10^{1}
10^{2}
10^{3}
10^{4}
Interval Breadth (Failure per Year)
Uncertainty (Fréchet)
Uncertainty (Independent)
Uncertainty (Perfect)

(c)

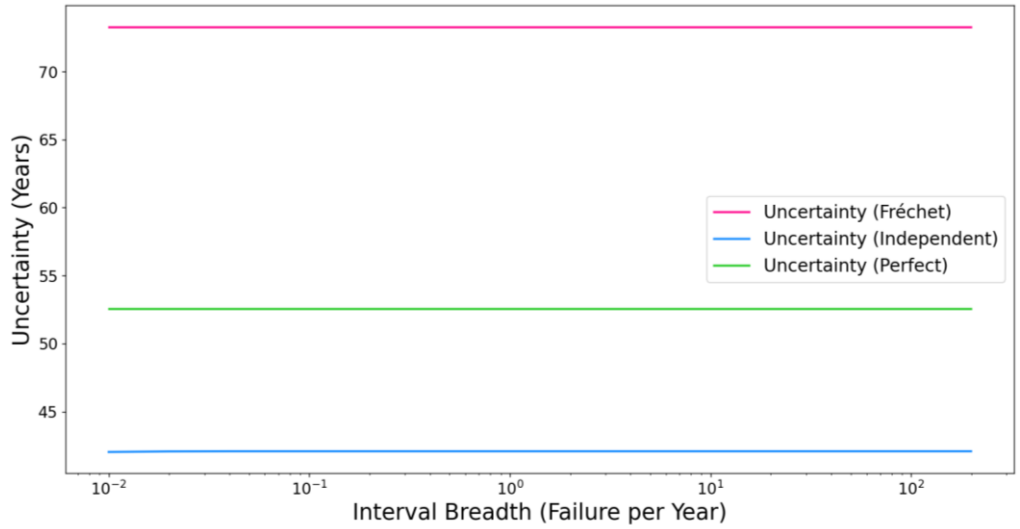
Uncertainty (Years)
70
65
60
55
50
45
10^{-2}
10^{-1}
10^{0}
10^{1}
10^{2}
Interval Breadth (Failure per Year)
Uncertainty (Fréchet)
Uncertainty (Independent)
Uncertainty (Perfect)

(d)

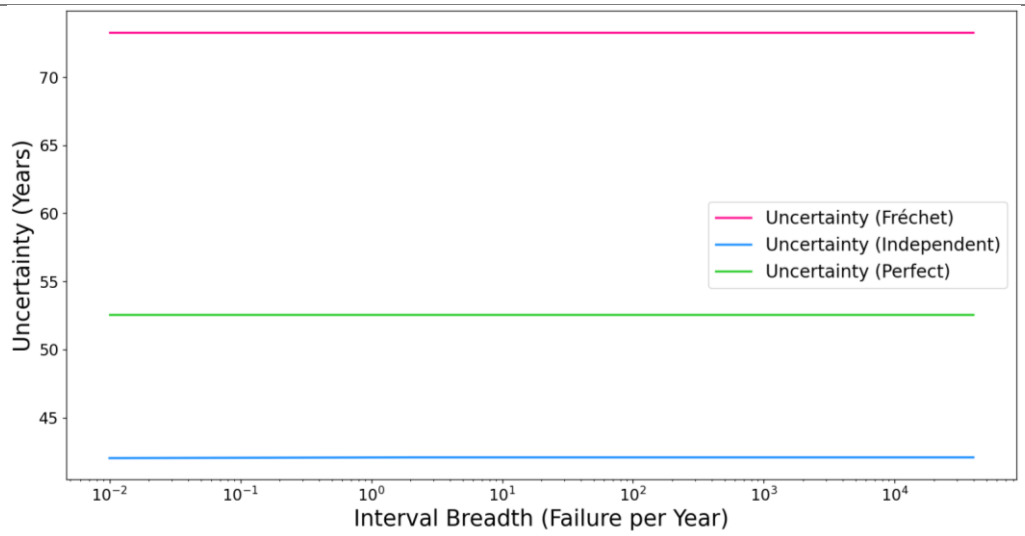

(e)

Figure 3. a) The change in the uncertainty for different types of dependency while λ_A was increased by 0.01 year 45 times. b) Change in the uncertainty for each type of dependency while λ_B was increased by 0.01 year 200 times. c) Change in the uncertainty for each type of dependency while λ_B was increased by 2 years 200 times. d) Change in the uncertainty for each type of dependency while λ_D was increased by 0.01 year for 200 times. e) Change in the uncertainty for each type of dependency while λ_D was increased by 2 years 200 times.

3.3. Demonstration Example 3

Considering the system in Figure 4.a, where the units B, C, and D are redundant with units E and F, and the failure rate of each unit is as follow: λ_A = [0.01,0.02], λ_B= [0.003,0.004], λ_C= [0.0035,0.0045], λ_D= [0.001,0.002], λ_E= [0.0035,0.0045], λ_F= [0.001,0.002] (failures/year). The corresponding time to failure p-boxes of these intervals are presented in Figure 4.b.

We are considering redundancy without repair, and it is assumed that failed redundant units remain failed until the whole system fails. Time to Failure of A in the system ($\overline{\underline{F}}^{*}_{q,i}$) is calculated through the following formula and presented in Figure 4.c:

$$\overline{\underline{F}}^{*}_{q,A} = \min_k \left(\overline{\underline{F}}_{q,A}\right), \left(\max_k \left(\left(\min_k \left(\overline{\underline{F}}_{q,B}, \overline{\underline{F}}_{q,C}, \overline{\underline{F}}_{q,D}\right)\right), \left(\min_k \left(\overline{\underline{F}}_{q,E}, \overline{\underline{F}}_{q,F}\right)\right)\right)\right) \quad (15)$$

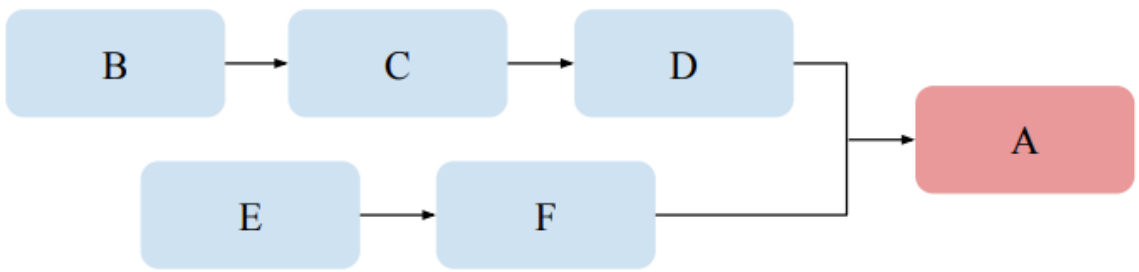

(a)

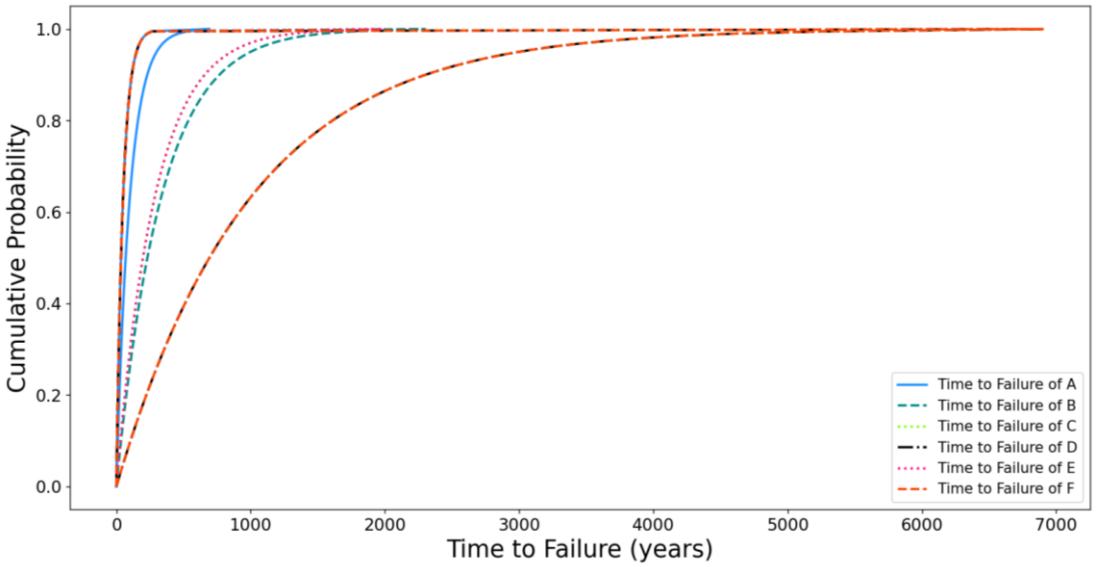
Cumulative Probability
Time to Failure (years)
Time to Failure of A
Time to Failure of B
Time to Failure of C
Time to Failure of D
Time to Failure of E
Time to Failure of F

(b)

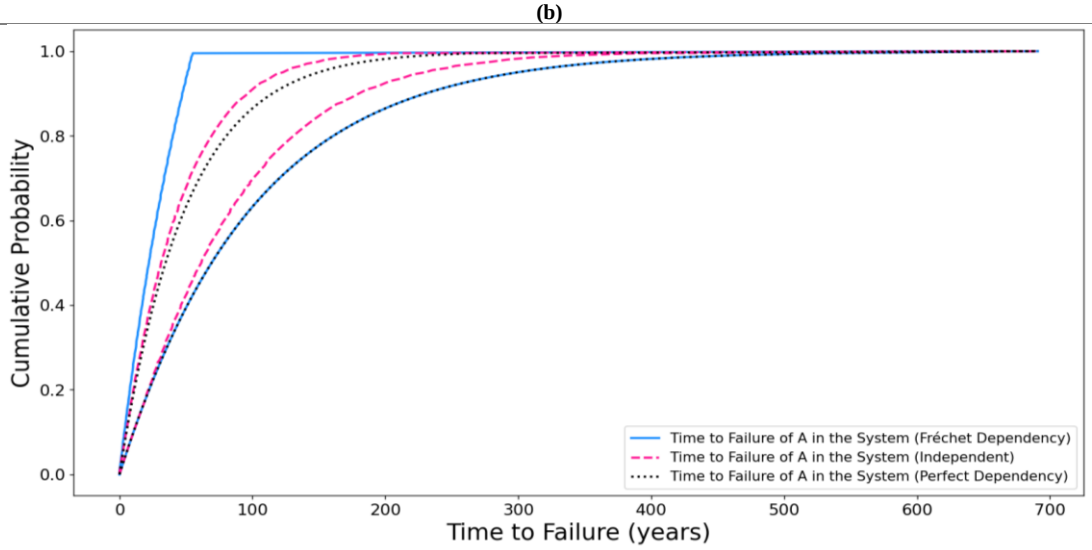
Cumulative Probability
Time to Failure (years)
Time to Failure of A in the System (Fréchet Dependency)
Time to Failure of A in the System (Independent)
Time to Failure of A in the System (Perfect Dependency)

(c)

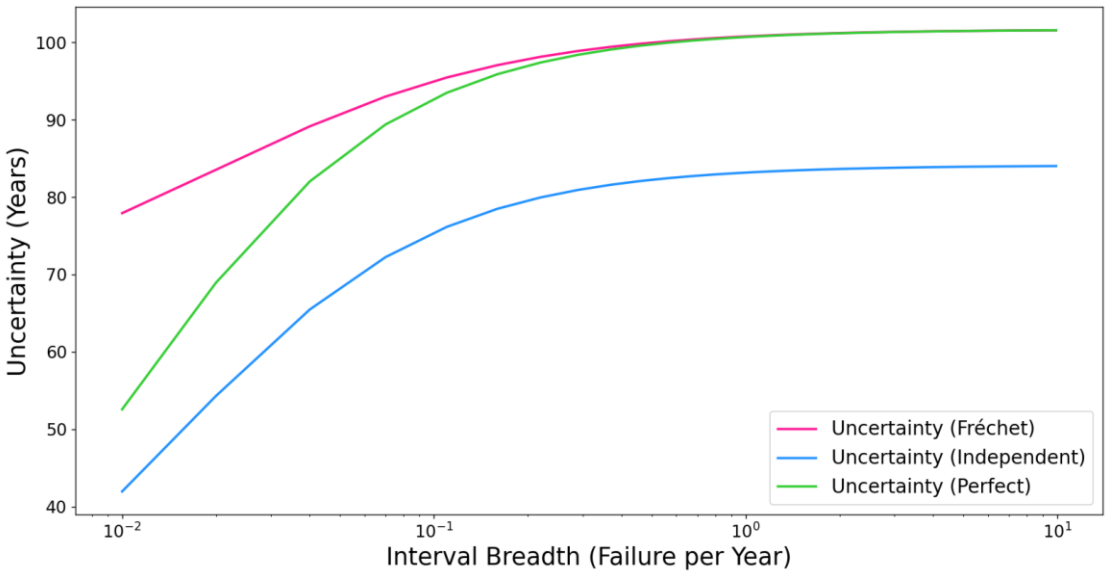
Uncertainty (Years)
Interval Breadth (Failure per Year)
Uncertainty (Fréchet)
Uncertainty (Independent)
Uncertainty (Perfect)

(d)

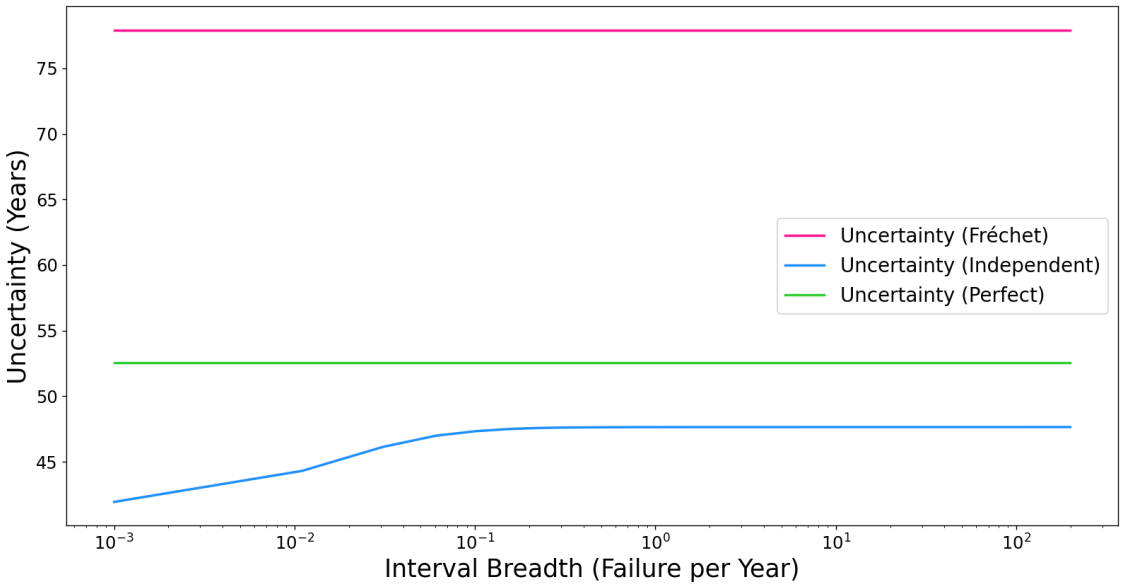

(e)

Figure 4. a) Redundant system composed of unit A with failure rate λ_A = [0.01,0.02], B with failure rate λ_B= [0.003,0.004], C with failure rate λ_C= [0.0035,0.0045], D with failure rate λ_D= [0.001,0.002], E with failure rate λ_E= [0.0035,0.0045], and F with failure rate λ_F= [0.001,0.002] (failure/year). b) Time to failure of units A, B, C, D, E, and F in Figure 4.a. c) Time to failure of the system (unit A in the system) in Figure 4.a, for different types of probabilistic dependency between time to failure of units A, B, C, D, E, and F. d) Change in the uncertainty for each type of dependency while λ_A was increased by 0.01 (failure/year) 45 times. e) Change in the uncertainty for each type of dependency while λ_B was increased by 0.01 (failure/year) 200 times.

We widen λ_A (Figure 4.d) and repeat the same procedure for λ_B (Figure 4.e) to investigate if the results in this case show a different pattern than the results of the system in the previous example, and to see how the structure of the system affects our previous conclusion. What we can see in this case (system with redundant parts) is that the width of the hazard rate interval is more important for the series part of the network, whereas the type of dependency will be the dominant factor in the amount of uncertainty in the estimated time to failure of the system for the redundant part of the network except for independent scenario in which changing the interval breath, can slightly increase the uncertainty. As a result, in such a case, the more practical approach would be to investigate the dependency type for the redundant parts of the network.

4. Practical case applications

Here we apply the proposed p-box methodology to the power grid and water and wastewater municipal infrastructure to demonstrate its applicability in these contexts. Subsequently we apply the method to the network of water and power components in an office building, including their functional dependence on the power grid and water and wastewater infrastructure to illustrate the use of the method for dealing with reliability of functional dependency networks.

4.1. P-boxes of the power grid

There are common measures that can be used to establish the time to failure and downtime p-boxes for the power grid. These are the System Average Interruption Frequency Index (SAIFI), the System Average Interruption Duration Index (SAIDI) and the Customer Average Interruption Duration Index (CAIDI) (IEEE 1999). The SAIFI describes the average number of sustained outages experienced by an average customer each year:

$$\text{SAIFI} = \frac{\text{Total number of customer interruptions in one year}}{\text{Total number of customers served}} \tag{16}$$

the SAIDI describes the total hours of sustained interruption experienced by an average customer each year:

$$\text{SAIDI} = \frac{\text{Total durations of customer intruption}}{\text{Total number of customers served}} \tag{17}$$

and the CAIDI = SAIDI/SAIFI describes the average time needed to restore service to a customer per outage, or:

$$\text{CAIDI} = \frac{\text{SAIDI}}{\text{SAIFI}} = \frac{\text{Total durations of customer intruption}}{\text{Total number of customer interruptions}} \tag{18}$$

The SAIFI is effectively λ from Equation 3, for the time to failure. CAIDI can be taken as m form Equation 5. However, since these individual indices are random variates, it is important to study their distribution, not just their mean point value (Billinton, 1988; Carpaneto & Chicco, 2004). For illustration purposes we can use data from Eto et al., (2012) to illustrate the distributions for SAIDI and SAIFI, and then we can calculate a distribution for CAIDI. Eto et al. (2012) provide a box plot for SAIDI and SAIFI from 2000 to 2009 with and without inclusion of major events. The SAIFI and SAIDI statistics are taken from 155 American utilities (about 50% of national electricity production), excluding major outage events, are summarized in Tables 6 and 7 in the Appendix. We use these quantities to formulate quantile derived distributions for SAIDI and SAIFI and generate their corresponding p-boxes for each year. To calculate the p-box for CAIDI we use Fréchet division since there is unknown dependence between SAIDI and SAIFI. For real-world application of this method utility specific, or even more location specific SAIFI and SAIDI data can be used. The resulting p-boxes for year 2009 are shown in Figure 5. Parts d and e of Figure 5 show the resulting time to failure and repair time p-boxes calculated from Equations 3 and 5, respectively. The medians for these curves range between 0.113 year and 6.418 years for time to failure and 0.001 hour and 65.110 hours for repair time. The means of these curves range from 0.162 year and 9.259 years for time to failure and 0.001 hour and 93.935 hours for repair time.

As reported by Eto et al., (2012), there is significant variation in the annual values of SAIDI and SAIFI, without including major events (mean of the coefficient of variations is greater than 20 percent). To account for the variation in electricity supply reliability measurements from year to year, the SAIDI and SAIFI p-boxes of each year (from 2000 to 2009) are mixed in the following step. Figure 6.a and 6.b show the resulting SAIDI and SAIFI p-boxes, respectively. In Table 1 we compare the mean and median of the year 2009 SAIFI and time to failure p-boxes with the SAIFI generated from combining SAIFI p-box of each year (from 2000 to 2009) and its corresponding time to failure p-box. The left endpoint of the median interval of the 10-year mixing SAIFI is equal to the median of the year 2009 SAIFI which is a scalar value (1.156 failures per year). Also, there is not a significant difference between the mean intervals of year 2009 SAIFI and 10-years mixing SAIFI (0.045 (failures/year) difference in the left endpoints and 0.419 (failures/year) difference in the right endpoints). Since the equation used to calculate time to failure (Equation 3) is an exponential function, even a small difference in failure rates (SAIFI) can result in a significant difference in estimated time to failure, as we can see in Table 1.

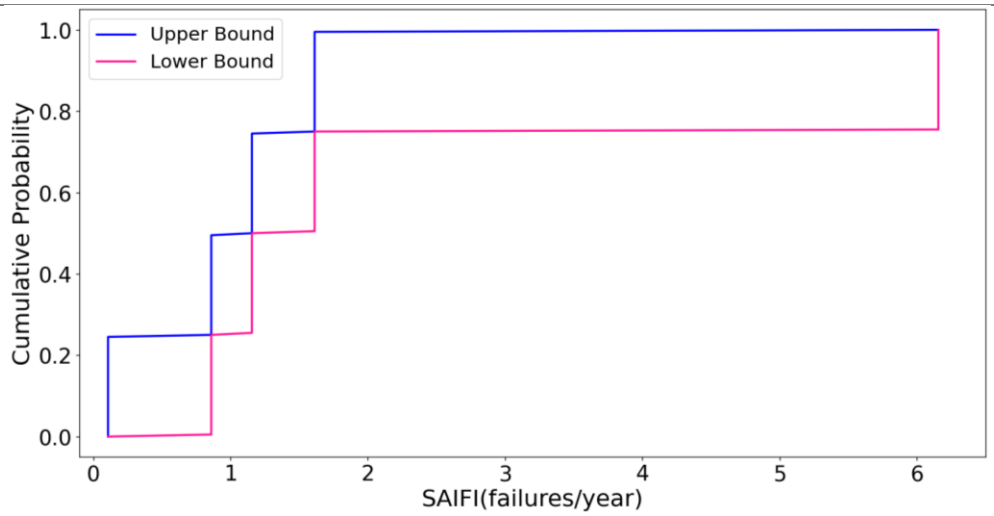
Upper Bound
Lower Bound
Cumulative Probability
SAIFI(failures/year)
0.0
0.2
0.4
0.6
0.8
1.0
0
1
2
3
4
5
6

(a)

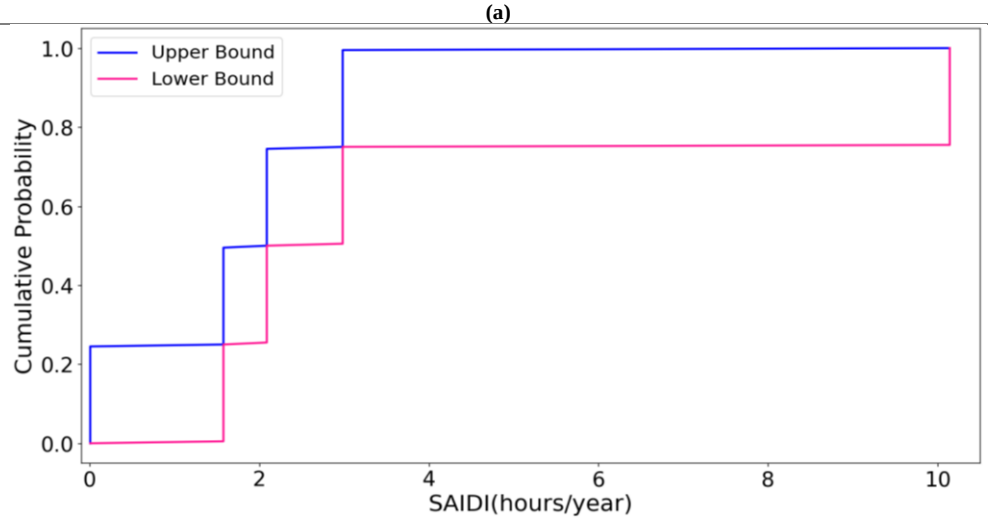
Upper Bound
Lower Bound
Cumulative Probability
SAIDI(hours/year)
0.0
0.2
0.4
0.6
0.8
1.0
0
2
4
6
8
10

(b)

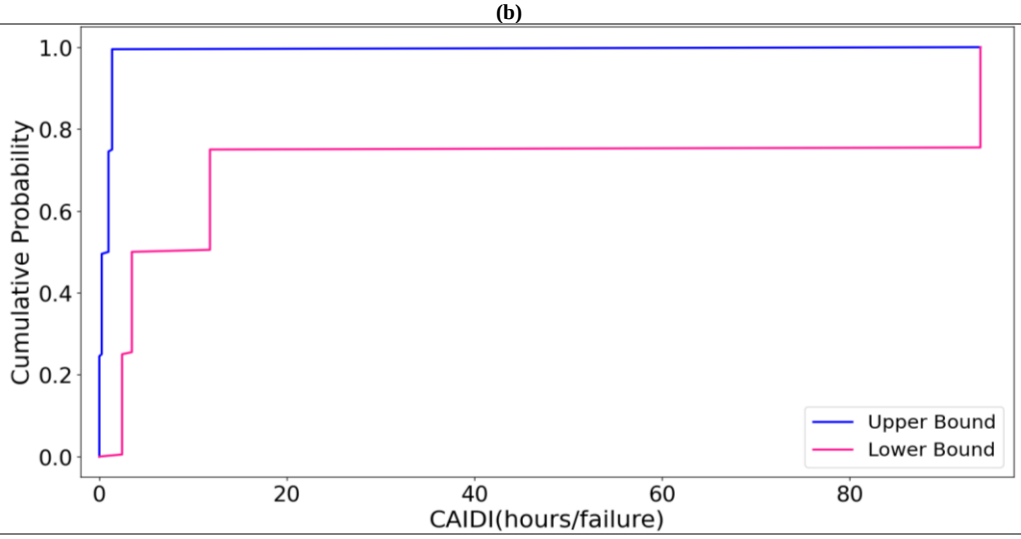
Upper Bound
Lower Bound
Cumulative Probability
CAIDI(hours/failure)
0.0
0.2
0.4
0.6
0.8
1.0
0
20
40
60
80

(c)

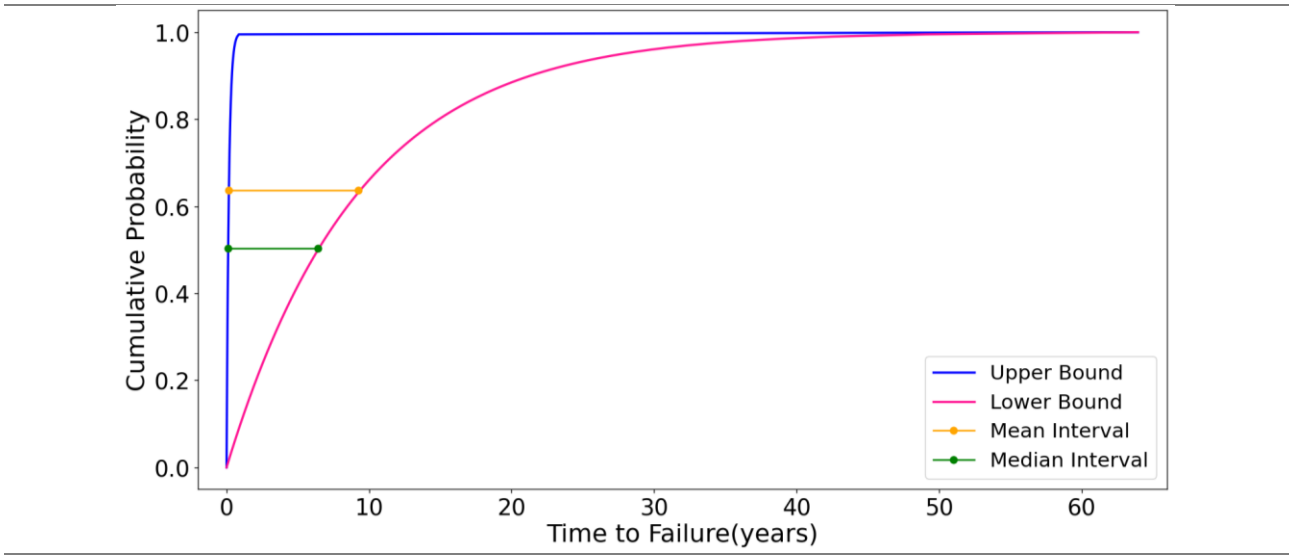

(d)

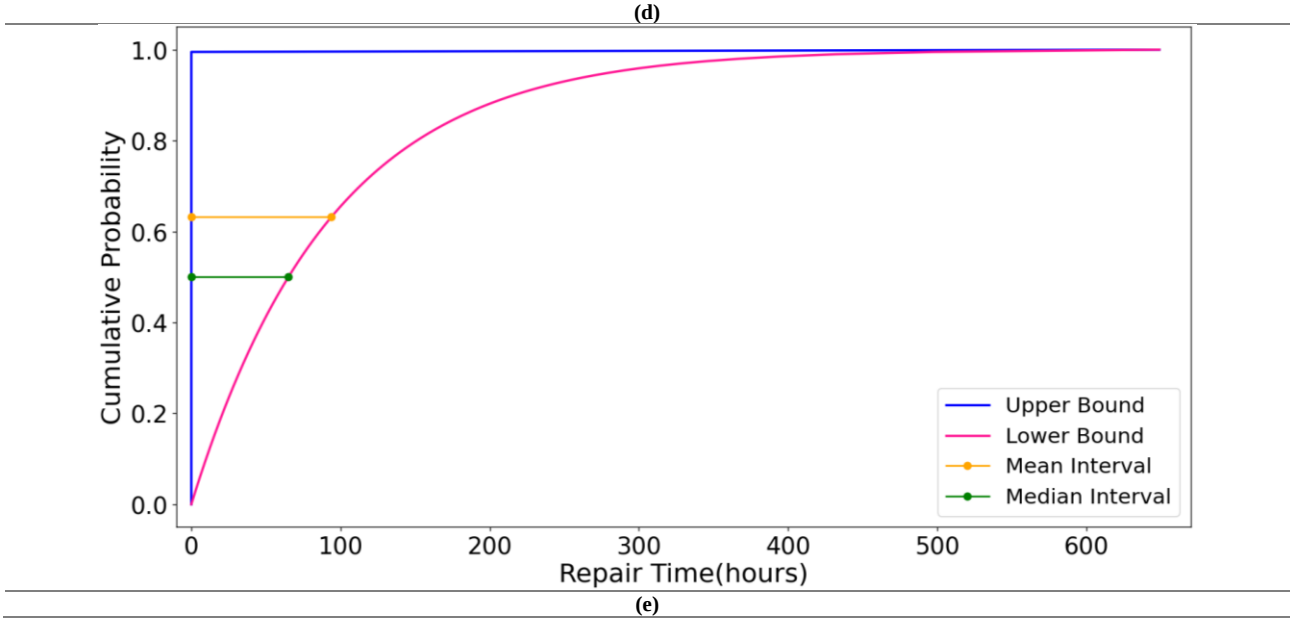

(e)

Figure 5. Electricity grid p-boxes, a) SAIFI, b) SAIDI, c) CAIDI, d) Time to failure, and e) Repair time.

Table 3. Mean and median of year 2009 SAIFI p-box and SAIFI p-box generated from mixing SAIFI p-box of each year (from 2000 to 2009), as well as mean and median of time to failure p-boxes derived from 2009 SAIFI p-box and mixing 10-year SAIFI p-box.

	SAIFI (failures/year)		**Time to Failure (years)**	
	2009	**Mix of 10 years**	**2009**	**Mix of 10 years**
Mean	[0.934, 2.446]	[0.979, 2.865]	[0.162, 9.259]	[0.048, 37.037]
Median	1.156	[1.156, 1.317]	[0.113, 6.418]	[0.033, 25.672]

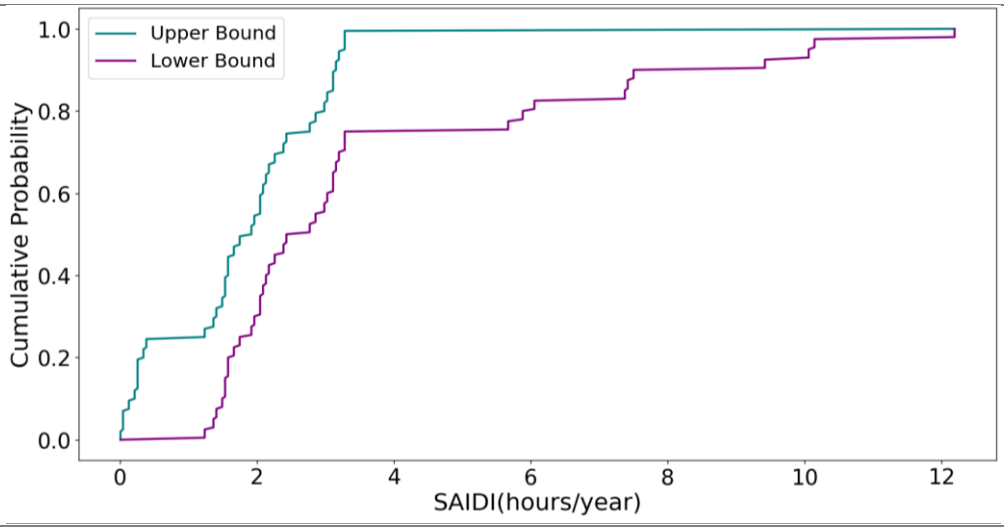

(a)

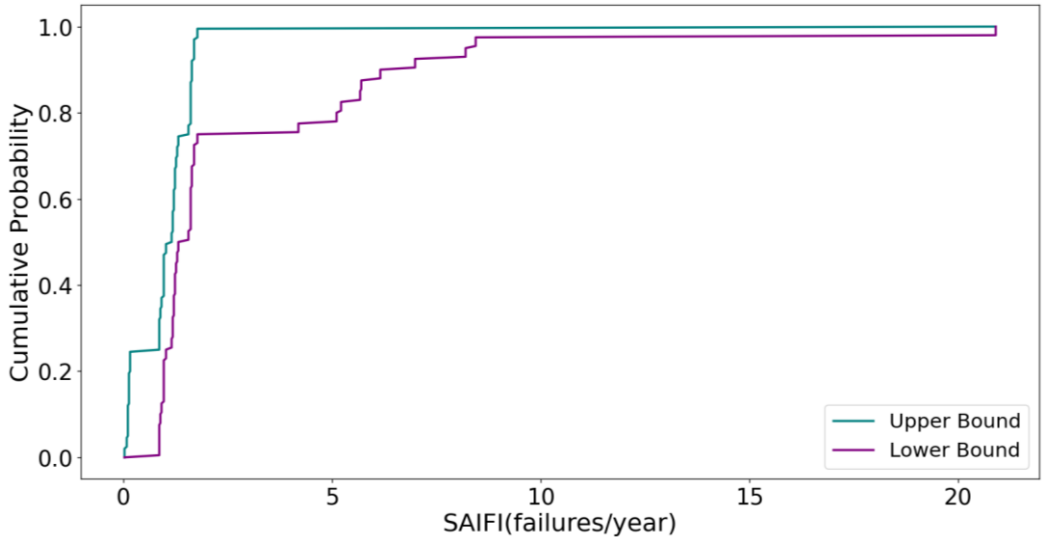

(b)

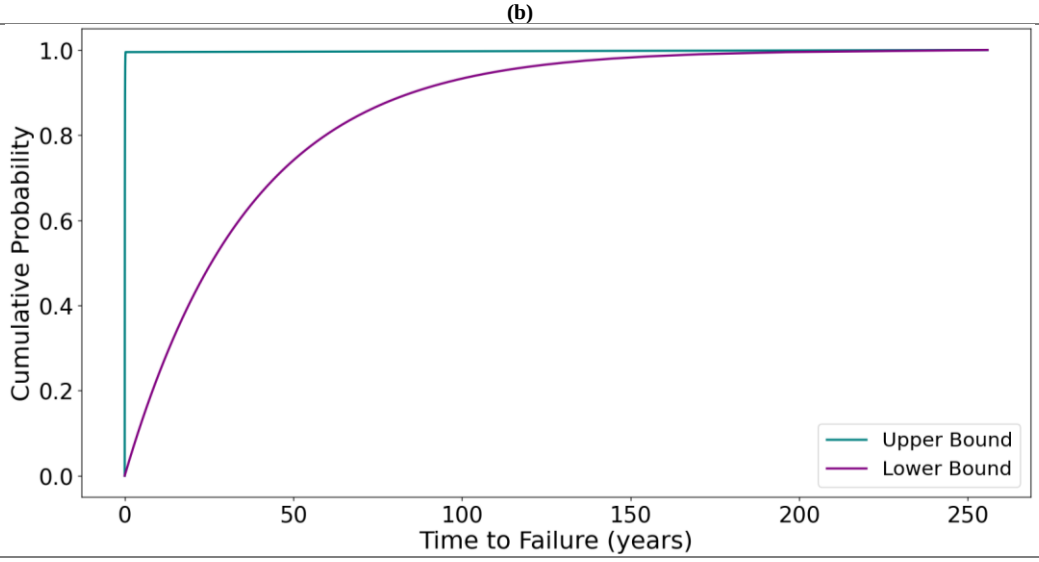

(c)

Figure 6. a) SAIDI (hours/year) p-box generated from mixing SAIDI statistics in each year (from 2000 to 2009) by considering equal weight, b) SAIFI (failures/year) p-box generated from mixing SAIFI statistics in each year (from 2000 to 2009) by considering equal weight, c) Time to failure p-box generated from mixture of SAIFI statistics in each year (from 2000 to 2009) as the failure rate.

As reported by Eto et al. (2012), the line with best fit to the mean SAIDI data is y = 1.84x + 133 with $R^2 = 0.46$ (where y is the mean SAIDI in year x, and x=1 (2000) to x=10 (2009)) and the line with best fit to the median SAIDI data is y = 2.06x + 113 with $R^2 = 0.45$ (where y is the median SAIDI in year x, and x=1 (2000) to x=10 (2009)). Considering best fit lines in Eto et al., (2012), the mean interval of SAIDI is [2.25, 2.52] hours and the median interval will be [1.92, 2.23] hours. The mean and median intervals from the SAIDI p-box generated by mixing SAIDI p-box of each year (Figure 6.a) are [1.73, 3.73] and [1.92, 2.43] hours respectively.

The line with best fit to the mean SAIFI data from Eto et al., (2012) is y = 0.0109 x + 1.35 with $R^2 = 0.22$ (where y is the mean SAIFI in year x, and x=1 (2000) to x=10 (2009)) and the line with best fit to the median SAIFI data is y = 0.0015 x + 1.21 with $R^2 = 0.01$ (where y is the median SAIFI in year x, and x=1 (2000) to x=10 (2009)). Therefore, according to these regressions, the mean interval of SAIFI is [1.36,1.46] failures per year and the median interval is [1.21,1.23] failures per year. The mean and median interval from SAIFI p-box generated by mixing SAIFI p-box of each year (Figure 6.b) are [0.98, 2.86] and [1.16, 1.32] failures per year, respectively. Considering the small R-squared values specially for SAIFI, using the mixture of the SAIDI and SAIFI p-boxes from each year, could be a better representation of the reliability metrics (SAIDI and SAIFI) observed in (Eto et al., 2012).

4. 2. P-boxes of municipal water and wastewater

American Water Works Association (AWWA) (AWWA 2020) defines an index similar to SAIFI, called the Disruption Frequency Index (DFI) measures outage frequency per 1,000 customers per year:

$$\text{DFI} = \frac{\text{Total number of service disrutpions per year}}{\text{Number of active accounts}}\,1000 \tag{19}$$

If we take 1,000 as the mean number of customers affected by each outage, then DFI is equivalent to SAIFI on the average.

AWWA also defines an index similar to CAIDI, called the Average Time to Address Service Disruptions Index (ATASDI). measured in hours:

$$\text{ATASDI} = \frac{\text{Total time to address service disruption}}{\text{Total number of service disruptions}} \tag{20}$$

These indicators can be measured for water and wastewater. We use DFIw and ATASDIw for water service and DFIs and ATASDIs for wastewater service. AWWA only provides the quartiles for these indicators, but we need the maximum and minimum to create a reasonably bounded p-box. A p-box built just from quartiles would have an infinite extent. Luo et al., (2018) and Wan et al., (2014) provide methods for estimating the sample mean ($\overline{x}$) and sample standard deviation (s_x) from quartile information, with and without a known maximum and minimum for normally distributed data as follows:

$$\overline{x} = \left(\frac{4}{4+n^{0.75}}\right)\frac{Q_{min}+Q_{max}}{2} + \left(\frac{n^{0.75}}{4+n^{0.75}}\right)Q_2 \tag{21}$$

$$\overline{x} = \left(0.7 + \frac{0.39}{n}\right)\frac{Q_1+Q_3}{2} + \left(0.3 - \frac{0.39}{n}\right)Q_2 \tag{22}$$

$$s_x = \frac{Q_{max} - Q_{min}}{2\phi^{-1}\frac{n - 0.375}{n + 0.25}} \tag{23}$$

$$s_x = \frac{Q_3 - Q_1}{2\phi^{-1}\frac{0.75n - 0.125}{n + 0.25}} \tag{24}$$

where Q_{min}, Q_1, Q_2, Q_3, Q_{max} are the minimum, first quartile, median, third quartile, and maximum respectively; ϕ^{-1} is the percent point function of the standard normal distribution and n is the sample size.

We can combine Equations 21 with 22 and 23 with 24 to produce a system of equation that can be solved for our unknowns Q_{min}, and Q_{max}. However, the equations from Luo et al., (2018) and Wan et al., (2014) are for normally distributed data, so first we must use a Box-Cost transformation to convert our quartile data (McGrath et al., 2020) and then do an inverse Box-Cox transformation to get back to our original scale.

These calculations result in the p-boxes shown in Figures 12 and 13 for the DFI and ATASDI quantities and for the resulting time to failure and repair times for water and wastewater systems.

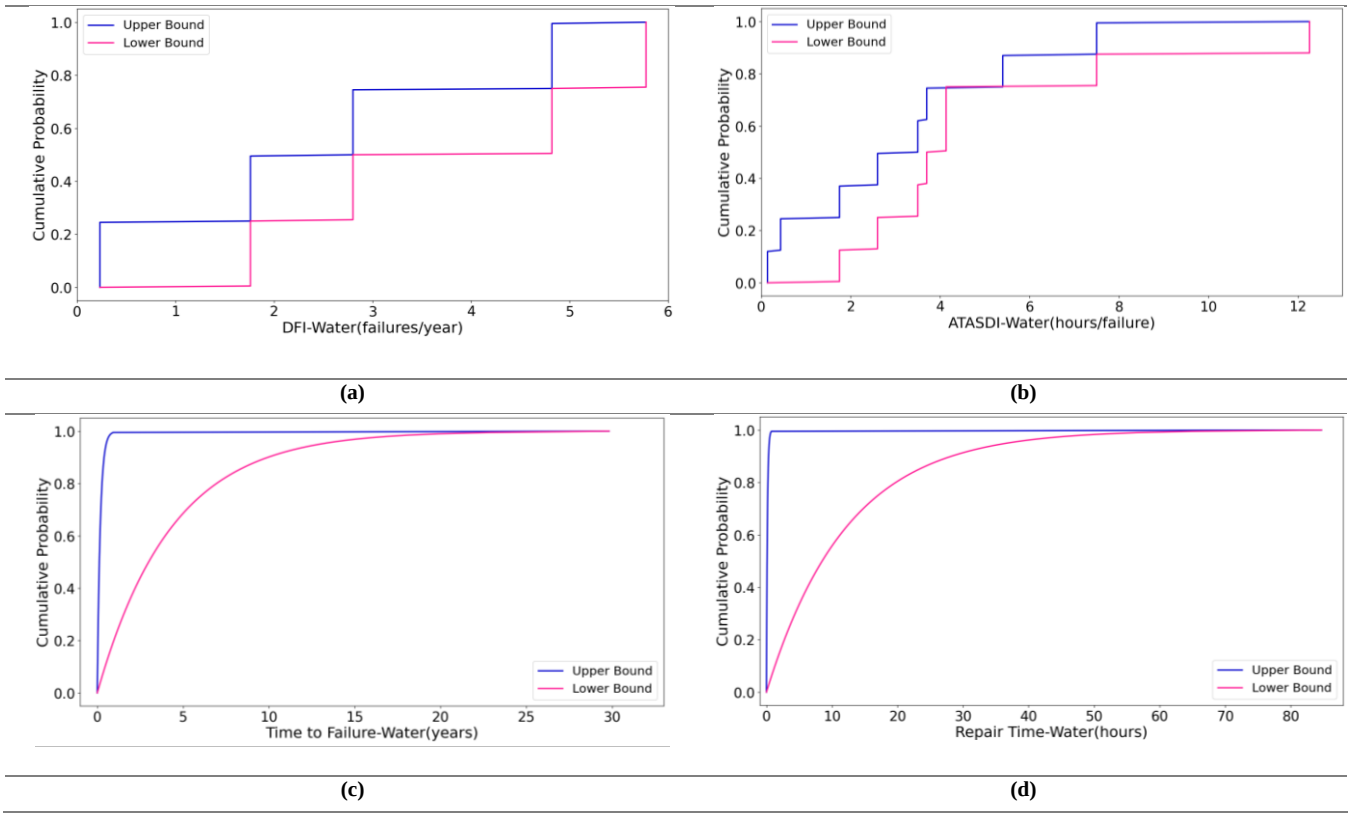

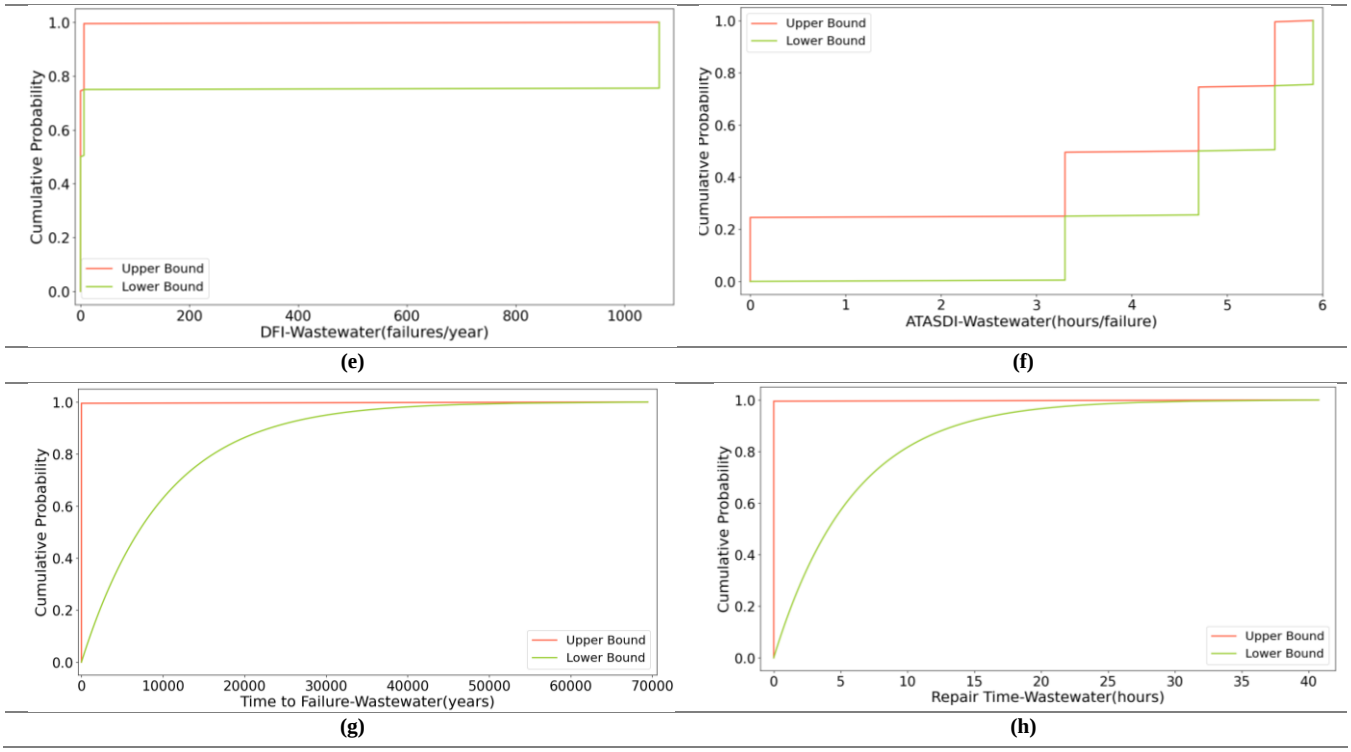

Figure 7. a) DFI p-box of water electricity grid, b) ATASDI p-box of water electricity grid, c) Time to failure p-box of water electricity grid, d) Repair time p-box of water electricity grid, e) DFI p-box of wastewater electricity grid, f) ATASDI p-box of wastewater electricity grid, g) Time to failure p-box of wastewater Electricity grid, h) Repair time p-box of wastewater electricity grid.

4. 3. Example networked application to an office building

For this case we examine a design from Johnson & Fallon, (2011), produced for the United States Army Core of Engineers. The building is a two-story office building with a total gross floor area of 3,582 m^2. We extracted the functional dependencies as shown in Figure 8 from the electrical, mechanical, and plumbing schedules in the building information model. Note that the set of functions presented is representative of many of the critical ones, as are the functional dependencies. A holistic risk assessment, however, would require an expanded list. Within this expanded list the building structure, envelope, and key roles like maintenance would be included. Additionally, it may be desirable to create a high-resolution model where functions and functional dependencies are decomposed into individual components, such as individual pipe or duct segments.

In this case study we are analyzing low consequence risks associated with reliability. For the system functions we are not considering disasters because of the data source. Also, for the external functions we use data without inclusion of disaster cases to align with the type of risks we have for system functions. We do not show any functional dependencies among the external functions (such as from the power utility to water service and sanitary service) for this reason. In reality, these are functional dependencies that tend to only be disrupted in large disasters.

Note that it is easiest to assess systems that do not have repeated functional dependencies. This is because: (1) p-box operations do not support repeated appearances of variables except in special cases, such as perfect dependence; and (2) unless you remember to check for these occurrences when applying the operations, the results will be incorrect. That being said, in case repetition is identified, duplicates of repeated p-boxes can be simply eliminated from the calculation. In the case of this model there are repeated functional dependencies. For example, the hot water heater depends

on the power utility via the inline pump and the panel. Therefore, care is made in calculations here to take recurring dependencies into consideration.

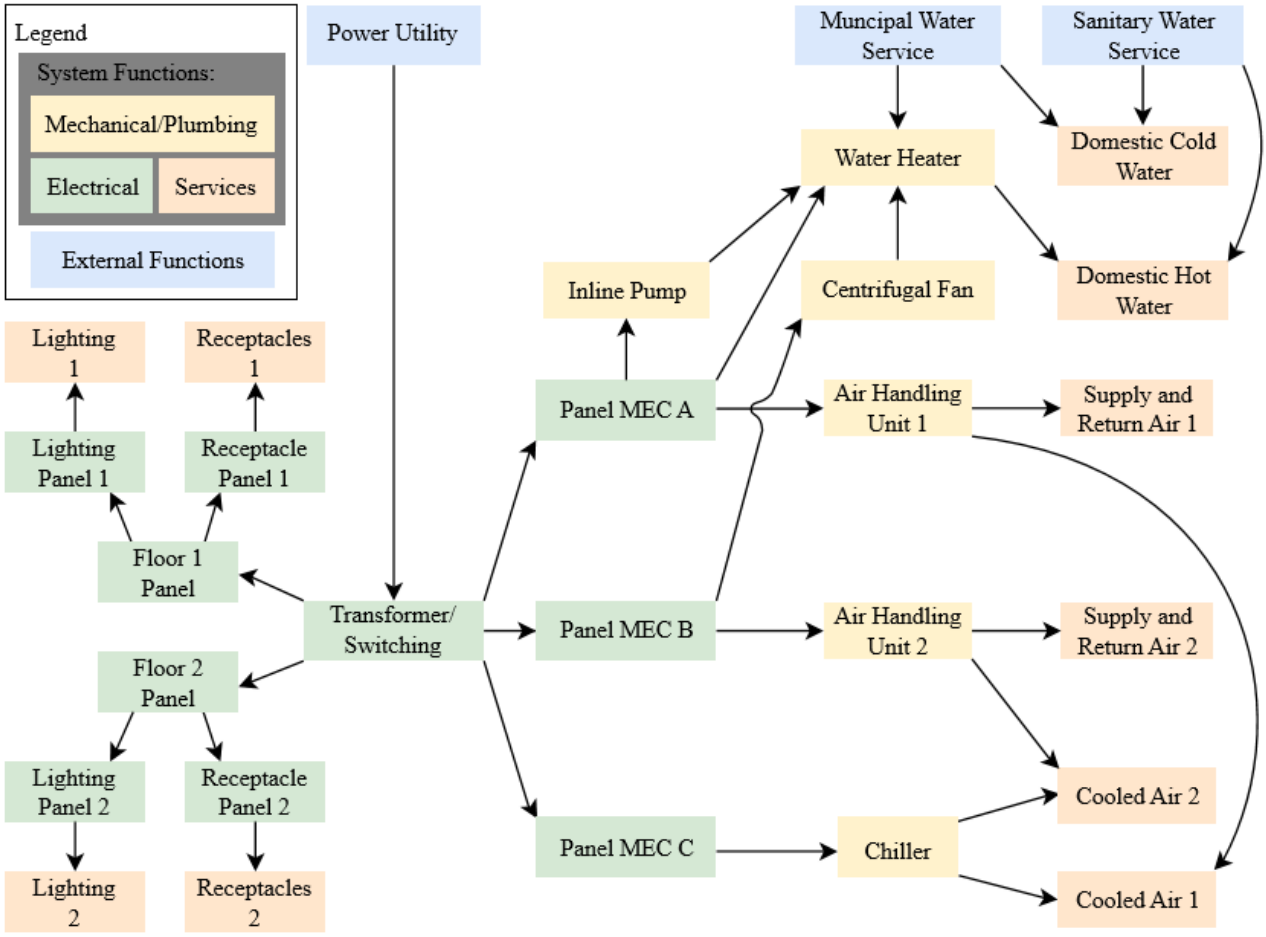

Figure 8. Functional dependencies of the building, where number 1 shows functions relate to the first floor only, and number 2 shows functions relate to the second floor only. Panels MEC A through C are electrical panels that specifically serve the mechanical and plumbing systems.

Table 2. Failure rate (λ) and mean repair time (r) for building components.

Function	**λ (failures/year)**	**r (hours/failure)**
Panels	[0.00002, 0.00011]	[3.098, 8.727]
Transformer/Switchboard	0.00949	4.308
Air Handling Units	0.011	99.036
Centrifugal Fan	0.01916	2.061
Chiller	0.0447	1.164
Inline Pump	[0.00422, 0.00821]	[0.246, 0.599]
Water Heater	0.04186	1.005

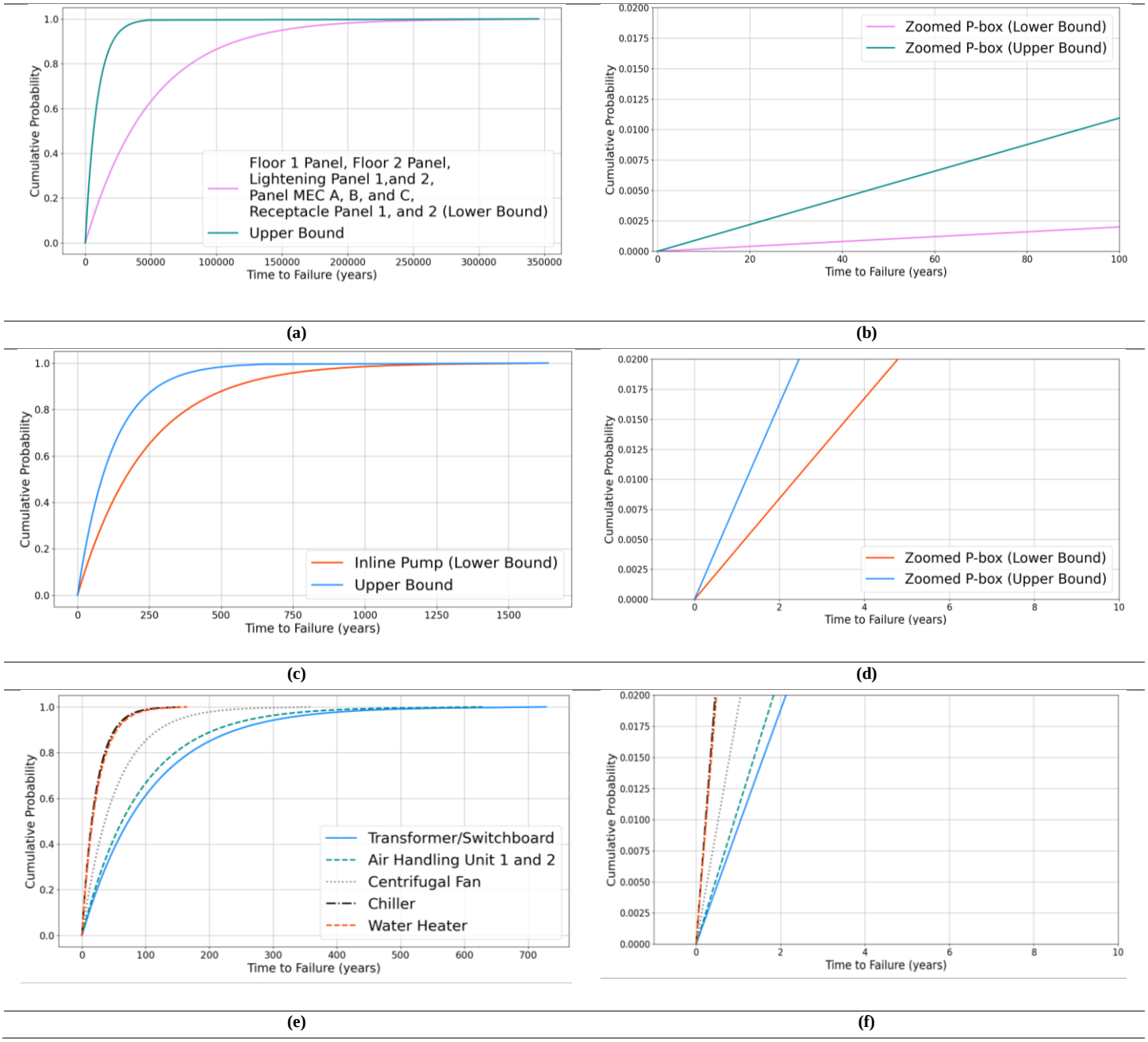

Figure 9. a) Time to failure p-box of floor 1 panel, floor 2 panel, lightening panel 1, lightening panel 2, panel MEC A, panel MEC B, panel MEC, receptacle panel 1, and receptacle panel 2, b) Zoomed in view of a, c) Time to failure p-box of inline pump, d) Zoomed in view of c, e) Time to failure of transformer/ switchboard, air handling unit 1, air handling unit 2, centrifugal, chiller, and water heater, f) Zoomed in view of e.

Table 3. Mean time to failure interval of the external functions and units in Figure 8.

	Time to Failure (Years)
Power Utility	[0.048, 37.037]
Municipal Water Service	[0.173, 4.317]
Sanitary Water Service	[0.001, 10052.06]
Floor 1 Panel, Floor 2 Panel, Lighting Panel 1, Lighting Panel 2, Panel MEC A, Panel MEC B, Panel MEC C, Receptacle Panel 1, and Receptacle Panel 2	[9090.909, 50000]
Inline Pump	[121.803, 236.967]
Transformer/Switchboard	105.3741

Air Handling Unit 1, Air Handling Unit 2	90.90909
Centrifugal Fan	52.19207
Chiller	22.37136
Water Heater	23.88915

We implement the model shown in Figure 8 as a network and, as we traverse through the network, we calculate and upgrade system time to failure considering the failure rate of each unit by applying Equation 8. Failure rates and mean repair time of the system units, as well as their mean time to failure interval and time to failure p-boxes are presented in Table 2, 3 and Figure 9 respectively. For the power utility, we employ time to failure p-box derived from combining SAIFI p-boxes of each year (Figure 6.c), and for the municipal water service and sanitary water service, we use time to failure p-boxes generated in sections 4.2. The resultant time to failure p-boxes that an average utility customer with a building design such as this may encounter is shown in Figure 10 for different type of functional dependency between the system units. Taking into account the external functions (power utility, water service, and sanitary water service), considerably reduces time to failure of the building, in other words it increases the probability of failure (Figure 10.a). Table 4 summarize mean time to failure (years) interval of the system in Figure 8, with and without considering the impact of failure in power utility, water service and sanitary water service, for different type of dependency between the units. As explained earlier, time to failure probability of the system where units are perfectly dependent is equal to the time to failure of the unit with the lowest time to failure (the highest failure probability) among the other units, in this case the chiller, when we do not consider the external functions. When considering the external functions, municipal water service will be the one that determines the time to failure of the entire system in the event of perfect dependency.

When we assume that the units are independent of one another, time to failure of the system is determined by multiplying time to failure probabilities of its individual units. Therefore, the resultant time to failure in this case will be smaller than the perfect dependency case, as we explain in section 3.1. Additionally, we can see that the uncertainty increases in perfect dependency scenario when external functions are considered. This is because, in the absence of external functions, the chiller, whose failure rate is precise, has the smallest time to failure, and as a result, the uncertainty in the estimated time to failure of the system will be smaller than the case where external functions are taken into account and the municipal water service, whose failure rate is an interval, serves as the unit defining the time to failure of the entire system.

The lower (right bound) of the system time to failure in Fréchet dependency scenario coincides with the lower bound of the perfect dependency, while its upper (left) bound is smaller than the upper bound of perfect dependency and independent cases.

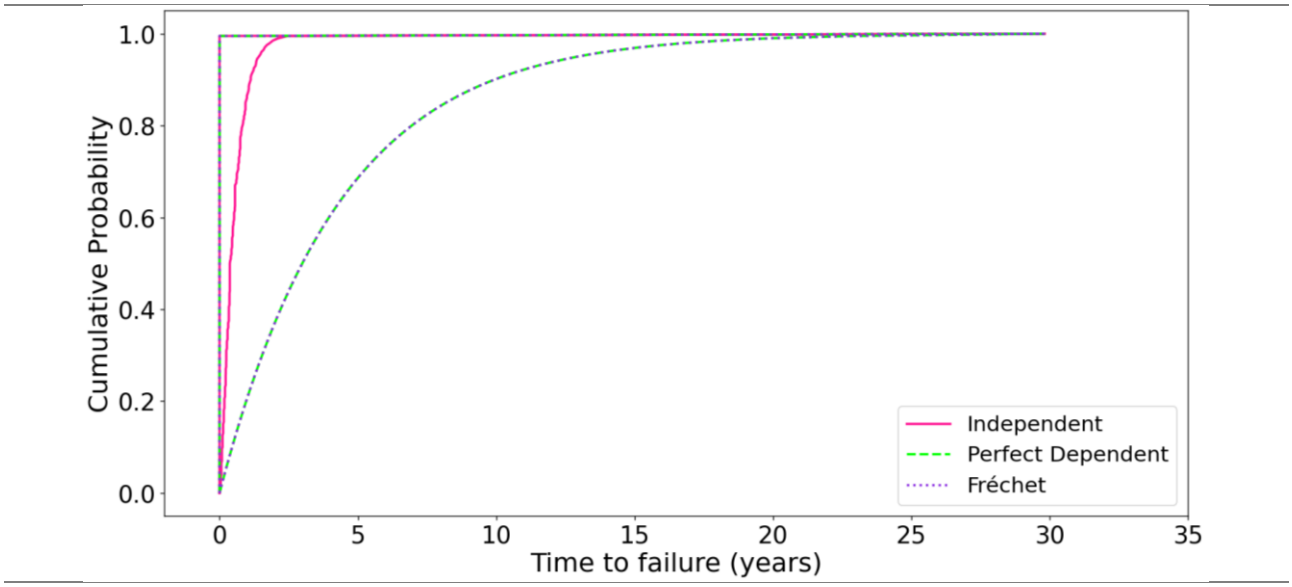

(a)

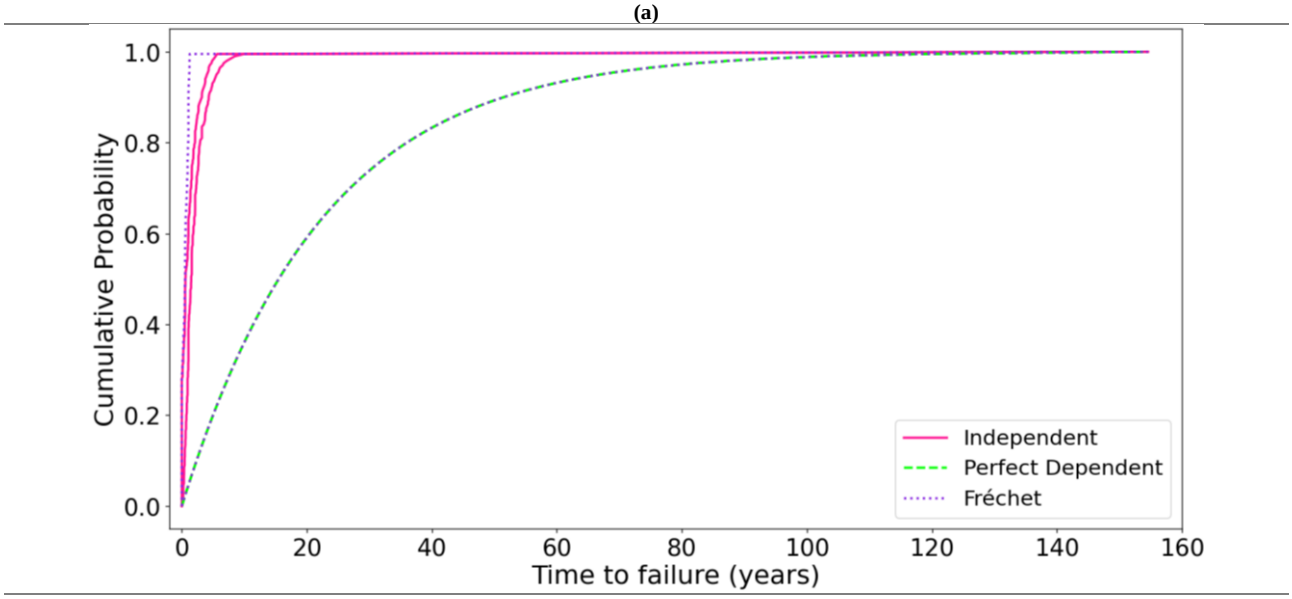

(b)

Figure 10. Time to failure of the system in Figure 8, a) with, and b) without considering the impact of failure in power utility, municipal water service and sanitary water service, for different type of dependency between the system components.

Table 4. Mean time to failure (years) interval of the system in Figure 8, with and without considering the impact of failure in power utility, municipal water service and sanitary water service, for different type of dependency between the units.

	Considering the external functions	**Without considering the external functions**
Independent	[8.3e-05, 0.68]	[1.11, 2.76]
Perfect Dependent	[0.001, 4.39]	[21.97, 22.74]
Fréchet	[2.6e-05, 4.39]	[0.50, 22.74]

Furthermore, we repeat the procedure for the system (without considering the external functions) after removing uncertainty in the input parameters, using the midpoint of each interval to determine how much of the remaining uncertainty is due to unknown dependency type between system components. Then we calculate the uncertainty for each type of dependency by averaging the subtraction of upper and lower bound for each probability (0.001,0.002, ..., 1). Table 5 summarizes

the findings. According to the results, unknown dependency is responsible for almost all the uncertainty in this case study since the uncertainty with λ as an interval is nearly the same as when it is a scalar.

Table 5. Uncertainty in the estimated time to failure of the building, before and after removing uncertainty in failure rates of the system components.

Dependency Type	Uncertainty (λ as an interval)	Uncertainty (λ as a scalar)
Perfect Dependent	0.7726796	0.7726796
Independent	1.644617	1.6287
Fréchet	22.24353	22.24088

5. Discussion

Quantifying and acknowledging the uncertainties is critical for effective uncertainty management. To prioritize reliability improvement design and activities, analysts must identify the main sources of uncertainty. The results of this study, however, demonstrate that the dominant uncertainty factors associated with reliability analysis is not always the same, and it varies depending on the system structure, the location of the influential component in the system, redundancy, and number of system components, and data on model parameters, to name a few. On the other hand, identifying dependency between components and subsystems of modern systems and networks is extremely challenging, if not often impossible, considering the continuous increase in their complexity. The suggested approach presented in this study can be used to assess the reliability of any complex system while taking into account various types of functional and probabilistic dependencies, ensuring a good balance of accuracy and efficiency, and defining the major sources of uncertainty. Our research can help with analysis during the initial stages of designing complex and multidisciplinary systems to maximize reliability while minimizing costs. It can also be applied to maintenance scheduling and planning.

Furthermore, we expect changes in the rate of failure (λ) and reliability of systems as a result of climate change and its impact on climatic loads and natural processes like wind, thermal, and snow loads, sea level rise, to name a few. The impact of nonstationary climatic conditions on failure rate and reliability has been recognized by a number of authors. Bruaset & Sægrov (2018), shows there is a significant correlation between temperatures and failure rates of drinking water pipes. The findings in Croce et al. (2019) suggest that structural reliability may decline over time due to effects of climate change. Rezaei et al. (2016) demonstrates how the reliability index of existing transmission line systems can be dramatically changed by changes in the mean value of extreme wind and ice events.

Using mixtures with equal or even different weights, our strategy in this study can be utilized to incorporate many potential ranges or beliefs on failure rate or any other variable. For instance, consider a complex network composed of numerous units in multiple locations, where we expect an alteration in reliability of the network caused by changes in failure rates of its units due to climate change. Additionally, we believe that some of those units may be more susceptible to change in their failure rate because of their location. Assume we hold a variety of beliefs on the rate of possible change in the failure rate of the network units. We can consider all those beliefs regarding the possible rate of change as an interval or a p-box and multiply it by the current failure rate of the units. We can also assign higher weight to the units that we expect to experience higher changes because of their location.

6. Conclusion

Evaluating uncertainty, particularly uncertainty brought on by indeterminacy in dependency, is a very complex task, and the available methods typically required a large amount of information such as correlation between variables or strength and criticality between them. In this study, we introduced a method that integrates probability bound analysis and reliability assessment to quantify the reliability of a complex system, while transparently acknowledging the associated uncertainty caused by imprecise data and indeterminacy of random variate dependency, with a very low computational cost. The applicability of the method was then illustrated through several examples. The functional dependence between utility suppliers was not taken into account in this analysis. Also, we did not consider failures caused by major events like hurricane or flood to highlight the unreliability of the system for an average customer in a typical circumstance. Therefore, future research could be conducted in more realistic settings by considering functional dependency between utility suppliers and including the catastrophic events. Furthermore, we can gain a better insight into the resilience of a city in case of a major event by applying the same approach in this study and estimating repair time of a residential, commercial, and industrial building as representative of different types of customers in a district or city.

Symbols

A Capital letters are sets, including random variables, some have specific uses or are exceptions, as noted below

α Lower-case letters are specific values of a set, some have specific uses or are exceptions, as noted below

T, t Time

i, j Indices

R Reliability

q Unreliability (Time to failure)

l Length of repair time (downtime)

c, v Cost, expense

Pr Probability

F (·) Cumulative distribution functions

f (·) Probability density function or probability mass function

S A set of functions that comprise a system

E A set of functions that exist in the system’s surrounding environment

D The union of S and G

G A subset (group) of functions of the system

$\in$ In

$\notin$ in

Z The set of integers

∪ Union

∩ Intersection

⊆ Subset

⊂ Proper subset (i.e., for B ⊂ A, B excludes at least one element of A)

Appendix

Table 6. SAIFI (failures/year) statistics observed for 155 American power utilities from 2000 to 2009.

	Min	25th	Median	75th	Max	Mean
2000	0.03	0.86	1.21	1.61	5.22	1.40
2001	0.08	0.86	1.18	1.56	5.67	1.34
2002	0.16	0.97	1.18	1.61	4.19	1.32
2003	0.13	0.91	1.26	1.61	5.11	1.34
2004	0.11	0.89	1.24	1.64	6.99	1.40
2005	0.11	0.97	1.32	1.77	20.90	1.53
2006	0.13	1.02	1.29	1.69	8.20	1.51
2007	0.16	0.97	1.21	1.64	8.44	1.45
2008	0.13	0.97	1.24	1.69	5.70	1.43
2009	0.11	0.86	1.16	1.61	6.16	1.37

Table 7. SAIDI (hours/year) statistics observed for 155 American power utilities from 2000 to 2009.

	Min	25th	Median	75th	Max	Mean
2000	0.13	1.24	2.05	3.03	9.42	2.43
2001	0.34	1.36	1.96	2.86	7.42	2.26
2002	0.04	1.41	2.05	3.11	7.37	2.34
2003	0.04	1.53	1.92	2.77	5.88	2.30
2004	0.26	1.53	2.17	3.11	5.67	2.43
2005	0.26	1.75	2.26	3.28	6.05	2.51
2006	0.21	1.58	2.39	3.20	7.50	2.60
2007	0.26	1.49	2.13	3.28	10.06	2.51
2008	0.38	1.66	2.43	3.15	12.19	2.69
2009	0.01	1.58	2.09	2.98	10.14	2.43

Chapter 5: Conclusions

1. Introduction

Overall, the findings of this thesis show that, in the absence of adaptation and mitigation measures, the total cost of climate change in urban areas could be very high, even in countries with substantial heating costs like Canada. Flood damage, for example, which is currently the most expensive natural disaster in Canada, will be much higher in the future if adaptation and mitigation measures are not implemented. Findings from Chapter 2 show that under the SSP5-8 scenario, pluvial flood hazards will intensify in the studied cities, exposing at-grade and underground infrastructure. Moreover, the deterioration state of intra-urban assets further amplifies their vulnerability, resulting in increased damage cost. Additionally, a comparison of the damage from the historic river flood scenario with the climate change-driven flood scenarios in Chapter 3 reveals significant vulnerability and exposure of residential buildings in Metro Vancouver and an urgent need for adaptation measures in the region.

To effectively mitigate potential losses from climate change impacts on cities and implement adaptation strategies, it is crucial to foster risk perception of climate change-induced risks in urban areas by considering all risk components, including hazards, vulnerability, and exposure. However, as evidenced by the findings in Chapter 4 and previous incidents such as August 14, 2003, blackout, which was caused by cascading failures across the northeastern United States and southern Canada and incurred significant costs for affected cities, neglecting interdependence in the analysis can have dire consequences. Therefore, when it comes to risk and reliability analysis in urban areas, we must take a comprehensive approach that considers all functional and probabilistic dependencies within and between systems and networks in the city.

2. Contributions

The contributions made in this thesis include the following points:

- Investigate changes in a wide variety of climate variables in seventeen Canadian cities under the SSP5-8 scenario, considering twenty-six global climate models.
- Show similarities and differences in rates of climate change across the cities using Euclidean distance.
- Detect regions with similar future climate stresses using Epps-Singleton test.
- Show climate change will have distinct effects on built environments of neighbouring coastal cities under the SSP5-8 scenario.
- Introduce a new methodology that combines damage functions and probability bounds analysis to understand and anticipate potential flood damage and its associated uncertainties at a regional scale.
- Assess and communicate the uncertainty caused by using sample data and imprecise measurements to decision makers while distinguishing between aleatory and epistemic uncertainty.
- Estimate the likelihood of direct tangible damage to 375,973 residential buildings along the Fraser River through Metro Vancouver, Canada, for a range of climate change driven flood scenarios.

- Suggest a new approach to assess the reliability of complex systems while taking into account various types of functional and probabilistic dependencies, ensuring a good balance of accuracy and efficiency, and defining the major sources of uncertainty.
- Estimate time to failure p-boxes for an average utility customer in a two-story office building in a typical circumstance, considering different types of internal and external (power grid, water, and wastewater infrastructure) functional dependencies of the building.

3. Summary of Chapters

Chapter 2

In chapter 2 we examine the rate and direction of changes in a wide variety of climate variables in seventeen Canadian cities, considering essential service reports and infrastructure performance data. To accomplish this, we use the modified Mann-Kendall test and Euclidean distance to analyse downscale data from twenty-six General Circulation Models (GCMs) from CMIP6 to the year 2100.

The findings of this chapter suggest that under SSP5-8.5, Canadian cities will experience more extreme heat and heavy rainfall but less extreme cold in the future. Using the Epps-Singleton test, we also compare climate change in neighbouring cities to see how similar adaptation plans are possible. The results show that coastal cities, even those located relatively close to one another, such as Vancouver and Victoria, follow distinct trends of change for most of their variables. Furthermore, by associating climate change velocity variables with impacts on different infrastructure, we provide a qualitative assessment of which aspects of the built environment of these cities may require more rapid modification than others.

Future Research 2

In future studies, the vulnerability of these seventeen cities can be assessed, and the findings can be integrated with the results of this study to provide a more comprehensive understanding of the potential risks induced by climate change. In addition, the same methods can be applied to data that has been downscaled by a different method than BCCAQv2 to determine how the choice of downscaling technique affects the direction and rate of change in climate variables, and the potential cost or damage to essential services and infrastructure.

Chapter 3

In chapter 3, we introduce a novel approach that combines damage functions and probability bounds analysis to quantify potential flood damage at the regional scale while accounting for the uncertainty introduced by using sample data and imprecise measurements.

In addition, we use the introduced method to estimate the likelihood of direct tangible damage to 375,973 one- and two-story residential buildings with and without basements in one coastal flood scenario and three climate change-driven river flood scenarios along the Fraser River in Metro Vancouver, Canada, and then compare the results with the historic flood scenario to evaluate the impact of climate change in terms of flood damage. The finding shows the major impact of finished basements on total flood damage as well as the effectiveness of mitigation measures aimed at finished basements. Furthermore, the results show that one-story buildings with and without basements are significantly more vulnerable to coastal floods than two-story buildings in the study area. Moreover, the findings suggest that, in the absence of adaptation measures, we should expect a significant increase in direct and indirect flood damages in Metro Vancouver by the end of the century. Finally, a comparison of the probability box and second-order Monte Carlo simulation shows that when the

sample size is small, the probability box should be the preferred method to avoid ignorance of the epistemic uncertainty involved in the analysis.

Future Research 3

In the future, we can use the same method to generate damage p-boxes caused by other flood impact parameters such as flow velocity and flood duration, and then combine the generated p-boxes with the ones in this study to gain a more comprehensive insight into potential losses caused by different climate change induced flood scenarios.

Chapter 4

Evaluation of the current state of infrastructure and service provision is very important for providing insights on what makes a system more reliable and improving resiliency to potential changes and extreme events. Considering the increasing complexity of infrastructure and networks, determining how the failure of one component or subsystem in a complex system can affect the entire city requires a great deal of knowledge and effort. Chapter 4 provides a new technique to evaluate the reliability of complex systems with imprecise variables and non-deterministic functional dependency using probability bounds (p-boxes) and considering uncertainty in the dependency between random variates. Throughout this chapter we investigate how dependence assumptions affect the quantitative results of reliability analysis.

Further, we examine the applicability of the proposed method by quantifying the time to failure and repair time of three real-world networks including power grid, municipal water, and wastewater. Finally, we calculate time to failure p-boxes that an average utility customer of a two-story office building with a specific area and design may experience for various types of functional dependency between the system units. The findings show that the dominant uncertainty factor associated with reliability analysis is not always the same, and it varies depending on the factors such as system structure, the location of the influential component in the system, redundancy, and number of system components, and data on model parameters to name a few.

Future Research 4

Future research can be conducted to assess the resiliency of a district or city in the event of major events such as a hurricane or flood by applying the proposed method in this study in more realistic settings (considering functional dependency between utility suppliers) and estimating the repair time of a residential, commercial, and industrial building as representative of different types of customers in a city.

References

1366-1998 - IEEE Guide for Electric Power Distribution Reliability Indices. (1999). https://doi.org/10.1109/IEEESTD.1999.89432

610-1990 - IEEE Standard Computer Dictionary: A Compilation of IEEE Standard Computer Glossaries. (1991). https://doi.org/10.1109/IEEESTD.1991.106963

Abboud, J. M., Ryan, M. C., & Osborn, G. D. (2018). Groundwater flooding in a river-connected alluvial aquifer. Journal of Flood Risk Management, 11(4), e12334. https://doi.org/10.1111/jfr3.12334

AECOM Consultants Inc. (2015). Toronto Hydro-Electric System Limited Climate Change Vulnerability Assessment; Application of the Public Infrastructure Engineering Vulnerability Assessment Protocol to Electrical Distribution Infrastructure. https://www.nrcan.gc.ca/sites/www.nrcan.gc.ca/files/energy/energy-resources/Toronto_Hyrdo-Electric_System_Limited-Climate-Change-Vulnerability-Assessment.pdf

Apel, H., Thieken, A. H., Merz, B., & Blöschl, G. (2004). Flood risk assessment and associated uncertainty. Natural Hazards and Earth System Sciences, 4(2), 295–308. https://doi.org/10.5194/nhess-4-295-2004

Apel, Heiko, Merz, B., & Thieken, A. H. (2008). Quantification of uncertainties in flood risk assessments. International Journal of River Basin Management, 6(2), 149–162. https://doi.org/10.1080/15715124.2008.9635344

Beer, M., Ferson, S., & Kreinovich, V. (2013). Imprecise probabilities in engineering analyses. Mechanical Systems and Signal Processing, 37(1–2), 4–29. https://doi.org/10.1016/j.ymssp.2013.01.024

Ben Alaya, M. A., Zwiers, F., & Zhang, X. (2020). An Evaluation of Block-Maximum-Based Estimation of Very Long Return Period Precipitation Extremes with a Large Ensemble Climate Simulation. Journal of Climate, 33(16), 6957–6970. https://doi.org/10.1175/JCLI-D-19-0011.1

Bhatnagar, M., Mathur, J., & Garg, V. (2018). Determining base temperature for heating and cooling degree-days for India. Journal of Building Engineering, 18, 270–280. https://doi.org/10.1016/j.jobe.2018.03.020

Bi, Daohua, Martin Dix, Simon Marsland, Siobhan O'Farrell, Arnold Sullivan, Roger Bodman, Rachel Law, Ian Harman, Jhan Srbinovsky, Harun A. Rashid, Peter Dobrohotoff, Chloe Mackallah, Hailin Yan, Anthony Hirst, Abhishek Savita, Fabio Boeira Dias, Matthew Woodhouse, Russell Fiedler, and Aidan Heerdegen. 2020. "Configuration and Spin-up of ACCESS-CM2, the New Generation Australian Community Climate and Earth System Simulator Coupled Model." Journal of Southern Hemisphere Earth Systems Science 70(1):225–51.

Billinton, R. (1988). Distribution system reliability performance and evaluation. International Journal of Electrical Power & Energy Systems, 10(3), 190–200. https://doi.org/10.1016/0142-0615(88)90035-X

Birolini, A. (2014). Reliability Engineering. Springer Berlin Heidelberg. https://doi.org/10.1007/978-3-642-39535-2

Bonnifait, L. (2005). Développement de courbes submersion-dommages pour l'habitat résidentiel 516 québécois.

Bosshard, T. et al. (2013) 'Quantifying uncertainty sources in an ensemble of hydrological climate-impact projections', Water Resources Research, 49(3), pp. 1523–1536. Available at: https://doi.org/10.1029/2011WR011533.

Breaden, J. P. (1971). The Generation of Flood Damage Time Sequences. https://doi.org/doi.org/10.7939/r3-h2xs-8404

Bruaset, S., & Sægrov, S. (2018). An Analysis of the Potential Impact of Climate Change on the Structural Reliability of Drinking Water Pipes in Cold Climate Regions. Water, 10(4), 411. https://doi.org/10.3390/w10040411

Brugmann, J. (2012) 'A Demand-Driven Approach to Development, Disaster Risk Reduction, and Climate Adaptation', in, pp. 383–390. Available at: https://doi.org/10.1007/978-94-007-4223-9_40.

Bryant, S. (2019). Accumulating Flood Risk A Model Study to Quantify Flood Damage Mitigation Measures under Dynamic Vulnerability.

Bubeck, P., de Moel, H., Bouwer, L. M., & Aerts, J. C. J. H. (2011). How reliable are projections of future flood damage? Natural Hazards and Earth System Sciences, 11(12), 3293–3306. https://doi.org/10.5194/nhess-11-3293-2011

Cannon, Alex J., Stephen R. Sobie, and Trevor Q. Murdock. 2015. "Bias Correction of GCM Precipitation by Quantile Mapping: How Well Do Methods Preserve Changes in Quantiles and Extremes?" Journal of Climate 28(17):6938–59.

Carpaneto, E., & Chicco, G. (2004). Evaluation of the Probability Density Functions of Distribution System Reliability Indices With a Characteristic Functions-Based Approach. IEEE Transactions on Power Systems, 19(2), 724–734. https://doi.org/10.1109/TPWRS.2003.821627

Chakraborty, L., Rus, H., Henstra, D., Thistlethwaite, J., & Scott, D. (2020). A place-based socioeconomic status index: Measuring social vulnerability to flood hazards in the context of environmental justice. International Journal of Disaster Risk Reduction, 43, 101394. https://doi.org/10.1016/j.ijdrr.2019.101394

Chen, S. and Gong, B. (2021) 'Response and adaptation of agriculture to climate change: Evidence from China', Journal of Development Economics, 148, p. 102557. Available at: https://doi.org/10.1016/j.jdeveco.2020.102557.

Chiotti, Q., Chan, K., Gulecoglu, E., Belaieff, A., & Noxon, G. (2017). PLANNING FOR RESILIENCY; Toward a Corporate Climate Adaptation Plan. https://assets.metrolinx.com/image/upload/v1663237658/Documents/Metrolinx/Planning_for_Resiliency_2017_EN_final.pdf

Cleary, S., & Willcot, N. (2022). The Physical Costs of Climate Change: A Canadian Perspective. https://smith.queensu.ca/centres/isf/pdfs/ISF-Report-PhysicalCostsOfClimateChange.pdf

Colquhoun, D. (2014). An investigation of the false discovery rate and the misinterpretation of p - values. Royal Society Open Science, 1(3), 140216. https://doi.org/10.1098/rsos.140216

Crespo, L. G., Kenny, S. P., & Giesy, D. P. (2013). Reliability analysis of polynomial systems subject to p-box uncertainties. Mechanical Systems and Signal Processing, 37(1–2), 121–136. https://doi.org/10.1016/j.ymssp.2012.08.012

Croce, P., Formichi, P., & Landi, F. (2019). Climate Change: Impacts on Climatic Actions and Structural Reliability. Applied Sciences, 9(24), 5416. https://doi.org/10.3390/app9245416

Crosbie, R.S. et al. (2011) 'Differences in future recharge estimates due to GCMs, downscaling methods and hydrological models', Geophysical Research Letters, 38(11), p. n/a-n/a. Available at: https://doi.org/10.1029/2011GL047657.

Curry, C. L., Islam, S. U., Zwiers, F. W., & Déry, S. J. (2019). Atmospheric Rivers Increase Future Flood Risk in Western Canada's Largest Pacific River. Geophysical Research Letters, 46(3), 1651–1661. https://doi.org/10.1029/2018GL080720

de Moel, H., Asselman, N. E. M., & Aerts, J. C. J. H. (2012). Uncertainty and sensitivity analysis of coastal flood damage estimates in the west of the Netherlands. Natural Hazards and Earth System Sciences, 12(4), 1045–1058. https://doi.org/10.5194/nhess-12-1045-2012

Dimitriadis, P., Tegos, A., Oikonomou, A., Pagana, V., Koukouvinos, A., Mamassis, N., Koutsoyiannis, D., & Efstratiadis, A. (2016). Comparative evaluation of 1D and quasi-2D hydraulic models based on benchmark and real-world applications for uncertainty assessment in flood mapping. Journal of Hydrology, 534, 478–492. https://doi.org/10.1016/j.jhydrol.2016.01.020

Dutta, D., Herath, S., & Musiake, K. (2001). DIRECT FLOOD DAMAGE MODELING TOWARDS URBAN FLOOD RISK MANAGEMENT.

Egorova, R., van Noortwijk, J. M., & Holterman, S. R. (2008). Uncertainty in flood damage estimation. International Journal of River Basin Management, 6(2), 139–148. https://doi.org/10.1080/15715124.2008.9635343*

Epps, T. W., & Singleton, K. J. (1986). An omnibus test for the two-sample problem using the empirical characteristic function. Journal of Statistical Computation and Simulation, 26(3–4), 177–203. https://doi.org/10.1080/00949658608810963

Eto, J. H., LaCommare, K. H., Larsen, P., Todd, A., & Fisher, E. (2012). An Examination of Temporal Trends in Electricity Reliability Based on Reports from U.S. Electric Utilities. https://doi.org/10.2172/1055706

Federal flood damage estimation guidelines for buildings and infrastructure. (2021). https://doi.org/10.4095/327001

Feng, G., Patelli, E., Beer, M., & Coolen, F. P. A. (2016). Imprecise system reliability and component importance based on survival signature. Reliability Engineering & System Safety, 150, 116–125. https://doi.org/10.1016/j.ress.2016.01.019

Ferson, S, Moore, D., Van den Brink, P., Estes, T., Gallagher, K., O'Connor, R., & Verdonck, F. (2010). Bounding Uncertainty Analyses. In Application of Uncertainty Analysis to Ecological Risks of Pesticides (pp. 89–122). CRC Press. https://doi.org/10.1201/EBK1439807347-c6

Ferson, S. (2020). pba.r Probability Bounds Analysis S4 library for the R.

Ferson, S., & Tucker, W. T. (2008). Probability boxes as info-gap models. NAFIPS 2008 - 2008 Annual Meeting of the North American Fuzzy Information Processing Society, 1–6. https://doi.org/10.1109/NAFIPS.2008.4531314

Ferson, S., Kreinovich, V., Ginzburg, L., Myers, D. S., & Sentz, K. (2003). Constructing Probability Boxes and Dempster-Shafer Structures.

Freni, G., La Loggia, G., & Notaro, V. (2010). Uncertainty in urban flood damage assessment due to urban drainage modelling and depth-damage curve estimation. Water Science and Technology, 61(12), 2979–2993. https://doi.org/10.2166/wst.2010.177

Gachon, P., Bussières, L., Gosselin, P., Raphoz, M., Bustinza, R., Martin, P., Dueymes, G., Gosselin, D., Labrecque, S., Jeffers, S., & Yagouti, A. (2016). A. (2016) Guide to identifying alert thresholds for heat waves in Canada based on evidence. Co-edited by Université du Québec à Montréal, Environment and Climate Change Canada, Institut National de Santé Publique du Québec, and Health Canada, Montréal, Qu. https://archipel.uqam.ca/9073/1/Gachon_et_al_2016_Guide_Heat_Waves_EN.pdf

GENIVAR. (2010). National Engineering Vulnerability Assessment of Public Infrastructure To Climate Change; Toronto and Region Conservation Authority Flood Control Dam Water Resources Infrastructure Assessment. https://pievc.ca/wp-content/uploads/2010/06/TRCA_Combined_Final-Report.pdf

Gillett, N. P., Cannon, A. J., Malinina, E., Schnorbus, M., Anslow, F., Sun, Q., Kirchmeier-Young, M., Zwiers, F., Seiler, C., Zhang, X., Flato, G., Wan, H., Li, G., & Castellan, A. (2022). Human influence on the 2021 British Columbia floods. Weather and Climate Extremes, 36, 100441. https://doi.org/10.1016/j.wace.2022.100441

Goerg, S. J., & Kaiser, J. (2009). Nonparametric testing of distributions—the Epps–Singleton two-sample test using the empirical characteristic function. The Stata Journal. https://journals.sagepub.com/doi/pdf/10.1177/1536867X0900900307

Goldberg, M. S., Gasparrini, A., Armstrong, B., & Valois, M.-F. (2011). The short-term influence of temperature on daily mortality in the temperate climate of Montreal, Canada. Environmental Research, 111(6), 853–860. https://doi.org/10.1016/j.envres.2011.05.022

Gouldby, B., Samuels, P., Klijn, F., Messner, F., Os, A. van, Sayers, P., & Schanze, J. (2009). Language of Risk – Project Definitions.

Government of Canada. (n.d.). Historical Climate Data. https://climate.weather.gc.ca/

Gray, N., Ferson, S., De Angelis, M., Gray, A., & Baumont de Oliveira, F. (2022). Probability bounds analysis for Python. Software Impacts, 12, 100246. https://doi.org/10.1016/j.simpa.2022.100246

Gutjahr, Oliver, Dian Putrasahan, Katja Lohmann, Johann H. Jungclaus, Jin-Song von Storch, Nils Brüggemann, Helmuth Haak, and Achim Stössel. 2019. "Max Planck Institute Earth System Model (MPI-ESM1.2) for the High-Resolution Model Intercomparison Project (HighResMIP)." Geoscientific Model Development 12(7):3241–81.

He, W. et al. (2019) 'Simulating evaluation and projection of the climate zones over China by CMIP5 models', Climate Dynamics, 52(5–6), pp. 2597–2612. Available at: https://doi.org/10.1007/s00382-018-4410-1.

Head, M. L., Holman, L., Lanfear, R., Kahn, A. T., & Jennions, M. D. (2015). The Extent and Consequences of P-Hacking in Science. PLOS Biology, 13(3), e1002106. https://doi.org/10.1371/journal.pbio.1002106

Health Canada. (2009). The Urban Heat Island Effect: Causes, Health Impacts and Mitigation Strategies. https://www.canada.ca/content/dam/hc-sc/migration/hc-sc/ewh-semt/alt_formats/hecs-sesc/pdf/pubs/climat/adapt_bulletin-adapt1/adapt_bulletin-adapt1-eng.pdf

Heinrich, D. F., & Penning-Rowsell, E. C. (2022). Flood risk management under uncertainty in transboundary basins: a delicate balancing act. International Journal of River Basin Management, 20(2), 215–224. https://doi.org/10.1080/15715124.2020.1837845

Henstra, D., & Thistlethwaite, J. (2017). Climate Change, Floods, and Municipal Risk Sharing in Canada. IMFG Papers on Municipal Finance and Governance No. 30.

Huang, W. K., Stein, M. L., McInerney, D. J., Sun, S., & Moyer, E. J. (2016). Estimating changes in temperature extremes from millennial-scale climate simulations using generalized extreme value (GEV) distributions. Advances in Statistical Climatology, Meteorology and Oceanography, 2(1), 79–103. https://doi.org/10.5194/ascmo-2-79-2016

Hughes, D.A., Mantel, S. and Mohobane, T. (2014) 'An assessment of the skill of downscaled GCM outputs in simulating historical patterns of rainfall variability in South Africa', Hydrology Research, 45(1), pp. 134–147. Available at: https://doi.org/10.2166/nh.2013.027.

IBI Group and Golder Associates. (2020). Flood Risk Assessment for BC's Lower Mainland.

IEA. (2022). Canada 2022 Energy Policy Review. https://iea.blob.core.windows.net/assets/7ec2467c-78b4-4c0c-a966-a42b8861ec5a/Canada2022.pdf

IPCC. (2023). AR6 Synthesis Report (SYR).1366-1998 - IEEE Guide for Electric Power Distribution Reliability Indices. (1999). https://doi.org/10.1109/IEEESTD.1999.89432

610-1990 - IEEE Standard Computer Dictionary: A Compilation of IEEE Standard Computer Glossaries. (1991). https://doi.org/10.1109/IEEESTD.1991.106963

Abboud, J. M., Ryan, M. C., & Osborn, G. D. (2018). Groundwater flooding in a river-connected alluvial aquifer. Journal of Flood Risk Management, 11(4), e12334. https://doi.org/10.1111/jfr3.12334

AECOM Consultants Inc. (2015). Toronto Hydro-Electric System Limited Climate Change Vulnerability Assessment; Application of the Public Infrastructure Engineering Vulnerability Assessment Protocol to Electrical Distribution Infrastructure. https://www.nrcan.gc.ca/sites/www.nrcan.gc.ca/files/energy/energy-resources/Toronto_Hyrdo-Electric_System_Limited-Climate-Change-Vulnerability-Assessment.pdf

Apel, H., Thieken, A. H., Merz, B., & Blöschl, G. (2004). Flood risk assessment and associated uncertainty. Natural Hazards and Earth System Sciences, 4(2), 295–308. https://doi.org/10.5194/nhess-4-295-2004

Apel, Heiko, Merz, B., & Thieken, A. H. (2008). Quantification of uncertainties in flood risk assessments. International Journal of River Basin Management, 6(2), 149–162. https://doi.org/10.1080/15715124.2008.9635344

Arora, N. K. (2019). Impact of climate change on agriculture production and its sustainable solutions. Environmental Sustainability, 2(2), 95–96. https://doi.org/10.1007/s42398-019-00078-w

Beer, M., Ferson, S., & Kreinovich, V. (2013). Imprecise probabilities in engineering analyses. Mechanical Systems and Signal Processing, 37(1–2), 4–29. https://doi.org/10.1016/j.ymssp.2013.01.024

Behrangi, A., Yin, X., Rajagopal, S., Stampoulis, D., & Ye, H. (2018). On distinguishing snowfall from rainfall using near-surface atmospheric information: <scp>C</scp> omparative analysis, uncertainties and hydrologic importance. Quarterly Journal of the Royal Meteorological Society, 144(S1), 89–102. https://doi.org/10.1002/qj.3240

Berardi, U., & Jafarpur, P. (2020). Assessing the impact of climate change on building heating and cooling energy demand in Canada. Renewable and Sustainable Energy Reviews, 121, 109681. https://doi.org/10.1016/j.rser.2019.109681

Bhatnagar, M., Mathur, J., & Garg, V. (2018). Determining base temperature for heating and cooling degree-days for India. Journal of Building Engineering, 18, 270–280. https://doi.org/10.1016/j.jobe.2018.03.020

Bi, D., Dix, M., Marsland, S., O'Farrell, S., Sullivan, A., Bodman, R., Law, R., Harman, I., Srbinovsky, J., Rashid, H. A., Dobrohotoff, P., Mackallah, C., Yan, H., Hirst, A., Savita, A., Dias, F. B., Woodhouse, M., Fiedler, R., & Heerdegen, A. (2020). Configuration and spin-up of ACCESS-CM2, the new generation Australian Community Climate and Earth System Simulator Coupled Model. Journal of Southern Hemisphere Earth Systems Science, 70(1), 225–251. https://doi.org/10.1071/ES19040

Billinton, R. (1988). Distribution system reliability performance and evaluation. International Journal of Electrical Power & Energy Systems, 10(3), 190–200. https://doi.org/10.1016/0142-0615(88)90035-X

Birolini, A. (2014). Reliability Engineering. Springer Berlin Heidelberg. https://doi.org/10.1007/978-3-642-39535-2

Bonnifait, L. (2005). Développement de courbes submersion-dommages pour l'habitat résidentiel 516 québécois.

Bosshard, T., Carambia, M., Goergen, K., Kotlarski, S., Krahe, P., Zappa, M., & Schär, C. (2013). Quantifying uncertainty sources in an ensemble of hydrological climate-impact projections. Water Resources Research, 49(3), 1523–1536. https://doi.org/10.1029/2011WR011533

Breaden, J. P. (1971). The Generation of Flood Damage Time Sequences. https://doi.org/doi.org/10.7939/r3-h2xs-8404

Bruaset, S., & Sægrov, S. (2018). An Analysis of the Potential Impact of Climate Change on the Structural Reliability of Drinking Water Pipes in Cold Climate Regions. Water, 10(4), 411. https://doi.org/10.3390/w10040411

Brugmann, J. (2012). A Demand-Driven Approach to Development, Disaster Risk Reduction, and Climate Adaptation (pp. 383–390). https://doi.org/10.1007/978-94-007-4223-9_40

Bryant, S. (2019). Accumulating Flood Risk A Model Study to Quantify Flood Damage Mitigation Measures under Dynamic Vulnerability.

Bubeck, P., de Moel, H., Bouwer, L. M., & Aerts, J. C. J. H. (2011). How reliable are projections of future flood damage? Natural Hazards and Earth System Sciences, 11(12), 3293–3306. https://doi.org/10.5194/nhess-11-3293-2011

Cannon, A. J. (2015). Selecting GCM Scenarios that Span the Range of Changes in a Multimodel Ensemble: Application to CMIP5 Climate Extremes Indices. Journal of Climate, 28(3), 1260–1267. https://doi.org/10.1175/JCLI-D-14-00636.1*

Cannon, A. J., Sobie, S. R., & Murdock, T. Q. (2015). Bias Correction of GCM Precipitation by Quantile Mapping: How Well Do Methods Preserve Changes in Quantiles and Extremes? Journal of Climate, 28(17), 6938–6959. https://doi.org/10.1175/JCLI-D-14-00754.1

Capacci, L., & Biondini, F. (2020). Probabilistic life-cycle seismic resilience assessment of aging bridge networks considering infrastructure upgrading. Structure and Infrastructure Engineering, 16(4), 659–675. https://doi.org/10.1080/15732479.2020.1716258

Carpaneto, E., & Chicco, G. (2004). Evaluation of the Probability Density Functions of Distribution System Reliability Indices With a Characteristic Functions-Based Approach. IEEE Transactions on Power Systems, 19(2), 724–734. https://doi.org/10.1109/TPWRS.2003.821627

Chakraborty, L., Rus, H., Henstra, D., Thistlethwaite, J., & Scott, D. (2020). A place-based socioeconomic status index: Measuring social vulnerability to flood hazards in the context of environmental justice. International Journal of Disaster Risk Reduction, 43, 101394. https://doi.org/10.1016/j.ijdrr.2019.101394

Chen, S., & Gong, B. (2021). Response and adaptation of agriculture to climate change: Evidence from China. Journal of Development Economics, 148, 102557. https://doi.org/10.1016/j.jdeveco.2020.102557

Chiotti, Q., Chan, K., Gulecoglu, E., Belaieff, A., & Noxon, G. (2017). PLANNING FOR RESILIENCY; Toward a Corporate Climate Adaptation Plan. https://assets.metrolinx.com/image/upload/v1663237658/Documents/Metrolinx/Planning_for_Resiliency_2017_EN_final.pdf

Cleary, S., & Willcot, N. (2022). The Physical Costs of Climate Change: A Canadian Perspective. https://smith.queensu.ca/centres/isf/pdfs/ISF-Report-PhysicalCostsOfClimateChange.pdf

Colquhoun, D. (2014). An investigation of the false discovery rate and the misinterpretation of p -values. Royal Society Open Science, 1(3), 140216. https://doi.org/10.1098/rsos.140216

Crespo, L. G., Kenny, S. P., & Giesy, D. P. (2013). Reliability analysis of polynomial systems subject to p-box uncertainties. Mechanical Systems and Signal Processing, 37(1–2), 121–136. https://doi.org/10.1016/j.ymssp.2012.08.012

Croce, P., Formichi, P., & Landi, F. (2019). Climate Change: Impacts on Climatic Actions and Structural Reliability. Applied Sciences, 9(24), 5416. https://doi.org/10.3390/app9245416

Crosbie, R. S., Dawes, W. R., Charles, S. P., Mpelasoka, F. S., Aryal, S., Barron, O., & Summerell, G. K. (2011). Differences in future recharge estimates due to GCMs, downscaling methods and hydrological models. Geophysical Research Letters, 38(11), n/a-n/a. https://doi.org/10.1029/2011GL047657

Curry, C. L., Islam, S. U., Zwiers, F. W., & Déry, S. J. (2019). Atmospheric Rivers Increase Future Flood Risk in Western Canada's Largest Pacific River. Geophysical Research Letters, 46(3), 1651–1661. https://doi.org/10.1029/2018GL080720

de Moel, H., Asselman, N. E. M., & Aerts, J. C. J. H. (2012). Uncertainty and sensitivity analysis of coastal flood damage estimates in the west of the Netherlands. Natural Hazards and Earth System Sciences, 12(4), 1045–1058. https://doi.org/10.5194/nhess-12-1045-2012

Di Virgilio, G., Ji, F., Tam, E., Nishant, N., Evans, J. P., Thomas, C., Riley, M. L., Beyer, K., Grose, M. R., Narsey, S., & Delage, F. (2022). Selecting CMIP6 GCMs for CORDEX Dynamical Downscaling: Model Performance, Independence, and Climate Change Signals. Earth's Future, 10(4). https://doi.org/10.1029/2021EF002625

Dimitriadis, P., Tegos, A., Oikonomou, A., Pagana, V., Koukouvinos, A., Mamassis, N., Koutsoyiannis, D., & Efstratiadis, A. (2016). Comparative evaluation of 1D and quasi-2D hydraulic models based on benchmark and real-world applications for uncertainty assessment in flood mapping. Journal of Hydrology, 534, 478–492. https://doi.org/10.1016/j.jhydrol.2016.01.020

Dutta, D., Herath, S., & Musiake, K. (2001). DIRECT FLOOD DAMAGE MODELING TOWARDS URBAN FLOOD RISK MANAGEMENT.

Egorova, R., van Noortwijk, J. M., & Holterman, S. R. (2008). Uncertainty in flood damage estimation. International Journal of River Basin Management, 6(2), 139–148. https://doi.org/10.1080/15715124.2008.9635343*

Epps, T. W., & Singleton, K. J. (1986). An omnibus test for the two-sample problem using the empirical characteristic function. Journal of Statistical Computation and Simulation, 26(3–4), 177–203. https://doi.org/10.1080/00949658608810963

Eto, J. H., LaCommare, K. H., Larsen, P., Todd, A., & Fisher, E. (2012). An Examination of Temporal Trends in Electricity Reliability Based on Reports from U.S. Electric Utilities. https://doi.org/10.2172/1055706

Federal flood damage estimation guidelines for buildings and infrastructure. (2021). https://doi.org/10.4095/327001

FEMA. (2018). Hazus Flood Model User Guidance.

Feng, G., Patelli, E., Beer, M., & Coolen, F. P. A. (2016). Imprecise system reliability and component importance based on survival signature. Reliability Engineering & System Safety, 150, 116–125. https://doi.org/10.1016/j.ress.2016.01.019

Ferson, S., & Tucker, W. T. (2008). Probability boxes as info-gap models. NAFIPS 2008 - 2008 Annual Meeting of the North American Fuzzy Information Processing Society, 1–6. https://doi.org/10.1109/NAFIPS.2008.4531314

Ferson, S, Moore, D., Van den Brink, P., Estes, T., Gallagher, K., O'Connor, R., & Verdonck, F. (2010). Bounding Uncertainty Analyses. In Application of Uncertainty Analysis to Ecological Risks of Pesticides (pp. 89–122). CRC Press. https://doi.org/10.1201/EBK1439807347-c6

Ferson, Scott. (2020). pba.r Probability Bounds Analysis S4 library for the R.

Ferson, Scott, Kreinovich, V., Ginzburg, L., Myers, D. S., & Sentz, K. (2003). Constructing Probability Boxes and Dempster-Shafer Structures.

Fischer, E. M., Oleson, K. W., & Lawrence, D. M. (2012). Contrasting urban and rural heat stress responses to climate change. Geophysical Research Letters, 39(3), n/a-n/a. https://doi.org/10.1029/2011GL050576

Freni, G., La Loggia, G., & Notaro, V. (2010). Uncertainty in urban flood damage assessment due to urban drainage modelling and depth-damage curve estimation. Water Science and Technology, 61(12), 2979–2993. https://doi.org/10.2166/wst.2010.177

Gachon, P., Bussières, L., Gosselin, P., Raphoz, M., Bustinza, R., Martin, P., Dueymes, G., Gosselin, D., Labrecque, S., Jeffers, S., & Yagouti, A. (2016). A. (2016) Guide to identifying alert thresholds for heat waves in Canada based on evidence. Co-edited by Université du Québec à Montréal, Environment and Climate Change Canada, Institut National de Santé Publique du Québec, and Health Canada, Montréal, Qu. https://archipel.uqam.ca/9073/1/Gachon_et_al_2016_Guide_Heat_Waves_EN.pdf

GENIVAR. (2010). National Engineering Vulnerability Assessment of Public Infrastructure To Climate Change; Toronto and Region Conservation Authority Flood Control Dam Water Resources Infrastructure Assessment. https://pievc.ca/wp-content/uploads/2010/06/TRCA_Combined_Final-Report.pdf

Gillett, N. P., Cannon, A. J., Malinina, E., Schnorbus, M., Anslow, F., Sun, Q., Kirchmeier-Young, M., Zwiers, F., Seiler, C., Zhang, X., Flato, G., Wan, H., Li, G., & Castellan, A. (2022). Human influence on the 2021 British Columbia floods. Weather and Climate Extremes, 36, 100441. https://doi.org/10.1016/j.wace.2022.100441

Goerg, S. J., & Kaiser, J. (2009). Nonparametric testing of distributions—the Epps–Singleton two-sample test using the empirical characteristic function. The Stata Journal. https://journals.sagepub.com/doi/pdf/10.1177/1536867X0900900307

Goldberg, M. S., Gasparrini, A., Armstrong, B., & Valois, M.-F. (2011). The short-term influence of temperature on daily mortality in the temperate climate of Montreal, Canada. Environmental Research, 111(6), 853–860. https://doi.org/10.1016/j.envres.2011.05.022

Gouldby, B., Samuels, P., Klijn, F., Messner, F., Os, A. van, Sayers, P., & Schanze, J. (2009). Integrated Flood Risk Analysis and Management Methodologies; Language of Risk – Project Definitions. www.floodsite.net.

Government of Canada. (n.d.). Historical Climate Data. https://climate.weather.gc.ca/

Gray, N., Ferson, S., De Angelis, M., Gray, A., & Baumont de Oliveira, F. (2022). Probability bounds analysis for Python. Software Impacts, 12, 100246. https://doi.org/10.1016/j.simpa.2022.100246

Gutjahr, O., Putrasahan, D., Lohmann, K., Jungclaus, J. H., von Storch, J.-S., Brüggemann, N., Haak, H., & Stössel, A. (2019). Max Planck Institute Earth System Model (MPI-ESM1.2) for the High-Resolution Model Intercomparison Project (HighResMIP). Geoscientific Model Development, 12(7), 3241–3281. https://doi.org/10.5194/gmd-12-3241-2019

Hamed, K. H., & Ramachandra Rao, A. (1998). A modified Mann-Kendall trend test for autocorrelated data. Journal of Hydrology, 204(1–4), 182–196. https://doi.org/10.1016/S0022-1694(97)00125-X

He, W., Zhao, S., Wu, Q., Jiang, Y., & Wan, S. (2019). Simulating evaluation and projection of the climate zones over China by CMIP5 models. Climate Dynamics, 52(5–6), 2597–2612. https://doi.org/10.1007/s00382-018-4410-1

Head, M. L., Holman, L., Lanfear, R., Kahn, A. T., & Jennions, M. D. (2015). The Extent and Consequences of P-Hacking in Science. PLOS Biology, 13(3), e1002106. https://doi.org/10.1371/journal.pbio.1002106

Health Canada. (2009). The Urban Heat Island Effect: Causes, Health Impacts and Mitigation Strategies. https://www.canada.ca/content/dam/hc-sc/migration/hc-sc/ewh-semt/alt_formats/hecs-sesc/pdf/pubs/climat/adapt_bulletin-adapt1/adapt_bulletin-adapt1-eng.pdf

Heinrich, D. F., & Penning-Rowsell, E. C. (2022). Flood risk management under uncertainty in transboundary basins: a delicate balancing act. International Journal of River Basin Management, 20(2), 215–224. https://doi.org/10.1080/15715124.2020.1837845

Henstra, D., & Thistlethwaite, J. (2017). Climate Change, Floods, and Municipal Risk Sharing in Canada. IMFG Papers on Municipal Finance and Governance No. 30.

Hughes, D. A., Mantel, S., & Mohobane, T. (2014). An assessment of the skill of downscaled GCM outputs in simulating historical patterns of rainfall variability in South Africa. Hydrology Research, 45(1), 134–147. https://doi.org/10.2166/nh.2013.027

Hunsaker, C. T., Whitaker, T. W., & Bales, R. C. (2012). Snowmelt Runoff and Water Yield Along Elevation and Temperature Gradients in California's Southern Sierra Nevada1. JAWRA Journal of the American Water Resources Association, 48(4), 667–678. https://doi.org/10.1111/j.1752-1688.2012.00641.x

Hwang, S., & Graham, W. D. (2013). Development and comparative evaluation of a stochastic analog method to downscale daily GCM precipitation. Hydrology and Earth System Sciences, 17(11), 4481–4502. https://doi.org/10.5194/hess-17-4481-2013

IBI Group and Golder Associates. (2020). Flood Risk Assessment for BC's Lower Mainland.

IEA. (2022). Canada 2022 Energy Policy Review. https://iea.blob.core.windows.net/assets/7ec2467c-78b4-4c0c-a966-a42b8861ec5a/Canada2022.pdf

IPCC. (2023). AR6 Synthesis Report (SYR).

Iqbal, M. S., & Öberg, T. (2013). Description and Propagation of Uncertainty in Input Parameters in Environmental Fate Models. Risk Analysis, 33(7), 1353–1366. https://doi.org/10.1111/j.1539-6924.2012.01926.x

Johnson, M., & Fallon, K. K. (2011). Experimental Building Information Models. https://doi.org/10.21236/ADA552634

Kam, P. M., Aznar-Siguan, G., Schewe, J., Milano, L., Ginnetti, J., Willner, S., McCaughey, J. W., & Bresch, D. N. (2021). Global warming and population change both heighten future risk of human displacement due to river floods. Environmental Research Letters, 16(4), 044026. https://doi.org/10.1088/1748-9326/abd26c

Kang, J.-L., Su, M.-D., & Chang, L.-F. (2005). LOSS FUNCTIONS AND FRAMEWORK FOR REGIONAL FLOOD DAMAGE ESTIMATION IN RESIDENTIAL AREA. Journal of Marine Science and Technology, 13(3). https://doi.org/10.51400/2709-6998.2126

Karanki, D. R., Kushwaha, H. S., Verma, A. K., & Ajit, S. (2009). Uncertainty Analysis Based on Probability Bounds (P-Box) Approach in Probabilistic Safety Assessment. Risk Analysis, 29(5), 662–675. https://doi.org/10.1111/j.1539-6924.2009.01221.x

Keller, A. A., Garner, K. L., Rao, N., Knipping, E., & Thomas, J. (2022). Downscaling approaches of climate change projections for watershed modeling: Review of theoretical and practical considerations. PLOS Water, 1(9), e0000046. https://doi.org/10.1371/journal.pwat.0000046

Kendall, M. G. (1975). Rank Correlation Methods. New York, NY: Oxford University Press.

Kompas, T., Pham, V. H., & Che, T. N. (2018). The Effects of Climate Change on GDP by Country and the Global Economic Gains From Complying With the Paris Climate Accord. Earth's Future, 6(8), 1153–1173. https://doi.org/10.1029/2018EF000922

Laframboise, K., & O'Malley, O. (2022). Heavy rainfall leads to flooding, sewer backups in Greater Montreal area. Globalnews.Ca. https://globalnews.ca/news/9128008/montreal-rainfall-flooding-highways-metros/

Lausselet, C., Borgnes, V., & Brattebø, H. (2019). LCA modelling for Zero Emission Neighbourhoods in early stage planning. Building and Environment, 149, 379–389. https://doi.org/10.1016/j.buildenv.2018.12.034

Lausselet, C., Ellingsen, L. A., Strømman, A. H., & Brattebø, H. (2020). A life-cycle assessment model for zero emission neighborhoods. Journal of Industrial Ecology, 24(3), 500–516. https://doi.org/10.1111/jiec.12960

Lee, W., Kim, H., Hwang, S., Zanobetti, A., Schwartz, J. D., & Chung, Y. (2017). Monte Carlo simulation-based estimation for the minimum mortality temperature in temperature-mortality association study. BMC Medical Research Methodology, 17(1), 137. https://doi.org/10.1186/s12874-017-0412-7

Lehmann, P., Brenck, M., Gebhardt, O., Schaller, S., & Süßbauer, E. (2015). Barriers and opportunities for urban adaptation planning: analytical framework and evidence from cities in Latin America and Germany. Mitigation and Adaptation Strategies for Global Change, 20(1), 75–97. https://doi.org/10.1007/s11027-013-9480-0

Lei, H., & Singh, C. (2016). Non-Sequential Monte Carlo Simulation for Cyber-Induced Dependent Failures in Composite Power System Reliability Evaluation. IEEE Transactions on Power Systems, 1–1. https://doi.org/10.1109/TPWRS.2016.2572159

Liu, X., Kuang, Z., Yin, L., & Hu, L. (2017). Structural reliability analysis based on probability and probability box hybrid model. Structural Safety, 68, 73–84. https://doi.org/10.1016/j.strusafe.2017.06.002

Lokoshchenko, M. A. (2017). Urban Heat Island and Urban Dry Island in Moscow and Their Centennial Changes. Journal of Applied Meteorology and Climatology, 56(10), 2729–2745. https://doi.org/10.1175/JAMC-D-16-0383.1

Luo, D., Wan, X., Liu, J., & Tong, T. (2018). Optimally estimating the sample mean from the sample size, median, mid-range, and/or mid-quartile range. Statistical Methods in Medical Research, 27(6), 1785–1805. https://doi.org/10.1177/0962280216669183

Luo, M., Liu, T., Frankl, A., Duan, Y., Meng, F., Bao, A., Kurban, A., & De Maeyer, P. (2018). Defining spatiotemporal characteristics of climate change trends from downscaled GCMs ensembles: how climate change reacts in Xinjiang, China. International Journal of Climatology, 38(5), 2538–2553. https://doi.org/10.1002/joc.5425

Malik, S., Pal, S. C., Sattar, A., Singh, S. K., Das, B., Chakrabortty, R., & Mohammad, P. (2020). Trend of extreme rainfall events using suitable Global Circulation Model to combat the water logging condition in Kolkata Metropolitan Area. Urban Climate, 32, 100599. https://doi.org/10.1016/j.uclim.2020.100599

Mann, H. B. (1945). Nonparametric Tests Against Trend. Econometrica, 13(3), 245. https://doi.org/10.2307/1907187

Marcotullio, P. J., & Schmeltz, M. T. (2021). Future Heat Risk in South Asia and the Need for Ecosystem Mitigation (pp. 225–252). https://doi.org/10.1007/978-981-16-4815-1_10

Maurer, E. P., & Hidalgo, H. G. (2008). Utility of daily vs. monthly large-scale climate data: an intercomparison of two statistical downscaling methods. Hydrology and Earth System Sciences, 12(2), 551–563. https://doi.org/10.5194/hess-12-551-2008

Maurer, E. P., Hidalgo, H. G., Das, T., Dettinger, M. D., & Cayan, D. R. (2010). The utility of daily large-scale climate data in the assessment of climate change impacts on daily streamflow in California. Hydrology and Earth System Sciences, 14(6), 1125–1138. https://doi.org/10.5194/hess-14-1125-2010

Maxwell, K. B., Julius, S. H., Grambsch, A. E., Kosmal, A. R., Larson, E., & Sonti, N. (2018). Chapter 11 : Built Environment, Urban Systems, and Cities. Impacts, Risks, and Adaptation in the United States: The Fourth National Climate Assessment, Volume II. https://doi.org/10.7930/NCA4.2018.CH11

McGrath, S., Zhao, X., Steele, R., Thombs, B. D., Benedetti, A., Levis, B., Riehm, K. E., Saadat, N., Levis, A. W., Azar, M., Rice, D. B., Sun, Y., Krishnan, A., He, C., Wu, Y., Bhandari, P. M., Neupane, D., Imran, M., Boruff, J., … Zhang, Y. (2020). Estimating the sample mean and standard deviation from commonly reported quantiles in meta-analysis. Statistical Methods in Medical Research, 29(9), 2520–2537. https://doi.org/10.1177/0962280219889080

McKeown, D. (2015). Update on Extreme Heat and Maximum Indoor Temperature Standard for Multi-unit Residential Buildings. https://www.toronto.ca/legdocs/mmis/2015/hl/bgrd/backgroundfile-85835.pdf

Merz, B., Kreibich, H., Schwarze, R., & Thieken, A. (2010). Review article "Assessment of economic flood damage" Natural Hazards and Earth System Sciences, 10(8), 1697–1724. https://doi.org/10.5194/nhess-10-1697-2010

Merz, B., Kreibich, H., Thieken, A., & Schmidtke, R. (2004). Estimation uncertainty of direct monetary flood damage to buildings. Natural Hazards and Earth System Sciences, 4(1), 153–163. https://doi.org/10.5194/nhess-4-153-2004

Merz, Bruno, & Thieken, A. H. (2009). Flood risk curves and uncertainty bounds. Natural Hazards, 51(3), 437–458. https://doi.org/10.1007/s11069-009-9452-6

Mohanty, M. P., & Simonovic, S. P. (2021). Changes in floodplain regimes over Canada due to climate change impacts: Observations from CMIP6 models. Science of The Total Environment, 792, 148323. https://doi.org/10.1016/j.scitotenv.2021.148323

Nakicenovic, N., Alcamo, J., & Davis, G. (2000). IPCC SPECIAL REPORT; EMISSIONS SCENARIOS.

Nematchoua, M. K., Orosa, J. A., & Reiter, S. (2019). Climate change: Variabilities, vulnerabilities and adaptation analysis - A case of seven cities located in seven countries of Central Africa. Urban Climate, 29, 100486. https://doi.org/10.1016/j.uclim.2019.100486

Nofal, O. M., van de Lindt, J. W., & Do, T. Q. (2020). Multi-variate and single-variable flood fragility and loss approaches for buildings. Reliability Engineering & System Safety, 202, 106971. https://doi.org/10.1016/j.ress.2020.106971

NRTEE. (2011). Paying the Price: The Economic Impacts of Climate Change for Canada.

O'Donnell, E. C., & Thorne, C. R. (2020). Drivers of future urban flood risk. Philosophical Transactions of the Royal Society A: Mathematical, Physical and Engineering Sciences, 378(2168), 20190216. https://doi.org/10.1098/rsta.2019.0216

Oberkampf, W. L., Tucker, W. T., Zhang, J., Ginzburg, L., Berleant, D. J., Ferson, S., Hajagos, J., & Nelsen, R. B. (2004). Dependence in probabilistic modeling, Dempster-Shafer theory, and probability bounds analysis. https://doi.org/10.2172/919189

Ogden, N., & Gachon, P. (2019). Climate change and infectious diseases: What can we expect? Canada Communicable Disease Report, 45(4), 76–80. https://doi.org/10.14745/ccdr.v45i04a01

Ormandy, D., & Ezratty, V. ronique. (2011). Health and thermal comfort: From WHO guidance to housing strategies. Energy Policy. https://doi.org/10.1016/j.enpol.2011.09.003

Ouyang, H., Tang, X., Zhang, R., Baklanov, A., Brasseur, G., Kumar, R., Han, Q., & Luo, Y. (2023). Resilience Building and Collaborative Governance for Climate Change Adaptation in Response to a New State of More Frequent and Intense Extreme Weather Events. International Journal of Disaster Risk Science. https://doi.org/10.1007/s13753-023-00467-0

P. Lees, F. (2005). Lees' Loss Prevention in the Process Industries : Hazard Identification, Assessment and Control (S. Mannan (Ed.); 3rd ed.).

Pacific Climate Impacts Consortium. (2021). Statistically Downscaled Climate Scenarios. University of Victoria. https://www.pacificclimate.org/data/statistically-downscaled-climate-scenarios

Palko, K. G., & Lemmen, D. S. (2017). Climate risks and adaptation practices for the Canadian transportation sector 2016. Ottawa, ON: Government of Canada. https://www.nrcan.gc.ca/sites/www.nrcan.gc.ca/files/earthsciences/pdf/assess/2016/ClimatRisk-E-ACCESSIBLE.pdf

PIEVC. (2010). Climate Change Engineering Vulnerability Assessment; Coquihalla Highway (B.C. Highway 5) Between Nicolum River and Dry Gulch. https://www2.gov.bc.ca/assets/gov/driving-and-transportation/environment/climate-action/hwy5_coquihalla.pdf

PIEVC. (2014). Climate Change Vulnerability Assessment for Selected Stormwater Infrastructure at Toronto Pearson International Airport. https://pievc.ca/wp-content/uploads/2021/01/gtaa_infrastructure_vulnerability_assessment_-_final-1.pdf

Pistrika, A., Tsakiris, G., & Nalbantis, I. (2014). Flood Depth-Damage Functions for Built Environment. Environmental Processes, 1(4), 553–572. https://doi.org/10.1007/s40710-014-0038-2

Rabinovich, S. G. (2005). Measurement errors and uncertainties: theory and practice.

Rezaei, S. N., Chouinard, L., Langlois, S., & Légeron, F. (2016). Analysis of the effect of climate change on the reliability of overhead transmission lines. Sustainable Cities and Society, 27, 137–144. https://doi.org/10.1016/j.scs.2016.01.007

Rivers, N., & Shaffer, B. (2020). Stretching the Duck: How Rising Temperatures will Change the Level and Shape of Future Electricity Consumption. The Energy Journal, 41(01). https://doi.org/10.5547/01956574.41.5.nriv

Roy, L. (2022). Downpour leads to flooded metro stations and overflowing roads in Montreal. CTVNewsMontreal.Ca. https://montreal.ctvnews.ca/downpour-leads-to-flooded-metro-stations-and-overflowing-roads-in-montreal-1.6067213

Sandink, D., Kovacs, P., Oulahen, G., & McGillivray, G. (2010). Making Flood Insurable for Canadian Homeowners: A Discussion Paper.

Schwalm, C. R., Glendon, S., & Duffy, P. B. (2020). RCP8.5 tracks cumulative CO 2 emissions. Proceedings of the National Academy of Sciences, 117(33), 19656–19657. https://doi.org/10.1073/pnas.2007117117

Simon, C., & Bicking, F. (2017). Hybrid computation of uncertainty in reliability analysis with p-box and evidential networks. Reliability Engineering & System Safety, 167, 629–638. https://doi.org/10.1016/j.ress.2017.04.015

Singh, V. P., Jain, S. K., & Tyagi, A. (2007). Risk and Reliability Analysis. American Society of Civil Engineers. https://doi.org/10.1061/9780784408919

Smith, D. I. (1994). Flood damage estimation - A review of urban stage-damage curves and loss functions.

Song, Y., Mi, J., Cheng, Y., Bai, L., & Chen, K. (2020). A dependency bounds analysis method for reliability assessment of complex system with hybrid uncertainty. Reliability Engineering & System Safety, 204, 107119. https://doi.org/10.1016/j.ress.2020.107119

Stein, L. (2022). Regina residents get surprised with flash flooding after heavy downpour. https://www.cjme.com/2022/07/19/regina-residents-get-surprised-with-flash-flooding-after-heavy-downpour/

Suter, L., Streletskiy, D., & Shiklomanov, N. (2019). Assessment of the cost of climate change impacts on critical infrastructure in the circumpolar Arctic. Polar Geography, 42(4), 267–286. https://doi.org/10.1080/1088937X.2019.1686082

Swain, S., Mishra, S. K., Pandey, A., Dayal, D., & Srivastava, P. K. (2022). Appraisal of historical trends in maximum and minimum temperature using multiple non-parametric techniques over the agriculture-dominated Narmada Basin, India. Environmental Monitoring and Assessment, 194(12), 893. https://doi.org/10.1007/s10661-022-10534-6

Tam, B. Y., Gough, W. A., & Mohsin, T. (2015). The impact of urbanization and the urban heat island effect on day to day temperature variation. Urban Climate, 12, 1–10. https://doi.org/10.1016/j.uclim.2014.12.004

Tate, E., Muñoz, C., & Suchan, J. (2015). Uncertainty and Sensitivity Analysis of the HAZUS-MH Flood Model. Natural Hazards Review, 16(3), 04014030. https://doi.org/10.1061/(ASCE)NH.1527-6996.0000167

Thieken, A. H., Müller, M., Kreibich, H., & Merz, B. (2005). Flood damage and influencing factors: New insights from the August 2002 flood in Germany. Water Resources Research, 41(12). https://doi.org/10.1029/2005WR004177

Transport Canada. (2021). Minister of Transport announces precautionary measures to address safety concerns resulting from extreme weather and wildfire risks. https://www.canada.ca/en/transport-canada/news/2021/07/minister-of-transport-announces-precautionary-measures-to-address-safety-concerns-resulting-from-extreme-weather-and-wildfire-risks.html

Tucker, W. T., & Ferson, S. (2003). Probability bounds analysis in environmental risk assessments. Applied Biomathematics.

U.S. National Research, & Council, C. on the H. D. of G. C. (1997). Environmentally Significant Consumption: Research Directions.

Vidgen, B., & Yasseri, T. (2016). P-Values: Misunderstood and Misused. Frontiers in Physics, 4. https://doi.org/10.3389/fphy.2016.00006

Wachinger, G., Renn, O., Begg, C., & Kuhlicke, C. (2013). The Risk Perception Paradox-Implications for Governance and Communication of Natural Hazards. Risk Analysis, 33(6), 1049–1065. https://doi.org/10.1111/j.1539-6924.2012.01942.x

Wagenaar, D. J., de Bruijn, K. M., Bouwer, L. M., & de Moel, H. (2016). Uncertainty in flood damage estimates and its potential effect on investment decisions. Natural Hazards and Earth System Sciences, 16(1), 1–14. https://doi.org/10.5194/nhess-16-1-2016

Walley, P. (1991). Statistical Reasoning with Imprecise Probabilities.

Wan, X., Wang, W., Liu, J., & Tong, T. (2014). Estimating the sample mean and standard deviation from the sample size, median, range and/or interquartile range. BMC Medical Research Methodology, 14(1), 135. https://doi.org/10.1186/1471-2288-14-135

Wang, H., & Chen, Q. (2014). Impact of climate change heating and cooling energy use in buildings in the United States. Energy and Buildings, 82, 428–436. https://doi.org/10.1016/j.enbuild.2014.07.034

Wang, L., Liu, X., & Brown, H. (2017). Prediction of the impacts of climate change on energy consumption for a medium-size office building with two climate models. Energy and Buildings, 157, 218–226. https://doi.org/10.1016/j.enbuild.2017.01.007

Wang, Yaping, & Pham, H. (2012). Modeling the Dependent Competing Risks With Multiple Degradation Processes and Random Shock Using Time-Varying Copulas. IEEE Transactions on Reliability, 61(1), 13–22. https://doi.org/10.1109/TR.2011.2170253

Wang, Yupeng, Berardi, U., & Akbari, H. (2016). Comparing the effects of urban heat island mitigation strategies for Toronto, Canada. Energy and Buildings, 114, 2–19. https://doi.org/10.1016/j.enbuild.2015.06.046

Warren, F., & Lulham, N. (2021). Canada in a Changing Climate: National Issues Report; Government of Canada, Ottawa, ON. https://www.nrcan.gc.ca/sites/nrcan/files/pdf/National_Issues_Report_Final_EN.pdf

Weber, E. U. (2010). What shapes perceptions of climate change? Wiley Interdisciplinary Reviews: Climate Change, 1(3), 332–342. https://doi.org/10.1002/wcc.41

Whibbs, K., & Postey, D. (2022). Heavy rain causes flooding, closes streets around Regina. CTV News Regina. https://regina.ctvnews.ca/heavy-rain-causes-flooding-closes-streets-around-regina-1.5993350

Williamson, R. C., & Downs, T. (1990). Probabilistic arithmetic. I. Numerical methods for calculating convolutions and dependency bounds. International Journal of Approximate Reasoning, 4(2), 89–158. https://doi.org/10.1016/0888-613X(90)90022-T

WSP Canada Inc. (2021). Assessment of Climate Change Impacts on Infrastructure in all NWT communities. Report produced for Government of Northwest Territories. https://www.maca.gov.nt.ca/sites/maca/files/resources/gnwt_pievc_report_final_released.pdf

Yamane, T. (1967). Statistics, An Introductory Analysis (2nd ed.). Harper and Row.

Yan, R., Huang, J., Wang, Y., Gao, J., & Qi, L. (2016). Modeling the combined impact of future climate and land use changes on streamflow of Xinjiang Basin, China. Hydrology Research, 47(2), 356–372. https://doi.org/10.2166/nh.2015.206

Yang, G., Huang, X., Li, Y., & Ding, P. (2019). System Reliability Assessment with Imprecise Probabilities. Applied Sciences, 9(24), 5422. https://doi.org/10.3390/app9245422

Yang, X., Li, Y., Luo, Z., & Chan, P. W. (2017). The urban cool island phenomenon in a high-rise high-density city and its mechanisms. International Journal of Climatology, 37(2), 890–904. https://doi.org/10.1002/joc.4747

Zhai, Y., Huang, G., Wang, X., Zhou, X., Lu, C., & Li, Z. (2019). Future projections of temperature changes in Ottawa, Canada through stepwise clustered downscaling of multiple GCMs under RCPs. Climate Dynamics, 52(5–6), 3455–3470. https://doi.org/10.1007/s00382-018-4340-y

Zhang, Q., Zeng, Z., Zio, E., & Kang, R. (2017). Probability box as a tool to model and control the effect of epistemic uncertainty in multiple dependent competing failure processes. Applied Soft Computing, 56, 570–579. https://doi.org/10.1016/j.asoc.2016.06.016

Ziehn, T., Chamberlain, M. A., Law, R. M., Lenton, A., Bodman, R. W., Dix, M., Stevens, L., Wang, Y.-P., & Srbinovsky, J. (2020). The Australian Earth System Model: ACCESS-ESM1.5. Journal of Southern Hemisphere Earth Systems Science, 70(1), 193–214. https://doi.org/10.1071/ES19035

Iqbal, M. S., & Öberg, T. (2013). Description and Propagation of Uncertainty in Input Parameters in Environmental Fate Models. Risk Analysis, 33(7), 1353–1366. https://doi.org/10.1111/j.1539-6924.2012.01926.x

Johnson, M., & Fallon, K. K. (2011). Experimental Building Information Models. https://doi.org/10.21236/ADA552634

Kam, P.M. et al. (2021) 'Global warming and population change both heighten future risk of human displacement due to river floods', Environmental Research Letters, 16(4), p. 044026. Available at: https://doi.org/10.1088/1748-9326/abd26c.

Kang, J.-L., Su, M.-D., & Chang, L.-F. (2005). LOSS FUNCTIONS AND FRAMEWORK FOR REGIONAL FLOOD DAMAGE ESTIMATION IN RESIDENTIAL AREA. Journal of Marine Science and Technology, 13(3). https://doi.org/10.51400/2709-6998.2126

Karanki, D. R., Kushwaha, H. S., Verma, A. K., & Ajit, S. (2009). Uncertainty Analysis Based on Probability Bounds (P-Box) Approach in Probabilistic Safety Assessment. Risk Analysis, 29(5), 662–675. https://doi.org/10.1111/j.1539-6924.2009.01221.x

Kendall, M. G. (1975). Rank Correlation Methods. New York, NY: Oxford University Press.

Kokelj, S. V., Tunnicliffe, J., Lacelle, D., Lantz, T. C., Chin, K. S., & Fraser, R. (2015). Increased precipitation drives mega slump development and destabilization of ice-rich permafrost terrain, northwestern Canada. Global and Planetary Change, 129, 56–68. https://doi.org/10.1016/j.gloplacha.2015.02.008

Kompas, T., Pham, V. H., & Che, T. N. (2018). The Effects of Climate Change on GDP by Country and the Global Economic Gains From Complying With the Paris Climate Accord. Earth's Future, 6(8), 1153–1173. https://doi.org/10.1029/2018EF000922

Laframboise, K., & O'Malley, O. (2022). Heavy rainfall leads to flooding, sewer backups in Greater Montreal area. Globalnews.Ca. https://globalnews.ca/news/9128008/montreal-rainfall-flooding-highways-metros/

Lehmann, P. et al. (2015) 'Barriers and opportunities for urban adaptation planning: analytical framework and evidence from cities in Latin America and Germany', Mitigation and Adaptation Strategies for Global Change, 20(1), pp. 75–97. Available at: https://doi.org/10.1007/s11027-013-9480-0.

Lei, H., & Singh, C. (2016). Non-Sequential Monte Carlo Simulation for Cyber-Induced Dependent Failures in Composite Power System Reliability Evaluation. IEEE Transactions on Power Systems, 1–1. https://doi.org/10.1109/TPWRS.2016.2572159

Liu, X., Kuang, Z., Yin, L., & Hu, L. (2017). Structural reliability analysis based on probability and probability box hybrid model. Structural Safety, 68, 73–84. https://doi.org/10.1016/j.strusafe.2017.06.002

Luo, D., Wan, X., Liu, J., & Tong, T. (2018). Optimally estimating the sample mean from the sample size, median, mid-range, and/or mid-quartile range. Statistical Methods in Medical Research, 27(6), 1785–1805. https://doi.org/10.1177/0962280216669183

Luo, M., Liu, T., Frankl, A., Duan, Y., Meng, F., Bao, A., Kurban, A., & De Maeyer, P. (2018). Defining spatiotemporal characteristics of climate change trends from downscaled GCMs ensembles: how climate change reacts in Xinjiang, China. International Journal of Climatology, 38(5), 2538–2553. https://doi.org/10.1002/joc.5425

Malik, S., Pal, S. C., Sattar, A., Singh, S. K., Das, B., Chakrabortty, R., & Mohammad, P. (2020). Trend of extreme rainfall events using suitable Global Circulation Model to combat the water logging condition in Kolkata Metropolitan Area. Urban Climate, 32, 100599. https://doi.org/10.1016/j.uclim.2020.100599

Mann, H. B. (1945). Nonparametric Tests Against Trend. Econometrica, 13(3), 245. https://doi.org/10.2307/1907187

Marcotullio, P. J., & Schmeltz, M. T. (2021). Future Heat Risk in South Asia and the Need for Ecosystem Mitigation (pp. 225–252). https://doi.org/10.1007/978-981-16-4815-1_10

Maurer, E. P., H. G. Hidalgo, T. Das, M. D. Dettinger, and D. R. Cayan. 2010. "The Utility of Daily Large-Scale Climate Data in the Assessment of Climate Change Impacts on Daily Streamflow in California." Hydrology and Earth System Sciences 14(6):1125–38.

Maxwell, K. B., Julius, S. H., Grambsch, A. E., Kosmal, A. R., Larson, E., & Sonti, N. (2018). Chapter 11 : Built Environment, Urban Systems, and Cities. Impacts, Risks, and Adaptation in the United States: The Fourth National Climate Assessment, Volume II. https://doi.org/10.7930/NCA4.2018.CH11

McGrath, S., Zhao, X., Steele, R., Thombs, B. D., Benedetti, A., Levis, B., Riehm, K. E., Saadat, N., Levis, A. W., Azar, M., Rice, D. B., Sun, Y., Krishnan, A., He, C., Wu, Y., Bhandari, P. M., Neupane, D., Imran, M., Boruff, J., … Zhang, Y. (2020). Estimating the sample mean and standard deviation from commonly reported quantiles in meta-analysis. Statistical Methods in Medical Research, 29(9), 2520–2537. https://doi.org/10.1177/0962280219889080

McKeown, D. (2015). Update on Extreme Heat and Maximum Indoor Temperature Standard for Multi-unit Residential Buildings. https://www.toronto.ca/legdocs/mmis/2015/hl/bgrd/backgroundfile-85835.pdf

Merz, B., Kreibich, H., Schwarze, R., & Thieken, A. (2010). Review article "Assessment of economic flood damage" Natural Hazards and Earth System Sciences, 10(8), 1697–1724. https://doi.org/10.5194/nhess-10-1697-2010

Merz, B., Kreibich, H., Thieken, A., & Schmidtke, R. (2004). Estimation uncertainty of direct monetary flood damage to buildings. Natural Hazards and Earth System Sciences, 4(1), 153–163. https://doi.org/10.5194/nhess-4-153-2004

Merz, Bruno, & Thieken, A. H. (2009). Flood risk curves and uncertainty bounds. Natural Hazards, 51(3), 437–458. https://doi.org/10.1007/s11069-009-9452-6

Mohanty, M. P., & Simonovic, S. P. (2021). Changes in floodplain regimes over Canada due to climate change impacts: Observations from CMIP6 models. Science of The Total Environment, 792, 148323. https://doi.org/10.1016/j.scitotenv.2021.148323

Nakicenovic, N., Alcamo, J., & Davis, G. (2000). IPCC SPECIAL REPORT; EMISSIONS SCENARIOS.

Nematchoua, M. K., Orosa, J. A., & Reiter, S. (2019). Climate change: Variabilities, vulnerabilities and adaptation analysis - A case of seven cities located in seven countries of Central Africa. Urban Climate, 29, 100486. https://doi.org/10.1016/j.uclim.2019.100486

Nofal, O. M., van de Lindt, J. W., & Do, T. Q. (2020). Multi-variate and single-variable flood fragility and loss approaches for buildings. Reliability Engineering & System Safety, 202, 106971. https://doi.org/10.1016/j.ress.2020.106971

Nordhaus, W. D., & Boyer, J. (2000). Warming the world: economic models of global warming.

NRTEE. (2011). Paying the Price: The Economic Impacts of Climate Change for Canada.

O'Donnell, E. C., & Thorne, C. R. (2020). Drivers of future urban flood risk. Philosophical Transactions of the Royal Society A: Mathematical, Physical and Engineering Sciences, 378(2168), 20190216. https://doi.org/10.1098/rsta.2019.0216

Oberkampf, W. L., Tucker, W. T., Zhang, J., Ginzburg, L., Berleant, D. J., Ferson, S., Hajagos, J., & Nelsen, R. B. (2004). Dependence in probabilistic modeling, Dempster-Shafer theory, and probability bounds analysis. https://doi.org/10.2172/919189

Ormandy, D., & Ezratty, V. ronique. (2011). Health and thermal comfort: From WHO guidance to housing strategies. Energy Policy. https://doi.org/10.1016/j.enpol.2011.09.003

Ouyang, H., Tang, X., Zhang, R., Baklanov, A., Brasseur, G., Kumar, R., Han, Q., & Luo, Y. (2023). Resilience Building and Collaborative Governance for Climate Change Adaptation in Response to a New State of More Frequent and Intense Extreme Weather Events. International Journal of Disaster Risk Science. https://doi.org/10.1007/s13753-023-00467-0

P. Lees, F. (2005). Lees' Loss Prevention in the Process Industries: Hazard Identification, Assessment and Control (S. Mannan (Ed.); 3rd ed.).

Pacific Climate Impacts Consortium. (n.d.). STATISTICALLY DOWNSCALED CLIMATE SCENARIOS. 2021. https://pacificclimate.org/data/statistically-downscaled-climate-scenarios

Palko, K. G., & Lemmen, D. S. (2017). Climate risks and adaptation practices for the Canadian transportation sector 2016. Ottawa, ON: Government of Canada. https://www.nrcan.gc.ca/sites/www.nrcan.gc.ca/files/earthsciences/pdf/assess/2016/ClimatRisk-E-ACCESSIBLE.pdf

PIEVC. (2010). Climate Change Engineering Vulnerability Assessment; Coquihalla Highway (B.C. Highway 5) Between Nicolum River and Dry Gulch. https://www2.gov.bc.ca/assets/gov/driving-and-transportation/environment/climate-action/hwy5_coquihalla.pdf

PIEVC. (2014). Climate Change Vulnerability Assessment for Selected Stormwater Infrastructure at Toronto Pearson International Airport. https://pievc.ca/wp-content/uploads/2021/01/gtaa_infrastructure_vulnerability_assessment_-_final-1.pdf

Pistrika, A., Tsakiris, G., & Nalbantis, I. (2014). Flood Depth-Damage Functions for Built Environment. Environmental Processes, 1(4), 553–572. https://doi.org/10.1007/s40710-014-0038-2

Rabinovich, S. G. (2005). Measurement errors and uncertainties: theory and practice.

Rezaei, S. N., Chouinard, L., Langlois, S., & Légeron, F. (2016). Analysis of the effect of climate change on the reliability of overhead transmission lines. Sustainable Cities and Society, 27, 137–144. https://doi.org/10.1016/j.scs.2016.01.007

Rivers, N., & Shaffer, B. (2020). Stretching the Duck: How Rising Temperatures will Change the Level and Shape of Future Electricity Consumption. The Energy Journal, 41(01). https://doi.org/10.5547/01956574.41.5.nriv

Roy, L. (2022). Downpour leads to flooded metro stations and overflowing roads in Montreal. CTVNewsMontreal.Ca. https://montreal.ctvnews.ca/downpour-leads-to-flooded-metro-stations-and-overflowing-roads-in-montreal-1.6067213

Sandink, D., Kovacs, P., Oulahen, G., & McGillivray, G. (2010). Making Flood Insurable for Canadian Homeowners: A Discussion Paper.

Schwalm, C. R., Glendon, S., & Duffy, P. B. (2020). RCP8.5 tracks cumulative CO 2 emissions. Proceedings of the National Academy of Sciences, 117(33), 19656–19657. https://doi.org/10.1073/pnas.2007117117

Simon, C., & Bicking, F. (2017). Hybrid computation of uncertainty in reliability analysis with p-box and evidential networks. Reliability Engineering & System Safety, 167, 629–638. https://doi.org/10.1016/j.ress.2017.04.015

Singh, V. P., Jain, S. K., & Tyagi, A. (2007). Risk and Reliability Analysis. American Society of Civil Engineers. https://doi.org/10.1061/9780784408919

Smith, D. I. (1994). Flood damage estimation - A review of urban stage-damage curves and loss functions.

Song, Y., Mi, J., Cheng, Y., Bai, L., & Chen, K. (2020). A dependency bounds analysis method for reliability assessment of complex system with hybrid uncertainty. Reliability Engineering & System Safety, 204, 107119. https://doi.org/10.1016/j.ress.2020.107119

Stein, L. (2022). Regina residents get surprised with flash flooding after heavy downpour. https://www.cjme.com/2022/07/19/regina-residents-get-surprised-with-flash-flooding-after-heavy-downpour/

Suter, L., Streletskiy, D., & Shiklomanov, N. (2019). Assessment of the cost of climate change impacts on critical infrastructure in the circumpolar Arctic. Polar Geography, 42(4), 267–286. https://doi.org/10.1080/1088937X.2019.1686082

Tate, E., Muñoz, C., & Suchan, J. (2015). Uncertainty and Sensitivity Analysis of the HAZUS-MH Flood Model. Natural Hazards Review, 16(3), 04014030. https://doi.org/10.1061/(ASCE)NH.1527-6996.0000167

Thieken, A. H., Müller, M., Kreibich, H., & Merz, B. (2005). Flood damage and influencing factors: New insights from the August 2002 flood in Germany. Water Resources Research, 41(12). https://doi.org/10.1029/2005WR004177

Tol, R. S. J. (2018). The Economic Impacts of Climate Change. Review of Environmental Economics and Policy, 12(1), 4–25. https://doi.org/10.1093/reep/rex027

Transport Canada. (2021). Minister of Transport announces precautionary measures to address safety concerns resulting from extreme weather and wildfire risks. https://www.canada.ca/en/transport-canada/news/2021/07/minister-of-transport-announces-precautionary-measures-to-address-safety-concerns-resulting-from-extreme-weather-and-wildfire-risks.html

Tucker, W. T., & Ferson, S. (2003). Probability bounds analysis in environmental risk assessments. Applied Biomathematics.

U.S. National Research and Council, C. on the H.D. of G.C. (1997) Environmentally Significant Consumption: Research Directions.

Vidgen, B., & Yasseri, T. (2016). P-Values: Misunderstood and Misused. Frontiers in Physics, 4. https://doi.org/10.3389/fphy.2016.00006

Wachinger, G. et al. (2013) 'The Risk Perception Paradox-Implications for Governance and Communication of Natural Hazards', Risk Analysis, 33(6), pp. 1049–1065. Available at: https://doi.org/10.1111/j.1539-6924.2012.01942.x.

Wagenaar, D. J., de Bruijn, K. M., Bouwer, L. M., & de Moel, H. (2016). Uncertainty in flood damage estimates and its potential effect on investment decisions. Natural Hazards and Earth System Sciences, 16(1), 1–14. https://doi.org/10.5194/nhess-16-1-2016

Walley, P. (1991). Statistical Reasoning with Imprecise Probabilities.

Wan, X., Wang, W., Liu, J., & Tong, T. (2014). Estimating the sample mean and standard deviation from the sample size, median, range and/or interquartile range. BMC Medical Research Methodology, 14(1), 135. https://doi.org/10.1186/1471-2288-14-135

Wang, H., & Chen, Q. (2014). Impact of climate change heating and cooling energy use in buildings in the United States. Energy and Buildings, 82, 428–436. https://doi.org/10.1016/j.enbuild.2014.07.034

Wang, L., Liu, X., & Brown, H. (2017). Prediction of the impacts of climate change on energy consumption for a medium-size office building with two climate models. Energy and Buildings, 157, 218–226. https://doi.org/10.1016/j.enbuild.2017.01.007

Wang, Y., & Pham, H. (2012). Modeling the Dependent Competing Risks With Multiple Degradation Processes and Random Shock Using Time-Varying Copulas. IEEE Transactions on Reliability, 61(1), 13–22. https://doi.org/10.1109/TR.2011.2170253

Warren, F., & Lulham, N. (2021). Canada in a Changing Climate: National Issues Report; Government of Canada, Ottawa, ON. https://www.nrcan.gc.ca/sites/nrcan/files/pdf/National_Issues_Report_Final_EN.pdf

Weber, E.U. (2010) 'What shapes perceptions of climate change?', Wiley Interdisciplinary Reviews: Climate Change, 1(3), pp. 332–342. Available at: https://doi.org/10.1002/wcc.41.

Whibbs, K., & Postey, D. (2022). Heavy rain causes flooding, closes streets around Regina. CTV News Regina. https://regina.ctvnews.ca/heavy-rain-causes-flooding-closes-streets-around-regina-1.5993350

Williamson, R. C., & Downs, T. (1990). Probabilistic arithmetic. I. Numerical methods for calculating convolutions and dependency bounds. International Journal of Approximate Reasoning, 4(2), 89–158. https://doi.org/10.1016/0888-613X(90)90022-T

WSP Canada Inc. (2021). Assessment of Climate Change Impacts on Infrastructure in all NWT communities. Report produced for Government of Northwest Territories. https://www.maca.gov.nt.ca/sites/maca/files/resources/gnwt_pievc_report_final_released.pdf

Yamane, T. (1967). Statistics, An Introductory Analysis.

Yan, R. et al. (2016) 'Modeling the combined impact of future climate and land use changes on streamflow of Xinjiang Basin, China', Hydrology Research, 47(2), pp. 356–372. Available at: https://doi.org/10.2166/nh.2015.206.

Yang, G., Huang, X., Li, Y., & Ding, P. (2019). System Reliability Assessment with Imprecise Probabilities. Applied Sciences, 9(24), 5422. https://doi.org/10.3390/app9245422

Zhai, Y., Huang, G., Wang, X., Zhou, X., Lu, C., & Li, Z. (2019). Future projections of temperature changes in Ottawa, Canada through stepwise clustered downscaling of multiple GCMs under RCPs. Climate Dynamics, 52(5–6), 3455–3470. https://doi.org/10.1007/s00382-018-4340-y

Zhang, Q., Zeng, Z., Zio, E., & Kang, R. (2017). Probability box as a tool to model and control the effect of epistemic uncertainty in multiple dependent competing failure processes. Applied Soft Computing, 56, 570–579. https://doi.org/10.1016/j.asoc.2016.06.016

Ziehn, Tilo, Matthew A. Chamberlain, Rachel M. Law, Andrew Lenton, Roger W. Bodman, Martin Dix, Lauren Stevens, Ying-Ping Wang, and Jhan Srbinovsky. 2020. "The Australian Earth System Model: ACCESS-ESM1.5." Journal of Southern Hemisphere Earth Systems Science 70(1):193–214.